BEDROCK-CONTROLLED FLUVIAL GEOMORPHOLOGY AND THE HYDRAULICS OF RAPIDS ON THE COLORADO RIVER

by

Christopher Sean Magirl

A Dissertation Submitted to the Faculty of the

DEPARTMENT OF HYDROLOGY AND WATER RESOURCES

In Partial Fulfillment of the Requirements
For the Degree of

DOCTOR OF PHILOSOPHY
WITH A MAJOR IN HYDROLOGY

In the Graduate College

THE UNIVERSITY OF ARIZONA

2006

THE UNIVERSITY OF ARIZONA
GRADUATE COLLEGE

As members of the Dissertation Committee, we certify that we have read the dissertation

Prepared by Christopher Sean Magirl

Entitled Bedrock-Controlled Fluvial Geomorphology and the Hydraulics of Rapids on the Colorado River

and recommend that it be accepted as fulfilling the dissertation requirement for the

Degree of Doctor of Philosophy

_____ Date: 10/30/06
Victor R. Baker

_____ Date: 10/30/06
Robert H. Webb

_____ Date: 10/30/06
Peter G. DeCelles

_____ Date: 10/30/06
Kevin E. Lansey

_____ Date: 10/30/06
Jon D. Pelletier

Final approval and acceptance of this dissertation is contingent upon the candidate's submission of the final copies of the dissertation to the Graduate College.

I hereby certify that I have read this dissertation prepared under my direction and recommend that it be accepted as fulfilling the dissertation requirement.

_____ Date: 10/30/06
Dissertation Director: Victor R. Baker

STATEMENT BY AUTHOR

This dissertation has been submitted in partial fulfillment of requirements for an advanced degree at the University of Arizona and is deposited in the University Library to be made available to borrowers under the rules of the Library.

Brief quotations from this dissertation are allowable without special permission, provided that accurate acknowledgment of source is made. Requests for permission for extended quotation from or reproduction of this manuscript in whole or in part may be granted by the head of the major department or the Dean of the Graduate College when in his or her judgment the proposed use of the material is in the interests of scholarship. In all other instances, however, permission must be obtained from the author.

Christopher Sean Magirl_____

ACKNOWLEDGEMENTS

For the bigger rapids, one usually gets out to scout. I began scouting the career shift to hydrology in 1997, sitting on my couch in San Diego. I was watching an extended episode of "A Desert Speaks" about the 1996 controlled flood in Grand Canyon. On the tube, a southern-drawled yahoo jumped up and down exclaiming, "Cool!" each time a chuck of soil cleaved into the rising river. I was hooked. I made it to Tucson in 1999.

Bob Webb, the previously-mentioned yahoo and my day-to-day boss at the USGS, has been a steady source of inspiration, encouragement, feigned indifference, and friendship during the ride. I'm amazed at his productivity and endless enthusiasm. Through battle calls of "BEANS!" and "COFFEE!," it's been a pleasure to work with one of the best. Vic Baker, my academic advisor, has been wonderfully supportive and insightful and I continue to enjoy the many thought provoking discussions. The other members of the committee, Pete DeCelles, Kevin Lansey, and Jon Pelletier have all been supportive. I was fortunate to benefit from such a skilled and distinguished committee.

Grand Canyon Monitoring and Research Center provided a large portion of my funding over the project. GCMRC's Ted Melis managed the project and has been a trusted advisor, benefactor, and friend. Soroosh Sorooshian and the National Science Foundation provided my first year's funding. And finally, the US Geological Survey filled in the sometimes sizeable funding gaps.

The past seven years were, at times, turbulent. Many good friends kept my head above water. Officemate *extraodinaire* Diane Boyer is a wonderful friend and colleague, and I'm indebted to her for her ear and compassion. Her counsel is golden. Peter Griffiths, a champion officemate in his own right, is a valued colleague and friend, adroit in most components of science, engineering, and philosophy. Peter has pulled me from more than one bind. Steve "do-you-work-out?" Young is a great friend, skilled professional, and all around go-to boatman. Tberry simply put us in places others could not. Steve Cunningham did an amazing job designing the deployment boom. Graeme Smart generously loaned the POEM, his technical brilliance, and warm friendship. Bill Knight is a brilliant physicist who graciously helped me with code and support. The recent partnership with Jeff Gartner was remarkably timely. Jeff's help in the instrumentation section of this study has been fantastic.

The total list of people who have helped me in this endeavor is long; these individuals deserve special recognition: Tillie Klearman, Mike Breedlove, Doug Neilson, Jen Cunningham, Joe Hazel, Jack Schmidt, Gordon Grant, Jim O'Connor, Dominic Oldershaw, Ellen Wohl, Bob Jarrett, Matt Kaplinski, Mike Strangstalien, Cassie Fenton, Elizabeth Deliso, Terry Kenney, Connor Watkins, Kirk Burnett, and Terrie Thompson.

Thanks to Seamus, a wonderful field assistant and a constant source of motivation, pride, and joy. Thanks, also, to my mother who, long ago, planted the vision of this life-long goal. And finally, my deepest gratitude must go to my wife, Kathy. She has been amazingly supportive and wonderful during the home stretch of this project. She motivated and righted me when I contemplated walking away. She offers me endless encouragement and happiness. She is my partner, counsel, best friend, and love.

DEDICATION

to

Robert Joseph Magirl (October 3, 1917 – November 26, 2001)

and

Seamus Alejandro Magirl (b. March 10, 1996)

TABLE OF CONTENTS

TABLE OF CONTENTS – Continued

LIST OF FIGURES

LIST OF FIGURES - Continued

LIST OF FIGURES - Continued

LIST OF FIGURES - Continued

LIST OF FIGURES - Continued

LIST OF FIGURES - Continued

LIST OF FIGURES - Continued

LIST OF FIGURES - Continued

LIST OF TABLES

ABSTRACT

The fluvial geomorphology of the Colorado River cutting across the Colorado Plateau in the western United States is bedrock controlled and largely governed by rapids. Rapids on the Colorado River control the water-surface profile and influence the bathymetry, the storage of sand, and the aquatic ecology. Despite their importance, little data on the hydraulics, sediment transport, and long-term stability of rapids have been collected.

By comparing water-surface profiles, the average rate of aggradation at the head of 91 rapids in Grand Canyon between 1923 and 2000 was calculated to be 0.26 ± 0.15 m. In addition, while in 1923, 50% of the cumulative drop through the river corridor occurred in just 9% of the distance, by 2000, the cumulative drop over the same distance increased to 66%.

A new hydraulic model, incorporating one-dimensional step-backwater theory, was constructed for the Colorado River in Grand Canyon. The model includes 2,690 cross sections and simulates discharge up to 5,600 m^3/s, offering the opportunity to simulate large floods, rare under the current regulated flow regime.

Flow velocities were measured directly in rapids using three separate flow measurement instruments. An acoustic Doppler velocimeter (ADV) was used to measure velocity in five Grand Canyon rapids. While the instrument was able to measure velocity in three dimensions up to 3.0 m/s, limitations rendered data unusable for flow above 3.0 m/s. An acoustic Doppler current profiler (ADCP) was used to measure the flow field in

rapids throughout the water column in Cataract Canyon. The peak average velocity measured by the ADCP was roughly 4.0 m/s. Similarly, average flow velocity of 5.2 m/s was measured in a Cataract Canyon rapid using a pitot-static tube. The pitot-static tube measured instantaneous flow velocities up to 6.5 m/s, one of the fastest velocity measurements made in a river. Using the combination of the ADCP and pitot-static tube, the flow structure and nature of turbulence within rapids were analyzed.

Finally, techniques were developed to enable the measurement and construction of detailed water surface, shoreline, and bathymetric maps directly in rapids on the Colorado River.

1. INTRODUCTION

Roughly 22,500 recreational river rafters run the Colorado River in Grand Canyon each year (Loomis *et al.*, 2005), and the waiting list for private launch dates can be many years. Many thousands more run other sections of the Colorado River, including Ruby-Horsethief Canyon, Westwater Canyon (Milligan, 2004), and the steepest reach on the Colorado, Cataract Canyon (Webb *et al.*, 2004). One of the primary attractions for these river runners is the collection of rapids distributed throughout the Colorado River basin. Over 100 named rapids exist in Grand Canyon alone (Stevens, 1983) including some of the largest and most well known in North America. Rapids on the Colorado typically form in bedrock-controlled reaches where collections of large boulders constrict the river, forcing a cascade over and around the boulder matrix (Howard and Dolan, 1981; Kieffer, 1987; Webb 1996; Kieffer, 2003; Webb *et al.*, 2004).

For the purposes of this study, a rapid is defined as a section of river characterized by flow constricted to near critical conditions resulting in a collection of breaking waves laterally spanning the width of the river. The International Whitewater Scale classifies rapids into a scored system of relative navigational difficulty ranging from one to six, one being the easiest and six being generally unnavigable (Belknap *et al.*, 1998). The only exception to this one-to-six scale is Grand Canyon, where commercial river companies adopt a one-to-ten rating scale (Belknap and Belknap, 1969; Stevens, 1983). The concept, nonetheless, remains the same: a category 10 rapid in Grand Canyon is a large, dangerous

rapid. Regardless of the definition, rapids offer the river runner an exhilarating ride with dowsing splashes, steep drops, and the potential for an extended swim.

Through the first half of the 20th century, however, river rafting was considered an extreme activity reserved for the explorer, thrill seeker, or scientist. The dangers were well known and navigation on the Colorado was respected if not outright feared. Indeed, more than a handful of the original river runners lost their lives running the Colorado (Ghiglieri and Myers, 2001). In the 1950s and 1960s, with the advent of safe, robust rafts constructed with military-grade rubber, river running went mainstream and soared in popularity. Today, on any given summer afternoon, hundreds of boats are on the water throughout the Colorado River network from the headwaters to Lake Mead.

Despite interest and popularity, relatively little formal scientific study of rapids is available in the literature. The extreme conditions of flow and force concentrated at rapids renders research a challenge, and slower sections of river have tended to garner greater scientific interest. This dissertation attempts to provide scientific insight into the formation, evolution, and denudation of rapids on the Colorado River, specifically the mechanics of the interaction between flowing water and the resistant boulders emplaced within the river.

1.1 Regulated River

The Colorado River flows 2,300 kilometers from its headwaters in the Rocky, Uinta, and Wind River Mountains of Colorado, Utah, and Wyoming to the Gulf of California south of Yuma, Arizona (Figure 1.1). Much of the river system cuts through

the Colorado Plateau, a high, arid desert contributing little to the Colorado's annual flow. The flow regime, instead, is dominated by spring snowmelt floods originating in the high elevation headwaters. These seasonally powerful floods helped the river carve into the Colorado Plateau forming, in places, deep bedrock canyons. Along the main stem, the largest of these is Grand Canyon in northern Arizona, which extends 445 km from Lee's Ferry in Northern Arizona to the Grand Wash Cliffs just east of Las Vegas, Nevada (Figure 1.1). At the western end of Grand Canyon, the river flows into the headwaters of Lake Mead, the reservoir created by the closure of Hoover Dam in 1935 (Stevens, 1988). Upstream of Lee's Ferry, the river carved Glen Canyon through roughly 300 km of Navajo Sandstone. Most of Glen Canyon now contains Lake Powell, the reservoir behind Glen Canyon Dam 25 km above Lee's Ferry (Martin, 1989). The steepest reach along the Colorado River is Cataract Canyon, known for its numerous and closely spaced rapids (Webb *et al.*, 2004). Much of the downstream section of Cataract Canyon is under Lake Powell in eastern Utah.

With its ample snowmelt, the Colorado River has become a source of water and power to tens of millions of residents of the western United States (Reisner, 1986; Boyer and Webb, in press). Dams throughout the Colorado River Basin, Hoover and Glen Canyon being the largest, divert water to agriculture and cities, generate power, and regulate flow to downstream canyons. The unregulated Colorado River had variable discharge, often experiencing floods over 3,000 m^3/s at Lee's Ferry in the early summer

Figure 1.1: Map of the Colorado River system. Lake Powell is the reservoir impounded by Glen Canyon Dam. Lake Mead is the reservoir impounded by Hoover Dam.

or during prolonged rainfall (Topping *et al.*, 2003). In contrast, the river's median January discharge was 146 m^3/s (Topping *et al.*, 2003). The river's temperature also fluctuated, seasonally varying between 0 to 29° C during the year (Webb *et al.*, 1999b; Webb *et al.*, 2002). Glen Canyon Dam, closed in 1963, almost entirely governs flow of the Colorado River through Grand Canyon. Today, the river in Grand Canyon is clear, cold, and rarely deviates from the dam-release discharge of 142-708 m^3/s (Schmit, *et al.*, 2005). The Colorado River through Cataract, in contrast, is only partially regulated (Webb *et al.*, 2004). This reach of river is still subjected to large snowmelt floods, fluctuating water temperatures, and a heavy sediment load.

1.2 Formation of Grand Canyon

The Colorado Plateau is a high, arid geographic region covering the four-corner states of Utah, Colorado, New Mexico, and Arizona. Known for its blue skies and scenic vistas, the Plateau is also known for conspicuous geologic features. Grand Canyon, at the southwestern edge of the Colorado Plateau, exemplifies the wealth, range, and scale of these active processes.

To many of the three million annual visitors to Grand Canyon National Park, a simple explanation of the formation of Grand Canyon will suffice. As the Kaibab Plateau rose due to tectonic action, the antecedent Colorado River cut down into older layers of rock, creating the spectacle visible today. The rate of lifting, and thus, rate of river incision, is very slow yet constant. In fact, John Wesley Powell (1895) originally formulated this theory of antecedence while navigating the river corridor in 1869 and

1872. Since the original Powell theory, geologists continue to speculate on the exact timing and precise sequence of geomorphic events behind the formation of one of the seven natural wonders of the world (Young and Spamer, 2001)

In contrast to the theory of antecedence, a new thinking arose in the 20th century tying Grand Canyon formation to a large-scale reversal of drainage patterns across the lower Colorado Plateau (Blackwelder, 1934; Lucchitta, 1972). Before basin and range faulting impacted the region of the Mojave and Sonoran Deserts, the Colorado Plateau was a topographically low basin flanked to the south by tall mountains. These southern highlands, located in central Arizona near the present-day Mogollon Rim, were the source for material flowing north and covering Paleozoic and Mesozoic strata in central and northern Arizona. These 'rim' gravels are found in several locations north of the Mogollon rim and illustrate drainage generally flowing to the northeast (McKee and McKee, 1972; Peirce, 1984; Young, 2001). With the onset of basin and range rifting at roughly 18-10 Ma, local drainages within the Mogollon region reversed and flowed southwest (Potochnik and Faulds, 1998). In addition, the Colorado Plateau rose along a normal fault at Grand Wash in western Arizona during the middle Miocene, though there is no evidence of post-late Miocene offset (Lucchitta, 1966). Powell might have suggested this uplift created the first opportunity for the river to cut down into the Plateau; however, there was one problem: The Colorado River did not exist in its present western Grand Canyon location until roughly 6 Ma, well after cessation of faulting at Grand Wash.

We know no river existed in western Grand Canyon for a number of reasons. First, the Peach Springs Tuff in western Arizona preserved early-Miocene river gravels emanating from the Mogollon Highlands to the south flowing northeast along strike valleys (Young and Brennan, 1974). Second, Lucchitta (1972) showed an alluvial fan originating from the Grand Wash Cliffs only 2 km north of the current Colorado River spans the mouth of the river, indicating the river was not present when the alluvial fan formed. Also, the Muddy Creek formation and Hualapai Limestone are deposited in the basin below Grand Wash Cliffs and show no evidence of a major through flowing or depositing river (Lucchitta, 1972). Though the Hualapai Limestone, youngest of the units, has not been dated, basalts and limestones in the Muddy Creek Formation have been dated to roughly 5-8 Ma (Anderson, 1978; Damon *et al.*, 1978). Other evidence demonstrating the absence of the Colorado in western Grand Canyon during the Miocene is a knob of mid-Miocene basalt capping gravels of Paleozoic rocks. A similar outcrop, presumably the same unit, covers a large area on the Shivwitz Plateau, several miles to the north.

Numerous data, however, suggest a river, or rivers, in the region of eastern Grand Canyon during the mid-Miocene. Hunt (1969) synthesized these data sets into a hypothesis that an early San Juan River and Little Colorado River helped cut the upper topography of eastern Grand Canyon. Hunt postulated these rivers, later combined with the Green, coalesced into the Colorado River we see today. While McKee *et al.* (1967) accepted the presence of an old and established Colorado River, they assumed the Miocene river flowed south from Utah, down the current course of Marble Canyon, but

then turned toward the southeast along the valley currently inhabited by the Little Colorado River, eventually linking up with the Rio Grande and dumping into the Gulf of Mexico. Evidence collected after 1967 argues against this hypothesis (Lucchitta, 1972; Lucchitta, 1975). The best explanation to reconcile both the presence of a Miocene river in the region of eastern Grand Canyon and concurrent absence in western Grand Canyon was proposed by Lucchitta (1972): The ancestral Colorado River flowed through eastern Grand Canyon and across the Kaibab Plateau, then diverged north along the Uinkaret region toward the Great Basin. The depth of the canyon, however, formed by this Miocene Colorado was not particularly grand.

By analyzing stratigraphic data in the lower Colorado, Lucchitta (1972) determined the Colorado River began debouching from Grand Wash Cliffs roughly 6 Ma. Though Hunt (1969) postulated groundwater flow could have supported the nascent river, many theories point to headward erosion from a fault induced knickpoint and subsequent stream capture of the Colorado River from eastern Grand Canyon. More recent theories suggest closed-basin spillover of paleolake on the Colorado Plateau may have caused incipient erosion of Grand Canyon (Meek and Douglass, 2001; Spencer and Pearthree, 2001). Most of the evidence linking the emergence of the Colorado comes from deposits along the lower Colorado River. For example, in the Imperial Valley, sediment deposited by the Colorado contain late Cretaceous foraminifers derived from Mancos Shale of the Colorado Plateau (Lucchitta, 1972), providing a link between lower Colorado river deposition and the upper basin. In addition, analysis of the estuarine Bouse Formation (older than 3 Ma) along the lower Colorado shows the advancement and eventual retreat

of a bay associated with the Sea of Cortes (Lucchitta, 1972). The northern reaches of the Bouse Formation show large fluvial input associated with the Colorado River.

By using K/Ar dating on basalt flows in Grand Canyon below the Toroweap fault, Hamblin (1994) found basalt deposits at river level ranged in age from 0.6-1.2 Ma. Synthesizing these dates, it appears western Grand Canyon started downcutting at 6 Ma with possible cessation of downcutting at 0.6-1.2 Ma. Some believe the river has ceased downcutting for the past 1 million years and achieved a state of equilibrium with the main-stem river, removing the volume of material dumped into the river corridor by tributaries. This idea gain some support by the presence of 3.3 Ma gravels just a few hundred feet above river level near Lake Mead (Lucchitta, 1972).

Recently, Fenton *et al.* (2001) used $^{3}He_{c}$ dating techniques to determine new dates for basalt flows near the Toroweap and Hurricane Faults, finding previously published data overestimated the ages of lavas in western Grand Canyon. They calculated displacements rates during the Quaternary for the Toroweap and Hurricane Faults to be 70-180 m/My and 70-170 m/My respectively. Pederson *et al.* (2002) later used U-series and $^{40}Ar/^{39}Ar$ dating to find displacement on the Toroweap Fault has continued over the past 500 ka at a rate of 94 m/My. Thus, both the Toroweap and Hurricane Faults continue to be active today (Huntoon, 1977), showing further lifting of the Kaibab Plateau and eastern Grand Canyon and concurrent downcutting of the river into bedrock. The formation, they speculate, of the inner Granite Gorge in eastern Grand Canyon results from continuous Quaternary uplift at the Toroweap and Hurricane Faults (Pederson *et al.*,

2002). It is surprising to realize, however, the present-day Colorado River in Grand Canyon (as well as Cataract Canyon) flows over a mantle of alluvial fill.

Recent analysis by Hanks and Webb (2006) shows a number of large convexities along the course of the Colorado River. They attribute these convexities to mounds of coarse-grained alluvium, speculating a sharp rise in debris flow activity during the Holocene buried long reaches of river. Their working hypothesis assumes the river was last cutting down into fresh bedrock in Grand and Cataract Canyons during the late Pleistocene when wetter, cooler conditions over the Colorado Plateau led to greater peak discharge in the main stem and more stable hillslopes. The shift to hotter, drier conditions in the Holocene led to smaller main-stem floods and less flow in the Colorado River. Coupled with an increase in debris flow activity due to more intense summer thunderstorms and less local vegetation to stabilize colluvial hillslopes, this climate shift on the Colorado Plateau led to long-term deposition and buildup of alluvium on the canyon floor.

Hanks and Webb (2006) estimate alluvium thickness up to 45 m in Grand Canyon. Unpublished geophysical data (R.H. Webb, USGS, personal communication, 2005) show the depth to bedrock at Spanish Bottom, the uppermost section of Cataract, to be about 80 m. Consistent with findings of earlier researchers (Howard and Dolan, 1981; Webb *et al.*, 1989), analysis demonstrates that streampower used to do work in Grand Canyon and Cataract Canyon today goes primarily into removing coarse-grained debris flow deposits, not into carving into fresh bedrock. Central to their analysis, Hanks and Webb (2006) spoke of convexities within the river corridor caused by mounds of coarse-

grained alluvium deposited by repeated debris flows. These convexities range in scale from long-wavelength features several tens of kilometers in extent down to the scale of individual rapids 100 m long. The formation, mechanics, and evolution of these short-wavelength features (*i.e.*, rapids) are the focus of this dissertation.

1.3 Fluvial Geomorphology

The character of the Colorado River through Grand Canyon consists of a series of long, quiet pools separated by turbulent rapids. The average slope of the Colorado in Grand Canyon is roughly 0.0015 (Hanks and Webb, 2006). The slope of rapids, however, often exceeds 0.01, and most of the drop of the river occurs in the relatively short distance taken up by rapids (Leopold, 1969). Using 1923 survey data collected by the USGS (USGS, 1924), Leopold (1969) calculated that 50% of the total drop in elevation of the Colorado River in Grand Canyon occurs in only 9% of the distance. Leopold (1969) termed this character the "pool-and-rapid" morphology. The importance of this morphology to the storage and deposition of sand and resultant impact on aquatic ecology is well documented (Schmidt, 1990; Schmidt and Graf, 1990; Parnell *et al.*, 1999). In the bedrock canyons of the Colorado River Basin, debris flows create and maintain this pool-and-rapid morphology.

The majority of work done by the river in Grand Canyon goes into removing material deposited by tributaries (Hanks and Webb, 2006). Mostly ephemeral, these Grand Canyon tributaries range in size from less than 1.0 km^2 to over 500 km^2 in drainage area and dump clays, sands, and cobbles into the river through flash flooding

(Webb *et al.*, 2000). When rainfall is intense, debris flows can initiate in tributaries, carrying large cobbles and boulders to the river. Once in the unconfined and flat river channel, debris flows lose their momentum, dewater, spread, and come to rest on the debris fan (Figure 1.2). If the debris flow is large enough, it can constrict the river, raising the water-surface elevation in the upper pool and creating a steeper, more energetic rapid (Kieffer, 1985). If the debris flow debouches into an otherwise quiet section of river, a new rapid can be created (Melis *et al.*, 1994).

Debris flow initiation in Grand Canyon results from one or more of three triggering mechanisms: 1) the failure of weathered bedrock, 2) the "firehose effect" of runoff falling onto unconsolidated colluvial wedges, and 3) direct failure of colluvial wedges (Melis *et al.*, 1994; Giffiths *et al.*, 1997). Most debris flows occur in conjunction with strong convective thunderstorms striking the region in middle to late summer. Less frequent, but sometimes larger, are debris flows resulting from wet, winter storms producing prolonged, heavy precipitation (Griffiths *et al.*, 1997). In either case, debris flows are associated with intense rainfall, usually on the order of 40 mm/hr or more, peaking near the end of the storm (Melis *et al.*, 1994). It appears that clay, commonly found in Hermit and Bright Angel Shales as well as Muav Limestone, is a critical ingredient for debris-flow rheology on the Colorado Plateau (Webb *et al*., in press). Grand Canyon debris flows contain between 1-8% clay-sized particles by weight, that, when saturated with water, act to lubricate the flow and increase buoyancy in the interstitial spaces of the slurry matrix (Griffiths *et al.*, 1996). These clays help support

Figure 1.2: Debris-flow fan emanating from Monument Creek at Grand Canyon, river-mile 93.7. Multiple debris-flow events have built the fan over time, forming Granite Fall Rapid (photograph by the Bureau of Reclamation, 1967).

larger boulders and promote slurry motion. In surveys of the largest boulders on 56 Grand Canyon debris fans, we found 86% contained at least one boulder larger than 2.0 meters (intermediate axis) and the largest boulder on 22% of fans exceeded 4.0 meters.

Where active tributaries repeatedly dump large boulders in the river, alluvial debris fans build over time, acting to constrict the river thus forming the small-wavelength convexities identified by Hanks and Webb (2006). Each new debris flow added to an existing fan has the potential to raise the water-surface elevation in the pool above the rapid as well as increase the navigational severity of the rapid. In December 1966, a large debris flow in Crystal Creek entered the Colorado at river mile 98.8 (Cooley *et al.*, 1977), creating one of the most feared rapids in Grand Canyon and pooling a long, quiet section of river upstream, locally known as "Lake Crystal." What had been a relatively minor and manageable rapid before the debris flow became a major impediment to navigation for 17 years. In 1983, a 2,700 m^3/s snowmelt flood on the Colorado River flowed past Glen Canyon Dam and into Grand Canyon. In addition to removing vegetation near the river and rebuilding beaches, the flood reworked many freshly aggraded debris fans, including the Crystal Creek debris fan (Kieffer, 1985; Webb *et al.*, 1989). While debris flows tend to raise the water-surface elevation of the upper pool and increase the slope of the rapid, main-stem floods do the opposite. By removing material, floods lower the elevation at the head of rapids and lessen the severity of slope through the drop.

The primary method of erosion from debris fans is physical removal of particles by flowing water. Fluid drag, the pushing force of flowing water, is proportional to the

square of the free-stream velocity (Fox and McDonald, 1985). Drag enables the river to move large rocks and is a function of the river discharge, channel width, and water slope. Where debris fans collect and water is forced around or over the fan complex, rapids adjust themselves to achieve a balance between discharge, width, and slope. Smaller clasts are removed from the fan, while the largest particles are immobile or shift until they reach stable positions. This process is termed reworking, and a fresh debris fan will continue to experience reworking as it experiences higher discharges (Webb *et al.*, 1999a).

For the largest boulders which the river cannot physically push, slow erosion from the rock surface occurs through chemical weathering and corrasion (Wohl, 1998; Sklar and Dietrich, 2004). Corrasion is the slow ablation of material from the rock surface from impinging water containing sand, gravel, or cobbles. In addition to mechanical corrasion, chemical erosion of the rock by the river occurs. Under the influence of impact from flowing sediment-laden water as well as water chemistry, large boulders are ablated until they are small enough to be removed by floods. Higher seasonal discharges, dissolved salts in the river, and high sediment load in the river all tend to enhance corrosion and chemical erosion. Though the rate of this denudation is not well understood, the removal of large clasts through superficial processes occurs over the time span of several hundreds of years. Examples of repeat photography show large boulders with no noticeable change after 100 years in the middle of Grand Canyon rapids (Webb, 1996). Due to the short time scales investigated, corrasion and chemical erosion are assumed to be zero in this study.

The balance between debris flows and main-stem floods in controlling the water-surface profile through Grand Canyon has only recently been fully recognized. Leopold (1969) looked at the longitudinal profile of the Colorado in Grand Canyon and tied the location and formation of rapids to a process he termed "quasi-equilibrium." Under quasi-equilibrium, rapids are balanced and spaced relative to each other to minimize overall fluvial energy. Though Leopold thought tributaries did create some rapids, he felt most rapids resulted from the quasi-equilibrium principle. In analyzing rapids throughout the basin, Graf (1979) mistakenly underestimated the role of debris flows in forming most rapids or rapid complexes with in the Colorado River system. For example, Graf stated that only 25% of rapids in Cataract Canyon were associated with tributaries and debris flows. We now know all rapids in Cataract Canyon were caused by debris flows (Webb *et al*., 2004). Dolan *et al*. (1978) were the first to correlate tributaries and rapids. Later, Howard and Dolan (1981) used aerial photography to tie alluvium production from tributaries to the formation of most rapids. They postulated that in the current post-dam flood regime, the pool-and-rapid morphology of the river is being continually enhanced with steeper, narrower rapids as well as the formation of new rapids. Studying the reworking of Crystal Rapid during the 1983 flood, Kieffer (1985) recognized the importance of debris flows to rapid formation as well as the interaction of debris flows and main-stem floods. She calculated the recurrence interval of both debris flows and large reworking floods was on the order of 100 – 10,000 years. She also calculated a large flood of 11,320 m^3/s is required to completely rework the larger debris fans along the river. Based on a wealth of direct field observations over the past two decades, we

now recognize debris flows from tributaries occur more frequently; on average, five debris flows occur in Grand Canyon each year (Griffiths *et al.*, 2004). In turn, the river reworks fresh deposits more efficiently than Kieffer postulated (Webb *et al.*, 1999a; Pizzuto *et al.*, 1999). Effective reworking has been observed at many locations in Grand Canyon with modest floods under 3,000 m^3/s (Webb *et al.*, 1989; Melis *et al.*, 1994; Webb *et al.*, 2000; Webb *et al.*, 2002).

Debris flows and river reworking are the primary force behind the formation of rapids and river morphology within Grand Canyon (Webb, 1996). Ultimately, the elevation of the water surface is governed by the aggradation of debris on the fan from active debris flows balanced against the erosion potential of reworking floods. In the short term, large floods perform most work on debris fans by removing smaller particles, widening debris-fan constrictions, and lowering the water-surface elevations in the upper pool. But even in the absence of large floods, the river removes material through corrasion and chemical erosion. Eventually, in the absence of new material from tributaries, or in a climatic or anthropologic shift toward a larger main-stem flood regime, the river would erode back down to bedrock.

In many ways, Cataract Canyon is a smaller, more-extreme version of Grand Canyon, with geomorphic and fluvial similarities. Owing to the relatively short fetch of its tributaries, the spacing and size of its rapids, the relative height of the rim above the river, and the bounding lithology, Cataract Canyon is most similar to the "Roaring Twenties" section of Grand Canyon, located 32-48 km (20-30 miles) below Lee's Ferry. Cataract Canyon contains over 25 rapids in a distance of roughly 25 km, thus justifying

Powell's (1895) name. While overall debris-flow activity in Cataract Canyon is less than in many sections of Grand Canyon (Webb *et al.*, in press), copious quantities of coarse-grained alluvium underlie the entire reach of river (Hanks and Webb, 2006). At its thickest, the depth of the alluvium fill beneath Cataract is 80 m (R.H. Webb, USGS, personal communication, 2005), and the steep slope of the river within the Cataract Canyon is, in large part, due to this coarse-grained alluvium (Webb *et al.*, 2004). The rapids in Cataract are as navigationally difficulty as those in Grand Canyon, but they tend to be more closely spaced with shorter interspaced pools The differences between Grand Canyon and Cataract Canyon, however, are important, particularly for scientific juxtaposition of the two.

Most salient of these differences is flow regulation. Flaming Gorge Dam on the Green River and a number of smaller reservoirs among the headwaters of the Colorado River control some of the flow to Cataract Canyon (Grams and Schmidt, 2002), yet large, predominantly snowmelt, discharges still occur; floods over 1,400 m^3/s are common. Cataract Canyon also has a heavy sediment load with the large seasonal swings in water temperature characteristic of the pre-development river. Because the Colorado through Cataract Canyon is similar to the river it was 100 years ago, directly comparing Cataract Canyon's fluvial geomorphology with the geomorphology of Grand Canyon offers insight into the potential influence of Glen Canyon Dam. A part of this dissertation, therefore, includes analysis and data of flow through selected rapids in Cataract Canyon.

1.4 Present Study

This dissertation represents a collection of research projects studying rapids, coarse-grained sediment, and reworking floods on the Colorado River. The work varies in focus between multiple time and spatial scales, yet is centered on the formation and denudation of rapids as a hydraulic feature and the concomitant relation between big rocks, rapids, and floods. More importantly, this document does not represent the sole contribution of its one author. The research contained in this study represents the efforts of many collaborative researchers in addition to the author; the collaborators on each section are named below.

Chapter Two looks at the geomorphic changes of the longitudinal water-surface profile through Grand Canyon over the course of the 20th century. By comparing the water-surface profile as measured in 1923 against the water-surface profile measured in 2000, the relative change in elevation of pools above 81 rapids was measured and analyzed. Chapter Two was published by the author along with coauthors Peter G. Griffiths and Robert H. Webb (Magirl *et al.*, 2005)

Chapter Three discusses the development and application of a one-dimensional step-backwater model to the entire river corridor through Grand Canyon, only the second of its kind developed for Grand Canyon. This model represents the collaboration between the author and Mike Breedlove from the Grand Canyon Monitoring and Research Center (GCMRC). A sister component of the step-backwater model is a GIS-based virtual shoreline tool that creates water inundation maps for any section of Grand Canyon at any discharge up to 5,600 m^3/s. The virtual shoreline tool was developed by Breedlove. This

model set (the step-backwater and GIS components) is currently being used within the Grand Canyon research community.

Chapter Four is a short study discussing the attempt to measure water velocity in rapids in Grand Canyon using an Acoustic Doppler Velocimeter (ADV). Velocity was measured in a small riffle in Glen Canyon. The ADV, however, was unable to measure velocities over 3.0 m/s, reducing the usefulness of this instrument in rapids. Bathymetry was measured using a Lowrance fathometer. This work was published by Magirl ***et al.*** (2006); Peter Griffiths and Robert Webb were coauthors.

Finally, Chapter Five builds on Chapter Four. To quantify the fluid mechanics governing flow within rapids, multiple flow-measurement techniques were applied to a number of rapids in Grand Canyon and Cataract Canyon. In addition to the ADV, an Acoustic Doppler Current Profiler (ADCP) and a rugged aqueous pitot-static tube were deployed. The ADCP and pitot-static tube performed reliably and show promise for future research. The instruments enabled construction of several maps including: three-dimensional flow velocity fields, bathymetry in rapids, topology of the water-surface through rapids, and spatial distribution of turbulence with rapids. The study in Chapter Five will be collected into a manuscript for submittal to *Water Resources Research*. The manuscripts coauthors include Jeffrey Gartner, Robert Webb, Steve Young, Terry Kenney, Steve Cunningham, and Graeme Smart.

2. CHANGES IN THE WATER-SURFACE PROFILE OF THE COLORADO RIVER IN GRAND CANYON, ARIZONA, BETWEEN 1923 AND 2000

Flowing through northwestern Arizona, the Colorado River in Grand Canyon (Figure 2.1) has long, flat sections of quiet water separated by steep, turbulent rapids. Periodic debris flows originating in tributaries build debris fans at tributary mouths and deposit large boulders into the river (Cooley *et al*., 1977; Webb *et al*., 1989; Melis *et al*., 1994). The Colorado River, confined by bedrock walls, pools upstream of the accumulated debris fans before descending as rapids over the fans, commonly plunging into downstream pools formed behind debris fans or boulder bars even further downstream. When viewed in profile, the water surface is stepped, termed by Leopold (1969) as the pool-and-rapid morphology. In this study, the term rapid is used to describe any short reach of river (typically 100 to 400 m in length) in which the water is choked to critical flow, descends down a relatively steep slope, and produces breaking waves which span the width of the channel.

The longitudinal configuration of pools and rapids results from the dynamic interplay between the addition of coarse-grained alluvium from tributaries and the subsequent removal, or reworking, of that material by main-stem Colorado River floods (Kieffer, 1985; Webb *et al*., 1999a). Reworking consists of both entrainment of smaller particles and the jostling of the largest particles until they settle into a stable matrix. Most reworking occurs during the rising stage of a flood, and by reducing the stream power of

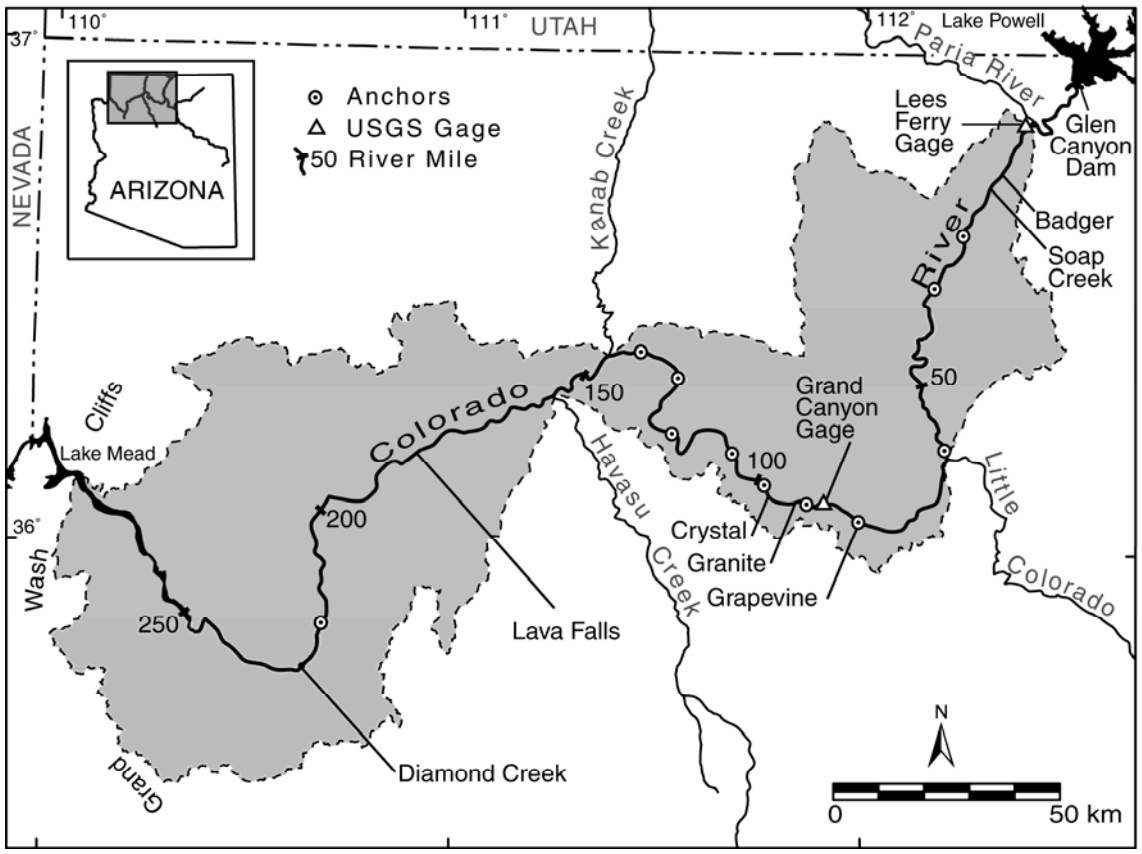

Figure 2.1: Map of Colorado River in Grand Canyon, Arizona showing the locations of 11 LIDAR anchors and prominent rapids. See Table 2.1.

a rapid, reworking can lower the water-surface elevation at the head of a rapid several centimeters in a matter of hours (Webb et al., 1999a). Repeat photography shows that the largest particles in a debris-fan matrix reworked by a flood of given discharge remain stable for at least a century unless subjected to a larger flood (Webb, 1996; Webb et al., 1999c). For stable debris fans, corrasion continues to remove material through ablation at the surface of individual boulders. Though not measured on the Colorado River, the rate of corrasion is probably several orders of magnitude less than the rate of change due to reworking.

The rates of both reworking and corrasion are strong functions of flood regime. Before Glen Canyon Dam, the mean annual peak discharge of the Colorado River was 2645 m^3/s (1921-1961; Schmidt and Graf, 1990). The largest flood during the period of record at the USGS streamflow gaging station at Lee's Ferry was 4800 m^3/s in 1921; a larger flood in 1884 was estimated to be 5900 m^3/s (O'Connor *et al*., 1994; Toppings *et al*., 2003). After closure of the dam in 1963, peak flows were reduced (Figure 2.2) with a mean annual peak discharge (1963-1996) of 920 m^3/s (Webb *et al*., 1999b). Howard and Dolan (1981) proposed that the reduction in flood peaks (and erosive potential) following the closure of Glen Canyon Dam would lead to accumulation of debris at tributary junctions, therefore increasing the severity and quantity of rapids on the Colorado River in Grand Canyon. The current study compares the modern water-surface profile of the Colorado River, surveyed in March 2000, with a 1923 USGS survey of the river corridor, measuring general trends of aggradation in the river corridor. The study also produces a new set of geomorphic statistics associated with this 2000 profile.

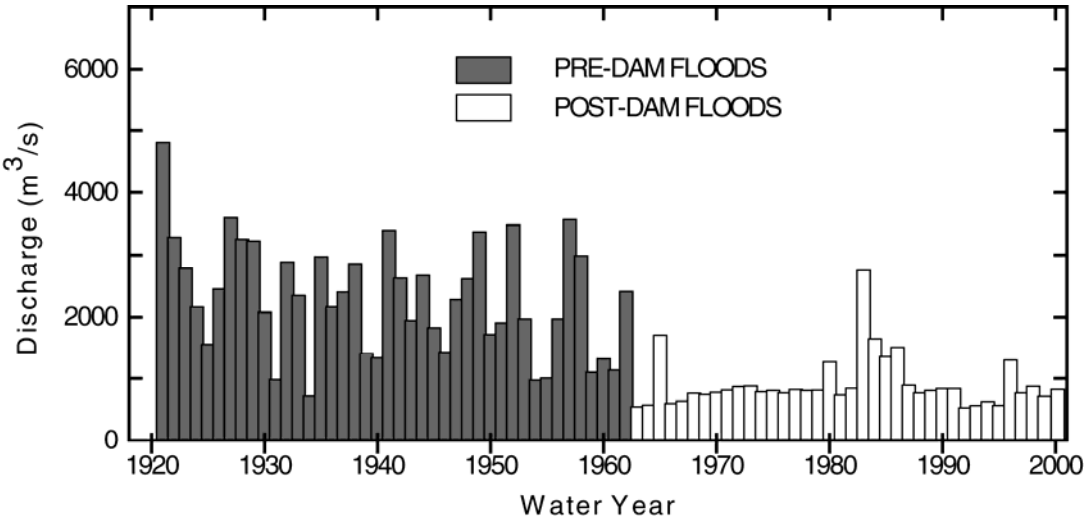

Figure 2.2: Annual peak flood series for the Colorado River at the USGS streamflow gage at Lee's Ferry, Arizona.

Though most data in this report are presented in metric units, position along the river corridor is reported in river miles relative to the gaging station on the Colorado River at Lee's Ferry (River Mile 0; RM 0). This convention, established by the USGS (1924), is the standard nomenclature for describing locations along the river. Indeed, many official place names are derived from river-mile position (*e.g.*, 60-Mile Canyon, 75-Mile Creek, 205-Mile Rapid). River mile locations originally published by the USGS (1924) and modified by Stevens (1983) were updated by the Grand Canyon Monitoring and Research Center (GCMRC) in September 2002 to fit a new river centerline. All references to river mile in this study are based on the GCMRC centerline.

2.1 Water-Surface Profile Surveys

2.1.1 1923 USGS Expedition

As part of a project to map the major rivers in the Colorado River Basin in search of potential dam sites, Claude H. Birdseye led a U.S. Geological Survey team though Grand Canyon. Starting at Lee's Ferry, Arizona on August 1, 1923, the survey party spent over two months mapping more than 400 km of the river corridor using theodolites and stadia rods (USGS, 1924). The total drop was more than 600 m. In addition to publishing topographic maps of the river and its tributaries, the USGS produced a water-surface profile map showing the location and elevation of pools and rapids along the river. Before 2000, this was the only such survey of the entire river corridor, although short segments have been surveyed in recent years (*e.g.*, Kieffer, 1988; Schmidt and Graf, 1990; Webb *et al*., 1999a). The published water-surface profile is constructed of

piecewise linear segments linking individually measured survey points. In the reach from Lee's Ferry to Diamond Creek, a distance of 364 km, 490 individual survey points were collected and published. The profile characterizes each long pool and the head of each significant rapid with a fall greater than 0.5 m.

The discharge during the Birdseye expedition fluctuated between 425 and 850 m^3/s except for a brief high flow of 3300 m^3/s on September 18. The final water-surface profile on published maps was normalized to 283 m^3/s using stage-discharge relations from the two newly established gaging stations in Grand Canyon (at Lee's Ferry and Grand Canyon). The survey team carried the survey lines continuously with fore and back sites (C.H. Birdseye, unpublished expedition diaries, National Archives, 1923). In addition to the benchmark at Lee's Ferry, the survey was tied into established benchmarks at Hance Trail (RM 77.2), Pipe Springs Creek (RM 89.4), Havasu Creek (RM 157.2), Diamond Creek (226.0), and Last Chance Rapid (RM 252.0). While vertical closure error at the end of the 405 km survey was approximately 1.4 m and subsequently corrected, specific estimates of error in the survey were not published and detailed survey notes have not been found. It is probable, however, that because Birdseye was the chief topographic engineer for the U.S. Geological Survey (Wilson, 1941), the survey crew followed standard USGS operating procedures detailed later by Birdseye (1928). Survey elevations were based on the North American Datum, later to become NGVD29.

2.1.2 2000 LIDAR Survey

In March of 2000, GCMRC commissioned a LIght Detection And Ranging (LIDAR) aerial overflight of Grand Canyon to collect high-resolution topographic data from the Colorado River corridor within Grand Canyon. An Altimeter Laser Mapping System (ALMS) LIDAR was flown at an altitude of 3048 m (Davis *et al*., 2002a). The ALMS LIDAR is a bi-directional, oscillating mirror system that operates at 1.064 μm wavelength. The average spot spacing was 3.75 m and the average spot diameter was 1.0 m. All elevation data were processed and delivered as orthometric heights (NVGD29, Geoid99) in Arizona state-plane coordinates (Davis *et al*., 2002b). Absolute vertical accuracy was found to be about 0.5 m (Davis *et al*., 2002b). The discharge released from Glen Canyon Dam was held constant at 227 m^3/s during all mapping flights.

Airborne laser-scanning systems work by firing a laser at the ground and measuring the return time of the beam reflected off the target surface. By comparing the return time of the laser beam and the relative global position of the aircraft, the location of the point of reflection in space is calculated (Wehr and Lohr, 1999). While some systems were designed specifically for the purpose of mapping aqueous and subaqueous surfaces (Irish and Lillycrop, 1999), the ALMS LIDAR flown over Grand Canyon in March 2000 was tuned to measure terrestrial relief. Therefore, all returns from the water surface of the river were removed and discarded by the LIDAR contractor in the final processing of the data. In order to produce a water-surface profile of the river, we salvaged and reanalyzed the water-surface returns. In rapids, LIDAR returns were plentiful and clustered near the centerline and largest waves. In contrast, there were fewer

returns in calm water, and these returns were generally located near river's edge. The broken surface and entrained air bubbles in rapids may have improved LIDAR reflectance. In contrast, calm water may tend to absorb or to reflect LIDAR energy from a range of depths, reducing the number of effective returns and increasing noise.

On average, we obtained 16 water-surface returns for every 10 m of river distance. In some reaches, however, water-surface returns were sparse with two or fewer measurements per 10 m. For unknown reasons, the paucity of water-surface data was particularly acute in western Grand Canyon, which made it difficult to find the precise location of the water surface. Therefore, in addition to analyzing water-surface returns, terrestrial elevation measurements within 9 m of the river shoreline were also plotted, producing an envelope that outlined the upper extent of the water surface. The density of shoreline data was typically around 15 counts per 10 m of river and never fell below 5 counts per 10 m. Where water-surface returns were sparse along the river corridor, shoreline data were used to augment the detection of the water surface.

To produce a water-surface elevation profile, each LIDAR point was first projected horizontally onto the river centerline to calculate its longitudinal position in river miles. Once projected onto the centerline, all river returns were plotted in profile with elevation values on the ordinate and river mile values on the abscissa. Despite noise, the LIDAR water-surface returns showed a discernable interface or pattern when plotted. This pattern was interpreted as the water surface. The perceived water surface was not ubiquitous; instead, the surface was only visible at certain points in pools and at the heads of rapids. As such, the resulting profile of the river surface is piecewise linear, not

continuous, from Lee's Ferry to below Diamond Creek. In all, 1221 profile points were generated in the 364 km between Lee's Ferry and Diamond Creek.

Using ground survey data from long-term monitoring sites, Davis *et al*. (2002a) determined that the root-mean-square error of the interpreted water-surface profile generated from LIDAR for this study ranged from 0.24 – 0.44 m relative to NGVD29 at four locations of tranquil water in upper Grand Canyon. We also evaluated the relative vertical precision of data points within the 2000 water-surface profile by comparing them to data collected during two detailed field surveys: one through Crystal Rapid (RM 98.8) and another through Dubendorff Rapid (RM 132.2) in May 2002. Both surveys evaluated more than 2.0 km of river that had not been altered between 2000 and 2002. After projection on the river centerlines, the data sets were referenced to each other by assuming that the pool elevation at the upper end of each survey was unchanged between 2000 and 2002 (Figure 2.3). Though the field survey shows some details of the water-surface profile not evident in the LIDAR water surface, the overall profiles are well aligned, indicating that the water-surface profile produced from the LIDAR data is accurate at the scale of rapids and pools. Root-mean-square error between the LIDAR profile and the field-survey data was 0.26 m at Crystal and 0.33 m at Dubendorff.

Using these field study results, combined with the accuracy measurements of Davis *et al*. (2002a) and the stated accuracy of the LIDAR data, we estimate the absolute accuracy of a given water-surface value to be within ±0.5 m of the true value relative to NGVD29. In other words, the actual elevation at a given location on the LIDAR water-

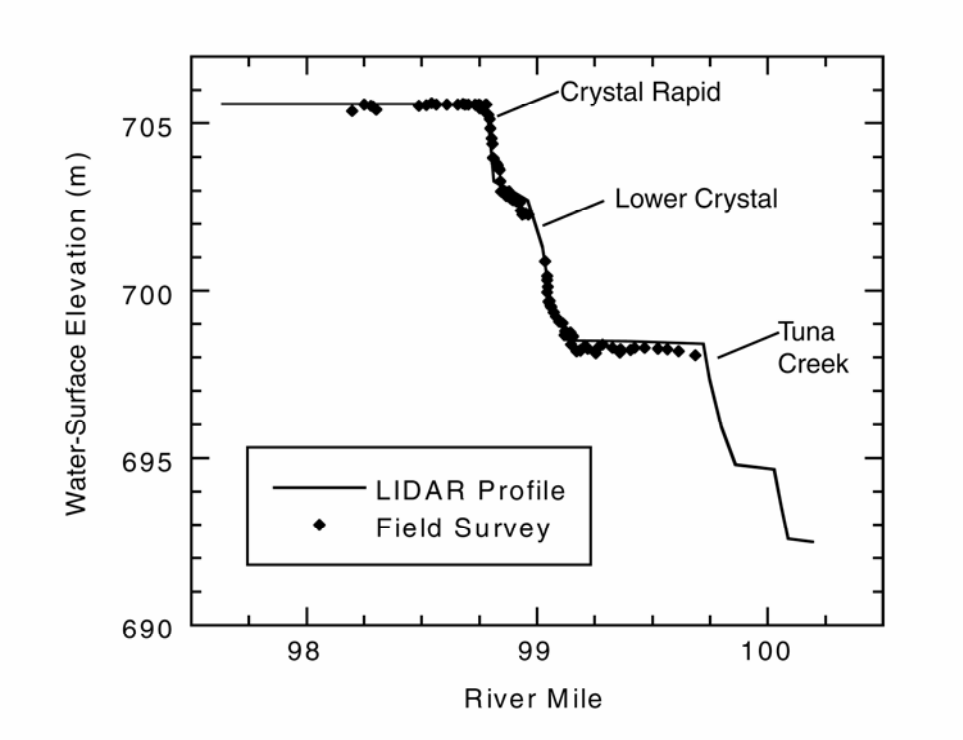

Figure 2.3: Comparison of 2002 survey data at Crystal Rapid with the 2000 water-surface profile generated from LIDAR data.

surface profile is likely within a half meter of the stated value referenced to the established vertical datum.

2.2 Comparison of 1923 and 2000 Profiles

The two elevation data sets are not directly comparable in raw form because they were generated on unique centerlines with different vertical reference data. The subjective choice of where to place the centerline differs slightly between the 1923 and 2000 surveys. To correct the longitudinal mismatch, the river miles of the 1923 survey were aligned to the LIDAR data by comparing the detailed river corridor maps produced by the two surveys. Adjustments were then made in the 1923 river miles to match the new centerline; the longitudinal adjustments ranged from –0.05 km to +1.22 km. The difference in vertical datum used for each survey resulted in discrepancies in absolute elevation. While this disparity in reference frame is potentially the largest source of error, it is also a disparity that can be eliminated by tying the surveys together at specific points along the river profile using essentially the same technique we used to compare the LIDAR data to our detailed survey data at Crystal and Dubendorff Rapids.

Both the 1923 and 2000 longitudinal profiles are tied to different external frames of reference, including a unique vertical datum for each survey. While one technique for comparison would involve converting the elevations to a common vertical datum (*e.g.*, from NGVD29 to NAVD88), such a conversion would not eliminate systematic error, or bias, present in each survey or error that arises from the comparison. Ideally, a better comparison would be achieved by linking together the surveys in a local vertical

reference frame using local benchmarks common to both surveys. The benchmarks used by Birdseye in 1923, however, have not been resurveyed and rectified into a modern coordinate system and, as such, are not available for integration. Instead, different local benchmarks were used to link the two surveys together.

Large rapids are prominent geomorphic features in the water-surface profile of the Colorado River in Grand Canyon. In the absence of new debris flows or large reworking floods, the hydraulics of rapids and the boulders that form them can be stable for a century (Webb, 1996; Webb *et al*., 1999a). At such locations, matched photographs suggest that the change in elevation of the water surface at the head of a rapid subjected only to corrasion is negligibly small, probably much less than 10 cm/century. Making the assumption that the change in water-surface elevation at the head of a stable rapid is zero between 1923 and 2000, we use these locations as "anchor points," or local benchmarks, to tie the two surveys together into a single vertical reference frame.

We identified anchor points using repeat photography and historical accounts of channel change (Webb *et al*., 1999a; Webb *et al*., 2002). Historic photographs used to identify anchor points came primarily from the Stanton collection of 1890 (Webb, 1996); these photographs allowed us to identify rapids with no new debris flows from 1890 to the present. Of 160 prominent tributaries in Grand Canyon photographed in 1890, 37 had no obvious debris flows that reached the river (Griffiths *et al*., 2004). Distinct and prominent rapid heads were readily discernible in both the 1923 and 2000 profiles at 11 of the 37 stable rapids. These 11 locations, unevenly spaced along the river corridor, were used as anchor points (Table 2.1). At each anchor location, the water-surface elevation of

Table 2.1: List of 11 Anchor Points (Stable Rapids) and Associated Tributaries Used to Register the 2000 LIDAR and 1923 Survey Data.

Rapid Name	River mile	Side Tributary Enters River	Tributary Drainage Area (km^2)
North Canyon	20.7	Right	407.27
29-Mile	29.4	Left	186.55
60-Mile	60.1	Left/Right	9.69
Grapevine	82.1	Left	30.82
Horn Creek	90.8	Left	4.28
Tuna Creek	99.7	Right	59.62
Ruby	105.2	Left/Right	7.47
Blacktail	120.7	Right	24.15
Dubendorff	132.3	Right	12.27
Fishtail	139.7	Right	19.63
217-Mile	217.7	Left	23.98

the 1923 survey was adjusted vertically to exactly match the elevation of the 2000 profile. Vertical adjustments of the anchors ranged from –2.02 m to +0.20 m. Intermediate points in the Birdseye survey between anchors were then adjusted vertically using linear interpolation in accordance with the ratio of the distance to the nearest upstream and downstream anchors. By linking the two surveys together with anchor rapids, both surveys can be directly compared without reference to an absolute global datum. Relative error, or precision of the survey data, however, remains an issue.

Error in change detection at specific rapids between 1923 and 2000 originates from several sources. First, errors occurred in the measurement of the water-surface elevation in both the 1923 and 2000 profiles intermediate to the anchor points. The relative precision of the LIDAR profile is probably not greatly different from the error of ±0.3 m measured when comparing the LIDAR profile and 2002 survey data collected at Crystal and Dubendorff Rapids. The relative precision of the 1923 profile is probably below ±0.5 m over 125 km, the greatest distance between adjacent anchors used in the current study.

Another source of error is the difference in discharge reported for each survey (283 m^3/s verses 227 m^3/s). Based on results from a step-backwater model developed by Randle and Pemberton (1987), the difference in stage of each discharge throughout the river reach is probably less than ±0.25 m. The greatest potential source of error lies in the process of tying to the two surveys together using the anchor points. If a given anchor location, which is assumed to remain unchanged between 1923 and 2000, does change, a systematic error, or bias, is introduced into any nearby change measurements. To

estimate the magnitude of potential error with the process of comparing the two profiles, each anchor was individually removed as an anchor and allow to float, adjusting to a new elevation determined by the influence of the nearest adjacent anchors. We have strong photographic evidence that these 11 anchors are unchanged and should report a difference in elevation of zero. The deviation from zero for the floating anchors gives an estimate of the overall error or accuracy in the process. The average measured change of the 11 floating anchors was +0.04 m with a standard deviation of ±0.68 m. These values suggest that while the anchoring process is relatively accurate, it is not particularly precise. Thus, we report, with a 95% confidence (*i.e.*, two standard deviations), that the error in measuring change of elevation for any individual rapid is ±1.4 m. While an individual measurement contains relatively large error, with multiple measurements, the standard error of the mean can be small.

Once the profiles were aligned using anchor points, an evaluation of changes in the water-surface profile was possible at many rapids. Comparison was easiest where a rapid was distinct and unambiguously related to a tributary junction in both the 1923 and 2000 surveys. Measurements of changes in the water-surface profile were taken only when there was no ambiguity in the identity of the rapid in both profiles. For such rapids, the vertical difference between the head of the rapid in 1923 and 2000 was measured and recorded as the net change in elevation. Some new rapids were evident in the 2000 profile that did not exist in 1923. Because the topographic survey in 1923 at these locations showed only flat water, these newly formed rapids were not included in the analysis.

While less common, reaches were also observed where a rapid measured in 1923 was flat water in 2000. These locations were also excluded from the analysis.

In evaluating the potential change in pool-and-rapid morphology within Grand Canyon between 1923 and 2000, the question of resolution of the two disparate surveys arises. In comparing the relative resolution of the LIDAR profile with the 1923 Birdseye profile, the higher density of profile points generated from the LIDAR data does not necessarily represent higher resolution. Both to facilitate further studies with Geographic Information Systems (GIS) and because it was inexpensive to do so, extra points were generated within long pools and rapids that were in line with other points of the LIDAR profile, providing no unique elevation information. As an exercise to evaluate density of points within the LIDAR survey, we removed extraneous data (*i.e.*, those data in line with adjacent points) from the LIDAR profile producing a survey of 777 points with no decrease in the resolution of features represented. Also, evidence discussed in the section below indicates more rapids exist in the river in 2000 than in 1923. Had Birdseye resurveyed in 2000 using 1923 techniques, more than 490 points would be needed between Lee's Ferry and Diamond Creek to capture the same resolution of detail. Finally, a sensitivity analysis was performed on the LIDAR profile, whereby points representing the smaller rapids were removed until only 490 remained. The sensitivity analysis showed that the geomorphic conclusions drawn below represent real changes in the pool-and-rapid morphology of the river, not a difference in the resolution of the techniques used to generate each water-surface profile.

2.3 Results

2.3.1 Overall Changes in the Water-Surface Profile

The Birdseye and LIDAR raw survey data are available in Appendix A. Determining the number of distinct rapids in Grand Canyon is difficult due to ambiguity in defining the difference between the smallest rapids and fast-moving water. Nonetheless, using the 2000 LIDAR profile, we identified 234 distinct features as rapids. In all, the change from 1923 to 2000 was determined at 91 rapids representing 39% of all rapids between Lee's Ferry and Diamond Creek. This collection includes data representing the zero change at the 11 anchor points. The magnitude of change was determined for 67% of the 99 named rapids (Stevens, 1983) in the reach.

The largest rise in elevation at the head of a rapid occurred at House Rock Rapid (+2.0 m), followed by Badger with a +1.8 m rise, Crystal Rapid with a +1.6 m rise, and Unkar Rapid with a +1.5 m rise (Table 2.2); all other increases were less than +1.4 m. Though generally not as large in magnitude as the increases, some elevation decreases were significant (Table 2.3). The greatest decrease was at 83-Mile Rapid (–1.5 m), while a rapid at river-mile 103.2 changed by –1.4 m. The head at no other rapid decreased more than –1.4 m. Given the 95% confidence limit of ±1.4 m, most estimates of change are less than the resolution of the measurement process. Overall, the mean change in elevation at the heads of all 91 measured rapids (including the anchors) was +0.26 m. Calculating the standard error of the mean for multiple measurements (Taylor, 1997), the average change in the elevation at the heads of rapids in Grand Canyon between 1923 and 2000 is +0.26 ±0.15 m.

Table 2.2: Ten Rapids with the Largest Net Elevation Increase at the Head of the Rapid, 1923 to 2000.

Rapid or Tributary Name	River mile	Net vertical change (m)	(Number of known debris flows[a]) Date of debris flow
House Rock	17.1	2.0	(1) 1966-71
Badger	8.0	1.8	(2) 1897-1909; 1994
Crystal	98.8	1.6	(2) 1966; 1973-86
Unkar	72.9	1.5	(2) 1890-1966; 1998
Doris	138.3	1.4	n.d.
Waltenberg	112.8	1.4	(4) 1890-1923; 1938-42; 1973-84; 2001
205-Mile	205.7	1.2	(2) 1937-56; 1998
Lava Falls	179.7	1.2	(6) 1939; ’54; ’55; ’63; ’66; ‘95
Havasu	157.2	1.2	(0) 1990[b]
209-Mile	209.2	1.1	(2) 1999; 2000

[a] Melis *et al.* (1994); Webb *et al.* (2000); n.d., no data for this site.
[b] Although debris flows have not occurred here, a 1990 flood moved significant gravel into this rapid (Melis *et al.*, 1996).

Table 2.3: Five Tributary Junctures with the Largest Net Elevation Decrease at the Head of the Rapid, 1923 to 2000.

Rapid or Tributary Name	River mile	Net vertical change (m)	(Number of known debris flows) Date of debris flow[a]
83-Mile	84.1	-1.5	n.d.
unnamed	103.2	-1.4	(1) 1890-1990
Zoroaster	85.3	-1.1	(0)
Nautiloid	35.0	-1.0	(1) 1980-1984
23.5-Mile	23.5	-0.8	n.d.

[a] Melis *et al.* (1994); Webb *et al.* (2000); n.d., no data for this site.

The spatial distribution of elevation change at the heads of rapids was analyzed (Figure 2.4). Several divisions of the river corridor into geomorphic reaches have been proposed (Leopold, 1969; Howard and Dolan, 1981; Schmidt and Graf, 1990; Melis, 1997). We applied a Kruskal-Wallis rank sum test (Helsel and Hirsch, 1992) to values of rapid-head elevation change gathered into six geomorphic reaches as defined by Melis (1997). The resulting p-value of 0.43 showed that there is little statistical difference between data grouped spatially (a p-value less than 0.05 is needed to show dependence). Thus, there is no correlation between changes in rapid-head elevation and geographic reach or position along the river.

The temporal distribution of rapid-head elevation change was also measured to test the hypothesis by Howard and Dolan (1981) that prolific coarse-grained alluvium generated in tributaries would overwhelm the regulated Colorado River leading to long-term aggradation at tributary mouths. The change data we analyzed were not detailed enough to allow a definitive evaluation of the temporal signal. We did not the have detail of information to tie the observed aggradation of +0.26 m specifically to closure of Glen Canyon Dam.

In Leopold's (1969) analysis of the pool-and-rapid morphology in Grand Canyon, one figure presents the cumulative drop of the river in 1923 as a function of cumulative distance for the first 241 km below Lee's Ferry. Leopold concluded that 50% of the total drop occurred in only 9% of the length of the river. We used 1923 survey data to recalculate and replicate Leopold's figure. We also produced an updated cumulative distribution curve based on the 2000 LIDAR data but expanded it to include 365 km of

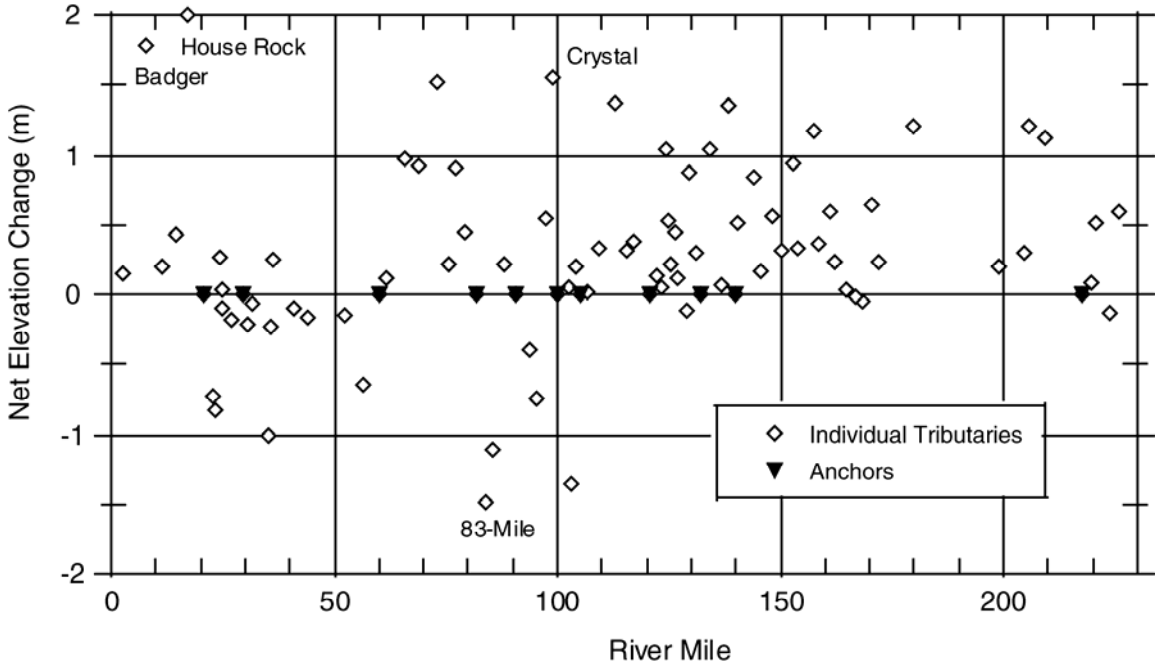

Figure 2.4: Measured net change at 80 rapids plotted as a function of river location. The anchor locations are also shown.

river from Lee's Ferry to below Diamond Creek (Figure 2.5). This extended scope gives a better overall representation of both eastern and western Grand Canyon. In 2000, 66% of the total drop in river occurred in only 9% of the length. When only the first 241 km of river is considered for direct comparison with Leopold (1969), 71% of the total rapid occurs in 9% of the distance, showing that eastern Grand Canyon has a more prominent pool-and-rapid morphology than western Grand Canyon. It is possible that the change illustrated in Figure 2.5 may have been caused by a difference in the resolution of data point density of the two surveys. As described above, a sensitivity analysis was performed on the LIDAR profile whereby the number of points representing the profile was reduced to 490 by removing redundant points and points around the smallest rapids. With this artificially reduced resolution, the altered 2000 profile had a 64% cumulative drop in only 9% of the length—a result still significantly different that the results calculated using 1923 data. Therefore, Figure 2.5 does represent a true and significant geomorphic change in the Colorado River between 1923 and 2000. Evidence of local rapid-head elevation increase (*e.g.*, Crystal Rapid, 18-Mile Wash) also points to a trend of steeper and more numerous rapids.

2.3.2 Specific Changes Documented in Grand Canyon 1923-2000

Comparisons at selected reaches illustrate the processes involved in maintaining the pool-and-rapid profile of the Colorado River. For example, Figure 2.6 juxtaposes the 1923 and 2000 water-surface profiles between Lee's Ferry (RM 0.0) and North Canyon (RM 20.7). The pool-and-rapid morphology is evident in the four large rapids: Badger

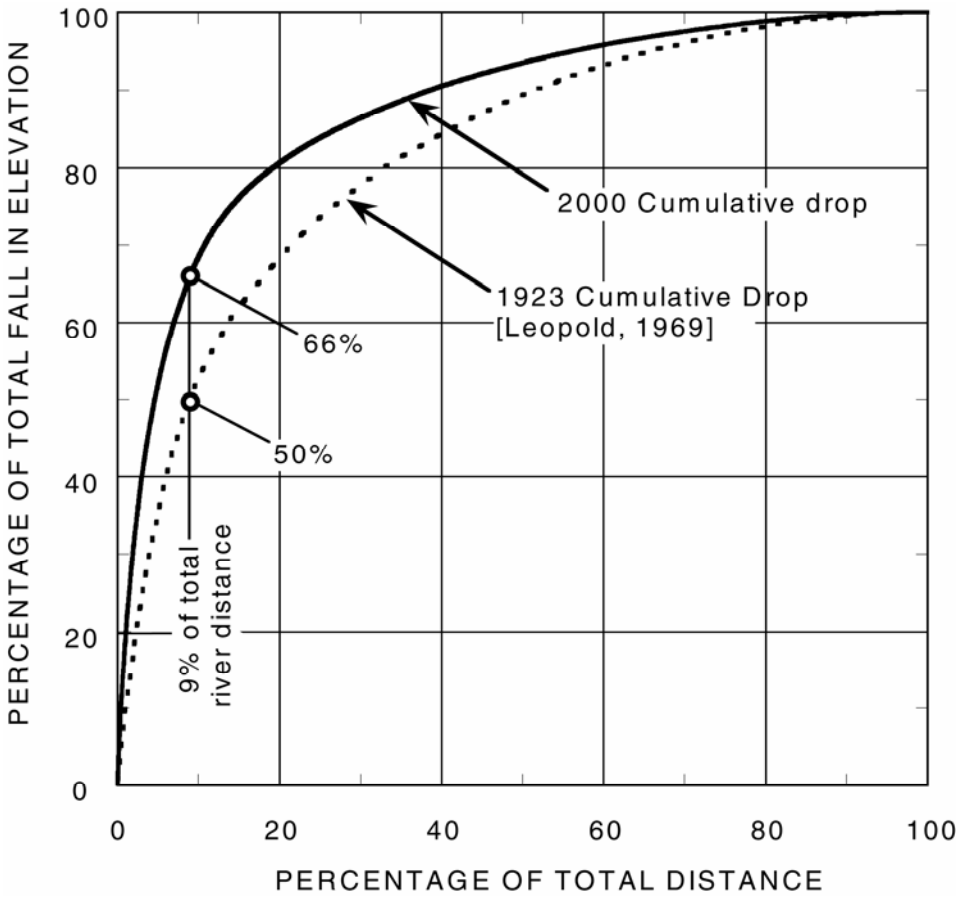

Figure 2.5: Cumulative vertical drop in the first 365 km of the Colorado River in Grand Canyon as a function of the total distance. In 2000, 66 percent of the drop occurs in just 9 percent of the river distance. The curve generated by Leopold (1969) is also included, when 50 percent of the drop occurred in 9 percent of the distance in the first 241 km below Lee's Ferry.

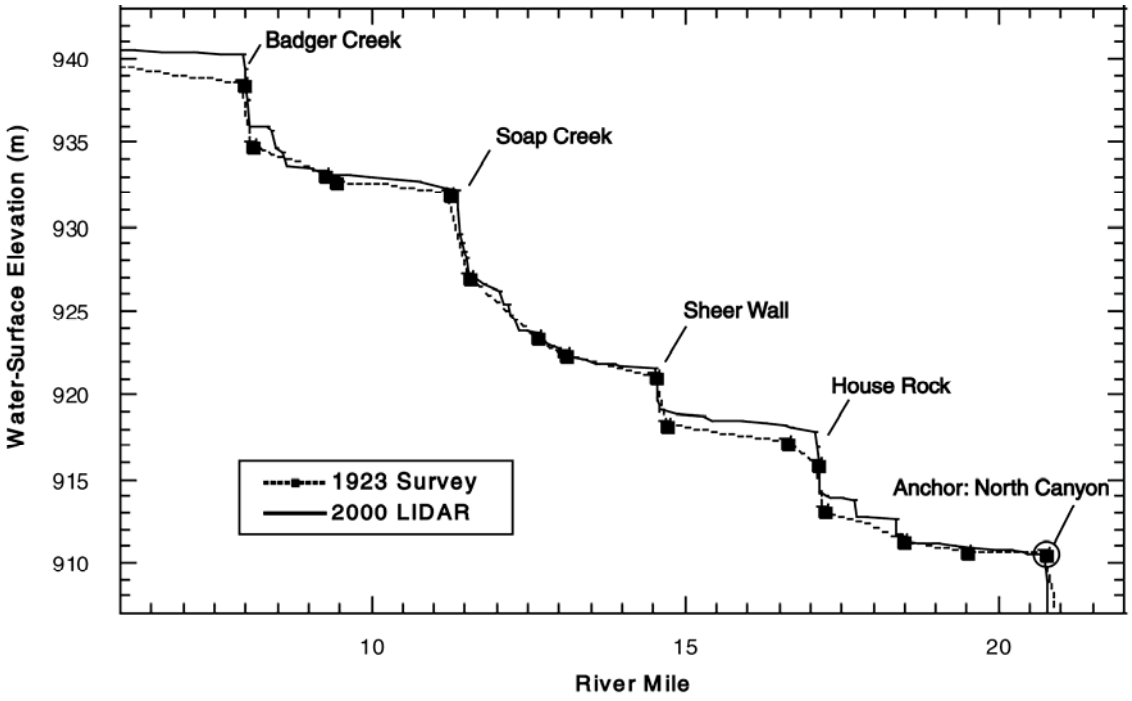

Figure 2.6: Comparison of 1923 and 2000 profiles of upper Marble Canyon. Note the prominent net increase in elevation at Badger Rapid and House Rock Rapid.

Rapid, Soap Creek Rapid, Sheer Wall Rapid and House Rock Rapid. The elevation at the head of Badger Rapid (RM 8.0) increased +1.8 m between 1923 and 2000, one of the largest changes observed (Table 2.2). Though a large debris flow enlarged the debris fan at Badger Creek between 1897 and 1909, the only known post-1923 debris flow came in 1994 from Jackass Canyon on river left. This debris flow, however, was relatively small (Melis *et al*., 1994) and probably does not account for the full elevation increase. One or more unidentified debris flows from either Badger Creek or Jackass Canyon most likely caused the observed aggradation. Downstream, Soap Creek Rapid (RM 11.4) had an increase in rapid-head elevation of only 0.2 m, despite two known debris flows since 1923, one between 1935 and 1941 and a second, smaller event between 1973 and 1984 (Melis *et al*., 1994). In addition, several pre-dam floods reworked the first debris flow, and a 2755 m^3/s flood in 1983 reworked the second, resulting in a relatively small net change. At Sheer Wall Rapid (RM 14.5), at least one debris flow between 1890 and 1990 raised the rapid-head elevation by +0.4 m.

A rise of +2.0 m at the head of House Rock Rapid (RM 17.1) was measured between 1923 and 2000, and this is the largest change we documented in the study. Between 1966 and 1971, one or more debris flows in Ryder Canyon on river right (Webb *et al*., 2000) enlarged the fan, constricted the rapid, and extended the upper pool to the base of Sheer Wall Rapid (Figure 2.7). Between House Rock and North Canyon Rapids, the 1923 survey mapped flat water, an observation confirmed by boatman H. Elwyn Blake who noted, “the river was smooth…for five miles” (H.E. Blake, unpublished diaries, National Archives, 1923). By 2000, however, two distinct rapids appeared in this

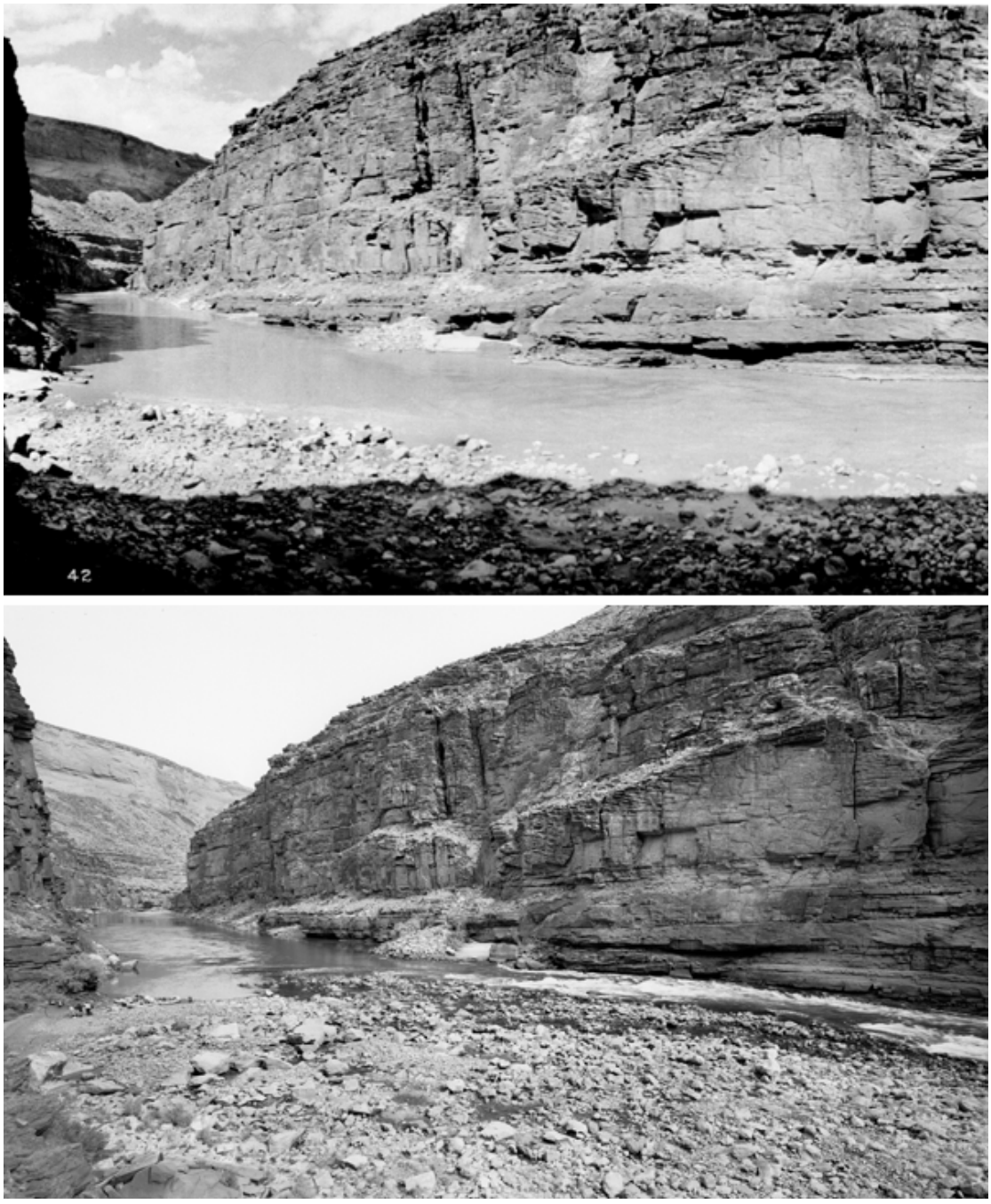

Figure 2.7: Repeat photographs of House Rock Rapid showing the large debris flow that constricted the right side of the river. (top) E.C. LaRue's photograph of the rapid taken during the 1923 survey (E.C. LaRue, number 348, courtesy of the U.S. Geological Survey Photographic Library). (bottom) Matching photograph taken in 1990 (R.H. Webb, stake 1701A).

reach. The first was Redneck Rapid (RM 17.7), created by a rockfall in 1979 (R. Dye, Grand Canyon Expeditions Co., personal communication, 2003), and the second is at 18-Mile Wash where a 1987 debris flow created a new rapid with a fall of 1.1 m (Melis *et al*., 1994). Because these two rapids formed after 1923 and no comparative topography was available in 1923, they were not included in the overall change analysis.

Within upper Granite Gorge, reliable anchors at Horn Creek and Tuna Creek Rapids allow confident analysis of the four major rapids (Figure 2.8). Though Monument Creek, the source of alluvium forming Granite Rapid, had three debris flows between 1966 and 1996 (Webb *et al*., 2000), the net change in rapid head elevation is -0.4 m. Due to the tight controls of close anchors and the distinct morphology, we are confident of this measurement. It is possible that each of these debris flows merely aggraded the subaerial debris fan and had little impact on the river, or that Granite Rapid was affected with a debris flow just before the 1923 survey that was subsequently reworked; the three new debris flows in the latter half of the 20th century could have then simply constricted the rapid again to its 1923 dimensions. Between Hermit and Tuna Creek Rapids, the most substantial change is at Crystal Rapid (RM 98.8), where a 1966 debris flow (Cooley *et al*., 1977) followed by the 1983 flood (Kieffer, 1985) created a net rise of +1.6 m. The rise in elevation at the head of Crystal Rapid created a rise at the base of Boucher Rapid 2.7 km upstream, decreasing its fall. Boucher Rapid itself also had a debris flow in 1951 or 1952 (Webb *et al*., 2002) that raised the upstream pool by +0.6 m and created the Fifth Wave in Hermit Rapid, a prominent hydraulic feature 2.7 km upstream from Boucher Rapid.

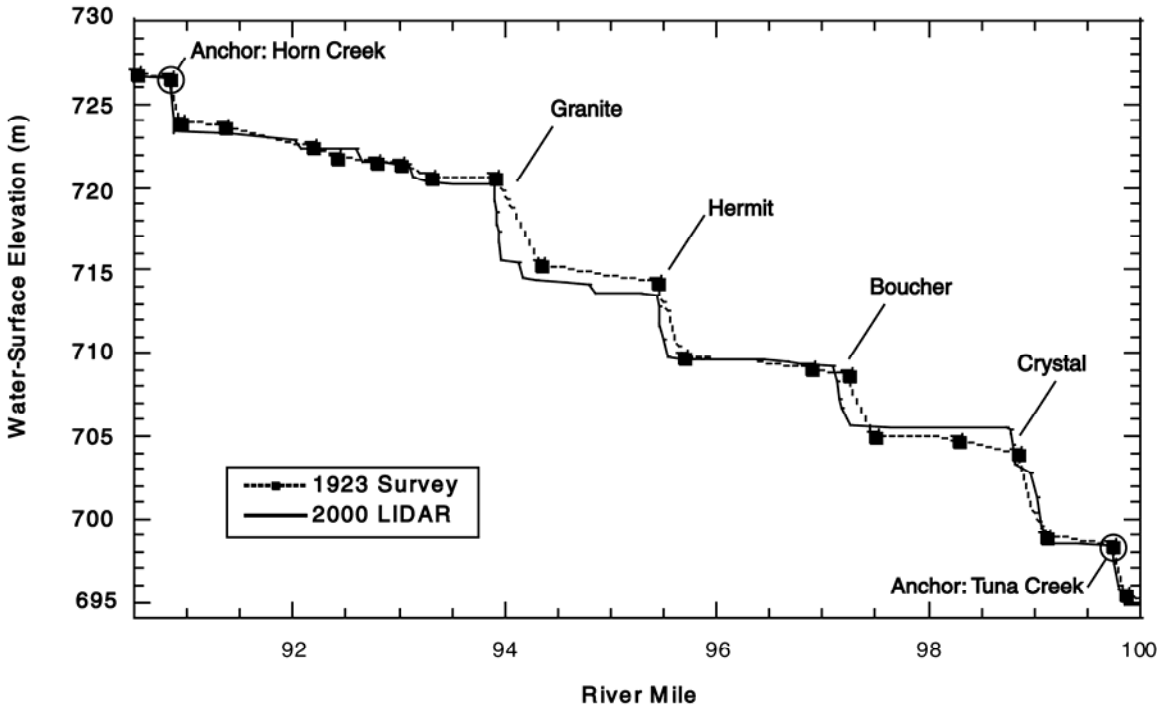

Figure 2.8: Comparison of 1923 and 2000 profiles in Upper Granite Gorge. Despite three debris flows, the head at Granite Rapid has changed little in 77 years. In contrast, aggradation from a debris flow at Crystal Rapids is clearly visible in the comparison.

One of the more complex stories of changing rapids in Grand Canyon is at Doris Rapid (RM 138.3). In 1890, Stanton photographed the canyon in the upstream and downstream directions from the alluvial fan, but he did not photograph the fan or the rapid. In his diary, he noted a 2.4 – 3.0 m rapid (Webb, 1996). During the 1923 survey, a total fall of only 0.3 m was recorded at this site. By 2000, however, the total fall at Doris Rapid again increased to 1.6 m (Figure 2.9). Using the three distinct observations and a chronology of reworking floods, we constructed a series of events to explain the changes observed at this rapid. First, because the largest flood on record in Grand Canyon (5900 m^3/s; O'Connor *et al*., 1994; Topping *et al*., 2003) would have removed all but the largest particles in the river in 1884, we assume that a debris flow created the Doris Rapid viewed by Stanton between 1884 and 1890. Between 1890 and 1921, this debris flow was removed by one of the many large floods common on the pre-dam Colorado River. When Birdseye encountered it in 1923, Doris Rapid was a one-foot riffle. Then, in 1940, early river runner Norm Nevills ran a newly enlarged rapid that took him by surprise; in fact, he was so unprepared that his wife Doris was ejected from the boat, lending her name to the restored rapid (Crumbo, 1981). Thus, it appears that a second debris flow enlarged Doris Rapid between 1923 and 1940. By piecing together historic observation and river hydrology in this manner, we identified these two previously unknown debris flows.

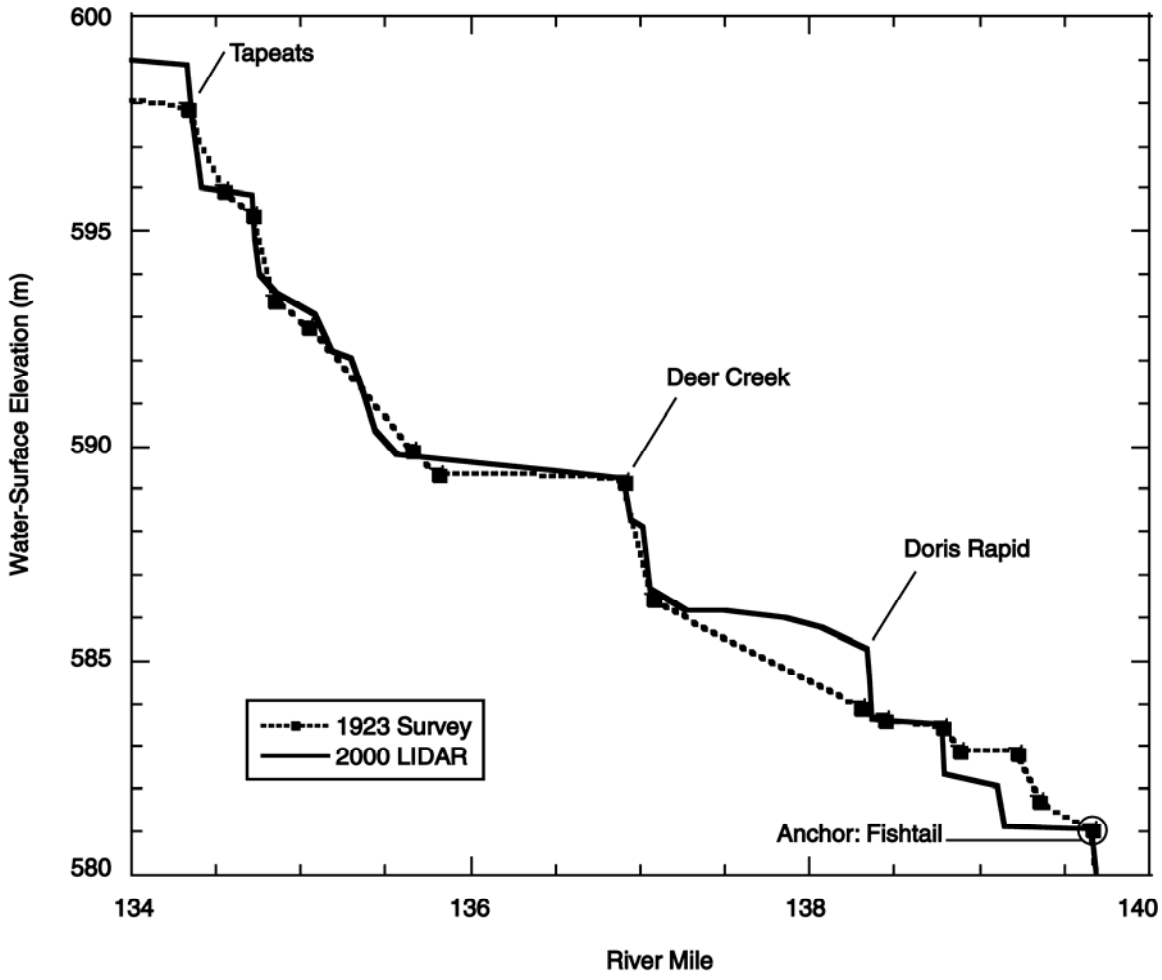

Figure 2.9: Comparison of the 1923 and 2000 profiles near Fishtail Rapid showing aggradation at Tapeats Rapid as well as the creation of a new rapid at Doris.

2.4 Discussion and Conclusions

Based on water-surface profiles derived from 1923 survey data and 2000 LIDAR data as well as repeat photography, geomorphic change detection on the Colorado River in Grand Canyon was determined at 91 locations between Lee's Ferry (RM 0.0) and Diamond Creek (RM 225.9), representing 39% of all rapids and 67% of named rapids. At these 91 locations, 11 rapids were known to have not changed between 1923 and 2000, 6 rapids exhibited a rise in the elevation at the head of the rapid of +1.4 m or more, and the elevation at the head of two rapids decreased more than –1.4 m. Though it has long been proposed that closure of Glen Canyon Dam would allow tributary input of coarse sediment to raise the level of the riverbed (Howard and Dolan, 1981; Kieffer, 1985; Webb *et al*., 1989; Melis *et al*., 1994; Griffiths *et al*., 2004), the precise rate of increase of the water-surface in the post-dam era throughout Grand Canyon was impossible to quantify without a new synoptic survey of the water-surface profile. This study shows that the water-surface elevation at the head of 91 rapids has increased by a mean value of +0.26 ±0.15 m from 1923 to 2000. The increase results primarily from channel constrictions in the river due to debris-flow input from tributaries. Thus, the current rate of aggradation in the main-stem Colorado at the confluence of a given tributary is roughly 3 cm/decade. While the general trend along the river is toward aggradation, several rapids were eroded with consequent lowering of the pool at the head of the rapid.

Also measured in the current study was an enhanced pool-and-rapid morphology within the river corridor. While in 1923, 50% of the cumulative drop through the river corridor occurred in just 9% of the distance, by 2000, this number increased to 66%. One

possible explanation for enhanced pool-and-rapid morphology could be increased debris-flow activity in Grand Canyon during the later half of the 20th century. However, previous research shows that debris-flow frequency in Grand Canyon has been constant over the past 100 years (Griffiths *et al*., 2004). Because debris-flow frequency did not change after 1923, aggradation in the river corridor can be principally tied to a reduced flood regime in the main stem. While continuous gaging records extend only back to 1921 at Lee's Ferry, gage records from the lower Colorado River and flood accounts from the late 19th century indicate that the general climate in the southwestern United Stated was cooler and wetter with larger floods. Fluctuation to a drier climate and subsequent reduced natural flood regime in the early 20th century may partially explain the net aggradation. The more probable cause for aggradation, however, is the introduction of a regulated flood regime due to closure of Glen Canyon Dam in 1963. Because the timeframe of measurement of change almost exactly spans the pre-dam and post-dam period, however, the current study is unable to determine specifically how Glen Canyon Dam might have affected the rate of aggradation.

Finally, while Kieffer (1985) stated that exceptionally large floods (11,320 m^3/s) are required to completely rework some large debris flows, we found several examples of small and moderately sized debris flows that were effectively reworked by modest floods. For example, it seems that a 2.4 – 3.0 m Doris Rapid was nearly completely removed by a 4800 m^3/s flood in 1921. While large floods are needed to rework large debris deposits, effective reworking can occur at a variety of flood magnitudes.

3. HYDRAULIC STEP-BACKWATER MODEL OF THE COLORADO RIVER IN GRAND CANYON

One of the first steps in studying the influence of discharge on hydraulics of rapids in Grand Canyon is to know the stage-discharge relation of water at specific locations along the Colorado River. Under flow regulation, stage heights from large floods in the pre-dam era are difficult to reconstruct because few dam releases approach the magnitude of pre-dam floods. To estimate the water surface of these larger floods, researchers rely on reconstructed water-surface elevations from photographs, stage-discharge relations from established gaging stations, or stage-discharge relations measured at specific study sites by Northern Arizona University (NAU). Many researchers also use Randle and Pemberton's (1987) one-dimensional step-backwater hydraulic model to estimate the water-surface elevation within Grand Canyon (BOR, 1996; Walters *et al.*, 2000).

3.1 Previous Research

3.1.1 The Randle-Pemberton STARS Model

Randle and Pemberton's (1987) STARS model was developed to predict sand transport down the river during typical dam releases. With closure of Glen Canyon Dam in 1963, the mean annual sediment supply at Lee's Ferry of 57±3 million metric tons (Topping *et al.*, 2000) was impounded behind the dam, and the retention of sand within

the corridor to preserve camping beaches and benefit native aquatic ecology became a salient management goal. To build their model, Randle and Pemberton started with 199 cross sections generated by Wilson (1986); the Wilson cross sections included both topography and bathymetry. All Wilson cross sections, however, were measured across slow pools in the river, not at rapids that control the overall water-surface profile. Randle and Pemberton therefore added another 508 interpolated cross sections to fill gaps in coverage. These interpolated cross sections were idealized trapezoids built using river width and channel shape measured from aerial photographs.

To calibrate the Randle and Pemberton model, synthetic bathymetry was built into each interpolated cross section; the depth of the synthetic bathymetry was adjusted up or down until the predicted water-surface profile closely matched a known water-surface profile measured along the river. The water-surface profile used for calibration was the USGS profile surveyed in 1923 (USGS, 1924). As such, the STARS model represents a hybrid topographic state of the river corridor with data measured in 1923 and the 1980s. The Randle and Pemberton model used a Manning's n value of 0.035 for all cross sections, though roughness coefficient is less important for step-backwater models in Grand Canyon owing to the dominant hydraulic control exerted by each rapid. Randle and Pemberton (1987) forced their model to a subcritical regime (*i.e.*, allowing conditions up to but not exceeding critical flow) assuming that while the river has critical flow at each rapid, no reach of the river has supercritical flow for any significant distance. This assumption proved appropriate as the model results appear to capture the behavior of the

river; this assumption is also consistent with the critical-flow theory for rivers with alluvial substrates proposed by Grant (1997).

Given the data and computational resources available at the time, Randle and Pemberton's (1987) STARS is a useful model, still widely used in the Grand Canyon research community. Two significant deficiencies, however, limit wider adoption of the model. First, the Randle and Pemberton model, originally designed as a tool to analyze sand transport for typical daily releases, cannot accurately simulate flows above 850 m^3/s, limiting its usefulness for understanding pre-dam floods. Secondly, the model was built with the best river-corridor data available at the time and more accurately represents the state of the river in 1923 rather than current-day post-dam conditions. Under the influence of dynamic geologic processes, the water-surface profile of the Colorado River in Grand Canyon changed measurably between 1923 and 2000 (Magirl *et al.*, 2005). Some magnitude of error is intrinsic in using a model built on 80-year-old data, and because the current research project needed a step-backwater model that exceeded the accuracy and performance of the STARS model, a new step-backwater model was constructed for flow in the Colorado River from Lee's Ferry to Diamond Creek (river miles 0.0 to 226.0).

3.1.2 Other Grand Canyon Hydraulic Modeling

Modeling the movement of sands and gravels, Bennett (1993) built on the work of Randle and Pemberton (1987), constructing step-backwater models at a reach from river miles 59.3-87.6 (Grand Canyon reach) and another short reach between river miles

164.0-166.6 (National Canyon reach). Bennett incorporated Randle and Pemberton cross sections into his model, then added 43% more cross sections to the Grand Canyon reach and 89% more cross sections to the National Canyon reach to improve precision.

O'Connor *et al.* (1994) constructed a step-backwater model for a short reach of the river below Lee's Ferry to estimate peak discharge of the paleofloods which left slackwater deposits at Axehandle Alcove.

An unsteady, one-dimensional hydraulic model was also developed for Grand Canyon. The model solved the St. Venant equations using reach-averaged normalized cross sections and predicted the propagation of dam releases through the river corridor (Wiele and Smith, 1996; Wiele and Griffin, 1997). This wave-routing model is fundamentally different from the deterministic step-backwater models developed by Randle and Pemberton (1987), Bennett (1993), and this study.

3.2 Model Construction

The new model was constructed in HEC-RAS version 3.1, a free shareware application developed by the US Army Corps of Engineers, Hydrologic Engineering Center (Brunner, 2001). With a fully integrated graphic user interface, wide acceptance within the civil engineering industry, and availability of the application, HEC-RAS proved to be an acceptable development platform. The model is one dimensional and uses the step-backwater approach (Henderson, 1966) to predict the water-surface elevation at specific cross sections. The model was developed for steady-state operation.

Topographic data used to construct the model came primarily from a data set of digital imagery and automated photogrammetry provided to Grand Canyon Monitoring and Research Center (GCMRC) by ISTAR America, Inc. ISTAR America collected and processed images captured during a series of May 2002 Grand Canyon overflights. In addition to digital imagery, a one-meter digital elevation model (DEM) built with photogrammetry (NGVD88) was assembled for the entire river corridor. The ISTAR DEM has an absolute vertical accuracy estimated by GCMRC to be better than 0.3 m (Steve Mietz, GCMRC, personal communication, 2003).

3.2.1 Selecting Cross Section Locations

Cross sections were chosen using the same approach adopted by Randle and Pemberton (1987), but with the availability of a high-quality DEM and computer processing capability far exceeding the capability available in 1987, many more cross sections could be created to better characterize the complex hydraulics of the Colorado River in Grand Canyon. In general, cross sections were selected as needed to most efficiently characterize the hydraulics of the river corridor. ISTAR aerial photography was used to facilitate cross-section selection.

At each rapid, a group of at least four cross sections were selected: one at the head of the rapid, a second about 15 m upstream from the head, a third about 45 m upstream from the head, and a fourth cross section at the foot of the rapid. For long rapids, additional cross sections were placed within the rapid as needed to capture the fall of the water surface moving down the rapid (Figure 3.1). A collection of four cross sections

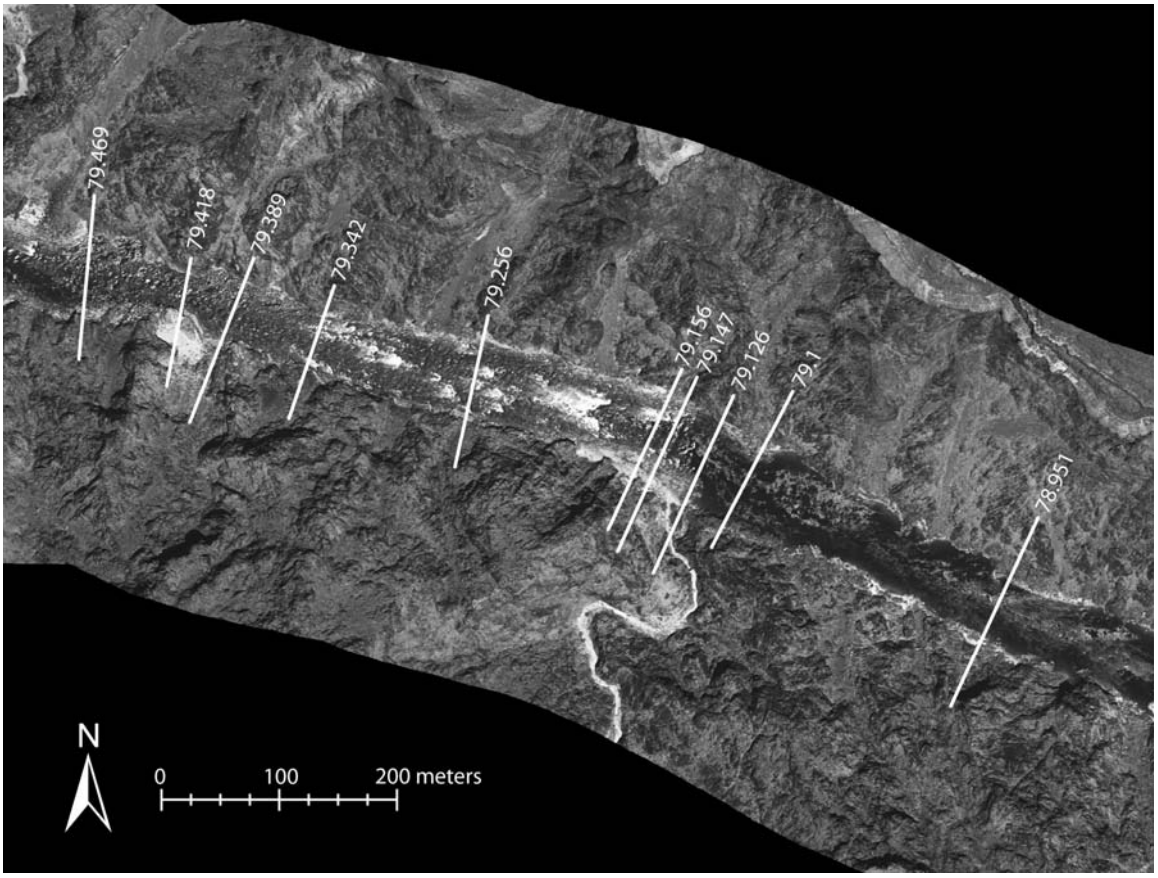

Figure 3.1: Typical cross section placement shown for the reach of river near Sockdolager Rapid. River is flowing right to left; cross section locations displayed as river-mile location adjacent each cross section.

were also placed at tributaries that flowed into otherwise quiet reaches of river. These tributaries, while associated with no rapid today, were assumed to have the potential to create rapids in the future. Placement of extra cross sections at currently quiet tributaries allows future modeling of tributary input; the model can also be quickly updated in the event of a rapid-creating debris flow. In slower sections of river away from tributaries, cross sections were spaced to best capture the progression of the river. Cross sections were also placed at river sections that widened or constricted abruptly (expansions and constrictions), consistent with recommended HEC-RAS procedures (Brunner, 2001). For continuity with the STARS model, cross sections were also generated at the locations of the Wilson (1986) cross sections.

3.2.2 Generating Cross Sections

A total of 2,690 cross sections were generated and built into the HEC-RAS model covering 364 km of river from Lee's Ferry to Diamond Creek. Consistent with HEC-RAS geometric conventions, each cross section was generated as a two-dimensional list of coordinates representing the station/elevation values of points along the cross section when viewed in the downstream direction. Points within a cross section were generally spaced 3 m apart. The cross sections were constructed perpendicular to the river centerline and extended away from the river shorelines, up the canyon walls, far enough to incorporate 30 m vertical elevation above the water surface on both sides of the cross section. This height of freeboard enabled the model to simulate discharge up to 5,600 m^3/s at every cross section. In addition, higher discharges can be simulated along specific

reaches where the predicted water surface does not overtop cross sections. The shoreline locations at each cross section were determined from aerial imagery and identified for each cross section.

In places, the DEM contains topographic surfaces that incorporate the tops of heavy stands of riparian vegetation, overestimating the true elevation of the ground on those surfaces. Each cross section was therefore post-processed and analyzed while juxtaposed against imagery to determine areas of vegetation-influence topography. Wherever high points in the cross section were identified with known stands of riparian vegetation, the cross section was edited to remove these higher elevation points (Figure 3.2). Similarly, some cross sections contained elevations below the known water-surface elevation. These elevation artifacts were removed by raising those points up to the known water-surface elevation.

Within the model for a given cross section, the distance to the next downstream cross section along the centerline, along the left bank, and along the right bank are required. HEC-RAS also requires roughness values for the channel, left-overbank (LOB), and right-overbank (ROB) regions. By considering the curvature of the river, HEC-RAS can calculate the distance water flows through different parts of the cross section, potentially affecting results. Because the current Grand Canyon model contains a uniform roughness value in the channel and overbank regions, downstream differences between centerline and overbanks length have no effect on model results. Nonetheless, to incorporate this feature of HEC-RAS, individual LOB and ROB distances were built into the model. To calculate downstream overbank distance, the width of the river, the

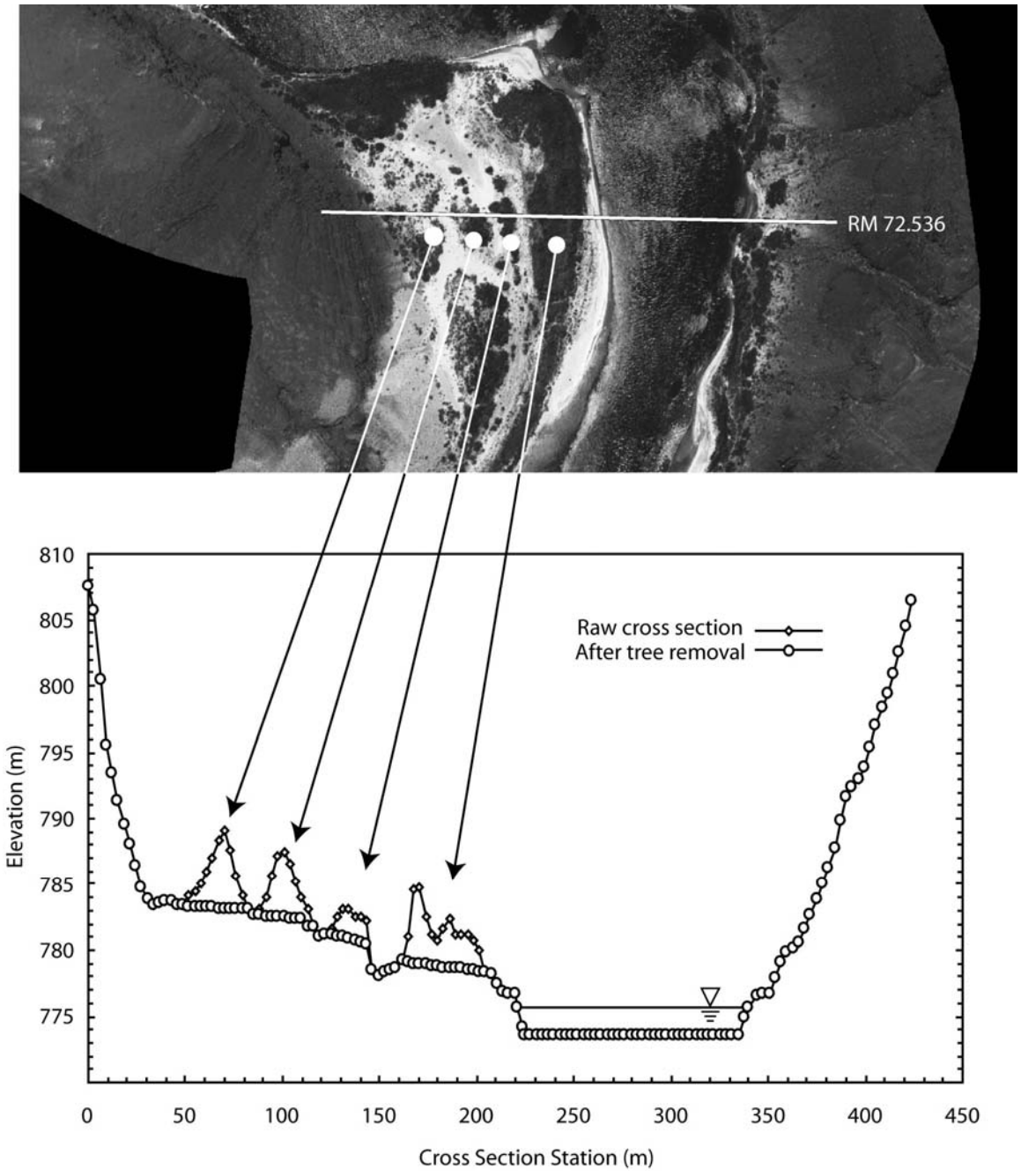

Figure 3.2: Cross section located at river mile 72.536 showing effect of trees on DEM topography. The top image is an aerial photo from ISTAR imagery data set; the white line represents the location of the cross section. The bottom graph shows the cross-section data (looking downstream) before and after the tree canopy was manually removed from the cross section.

curvature of the river for the current cross section, and the curvature of the river for the next downstream cross section are required. Curvature is given as an angle between the downstream flow vectors of sequential location along the river; counter clockwise is positive. The downstream distance between cross sections along the centerline, *D*, is determined by the cross section locations which are referenced to the river centerline. Once D is determined, the overbank distances are calculated using,

$$D_{LOB} = D_{ch} - \frac{w}{2}(\tan\theta_1 + \tan\theta_2) \tag{3.1}$$

and

$$D_{ROB} = D_{ch} + \frac{w}{2}(\tan\theta_1 + \tan\theta_2) \tag{3.2}$$

where *w* is the channel width at the target cross section, θ_1 is the curvature at the target cross section, and θ_2 is the curvature at the next cross section downstream.

3.2.3 Water-Surface Elevation

The elevation of the water-surface profile at each cross section was reported in each cross section and represents the known water-surface elevation (target elevation) to which the model is calibrated. The water surface was determined by laying the water-surface profile as measured in 2000 by Magirl *et al*. (2005) directly over the ISTAR DEM and adjusting points up or down until the spatial coverage of the water surface closely matched the extent of the river shoreline shown in the ISTAR imagery. This adjustment process produced a water-surface profile matching the geomorphic conditions of the DEM used to generate cross sections and best represents the state of the river in

2002.The discharge for the water surface reported by Magirl *et al.* (2005) was 227 m^3/s, as was the discharge during the 2002 overflights used to build the ISTAR DEM. A standard discharge of 227 m^3/s has been adopted for all remote-sensing overflights coordinated by GCMRC, and the model was calibrated to this standard 227 m^3/s discharge. The water-surface profile used for calibration is available in Appendix A.

3.2.4 Roughness Coefficient

Following the lead of Randle and Pemberton (1987), a standard Manning's n roughness value of 0.035 was chosen for all channel and overbank regions in the model. The bed of the Colorado River in Grand Canyon is a mixed substrate ranging from sand with various bed forms in slow reaches of the river to cobbles and boulders where flow velocity is high or where tributaries enter the river corridor (Howard and Dolan, 1981). Just as bathymetry is generally unknown in most reaches of river, the substrate for any given cross section is generally unknown. The roughness value of n=0.035 chosen for the channel represents a best guess synthesis all the roughness elements of the Colorado River in Grand Canyon. This roughness estimate follows the recommendations of Chow (1959).

The roughness in overbank regions is variable. The overbank region of some cross sections spans talus slopes with large particles and little vegetation. Other cross sections can have dense riparian vegetation. Still other cross sections have vegetation close to the shoreline with open, low-roughness sections away from shore. The

Manning's n value of 0.035 in the overbanks area may underestimate the actual value of roughness, but specific information for each of the 2,690 cross sections was not available.

Ultimately, the step-backwater model in Grand Canyon is largely controlled by critical flow constrictions widely located throughout the river corridor. For all simulations of the HEC-RAS model, subcritical flow conditions were selected. This flow-condition choice is consistent with the approach taken by Randle and Pemberton (1987) as well as the findings of Grant (1997) and best represents the conditions of flow of the Colorado River in Grand Canyon. As determined by Randle and Pemberton (1987), a step-backwater model in Grand Canyon is largely controlled by the critical flow at rapids and less by the roughness values entered at each cross section. Wherever flow is constricted to critical conditions in the channel, the water-surface elevation just upstream of the constriction is predominantly determined by the water-surface elevation at the constriction and independent of roughness coefficient. The farther upstream from a constriction with critical flow, the greater the influence roughness can have on predicted water-surface elevation.

3.2.5 Synthetic Bathymetry

Because the ISTAR DEM has no river bathymetry data built into it, the cross sections contain only subaerial topography away from the river. Synthetic bathymetry, therefore, was created for each cross section, mimicking the approach of Randle and Pemberton (1987). The total depth for each cross section was initially set to a value based on a bathymetric trace collected by the Bureau of Reclamation in the 1980s (Tim Randle,

BOR, personal communication, 2003). This initial bathymetry was somewhat arbitrary and ultimately irrelevant as the bathymetric depths were later reset by the calibration process. The shape of the bathymetry at each cross section was assumed to be one of four styles based on the proximity of the cross section to tributaries. For cross sections adjacent to a tributary, a triangular shape was used to best represent the subaqueous wedge of coarse-grained alluvium debouched from the tributary. For example, if the cross section was adjacent to a tributary that entered from river left, a triangular shape was chosen with the thalweg located four-fifths of the total channel width away from the left bank (Figure 3.3b). Similarly, for cross sections near tributaries that entered from river right, a triangular shape was chosen with the thalweg located four-fifths of the total channel width from the right bank (Figure 3.3c). For cross sections with tributaries entering from both sides, a triangular shape was chosen with the thalweg placed in the channel center (Figure 3.3d). The bathymetry of the river not influenced by tributaries tends toward a trapezoidal shape. For cross sections away from any tributary, therefore, the bathymetry was assumed to be trapezoidal with 1:1 side slopes (Figure 3.3a). Similarly, for the few cross sections that had an island and two separate flow channels, the bathymetry for each channel was assumed trapezoidal with 1:1 side slopes. These cross-section shapes are consistent with the trends of channel shape in Grand Canyon reported by Flynn and Hornewer (2003).

Occasionally, cross sections showed small exposed boulders in the middle of the river. These particles were, for the most part, removed from the cross section. An

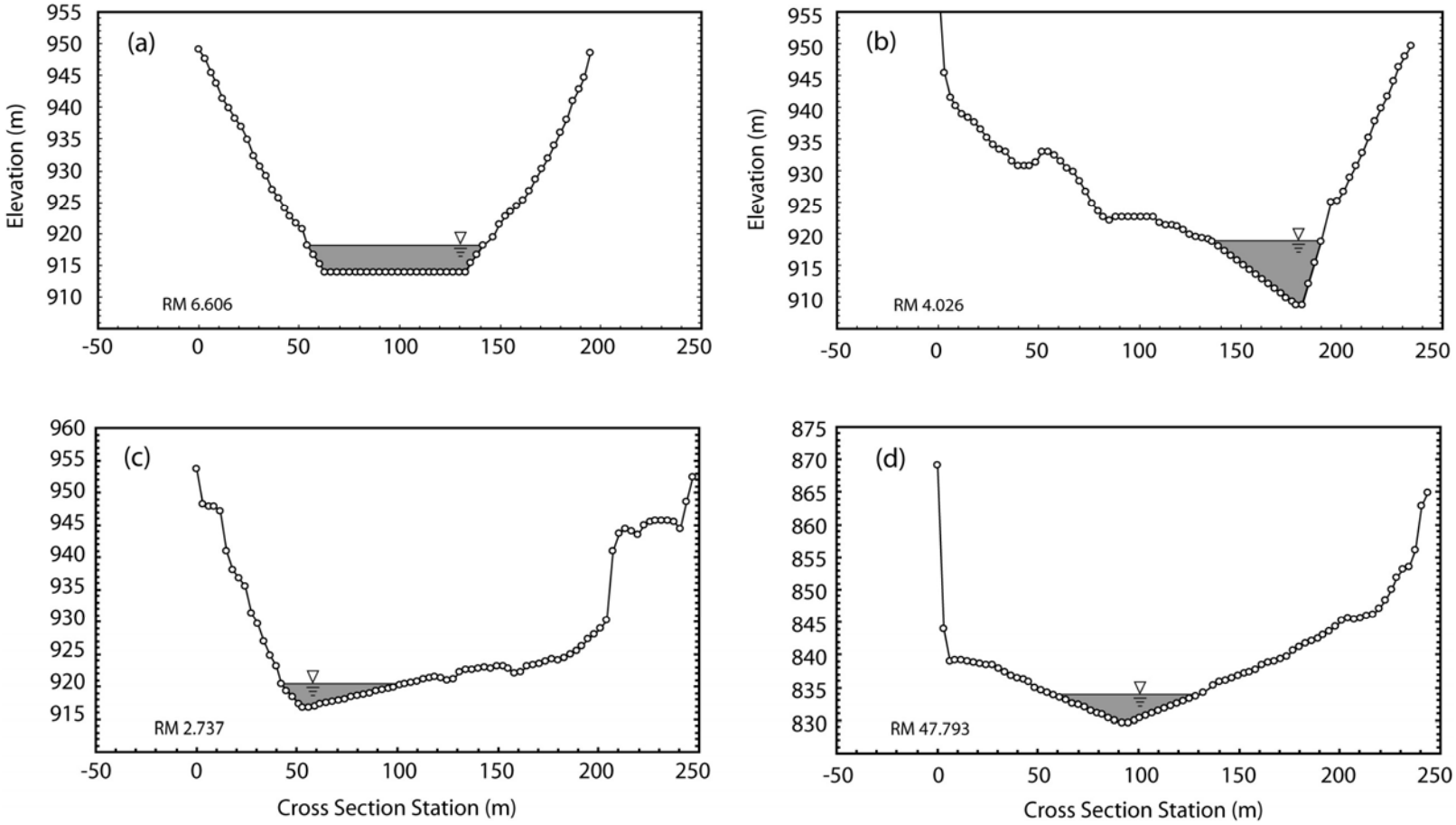

Figure 3.3: Example cross sections showing shape of synthetic bathymetry in (a) open sections of river, (b) section of river with tributary entering from river left, (c) section of river with tributary entering from right, and (d) section of river with tributaries entering both sides.

exception to this rule was the large boulder at river mile 18.746, several meters wide in the middle of the channel. This large boulder was retained in the model as an island.

For the calibration, the HEC-RAS model was run at a steady flow of 227 m^3/s under subcritical conditions. The farthest downstream cross section of the model was positioned within the rapid at Diamond Creek; the downstream boundary condition was selected as critical flow. When changing bathymetry during the calibration process, an adjustment value (*e.g.*, +0.5 m or -1.2 m) was estimated for all the cross sections to be changed, then all station/elevation points within that cross section below the known water-surface elevation were adjusted; the adjustment at a particular station/elevation point was made proportionately according to the relative depth of the point so that the prismatic shape of the bathymetry at that cross section remained consistent. Adjustments that would result in a water depth less than 1.52 m were not made; in other words, the minimum allowable water depth for a cross section was 1.52 m.

The calibration process began by running the model with the assumed bathymetry and visually inspecting the difference between the predicted water-surface elevation and the known water-surface elevation at a given target cross section. Owing to the subcritical flow conditions of the model, calibration progressed in an upstream manner. Changes to the bathymetry at any given cross section impacted only the water-surface elevations upstream from that cross sections—the closer the cross section, the stronger the effect. Attempting to correct error at a target cross section, the synthetic bathymetry was then raised or lowered at the target cross section and its closest downstream neighbors. Rerunning the HEC-RAS model, a new predicted water-surface profile could again be

compared to the known water-surface profile thus suggesting how the next adjustment might best achieve the target goals. This iterative process of evaluating error, adjusting bathymetry, then reevaluating error continued upstream until the model was fully calibrated.

For the calibration, the target error tolerance between the known and predicted water-surface profiles was 30 mm. For the final calibrated model (a total of 2,690 cross sections), 88% fell within this target error tolerance. Most of this error was confined to rapids, which cannot be accurately modeled using one-dimensional hydraulics. When flow in a one-dimensional prismatic channel passes through a constriction without energy loss, the water surface at the constriction drops in elevation relative to the flow upstream and downstream of the constriction (Chow, 1959). When modeling rapids with a step-backwater approach, the depressed water surface at the constriction—commonly 1-2 m—can be pronounced. Therefore, the target tolerance in the middle of rapids (both steep rapids and less-steep riffles) was, at times, discarded in favor of accuracy in the pools above the rapids. In fact, the standard approach of the calibration process near rapids was to first correct the predicted water surface in the pool at the head of the rapid, then attempt to match the water-surface profile in the core of the rapid as closely as possible. Examining the model calibration only in the pools (*i.e.*, cross sections where the water-surface slope from the next upstream cross section is less that 0.001), 98.0% of the calibrated predictions were within the 30 mm tolerance, and 99.8% were within 60 mm of the known water-surface elevation.

Future users of the model need to be aware of these water-surface elevation depressions for two reasons: (1) model accuracy is always suspect in the core of rapids or even riffles—the model should not be used to make predictions about the water-surface elevation within rapids—and (2) the user should post-process all water-surface profiles taken directly from HEC-RAS by backfilling all water-surface depressions from downstream to upstream. More importantly, users need to understand that the model is better at predicting the water-surface elevation in the pools, particularly the pools directly above rapids.

3.3 Results

3.3.1 Error Estimate

Because the model was calibrated to a water-surface elevation for a steady discharge of 227 m^3/s, performance of the model at discharges near 227 m^3/s is excellent (as discussed in Section 3.2.5). To answer how well the model predicts water-surface elevations in pools for discharges other than 227 m^3/s, the model predictions were compared to stage-discharge relations for select NAU monitoring sites. In all, 18 NAU sites were used to estimate model error (Joe Hazel, Northern Arizona University, personal communication, 2005). Under a long-term monitoring program, NAU routinely measures topography and stage at 52 prominent sand bars in Grand Canyon constructing stage-discharge relations for the sites at flows from 142 to 1,700 m^3/s. Of all the sites, 18 were chosen for comparison to the model due to their proximity to model cross sections and their position relative to pools (Figure 3.4). Some NAU sites are located in fast water

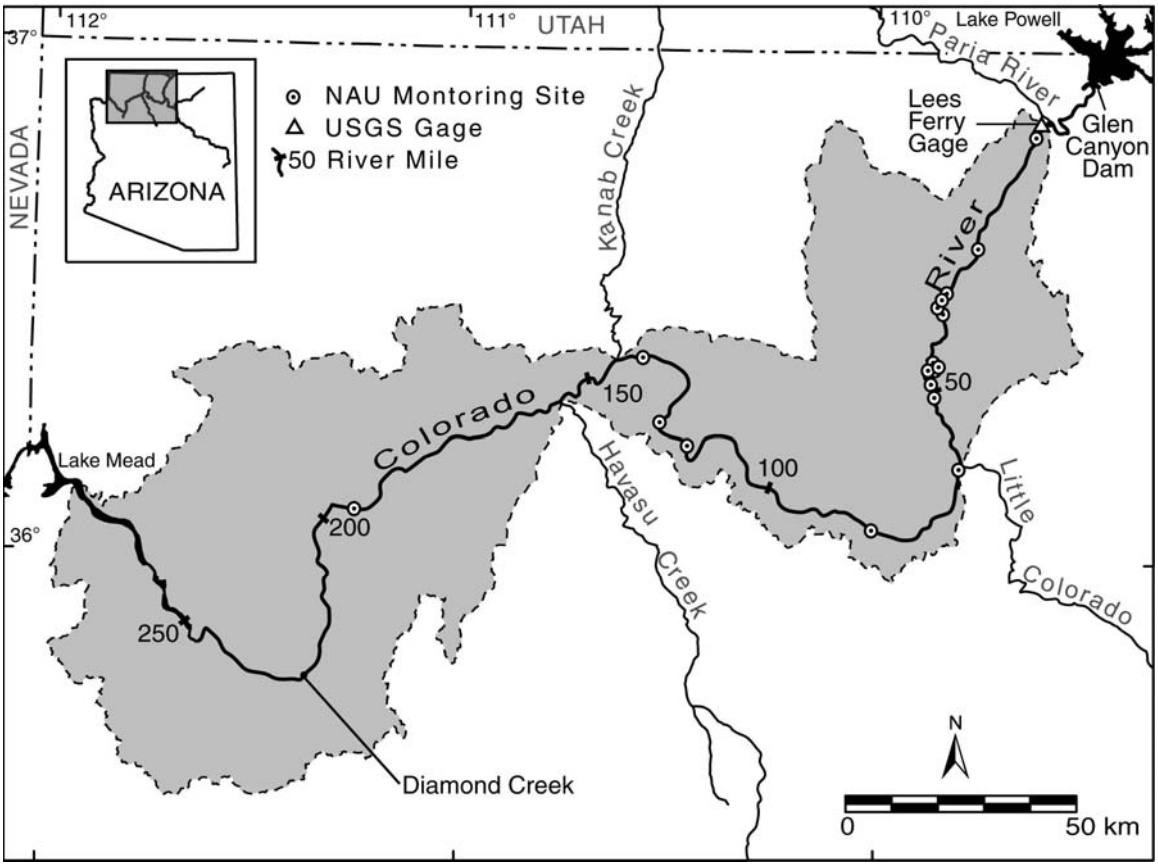

Figure 3.4: Map of Grand Canyon showing the 18 NAU monitoring sites used to evaluate the stage-discharge prediction accuracy of the HEC-RAS model. Most NAU are located between Lee's Ferry and the Little Colorado River.

or small rapids that are not conducive to evaluating the model results; only sites located unambiguously in pools were chosen for comparison. For a given NAU site, the predicted water-surface elevation from the HEC-RAS model was calculated by linearly interpolating values from the two cross sections in the model bounding the NAU site. Because each of the 18 sites were in pools, there was little difference in elevation between the two bounding cross sections.

Figure 3.5 shows the prediction error of the HEC-RAS model for a range of discharges at the 18 sites. Also shown is the root mean squared error at each discharge. The prediction error is the value of the predicted water-surface elevation at a given site minus the known water-surface elevation for the site from the NAU data. Not surprisingly, Figure 3.5 shows that prediction error is smallest for a discharge of 227 m^3/s, the discharge used for model calibration. At lower flows, 142 m^3/s, the prediction error becomes slightly negative showing the model predicting a water surface slightly below the actual water surface. As the discharge rises above 227 m^3/s, the error rises to a maximum negative value of -0.31 m from 900 to 1,300 m^3/s; discharges in this range begin to inundate the overbank regions. Heavy riparian vegetation on the lower sections of the overbanks may result in a larger roughness and a higher water-surface elevation than the model predicts. Pre-dam floods periodically scoured riparian vegetation from the Colorado River corridor, leaving the near shoreline area relatively free of vegetation. The regulated flow regime in the post-dam Grand Canyon, however, allowed growth of willow, arrow weed, tamarisk, and other woody vegetation near the shore (Turner and

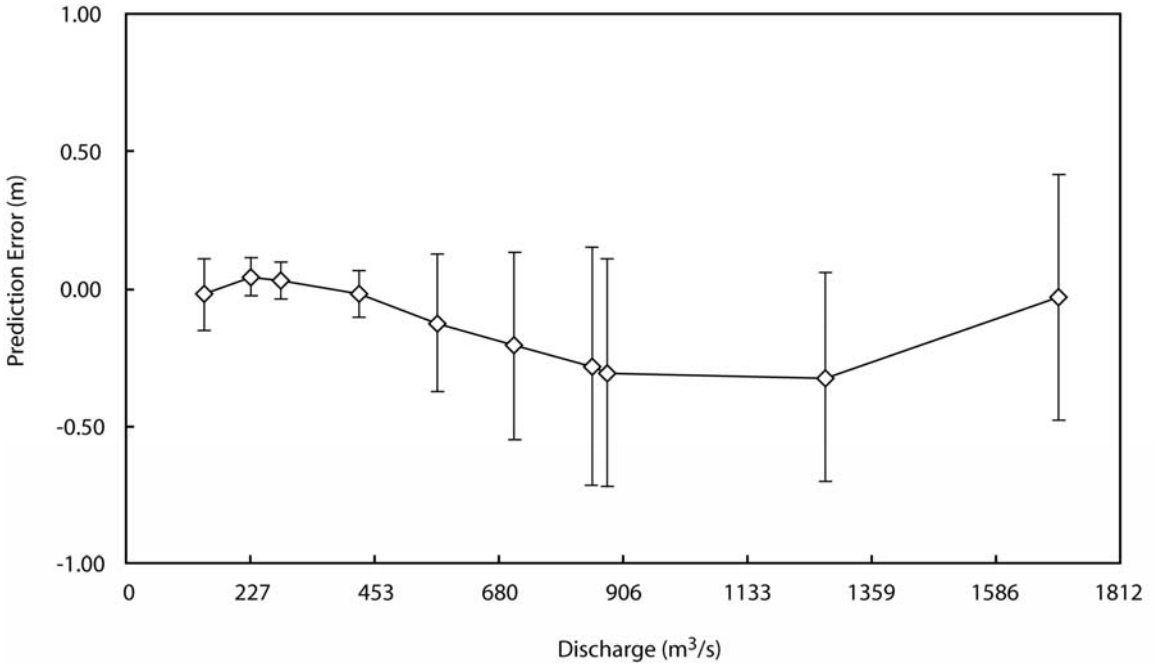

Figure 3.5: The average absolute error of the HEC-RAS model predictions compared against stage-discharge values known at 18 permanent NAU monitoring sites. The error bars represent the root mean squared error of the residuals. The HEC-RAS model was calibrated at 227 m^3/s, the discharge showing the smallest error.

Karpiscak, 1980; Kearsley and Ayers, 1999). The model, with a constant 0.035 roughness coefficient, fails to capture energy losses from extra vegetation on the overbanks.

For larger floods approaching 1,700 m^3/s, the average prediction error actually improves to -0.03 m. The root mean squared error, however, continues to increase owing to the uncertainty of model prediction for large flows. For extremely large floods, the relative size of the roughness elements in the domain decreases and the actual roughness values tend to fall with increasing depth of flow. Because the model uses a constant roughness value regardless of discharge and depth of flow, the model tends to over predict the level of water surface for extreme floods. Figure 3.5 shows this tendency of the model to over predict for larger floods.

To evaluate the sensitivity of the model to different values of Manning's n, global roughness values of 0.025 to 0.045 were evaluated and compared to the standard n=0.035 (Figure 3.6). Underprediction of the water-surface elevation at moderate discharges of 900 – 1,300 m^3/s is present for all values of roughness evaluated. At the smallest discharge evaluated, 142 m^3/s, average error changes roughly 36 cm as roughness is raised from n=0.025 to n=0.045. At the largest discharge, 1699 m^3/s, average error changes roughly 84 cm over the span of roughness values evaluated. Figure 3.6 may suggest a higher roughness value better approximates the conditions in the river simply because the top curve (n=0.045) in Figure 3.6 appears to have less overall difference in the error over all discharges. For discharges above 1699 m^3/s, however, a large roughness value would produce large overpredicted values. In fact, for extremely large

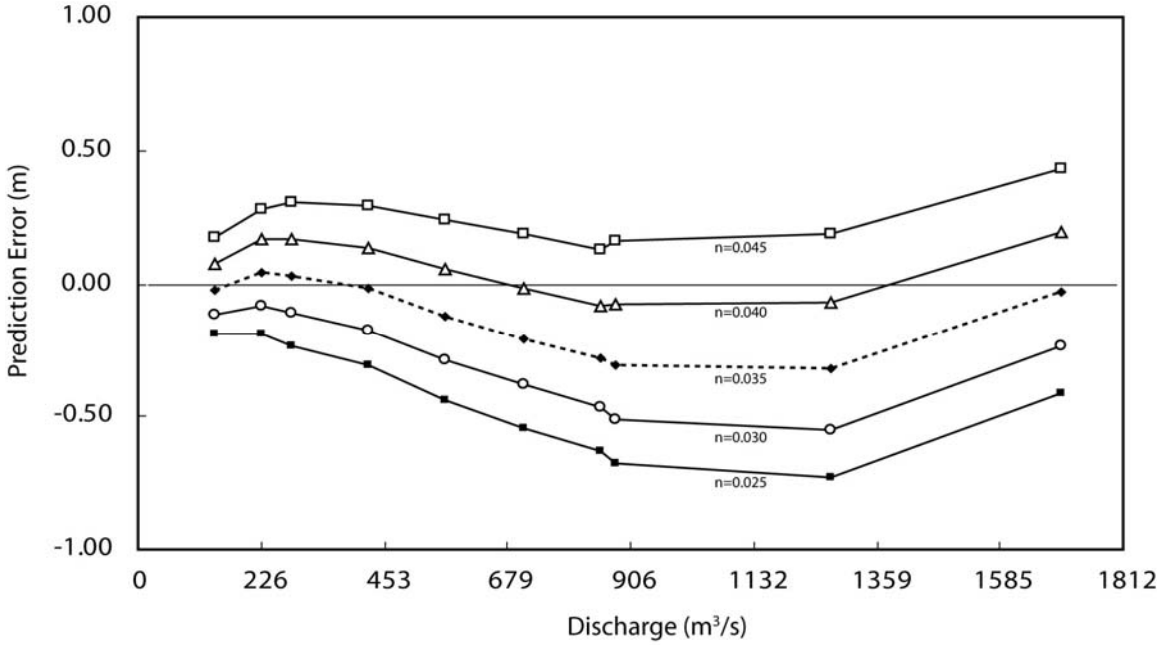

Figure 3.6: Sensitivity analysis of the model prediction error (averaged for all 18 NAU sites) for different values of Manning's n.

floods, smaller roughness values seem to best approximate the water-surface elevation.

3.3.2 Model Performance at Select Sites for Large Floods

Driftwood lines from large pre-dam floods are visible today throughout Grand Canyon. Assuming these driftwood lines represent the high-water mark from a flood event and driftwood lines can be correlated with a particular flood event, an evaluation of model performance for large floods can be made. Based on the driftwood lines left near Palisades Creek near river mile 66 (David Topping, USGS, personal communication, 2005), the HEC-RAS model over predicts the water-surface elevation in this reach by 1.11 m at 5,000 m^3/s and 1.40 m at 5,600 m^3/s. More recently, numerous driftwood piles were left throughout the river corridor from a 3,570 m^3/s flood in 1957. This was the last large flood before closure of Glen Canyon Dam in 1963, and it was the largest flood in Grand Canyon in the past 79 years.

One prominent location where driftwood was left from this 1957 flood is the top of the huge boulder at Boulder Narrows in Marble Canyon (river mile 18.746). In 1957, P.T. Reilly, remarkably, ran his boat through Grand Canyon at this flood stage. Duane Norton fortuitously snapped a photograph of Reilly running Boulder Narrows showing the height of inundation of the flood (Figure 3.7). In 2003, Steve Young matched the photo showing the stranded driftwood and a much lower water-surface (Figure 3.7). When this section of river is simulated with the HEC-RAS model, the predicted water-surface elevation falls about a meter below the top of the boulder (Figure 3.8). It appears

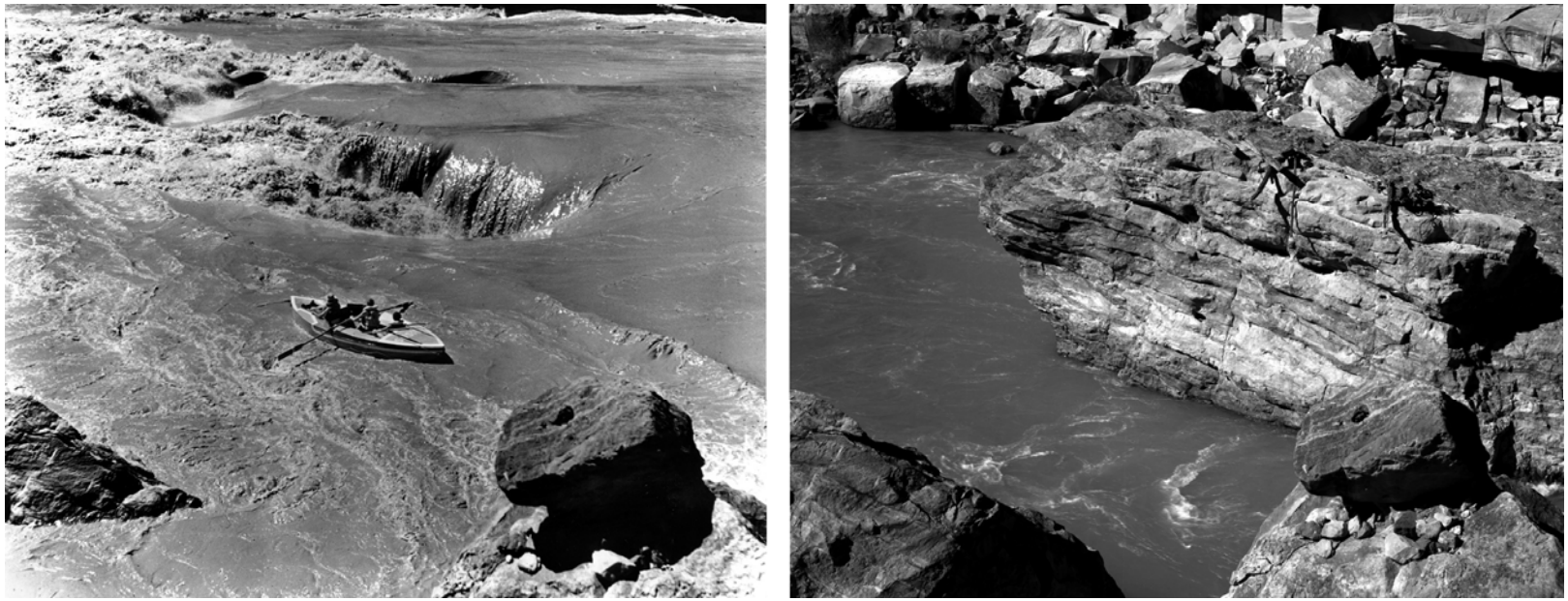

Figure 3.7: Matched photos showing the section of river at Boulder Narrows (river mile 18.746) during (left) 3,570 m^3/s flood with P.T. Reilly rowing on 6/11/1957 (Duane Norton: photo courtesy P.T. Reilly) and (right) low flow of roughly 340 m^3/s photographed 3/1/2005 (Steve Young, stake #4810). The driftwood left stranded on top of the mid-channel boulder was left by the high water of the 1957 flood, the last large flood in Grand Canyon before closure of Glen Canyon Dam.

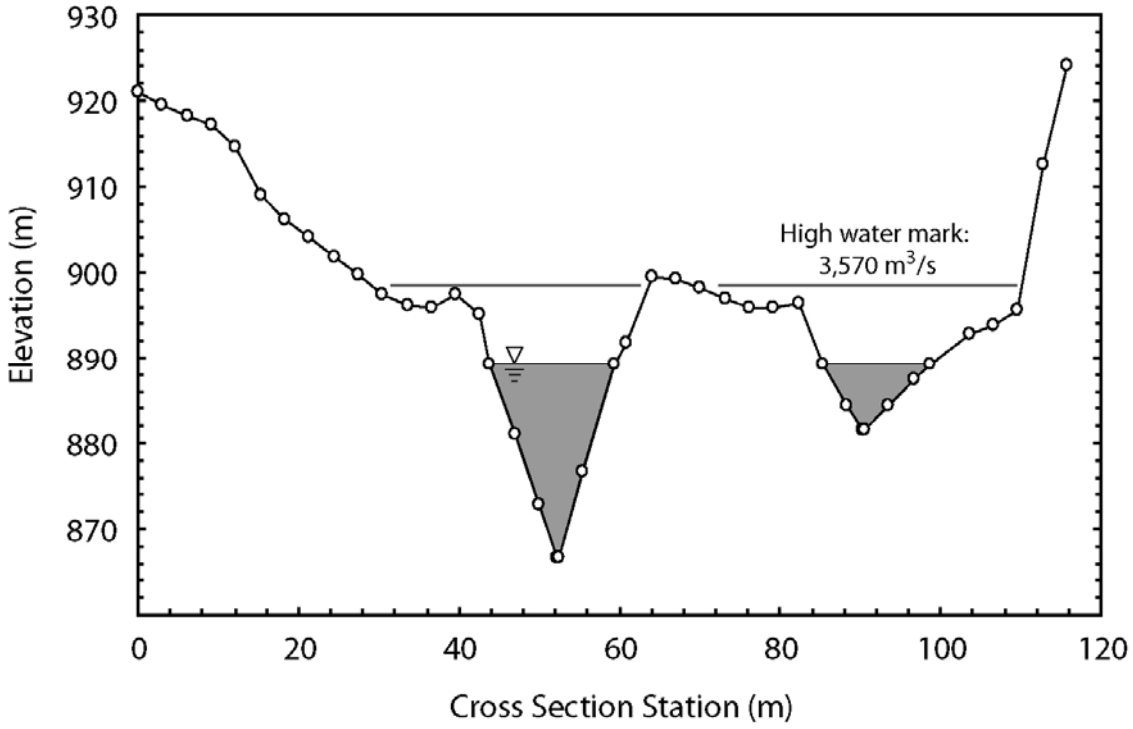

Figure 3.8: HEC-RAS cross section at river mile 18.746 (Boulder Narrows) showing predicted water-surface elevation at 227 m^3/s (the shaded area) and the predicted high water mark of the 3,570 m^3/s flood that occurred in Grand Canyon in 1957. The peak of the actual flood overtopped the boulder (Figure 3.7); the model under predicts the location of the flood high-water mark by about a meter.

that in this section of the river for a flood of 3,570 m^3/s, the model actually under predicts the height of the water surface.

Granite Park, located near river mile 209, is a relatively wide expanse of river corridor caused by faulting of the Granite Park Fault (Figure 3.9). Just upstream of the expansion, three closely spaced tributaries dump copious amounts of coarse-grained sediment into the river which has been reworked into a large boulder-strewn island which rises in elevation in the downstream direction. At low flows, the river flows entirely around the right edge of the island; with increasing discharge, the river bifurcates around the island with its highest point at the farthest downstream point of the bar. Extremely large flows (> 5,500 m^3/s) completely submerge the island. The flood of 1957, however, did not overtop the bar and left large driftwood piles in the lower middle section of the island. The dark gray splotches shown on Figure 3.9 at cross section 209.445 are the remnants of those driftwood piles. To test the accuracy of the HEC-RAS model for the 1957 flood at Granite Park, the predicted water-surface elevations at each cross section were analyzed. In the model, the cross section at river mile 209.368 was completely submerged while the cross section at river mile 209.501 still showed a prominent island. The predicted water surface just touched the top of the boulder bar at cross section 209.445, accurately predicting the location of the driftwood piles left in 1957 (Figure 3.10).

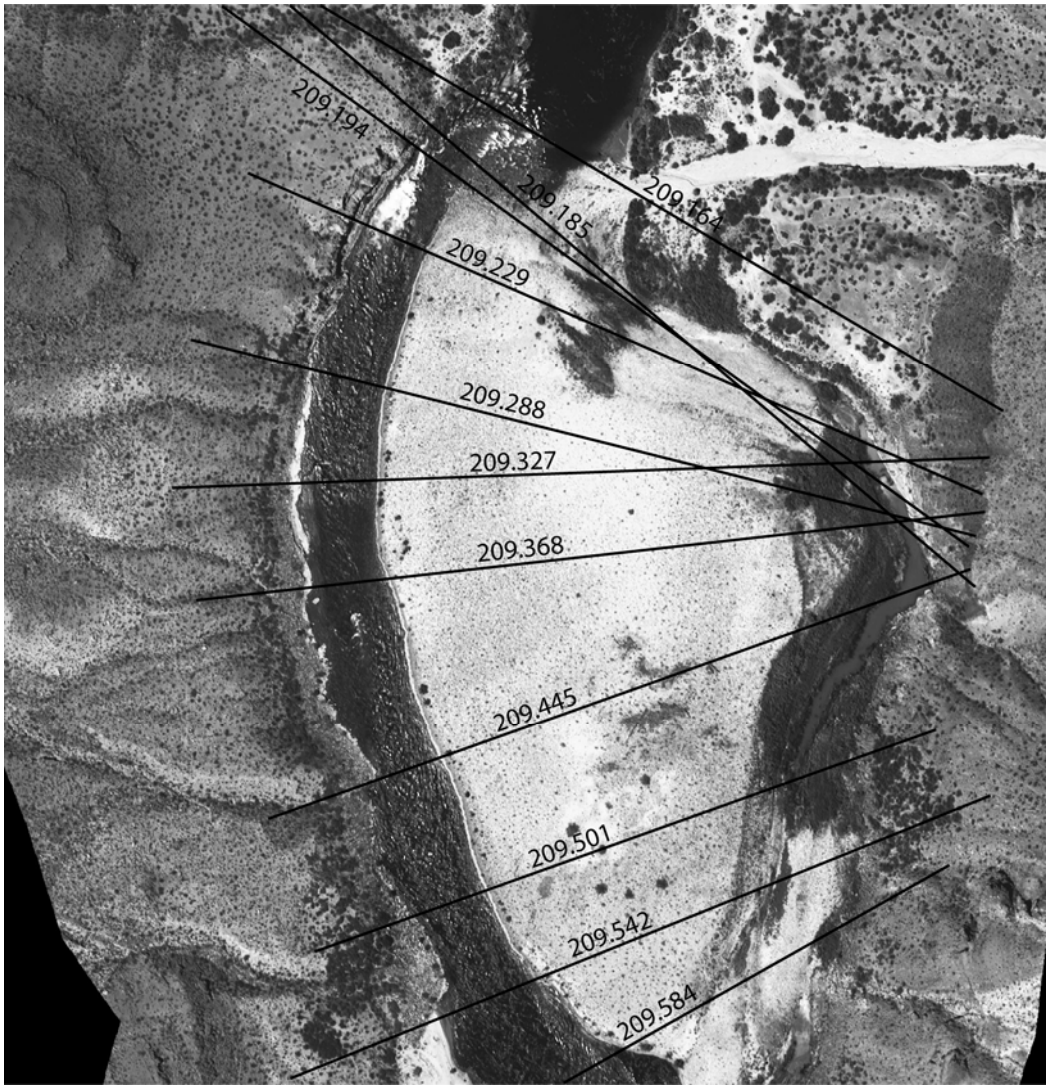

Figure 3.9: Reach of river in Granite Park (river mile 209) showing the broad boulder bar formed from reworked particles entering tributary from river left. The flow of the river in the image is from top to bottom. Collections of driftwood left by the 1957 (3,570 m^3/s) flood are visible toward the middle of the boulder bar where cross section 209.445 cuts the domain.

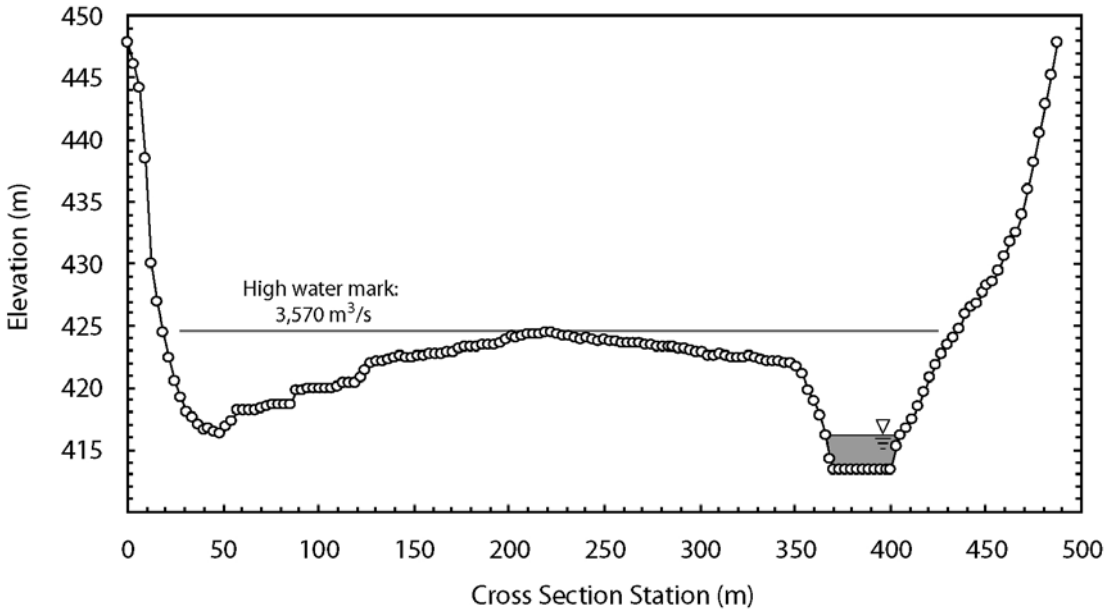

Figure 3.10: HEC-RAS model prediction of the water-surface elevation at river mile 209.445. The inundation of 227 m^3/s is shown as the gray area. The high water mark of the 1957 flood (3,570 m^3/s) is also shown illustrating the prediction accuracy for high discharges for this reach of river.

3.4 Applications

The most immediate application of the HEC-RAS model is for the correction of water-surface profiles surveyed in Grand Canyon. The hydrograph released from Glen Canyon Dam is variable, commonly ranging from 142-708 m^3/s diurnally (Schmit, *et al.*, 2005). Water-surface surveys in Grand Canyon are commonly measured on the rapidly rising or falling limb of the hydrograph or at significantly different flow conditions. Because water-surface profiles are one common metric to analyze change at rapids (Webb *et al.*, 1999a; Webb *et al.*, 1999c), normalizing the measured water surface of disparate surveys to a common discharge is essential to make direct comparisons. Yanites *et al.* (2006) recently used the stage-discharge relations predicted from the Grand Canyon HEC-RAS model to normalize separate surveys spanning 6 years at Granite Falls Rapid and Nevills Rapids. With the normalized water profiles, they were able to tie aggradation and denudation of the water profile at these sites to specific geomorphic events. Similarly, the current study uses the HEC-RAS predicted results to normalize water-surface elevations collected during velocity measurements in Grand Canyon (see Chapter 5 and Chapter 6).

Demand for a replacement to the STARS model is high within the Grand Canyon research community, and ignoring the fact that the model has not been formally released or published, several researchers are today using its results (Helen Fairley, GCMRC, personal communication, 2006). Notwithstanding its popularity, the model will be valuable in extending the current research. Though not able to be incorporated into the

current study, a river-profile evolution model, built of the foundation of the Grand Canyon HEC-RAS model, is currently in an advanced stage of development.

3.5 Conclusions

A one-dimensional step-backwater model was constructed for 364 km of Colorado River in Grand Canyon. The model was built using topography collected in 2002 and best represents the state of the river in 2002. The model was designed to be a replacement to the Randle and Pemberton (1987) Grand Canyon step-backwater model. The new model, however, handles extreme flood events (up to 5,600 m^3/s) with 2,690 cross sections using a consistent morphologic data set. The model was built in HEC-RAS and has a convenient graphic user interface for easier display and analysis.

Based on independently collected stage-discharge data from NAU, the absolute error of predicted water-surface elevations from the model is less than 0.25 m for flows less than 450 m^3/s. For flows between 450-1,600 m^3/s, model error is less than 0.75 m. For extremely large floods of 5,600 m^3/s, the model tends to over predict the water-surface elevation by roughly 1.4 m. Anecdotal analysis of the 1957 flood at Boulder Narrows and Granite Park show good agreement between the model and the actual behavior of pre-dam flooding, showing the potential usefulness of the model as a research tool.

4. ADV POINT MEASUREMENT OF VELOCITIES WITHIN RAPIDS OF THE COLORADO RIVER IN GRAND CANYON

Rapids on the Colorado River in Grand Canyon are formed predominantly by the accumulation of coarse-grained sediment debouched from ephemeral tributaries by debris flows (Webb *et al.*, 1989; Melis *et al.*, 1994). These debris flows transport boulders well over 1.0 m in size into the main channel. Over time, the accumulation of debris on an active debris fan pools the river upstream of the fan, constricts the river forming the rapid, and creates a deep scour pool below the rapid. Depending upon how they are defined, roughly 200-300 rapids exist along the 380 km of river between Lee's Ferry and Lake Mead. The rapids and their associated pool-and-rapid morphology form the basic geomorphic control of the river corridor in Grand Canyon (Leopold, 1969; Howard and Dolan, 1981; Schmidt and Rubin, 1995). Sand deposition, fish habitat, and even bedrock down cutting are driven by debris fan location and the hydraulics of the resulting rapids. Despite the scientific importance of rapids on the Colorado River, little quantitative data exists describing the hydraulics in rapids.

Velocity measurements in rivers are usually taken with mechanical current meters, but most current meters average flow in all directions and are ill-suited to measure flow in turbulent or rapidly flowing rivers and steams. Flow velocities in a turbulent mountain stream were collected by Smart (1994) using a pitot-static tube. More recently, electromagnetic current meters have been used to measure flow and turbulence

in rivers (Roy *et al.*, 1999). Recent developments in acoustic flow instruments has led to widespread and routine measurements of velocity and discharge in rivers (Yorke and Oberg, 2002; Morlock and Fisher, 2002). Using an acoustic Doppler current profiler (ADCP) and BoogieDopp river discharge measurement system, Cheng and Gartner (2003) measured velocity profiles that extended closer to the free surface than normally possible with an ADCP alone.

Acoustic Doppler velocimeters (ADVs) are also commonly used to measure flow velocity at a point location. Lane *et al.* (1998) completed an extensive study of 3-D flow fields in rivers using an ADV. Detailed studies with ADVs have also been made of the 3-D flow field above a gravel-bed flume (Ferro, 2003), in scour hole abutments (Dey and Barbhuiya, 2006), and in the surf zone (Elgar *et al.*, 2005). In an application similar to the present study, Hotchkiss *et al*. (2003) used an ADV to measure the fluid velocity entering a spillway weir. Yet in each application described above, maximum measured flow velocity was much less than velocity magnitudes expected in the core of Grand Canyon rapids.

Kieffer (1987) was one of the first to attempt to quantify the hydraulics of Grand Canyon rapids. She cleverly used a calibrated video camera and floating tracer particles to measure, in a Lagrangian frame of reference, velocity along trace lines through rapids. Using tracking particles for measuring flow velocity, however, has some disadvantages. First, particle trajectories cannot be controlled; also, being on the surface, particles are susceptible to jostling by waves and wind thus reducing the particle velocity relative to the true free-stream velocity. Nonetheless, Kieffer (1987) reported velocities as high as

7.5 m/s and made a preliminary attempt at measuring bathymetry within the rapids, with mixed results. These efforts suggest complete data sets describing river flow velocity, surface elevation, and bathymetry in rapids is an elusive problem. The present work attempts to build on the work of Kieffer (1987) by quantifying flow values within a Grand Canyon rapid in addition to measuring the morphology of the water surface and the bathymetry below the rapid.

4.1 Field Locations and Measurement Techniques

The main challenge in making in-situ measurements of water velocity in rapids of the Colorado River in Grand Canyon is the logistical difficulty of holding an instrument in a fixed position within the flow. Most boaters are motivated to safely navigate a given rapid as quickly as possible; few are interesting in loitering in the midst of whitewater. The waves in the rapids and the force of the moving water can make small errors potentially catastrophic, even in small rapids. Also, because the study area is a national park, measurement techniques cannot damage the landscape and no structures can be left behind. Vehicle access to the river is available only at Lee's Ferry and at Diamond Creek, 364 km downstream of Lee's Ferry. All field equipment is typically brought in by boat.

The site chosen for measurement in this study was Upper Rattlesnake Rapid, located 119 km below Lee's Ferry. The measurements were made in March 2005 at a river discharge of 540 m^3/s. Within the river corridor, Upper Rattlesnake Rapid is situated between the better known Unkar Rapid upstream and Nevills Rapid downstream. A debris flow at Upper Rattlesnake Rapid in 2002 changed the riffle into a small rapid.

Another site at Minus 4-Mile Bar in Glen Canyon was measured in April 2003 at a river discharge of 340 m^3/s. Glen Canyon is a bedrock controlled reach of the Colorado River just upstream from Lee's Ferry. The site is 18 km below Glen Canyon Dam and consists of a large cobble bar on river right just before a large right-trending meander. In contrast to Grand Canyon, Glen Canyon has no rapids and its fluvial geomorphology is more characteristic of an alluvial river. Due to the dam, little sand or clay is present in the reach and the bed is composed predominantly of gravels and cobbles. Measuring sites in Glen Canyon and Grand Canyon allowed a comparison of the measurement techniques on a rapid as well as in an alluvial reach.

A 10Hz Argonaut ADV manufactured by Sontek/YSI was used for velocity measurements (Figure 4.1). The instrument was fitted with a 3D side-looking transducer probe arrangement. ADVs operate on the Doppler principle utilizing the fact that sound reflected from particles suspended in the moving fluid is shifted in frequency according to the direction and speed of flow. By using three transmitters/receivers oriented in a spread array, the velocity of a 0.25 cc point within the flow can be calculated. The sample volume is nominally 10 cm from the probe. During this study, measured 3-D velocities consisted of the vector average of a 5-second burst of measurements (made at a 10Hz sample rate). A review of the operation of the ADV can be found in Lane *et al*. (1998) and Morlock and Fisher (2002).

The boat was a 19-foot J-snout, consisting of two rubber tubes supporting a rigid aluminum frame. A Mercury 50-hp outboard motor powered the boat with enough speed to up-run many smaller rapids. A stainless-steel rotating boom was mounted on the front

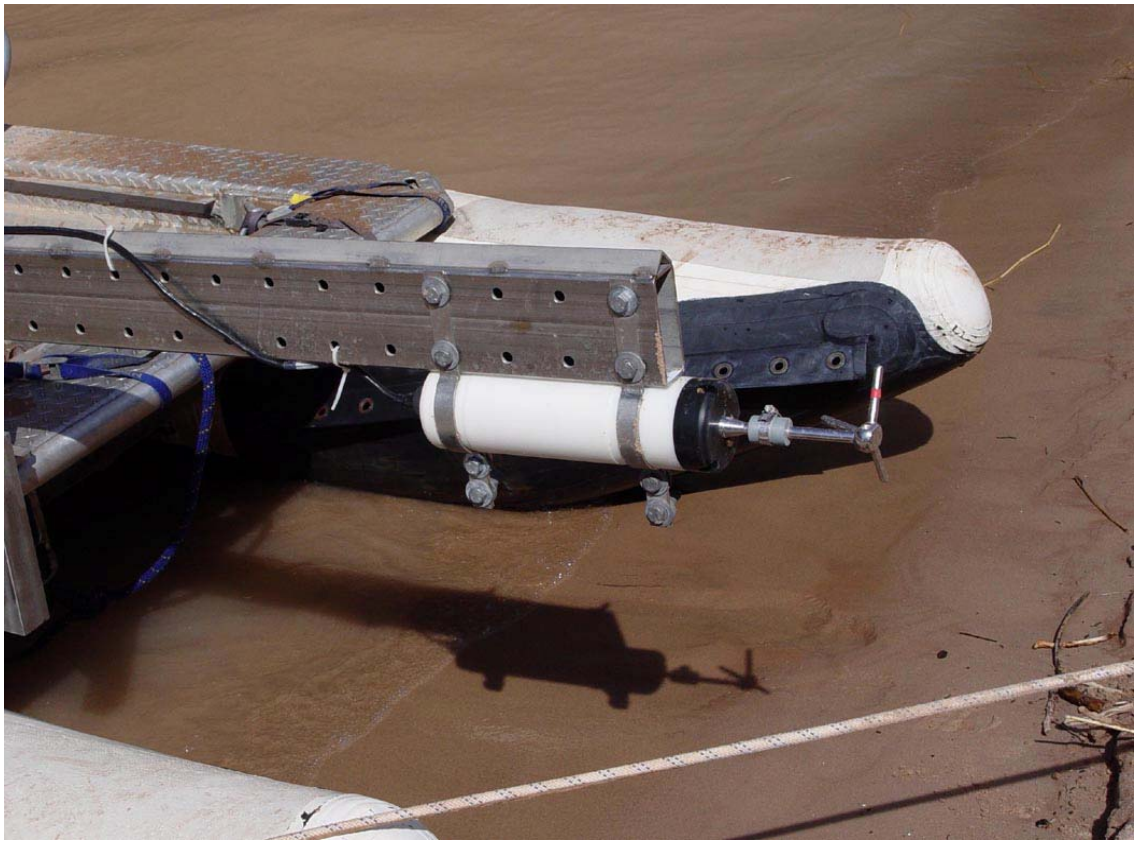

Figure 4.1: ADV shown mounted on rotating boom. The boom was rotated down into the water for measurements, positioning the ADV probe 80 cm below the water surface (photograph by C. Watkins).

of the boat allowing rapid deployment of the ADV instrument (Figure 4.2). When the boat was in position to make measurements, the boom was pivoted down into the river. All measurements were made 80 cm below the water surface. With this mounting arrangement, the boom could be quickly pulled from the water and secured at any time. This safety feature was essential to ensure the boat could be made navigation-ready in an instant. Stainless steel was chosen for the mounting boom because of its strength and non-magnetic properties, necessary to minimize magnetic interference because the ADV has a built-in compass to reference measurements to magnetic north.

Velocity data were post-processed using software supplied by the vendor. While the ADV software has the ability to use the instrument's built-in compass/tilt sensors to report velocity vectors in globally referenced East-North-Up (ENU) coordinates, the high velocities and extreme turbulence within the flow rendered ENU coordinates suspect. Instead, velocity data reported in a raw XYZ coordinate system were used for all analysis. Because the boat was positioned facing against the river current, the instrument was oriented so the probe looked across, or orthogonal to, the oncoming flow. The X component of velocity was defined along the predominant flow, the Y component of velocity orthogonal to the boat direction, and the Z component of velocity in the vertical. In this orientation, the maximum velocities could be measured along the axis of the boat (X component) with smaller fluctuations measured along the two remaining axes (Y and Z components). For a particular measurement location, a scalar magnitude of the overall horizontal velocity vectors, X and Y, was calculated.

Figure 4.2: Photos of operation of ADV boat (left) in quiet water above the rapid and (right) within the wave field of the rapid (photographs by C. Watkins).

The boat heading, as reported by the compass in the instrument, was used to determine the direction of horizontal velocity. Instrument specifications list the maximum velocity measurement capability to be 4.5 m/s, but small changes in the orientation of the probe relative to the flow reduced three flow axes, the instrument will experience an "ambiguity jump," in which case either the velocity values are reported as negative or the reported vertical velocity is well above 2.0 m/s and the corresponding horizontal components of velocity are reported to be nearly zero—a physically unrealistic condition in most rivers. Because measurements were always made with the boat positioned into the oncoming flow, any data in which the Y or Z components of velocity exceeded the magnitude in the X component of velocity were discarded as potential ambiguity jumps.

Water depth values were determined using a Lowrance X59DF fathometer mounted near the rear of the boat. The X59DF is a 50/200kHz instrument with a digital LCD display and a reported depth range of 400 m.

The ADV was connected to a laptop computer mounted in the boat and data were continuously fed to the laptop during each experiment. A multi-directional survey prism was placed at the top of the boom to allow the position of the instrument to be determined using an on-shore total-station surveying instrument. When making measurements, the boat was first positioned at a target location in the river and allowed to stabilize in the flow. ADV measurements were then taken for at least 15 seconds. The water depth under the boat, as reported by the fathometer, and the position of the boat measured with the total station was also recorded.

Finally, tetherballs were used as surface floats to measure flow velocity at Upper Rattlesnake Rapid. In a Lagrangian measurement technique analogous to the Kieffer (1987) work, the tetherballs were tossed into the water above the rapid and free-floated down the middle of the tongue of the rapid. By timing the passage of each tetherball, an average velocity in the tongue of the rapid was calculated and recorded. Fifteen tetherballs were tossed, timed, and results recorded.

4.2 Results

During the ADV measurement in Upper Rattlesnake Rapid, ambiguity jumps occurred frequently as flow velocities exceeded 3.0 m/s. In fact, measurements made in the core of the rapid typically reported vertical velocities approaching 6.0 m/s with concurrent horizontal velocities near zero—a physically unrealistic result. For Upper Rattlesnake Rapid, only 62% of all measurements were usable. In the slower water of Minus 4-Mile Bar, 87% of the measurements were salvaged.

While attempts were made to minimize magnetic interference with the ADV compass, the system had problems. While the stainless-steel ADV boom was not magnetic, the stainless steel bolts held the instrument to the boom were slightly magnetic. This problem was discovered while post-processing the data. In addition, it appeared that for the measurement session at Upper Rattlesnake, a local magnetic field developed around the boat itself. In the adjacent transects measured in the pool above the rapid, where the flow velocity is uniform and directed into the rapid below, compass headings (and in turn, the processed velocity vectors) were deflected as much as 30˚ depending on

whether the transect was cut from river left toward river right or the other way. Before making a measurement, the boat was allowed to dwell in a location for roughly 15 seconds. This dwell offered ample time to let the boat adjust to the oncoming flow. We also know from direct observations that the flow leading into the rapid, while turbulent, is smooth and uniform. Because the ADV was mounted forward and centered on the boat, our only remaining explanation for this compass artifact is the presence of a magnetic field, probably generated from the boat motor. This problem was intermittent and not observed at Minus 4-Mile Bar. Due to the error induced in the ADV compass by the magnetic bolts and this apparent magnetic field, a compass correction was required for each site. This correction was applied to all the data from a site until the velocity vectors flowing into the study section were pointed reasonably downstream. The correction at Minus 4-Mile Bar was -40˚ and the correction at Upper Rattlesnake was -35˚. This compass correction does not affect the reported velocity magnitudes, only the direction of the velocity vector as shown in the flow-field maps.

The velocity flow field and the bathymetry from Minus 4-Mile Bar are shown in Figure 4.3. Roughly 13 transects were made covering a distance of just over 1.1 km. The river centerline is shown, expressed as a distance in miles above Lee's Ferry. As the flow entered the study reach, a wide, shallow, 1-2 m deep section with low velocities (around 1.0 m/s) was pinched by a long cobble bar forming along the right side of the river. The flow was pushed to the left and accelerated to over 2.0 m/s. The depth in this faster section of the channel increased to roughly 5.0 m. The flow then curved toward the right in a meander bend with a deep channel near the outer bank and reduced flow velocities.

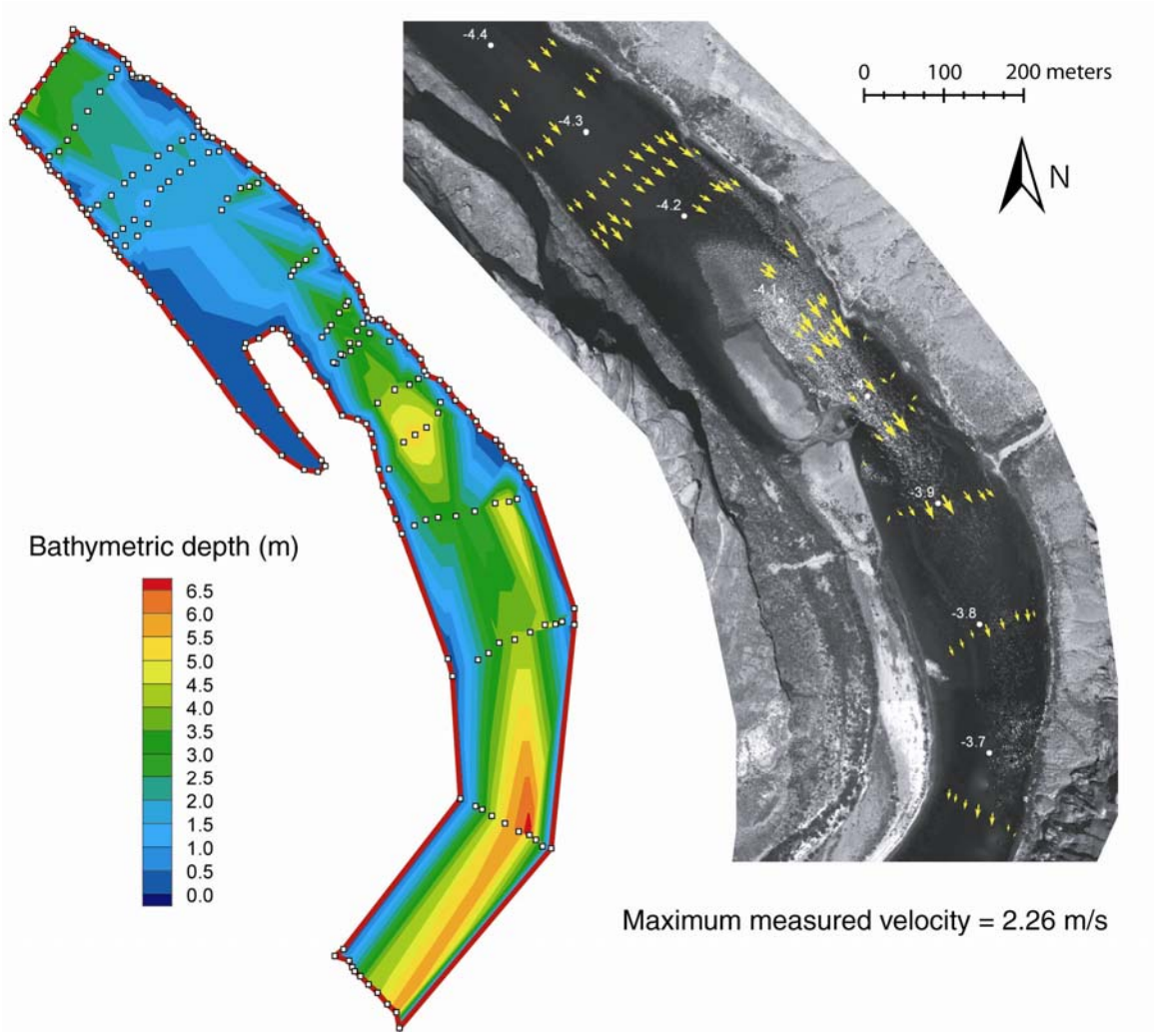

Figure 4.3: Bathymetry (left) and velocity (right) maps of Minus 4-Mile Bar in Glen Canyon. River miles relative to Lee's Ferry are indicated with the white dots. The greatest depth measured was 6.8 m, on the outside of the bend.

The greatest depth measured at this site, 6.8 m, occurred in this meander bend; velocities here dropped to below 1.0 m/s. Overall, the highest velocity measured at Minus 4-Mile Bar was 2.26 m/s and all velocities appeared to be within the capability of the instrument. It is interesting to note that in the clear water of Glen Canyon, the signal strength of the instrument was unusually low—typically below 100 counts. Signal strength is an internal instrument metric that reports the strength of the return signal from particles in the water; one count equals 0.72 dB. Signal strength is a function of the amount and type of particulate matter in the water. In Grand Canyon, where suspended sediment is much higher, signal strength ranged from 180 to 200.

Overall velocity magnitudes in Upper Rattlesnake Rapid (Figure 4.4) were higher and more variable than in Glen Canyon. Velocities were measured in the smooth water above the rapid, but most measurements from the core of the rapid were unusable due to ambiguity jumps. Below the rapid, waves and turbulence jostled the boat, and ambiguity jumps were common. In all, 63 velocity measurements were made at Upper Rattlesnake with a peak value of 3.19 m/s. Figure 4.4 also shows the velocity direction switch in the alternating transects of the upper pool we attribute to a boat-based magnetic field.

At Upper Rattlesnake Rapid, a total of 101 depth measurements were made throughout the rapid complex, allowing us to create a map of the river bottom (Figure 4.4). River depths leading into the rapid were 6-8 m, and a deep scour hole of 23.4 m was measured below the rapid. This deep scour hole was comparable to scour holes measured on other large rapids in Grand Canyon (Howard and Dolan, 1981), suggesting Upper Rattlesnake was once a larger rapid. The depth in the shallowest part of the rapid was

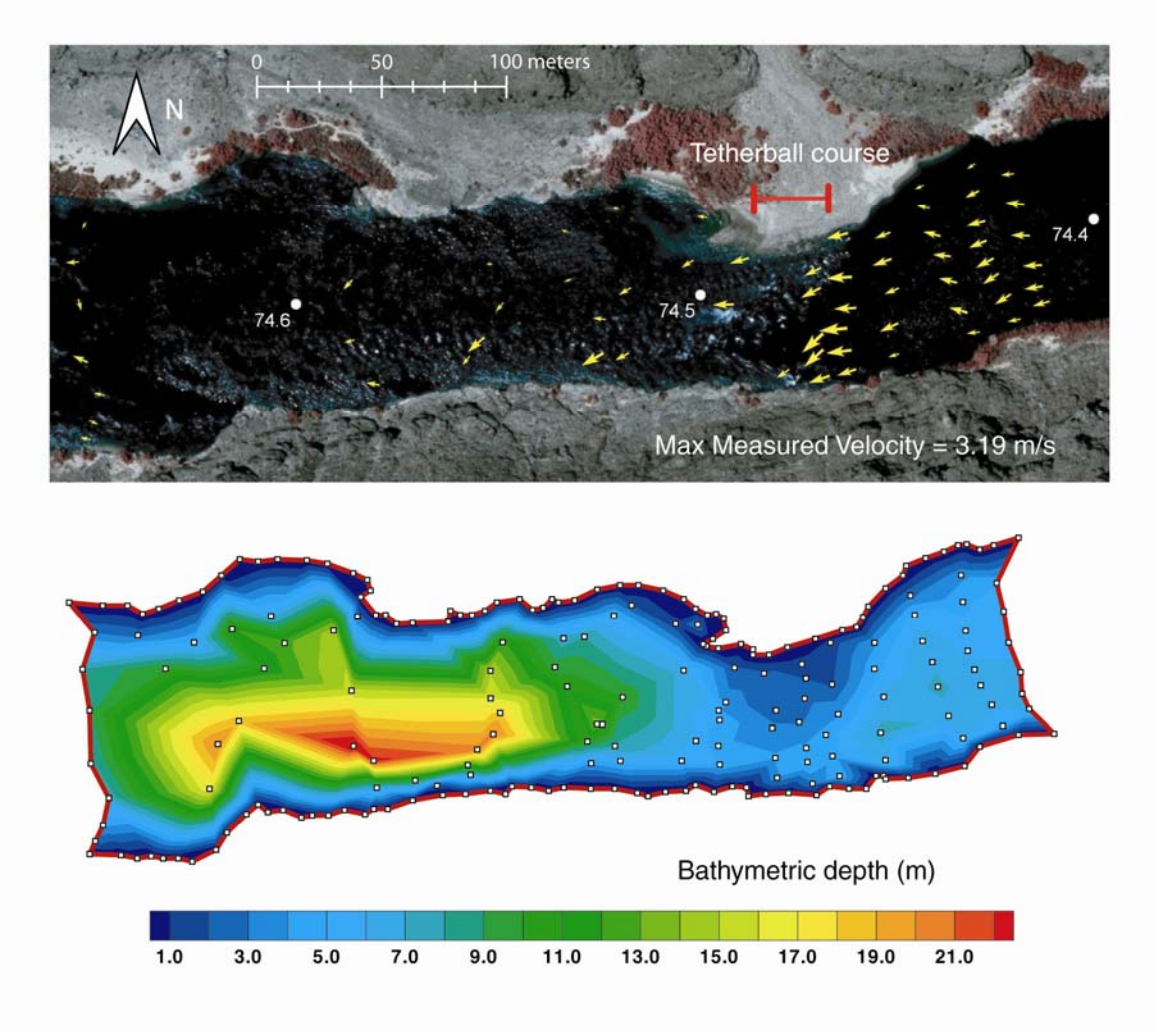

Figure 4.4: Velocity (top) and bathymetry (bottom) maps from Upper Rattlesnake Rapid. River miles relative to Lee's Ferry are indicated with the white dots. The 30 m tetherball course is shown. The maximum depth of 23.4 m is found in the below-rapid scour hole.

4.15 m, and a sub-aqueous debris mound is visible at the tributary mouth. While a number of researchers have measured depth traces floating through rapids (Leopold, 1969; Randle and Pemberton, 1987), to the best of our knowledge, this is the first bathymetry map measured in the core of a Grand Canyon rapid. The fathometer used in the study was a capable instrument. While it would occasionally fail in the largest, most turbulent and aerated zones, it generally was able to return data for almost every part of the rapid surveyed.

Tetherball speeds were measured at Upper Rattlesnake just before the ADV run. The average velocity of all 15 tetherballs was 3.94 ± 0.09 m/s. The tetherball course was 30 m long and integrated the velocity of the path of the tetherballs leading into the middle of the rapid.

4.3 Discussion

Figure 4.5 shows a composite of velocity measurements as a function of river mile for both study sites. At Minus 4-Mile Bar, velocities slowly increased from roughly 1.2 m/s to a maximum of 2.26 m/s over a span of 600 m. This maximum velocity occurred where the cobble bar constricted the flow. Within Upper Rattlesnake Rapid, flow velocities accelerated more quickly; rising from a free-stream value of roughly 2.0 m/s to over 3.19 m/s in a distance of 25 m. Flow velocities in the rapid rose well above 3.5 m/s and are at least 3.94 m/s, the value measured with tetherballs tracers. Direct measurements of flow in the core of the rapid could not be made with the ADV instrument. Kieffer (1987) measured flow velocity in Grand Canyon rapids as high as 7.5

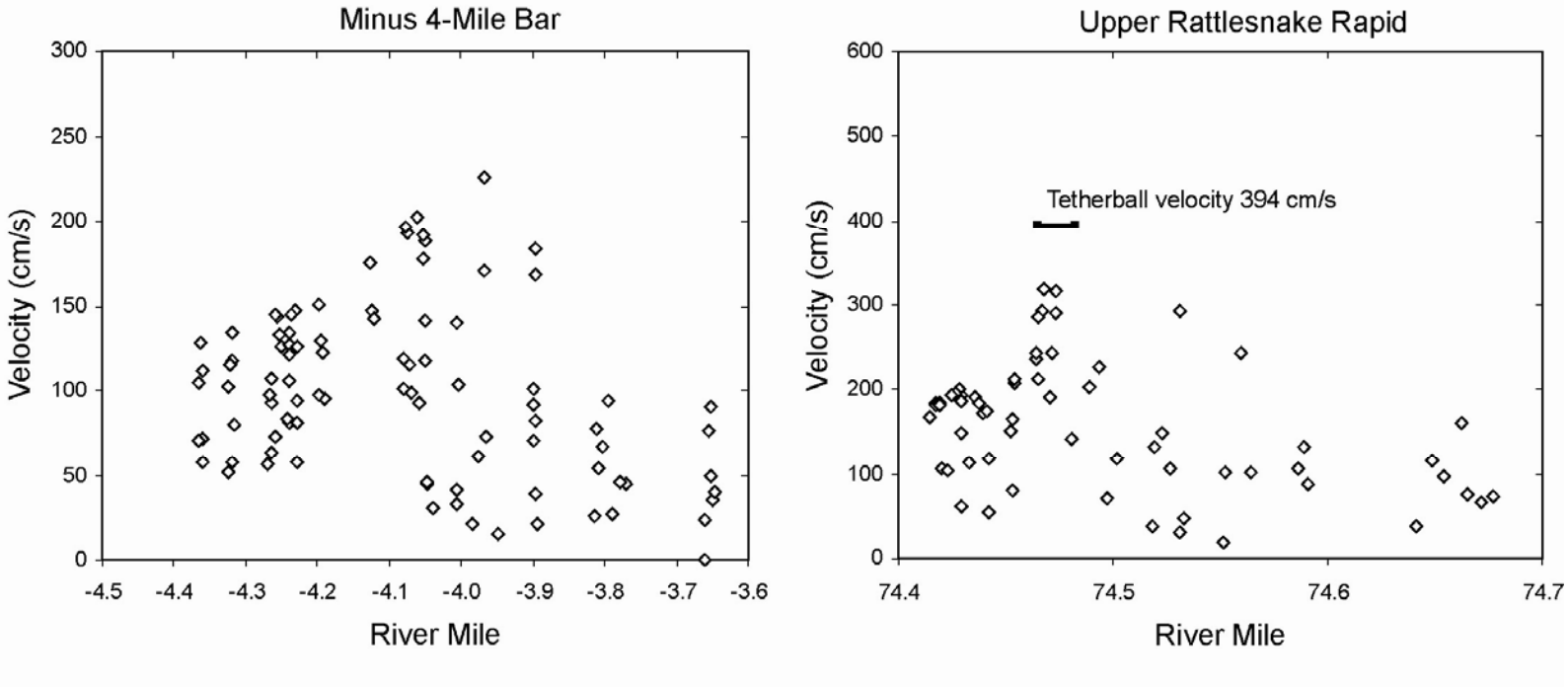

Figure 4.5: Graph showing horizontal velocity values for Minus 4-Mile Bar (left) and Upper Rattlesnake Rapid (right). Note the axes are at different scales. Also included on the Upper Rattlesnake graph is the surface velocity from the 15 tetherballs.

m/s, and the peak flow in Upper Rattlesnake Rapid probably approaches 6 m/s.

As a byproduct to collecting velocity and bathymetry data, the morphology of the water surface was also determined. Figure 4.6 shows the water-surface profiles of both sites. The fall in water surface through Minus 4-Mile Bar occurred mostly upstream of the cobble bar. The slope was small, just 0.4 m in 800 m. Comparing Figures 4.5 and 4.6, the greatest velocities occurred near the bottom of the long fall at Minus 4-Mile Bar. In contrast, the greatest velocities in Upper Rattlesnake Rapid occurred at the top of the fall. The overall drop through Upper Rattlesnake Rapid is 0.8 m and occurred within 65 m. The higher consumption of river energy in this rapid (*i.e.*, dissipation of stream power) offered a simple explanation as to why Upper Rattlesnake contained large breaking waves and high turbulence while Minus 4-Mile Bar did not.

4.4 Conclusions

This study attempts to use modern acoustic instrumentation to directly measure flow velocities in a rapid on the Colorado River. Valuable flow data in all but the highest-velocity regions of Upper Rattlesnake Rapid in Grand Canyon were recorded and mapped. Within the alluvial reach of Minus 4-Mile Bar in Glen Canyon, a comprehensive flow field of velocity vectors was mapped. In addition, extensive bathymetric mapping was successful for both study sites. In the case of Upper Rattlesnake Rapid, the resulting depth chart is the best and most comprehensive data set reported for a rapid in Grand Canyon. Finally, the 3-D water-surface elevations measured in each study reach offer a

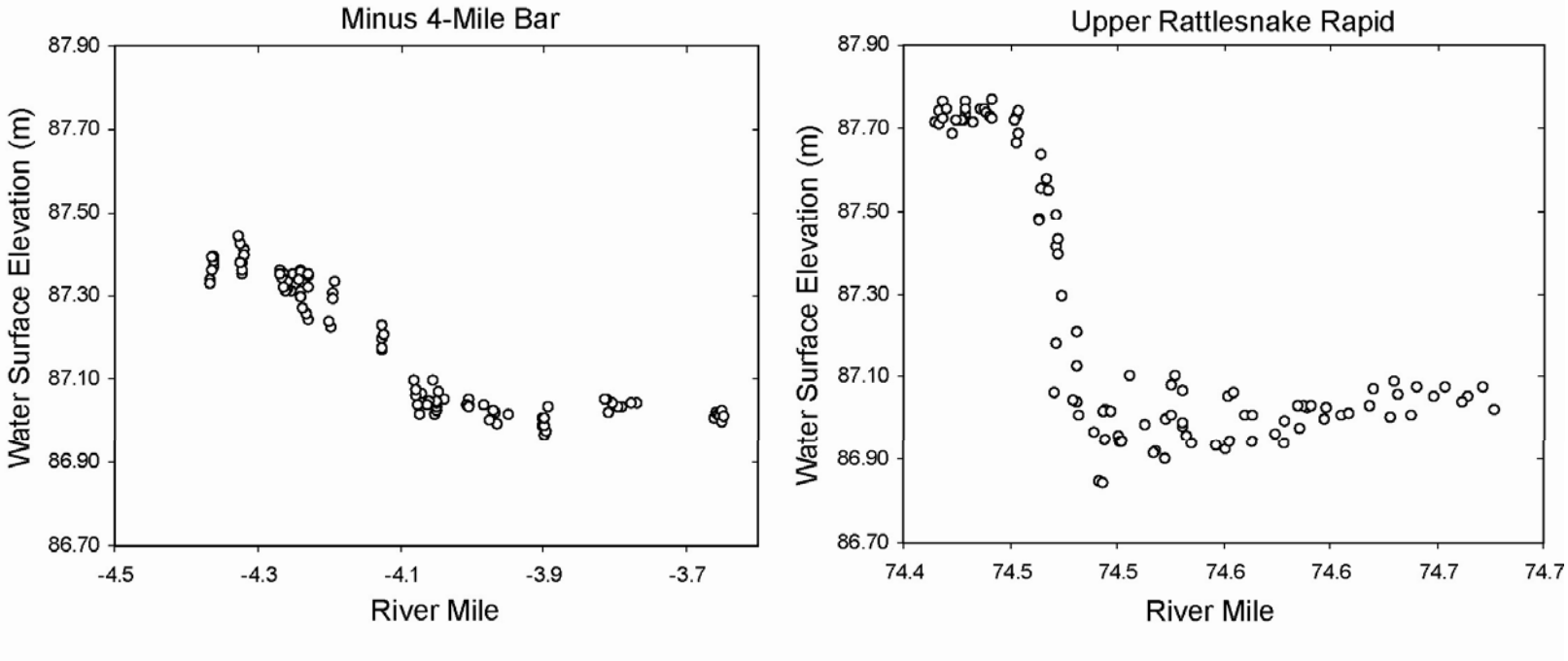

Figure 4.6: Graph showing water-surface profile for Minus 4-Mile Bar (left) and Upper Rattlesnake Rapid (right). The elevations are expressed in similar relative vertical scales, but the horizontal scales are different.

valuable morphological data set that can be used to characterize the river and its free surface.

One of the goals of this study was to measure top velocities in the core of Grand Canyon Rapids. While the ADV did measure flow velocities in Glen Canyon and the slower sections of Grand Canyon, the instrument as configured was unable to measure many higher velocities found within rapids. The instrument chosen used a side-looking probe arrangement; a downward-looking probe arrangement would have been better at measuring horizontal velocities and may have had a higher upper limit than 3.0 m/s. Either way, the ADV family of instruments has an upper measurement limit of 4.5 m/s and cannot measure peak velocities of Grand Canyon rapids.

For future research, the goal of directly measuring velocities in the core of rapids remains important. Such data would lead to insight into the transport processes distributing coarse-grained sediment in bedrock-controlled rivers. ADCPs may be a more appropriate tool for measurement purposes, although turbulence and bubbles in the rapid may create challenges. It is likely a fundamentally different flow measurement technique is needed.

5. FLOW MEASUREMENT IN RAPIDS AND FAN-EDDY COMPLEXES OF THE COLORADO RIVER

Rapids occur in bedrock-controlled rivers where constrictions accelerate the flow to near-critical conditions, resulting in breaking waves, air entrainment, and a steep localized slope. Along the Colorado River and its major tributaries in the western United States most rapids form in response to the collection of coarse-grained sediment at the mouths of tributaries (Cooley *et al.*, 1977; Howard and Dolan, 1981; Kieffer, 1985; Kieffer, 1987; Melis *et al.*, 1994; Webb 1996; Webb *et al*., 2000; Webb *et al.*, 2004). In turn, coarse-grained sediment and the rapids they create dominate the morphology in most bedrock-controlled reaches of the river, leading to alternating sections of rapids and pools.

In Grand Canyon, Leopold (1969) termed the sequence of slower reaches of water alternating between steep constrictions the "pool-and-rapid" morphology. The same morphology is present in other river reaches where debris flows occur, including Cataract Canyon in central Utah. When viewed in profile, the pool-and-rapid morphology gives the river a stair-step appearance, and this morphology is termed the fan-eddy complex when observed in plan view. Schmidt and Rubin (1995) demonstrated the role of the fan-eddy complex in storing sand in eddy bars near rapids. Hazel *et al*. (2006) showed most sand storage within Grand Canyon is within the eddy bars associated with rapids.

Rapids not only dominate the fluvial geomorphology on the Colorado River, they also strongly influence the aquatic ecology. The first large rapids below Lee's Ferry efficiently saturate the river's level of dissolved oxygen, and periodic rapids in Grand Canyon maintain saturated oxygen conditions throughout the river corridor (Stevens *et al.,* 1997). In addition, biomass production in Grand Canyon is greatest on the coarse-sediment substrate of the rapids and riffles (Stevens *et al.,* 1997). Biologists speculate the native fish population evolved to survive the extreme velocity and turbulence of the Colorado River pool-and-riffle morphology (Douglas and Marsh, 1996).

Rapids can also be an important recreational resource for the public (Loomis *et al.*, 2005). The rapids within Grand Canyon and Cataract Canyon are the principal attraction for thousands of river runners who use the river annually. Those rivers offering rapids with navigational difficulties (*i.e.*, fast water and large hydraulic features—waves) tend to be popular.

Despite their importance, the scientific literature offers relatively little quantitative data on rapids. Little is known of the peak velocities through rapids; less is known of the flow structure throughout the water column and the strength and direction of shear stresses acting on the bed. Even fundamental topologic data sets consisting of bathymetry and water-surface topography are generally unavailable. Such fundamental data would be needed to build complicated numerical models (*e.g.*, computational fluid dynamics, CFD) offering insight into the mechanics of rapids. New flow-measurement techniques developed in this study are enabling the collection of hydraulic and bathymetric data from rapids.

5.1 Previous Velocity and Bathymetry Measurements in Rapids

Kieffer (1987) was one of the first to measure velocities in rapids. Using a calibrated video camera and floating tracer particles, she videotaped the movement of particles through large rapids in Grand Canyon to measure, in a Lagrangian frame of reference, velocity along trace lines. She measured velocities as large as 7.5 m/s. While the measurement technique was clever, the floating particles were subject to waves and wind at the surface affecting measured flow values. Webb *et al.* (1997) also used floating tetherballs to measure surface velocity through a number of rapids in Grand Canyon. Cluer (1997) used an acoustic Doppler current profiler (ADCP) to measure flow in a recirculation eddy near Mohawk Canyon in western Grand Canyon. His work, however, focused on the erosion of sand bars on the lower portion of the fan-eddy complex, and he did not measure velocities directly in the rapid. An ADCP was also used to measure velocity, shear, and sand transport processes in the tail waters of a fan-eddy complex in eastern Grand Canyon during the flood of 2004 (Wright and Gartner, 2006). Tinkler (1997) used floating particles to measure flow velocity in rapids in bedrock channels. He then correlated velocity and the wavelength of wave crests in the rapids, providing a visual method to estimate water velocity safely from the shore. Hotchkiss *et al*. (2003) used an acoustic Doppler velocimeter (ADV) to measure velocity of water funneling into a dam spillway, and Lai (2005) published ADCP data measuring velocities in the recirculation eddies below a dam spillway. Recently, Magirl *et al*. (2006) used an ADV mounted on a powered boat to measure the velocity field 40 cm below the surface at a small rapid in Grand Canyon and a riffle in Glen Canyon. They also recorded depths

below the rapid with a digital fathometer, creating coarse yet useful bathymetric maps of both the rapid and riffle.

The present study builds on the ADV work of Magirl *et al*. (2006) applying two new flow measurement technologies to the problem of quantifying the mechanics of hydraulics in rapids. The first of the new technologies is an ADCP. Long used for discharge measurements and determining velocity profiles in alluvial rivers (Yorke and Oberg, 2002), the ADCP has the ability to measure velocities throughout the vertical water column and simultaneously record bathymetry. The second instrument is a pitot-static tube designed and built at New Zealand's National Institute of Water and Atmospheric Research. The instrument is known as the Pressure Operated Electronic Meter (POEM) and was used by Smart to measure velocity and turbulence in swift mountain streams (1994; 1999). Nikora and Smart (1997) also used the POEM to characterize turbulence, velocity, and velocity structures for a number of fast-flowing gravel-bed rivers in New Zealand. ADV data were collected in Grand Canyon whereas ADCP and POEM data were collected in Cataract Canyon.

5.2 Hardware and Instrumentation

All velocity measurements were made from a 5.5 m boat designed to navigate rapids. The boat had a catamaran design with two 6 m inflatable tubes providing buoyancy; a rigid aluminum frame strapped between provided structural support and a working platform (Figure 5.1). The boat was powered by a 50 HP outboard motor and, when stripped of gear, was swift enough to travel up many rapids. A personal computer

Figure 5.1: Boat equipped to make flow velocity measurements in Salt Creek Rapid within Grand Canyon. Diane Boyer is under the sun shade monitoring the computer and making field notes (photograph by C. Watkins).

was used to operate the instrumentation and was strapped in a water-resistant case, easily stowed if necessary. Power for all instrumentation and computers was taken directly from the motor's alternator, which was attached to a marine battery mounted next to the motor. The 12-volt DC power source from the alternator was tied into a 120-volt AC power inverter mounted safely in a dry aluminum cross box in the center of the boat. Instruments and computers were plugged directly into the inverter as needed.

5.2.1 Flow Instrument Deployment: Boom Design

A pivoting boom attached to the front of the boat (Figure 5.1) provided the means to deploy each flow-measurement instrument. A number of considerations, safety and robust reliability being most important, governed the boom design. The original design required that one person was able to deploy and retract the instrument in less than 3 s. In the maximum design flow velocity (12 m/s), the boom could deflect no more than 5 cm and the amplitude of any flow-induced oscillations needed to be less than 1 cm. Minimizing the drag force on the boom while keeping the design as simple as possible was important. While the device was designed to position the instrument up to 3 m below the water surface, subsequent testing indicated the boat operation was compromised at deployment depths greater than 1.5 m. Also, while unlimited depth resolution during deployment was initially desired, it was determined that fixed adjustments within a 76 mm resolution was acceptable.

A number of worst-case scenarios were considered in the design. The most probable event would be damage to the instrument from striking a submerged obstacle

while the operator was trying to retract the boom. The most dangerous event would be loss of ability to keep the boat pointed upstream while the boom was deployed. If the boat began to turn sideways in the flow, the boom could act as a keel, quickly and forcefully pivoting the boat. If the instrument or boom were to hit a submerged boulder during this violent rotation, the possibility of capsizing was high.

A single-motion retraction of the boom was determined to be a requirement to minimize the possibility of flipping the boat. Rotation about a single axis was significantly less complicated than a rack-and-pinion mechanism, eliminating the possible failure modes of gear and/or ratchet malfunction. The primary advantage of rotating the boom about an axis for deployment and retraction is being able to retract the boom from the water quickly in an emergency. Furthermore, a rack-and-pinion gear-driven system would require a large gear ratio to enable retraction of the system manually in less than three seconds. Also, complete retraction of the instrument above the water line would require the system be mounted at least a 30 cm higher than the top of the boat pan. “Telescoping,” or deployment of the boom like a car antenna, was quickly dropped as a design alternative due to its inherent complexity, cost, and lack of rigidity.

Initial calculations of drag forces on different boom shapes pointed to the necessity of minimizing the projected area and using a stiff material to achieve the deflection performance. The ADV and ADCP flow instruments were found to contribute a large proportion of the deflection force, due to the amount of area exposed to flow and distance from the pivot point. Flexibility in depth adjustment made it impractical to use a boom shape without flat features to mount to the rotational plate and instrument. Sail boat

extruded mast shapes were initially investigated owing to stiffness and low drag coefficients; drag coefficients for a 127 x 89 mm airfoil mast extrusion were five to ten times less than a cylindrical cross section of the same frontal area. The main drawback with using an airfoil-shaped boom was the difficultly in adjustment of the instrument depth; the non-flat sides would require a custom clamping mechanism to fix the boom in place. Also, high clamping forces required to fix the boom in position would potentially crumple the mast. Prismatic pipe and rod shapes were also analyzed for deflection performance. These geometries did not work because increasing the diameter or sidewall length to provide stiffness also increased the frontal area exposed to the force of the water making a cylinder or prismatic system impractical for the anticipated forces and depths of flow.

Eventually, a 127 x 51 mm cross section of schedule 80 structural stainless steel tubing (box-beam) was selected for the design. In addition to strength, the stainless steel minimized magnetic interference to the flow instruments: both the ADV and ADCP use a compass to reference flow velocity vectors to magnetic north. The tubing of the boom was augmented with a piece of angle iron welded on the frontal face to approximate an airfoil shape and reduce drag (Figure 5.2). This shape had the benefits of being easy to source, easy to manufacture, and easy to configure as required. This shape was also cost effective. Without considering the reduction in drag effect resulting from the leading angle-iron nose, this shape met the worst case goals of less than 5 cm deflection when deployed at 3 m depth and exposed to 12 m/s flow. A series of holes were drilled through the tube to allow adjustment of the boom depth in 76 mm increments. A standard 25.4

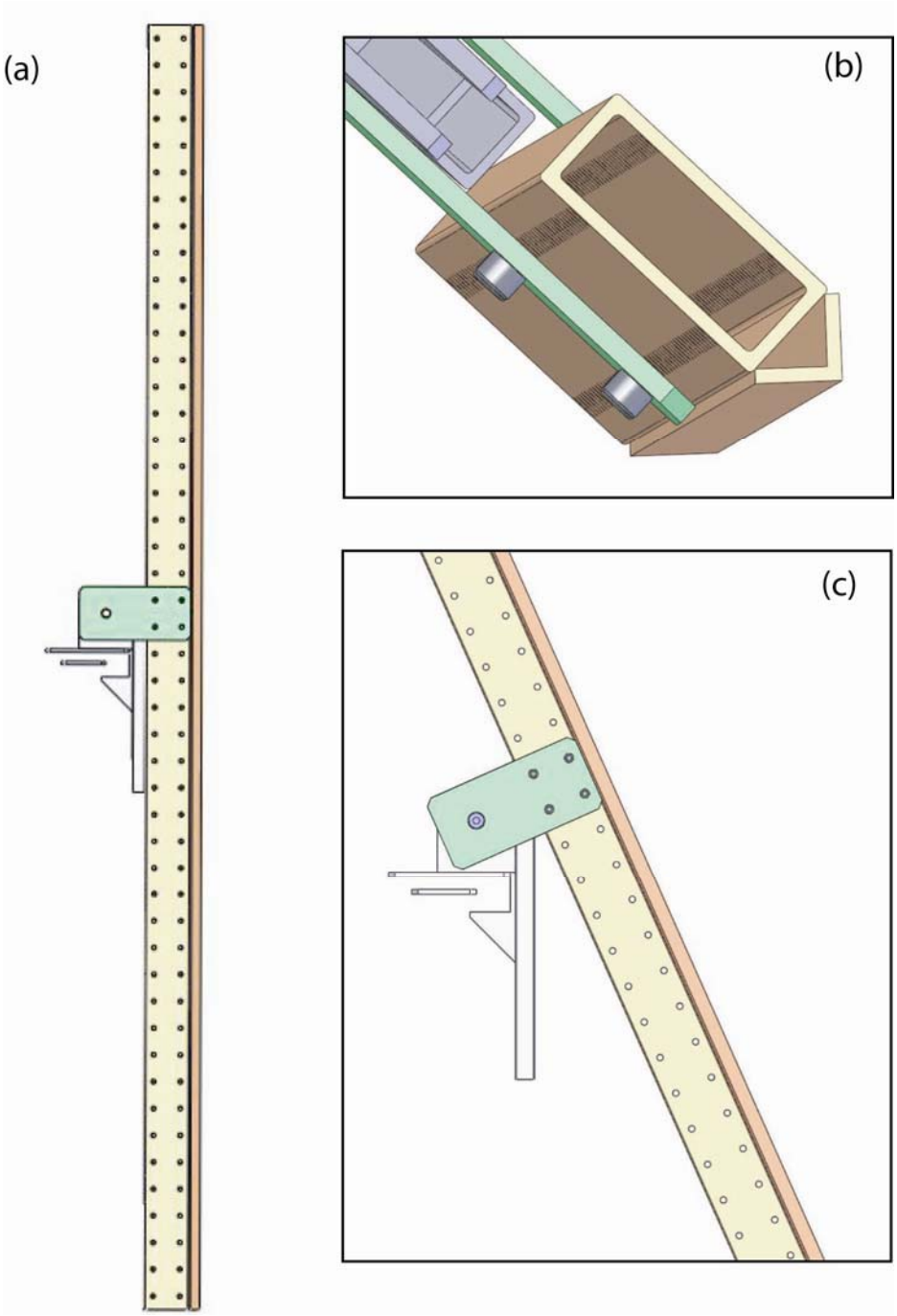

Figure 5.2: Computer generated drawings of the flow-instrument boom assembly: (a) in side view showing the mount to the boat, (b) an isometric view showing the mast cross section, and (c) the boom rotating around the pivot during instrument deployment (illustrations by S. Cunningham).

mm diameter shoulder bolt was used as the pivot axis. Welds were added to all non-moving connections to increase strength. Mounting to the boat was designed to be accomplished with clamp plates sandwiching the boat pan but, in the end, it was decided that standard C-clamps were easier to implement and provided sufficient strength.

The boom's robust design and hole-mount pattern, 76 mm center-squared, allowed flexibility in mounting any of the intended flow-measurement instruments. While desirable to deploy multiple instrument simultaneously, power concerns, complexity, and safety dictated that no more than one instrument would be operated at any given time. Ultimately, the boom design proved both robust and safe. The deployment/retraction time of the boom was less than one second, and the stainless steel design has thus far survived a number of heavy collisions with boulders and bedrock while in transit through several hundred kilometers of river.

5.2.2 Point Velocity Measurements

A 10 Hz Argonaut acoustic Doppler velocimeter (ADV), manufactured by Sontek/YSI, was used for point velocity measurements in Grand Canyon and Glen Canyon (Magirl *et al.*, 2006). The instrument operates by pinging acoustic energy at a known frequency into the flowing water using an array of three pressure transducers. By evaluating the Doppler shift in the frequency of the sound waves bouncing off particles suspended in the flow, the three-dimensional velocity of the those particles relative to the instrument probe is calculated. The instrument is able to measure velocity at a 1.0 cm^3 point volume located 10 cm in front of the transducer probe. With a built-in compass and

tilt meters, the instrument reports velocity in a global reference frame, V_{east}, V_{north}, and V_{up}. The averaging time for a given measurement must be at least 3 s, requiring at least 30 pings. Five seconds of averaging was used in this study. In theory, the instrument is capable of quantifying turbulence in the flow, but with the required averaging time of 3 s, an exceptionally long dwell would be needed to measure the standard deviation of turbulent fluctuations.

The adopted procedure for ADV measurements required a dwell of 15 s to collect at least 3 averaged velocity vectors. The instrument probe was placed 40 cm below the water surface. The instrument had a three-dimensional side-looking transducer probe. After obtaining the instrument, we learned the side-looking probe, while good for making measurements in shallow water, was a poor choice for flow measurement in rapids. According to the manufacturer, the alternative down-looking probe is able to measure greater water velocity (Craig Huhta, Sontek/YSI, personal communications, 2006). If the flow velocity across the probe is too fast, the returning Doppler-shifted pings will be so extreme as to confuse the instrument processor into reporting unrealistic velocity values. This error condition is known as an "ambiguity jump" and is manifested in the Grand Canyon data as exceptionally high vertical velocity with corresponding small horizontal velocities (Craig Huhta, Sontek/YSI, personal communications, 2006). All data exhibiting the characteristics of ambiguity jumps were discarded.

In Cataract Canyon, the POEM used by Smart (1999) was employed to measure point velocity and turbulent fluctuations. Essentially the same flow-measurement technology used in aircraft for nearly a century, the POEM is a streamlined pitot-static

tube with a built-in, fast-response (28 Hz) differential pressure transducer. With the POEM, the measurement procedure required a dwell in a given location for 60 s. In all 1,686 individual velocity values were collected from a measurement location. Measuring the difference between the oncoming flow's stagnation and static pressures, the instrument uses Bernoulli's principle to estimate free-stream flow velocity (Fox and McDonald, 1985). Electronics housed within the instrument convert the pressure signal to an analog radio frequency that is transmitted by wire to an A/D converter located on the boat. Conversion of the signal to radio waves in the instrument allows communication wires to be exposed to water without electrical shorting of the signal. The POEM was mounted 39 cm below the water surface and attached to the end of the boom assembly with a pivoting steel rod. The pivot of the rod (roughly ±15° around an axis parallel to the boom-rotation axis) allowed the streamlined POEM to self-adjust its angle of attack to the oncoming flow. The hydrodynamic design of the POEM was extremely stable in fast water, and in contrast to the ADV or ADCP, the combined drag of the boom and the POEM was small allowing nimble response of the boat in fast water. The POEM returned only a scalar quantity of velocity magnitude. To determine the direction of the vector of the oncoming flow, the angle of direction of the boat relative to the shore was recorded during a given measurement.

The fast-response pressure transducer allows the instrument to sample high-frequency turbulence (Nikora and Smart, 1997), and turbulence analysis was performed using the POEM-collected data. Following the averaging concepts introduced by Reynolds (1895), time averaging is appropriate for stationary turbulence unchanging in

time or space (Wilcox, 1993). Looking at the instantaneous velocity, $u_i(x,t)$, of turbulent flow shown in Figure 5.3, we see the velocity can be expressed as the sum of an average part, $U_i(x)$, and a fluctuating part, $u'_i(x,t)$, such that

$$u_i(x,t) = U_i(x) + u'_i(x,t) \tag{5.1}$$

In processing the POEM data collected from Cataract Canyon, the mean-flow velocity, U_E, was readily calculated from,

$$U_E = \frac{1}{T}\int u_i(x,t)dt \tag{5.2}$$

The relative turbulent intensity, $\hat{u}$, is defined as the root-mean-squared of the velocity fluctuations normalized against mean velocity,

$$\hat{u} = \frac{\sqrt{\overline{u'^2}}}{U_E} \tag{5.3}$$

and represents the strength of the turbulent fluctuations relative to the magnitude of the free-stream flow velocity (Wilcox, 1993). Similarly, turbulent kinetic energy (TKE) is defined as,

$$k = \frac{1}{2}\left(\overline{u'^2} + \overline{v'^2} + \overline{w'^2}\right) \tag{5.4}$$

where v' and w' are the velocity fluctuations in the y and z directions (Wilcox, 1993). If the turbulence is isotropic,

$$\overline{u'^2} \approx \overline{v'^2} \approx \overline{w'^2}$$

and equation (5.4) reduces to

$$k = \frac{3}{2}(\overline{u'^2}) \tag{5.5}$$

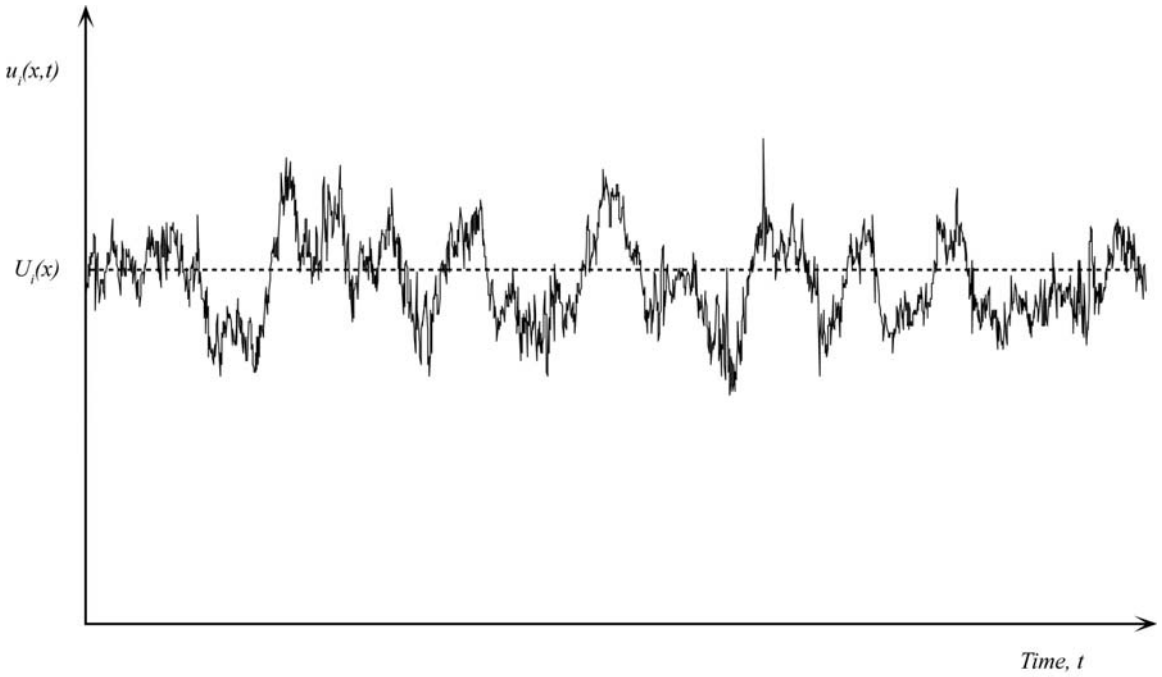

Figure 5.3: Example of turbulent velocity measured by the POEM. The instantaneous velocity, u_i, at a given location, x, is a function of time, t.

While there is no way of knowing *apriori* if the turbulent structures in the Colorado River are isotropic, this assumption was made to enable the use of equation (5.5) to calculate a value of TKE. Because measurements were made near the water surface, away from the shear zone at the boundary of the bed, this first-order assumption of isotropic flow may be sound.

Dynamic fluids dissipate energy with turbulence. If the Reynolds number is large enough, energy is imparted into a flow at zones of high shear. Flow past a solid surface, whether it be a baseball, an airfoil, or the wetted boundary of water in an open channel, will generate turbulent eddies in the shear zone near the surface that quickly advect into the main flow. The largest eddies are generated directly from the shear zone. These large eddies stretch and break into smaller eddies which, in turn, break into still smaller eddies. This breakdown of the eddy structure continues down to the smallest scales of turbulence in a process termed the energy cascade (Pope, 2000). The smallest eddies dissipate turbulent motion into heat. The rate of the energy cascade is controlled not by the smallest eddies but rather, by the rate of generation of the largest turbulent eddies in the flow (Pope, 2000). In addition, the characteristic eddy length of the largest eddies in the flow are on the same order of magnitude as the features generating the turbulence (Wilcox, 1993). If the turbulence is generated by a flow past a baseball, the largest eddies will be on the order of magnitude of the baseball. Similarly, if the turbulence is generated by a river, the largest turbulence eddies will be similar in size to the width of the river. The fast-response pressure transducer in the POEM is able to resolve all length scales of turbulent structures in flowing water, including the smallest eddies which dissipate into

heat. Analysis of the POEM data allowed insight into the turbulent structures of flow directly in a rapid.

5.2.3 Velocity Profile Measurements

An ADCP was employed for making velocity measurements throughout the water column. ADCPs collect bathymetry concurrent with velocity measurements. The ADCP's theory of operation is well documented (RDInstruments, 1996; Gartner and Ganju, 2002; Yorke and Oberg, 2002). An ADCP pings acoustic energy into the water column with four separate transducers pointed 20° away from the primary instrument axis. The transducers are oriented toward the front, back, left, and right of the instrument in such a fashion to evaluate the flow conditions along each beam. From each transducer, the ADCP pings a known acoustic frequency; this acoustic energy bounces off suspended particles moving with the flow and allows the instrument to calculate particle velocity by evaluating the Doppler shift of the returning signal along each beam. A collection of pings, or an ensemble, represents the averaged measurement of multiple pings. By filtering the return signal, velocity at set distances away from the instrument, termed bins, are calculated. If tracking across a river while collecting measurements, the instrument builds a map of water profiles in the water column where the bins represent velocity at different depths and the ensembles represent the position along the boat path. If the boat is held stationary while making measurements, the ensembles represent different velocity measurements at a given fixed location as a function of time. Each ensemble consists of two water-profile pings and three bottom-track pings, rendering the approximate sample

rate to be roughly 1 Hz for the data collected in this study. In calculating velocity within a particular bin, the instrument assumes flow is homogeneous, a required assumption because the ADCP uses multiple beams to calculate flow velocity. Occasionally, individual bins, or even entire ensembles, are lost during data collection. Missing bins and missing ensembles can result from swirling flow, excessive turbulence, or attenuation by air bubbles in the water column. By collecting multiple data at a single location, missing bins and missing ensembles are averaged out of the final data set.

Two separate ADCPs, manufactured by Teledyne RD Instruments, were used to make velocity measurements in Cataract Canyon. The first was a 600 kHz Workhorse suited to making lower-resolution measurements in sediment-heavy flow. The second instrument was a 1,200 kHz Rio Grande providing better relative accuracy (*i.e.*, a smaller standard error) with the drawback that its acoustic signal is attenuated more quickly in water with high suspended load. In addition, the user of the 1,200 kHz ADCP can chose to reduce the relative accuracy of the instrument and increase the number of bins, essentially increasing the measurement resolution in the water column. The instrument transducers were placed 69 cm below the water surface for most measurements. A shallower placement of 38 cm proved problematic with the velocity signal essentially dropping out while in the faster water near the rapid. A large bow wave formed on the instrument at a mounting depth of 38 cm suggests air entrainment under the transducers likely interfered with the acoustic signal. The bin size for the 600 kHz machine was set to be 0.50 m with the center of the first bin 1.55 m below the surface; the bin size for the 1,200 kHz machine was set to be 0.25 m with the center of the first bin 1.30 m below the

surface. A blank distance of 25 cm was used for both instruments. Water Mode 1 was chosen as the sample mode for both instruments; this sample mode is the most robust of the sample modes and should be good for water velocity up to 10 m/s. This mode is generally assumed to operate well even in flows with high shear and turbulence.

For the ADCP measurements, two modes of data were collected: dwell and interdwell data. Each mode exhibiting advantages and disadvantages when measuring velocity or bathymetry. During a particular ADCP measurement session, transects were measured in the pool above the rapid progressing downstream until the hydraulics of the rapid became too severe to continue. As was done with the POEM, ADCP measurements were made at given locations for a dwell period of about 60 s; the final data from a given dwell location represented roughly one minute of integrated flow. The benefit of capturing multiple data at a single dwell location lies in ensemble averaging; the standard error of a measured ADCP profile decreases by a factor of the square root of the number of measurements averaged, improving the overall measurement quality. As the boat tracked between dwell positions, velocity and depth were continuously recorded by the ADCP. These interdwell data, in contrast to the 60 s averaged dwell data, had higher variability in the velocity measurement owing to the lack of ensemble averaging.

Bathymetry data collected during interdwell measurements, however, were more robust, not requiring ensemble averaging. ADCP bathymetric data is collected along each of the four beams oriented 20° from the instrument axis. The instrument averages the depths measured from the four beams, assuming the bathymetry directly below the instrument is equivalent to this average.

The ADCP uses bottom-tracking algorithms and a GPS signal to calculate its relative position in the river. When bedload is present, the moving bed creates a drift error in the bottom-track algorithm and GPS tracking is used exclusively. A Trimble AG132 differential GPS unit was attached to the ADCP to aid in tracking, particularly for the interdwell measurements. While the steep canyon walls of Cataract occasionally blocked visibility to satellites, the position of the boat was surveyed into local coordinates at each dwell location allowing correction of the GPS position and improved positional accuracy of any given ADCP measurement.

Velocity profiles in alluvial rivers and prismatic channels are well characterized (Chow, 1959; Leopold *et al.*, 1964; Henderson, 1966). Velocity typically follows a logarithmic profile of the form:

$$\frac{u(y)}{U} = \ln\left(\frac{y}{H}\right) \tag{5.6}$$

where *u(y)* is the velocity at a given height above the bed, y. U is a velocity scaling factor and H is a height scaling factor (Allen, 1985). In analyzing the hydraulic structures in rapids using ADCP data, one of the salient questions is whether the logarithmic velocity profile assumption holds. To answer this question, logarithmic regression curves were fitted to each of the velocity profiles collected with the ADCP. The correlation coefficient, R^2, quantifies the quality of fit of the logarithmic trendline to the data.

5.2.4 Bathymetry

In addition to collecting bathymetric data with the ADCP, depths were recorded with depth soundings measured with a Lowrance X59DF dual-frequency fathometer. When working with the ADV or POEM, bathymetry could only be collected with the fathometer. Details of the fathometer can be found in Magirl *et al*. (2006). At each dwell location, where velocity data were collected, the depth, as measured by the fathometer, was manually recorded. The fathometer transducer was mounted to the back of the boat, approximately 5 m away from the velocity instrument. In processing bathymetry for a given site, all the acceptable bathymetry data were integrated into a three-dimensional map. The bathymetry map, therefore, can include data collected with either ADCP or fathometer and may include data collected on different days. For Grand Canyon, all bathymetry data were normalized to a standard 227 m^3/s discharge using stage-discharge relations generate with the Grand Canyon HEC-RAS model (see Chapter 3). The discharge in Cataract during the April 2006 trip was steady enough to assume the water-surface elevation did not change appreciably between sessions.

5.2.5 Measuring Topography of Rapids

A 360° mirrored prism mounted to the top of the boom assembly allowed the position of the boat to be surveyed with a total surveying station (Figure 5.4). The total station was typically placed on a prominent point above the river far from the rapid offering its operator an unobstructed the boat. The total station was also used to measure water-surface profiles within the measurement reach.

Figure 5.4: View of the front of the boat in Rapid 13 of Cataract Canyon while the ADCP is deployed. The 360° prism and the bottom of the GPS receiver are shown mounted to the top of the boom assembly (photograph by T. Kenney).

Target velocity-measurement locations in the river were chosen to balance safety against the desire to capture the most comprehensive and insightful data. Some locations in the river were too turbulent, unstable, or unsafe to make measurements. When attempting to make measurements at dwell sites, the boat was held as close to stationary as possible at a single point in the river for the pre-determined dwell time, either 15 s or 60 s depending on the instrument. Due to boat drift during the dwell (while measuring velocity), the horizontal accuracy of a given survey point is probably no better than 1.0 m. This accuracy improved in slower water.

The survey of the boat dwell location allowed rectification of the collected velocity data into a site-specific map. Combining the water's edge survey data with the water surface data collected with the surveyed boat allowed the construction of a three-dimensional representation of the water surface for a given rapid complex. Combined with the bathymetric data from a particular site, this three-dimensional water surface allowed the entire topologic domain (*i.e.*, the water surface, shorelines, and bathymetry) of the water in the rapid to be fully characterized.

5.3 Site Selection

The attempt to quantify velocity fields in rapids of the Colorado River for this study spans several years and a number of river trips. Table 5.1 lists each of the successful measurement sessions from 2003 to 2006. The ADV was purchased in late 2001 and collected all the velocity data in this study from Grand Canyon. The Cataract Canyon velocities were collected with the two ADCPs and the POEM during an April

Table 5.1: List of sites where velocity and bathymetry were collected for this study.

Site	Canyon	Tributary name	Rapid name	River mile[a]	Date	Discharge (m^3/s)	ADV	ADCP	POEM	Lowrance bathymetry	ADCP bathymetry
Minus 4-mile Bar	Glen	Waters Hole Canyon	n/a	-4.0	4/8/03	332-338	x			x	
Comanche	Grand	Comanche Creek	n/a	67.7	3/18/03	554-527	x			x	
"	"	"	"	67.7	3/3/05	415-375	x			x	
Rattlesnake	Grand	unnamed	n/a	74.5	3/20/03	417-384	x			x	
"	"	"	"	74.5	3/21/03	571-544	x			x	
"	"	"	"	74.5	3/5/05	560-541	x			x	
Escalante	Grand	Escalante Creek	n/a	75.4	3/21/03	468-430	x			x	
"	"	"	"	75.4	3/5/05	480-429	x			x	
Salt	Grand	Salt Creek	Salt Creek	93.1	3/25/03	565-557	x			x	
"	"	"	"	93.1	3/26/03	217-299	x			x	
"	"	"	"	93.1	3/8/05	539-500	x			x	
RM 189.7L	Grand	unnamed	n/a	190.1	3/30/03	506-484	x			x	
"	"	"	"	190.1	3/11/05	324-317	x			x	
"	"	"	"	190.1	3/12/05	503-450	x			x	
Range	Cataract	Range Canyon	Rapid 13	-204.9	4/23/06	640		x		x	x
"	"	"	"	-204.9	4/24/06	617		x	x	x	x
Teapot	Cataract	Teapot Canyon	Rapid 21	-202.8	4/25/06	633			x	x	
Imperial	Cataract	Imperial Canyon	Rapid 27	-200.3	4/26/06	648		x	x		x

[a] Relative to Lee's Ferry (GCMRC, 2002; Belknap *et al.*, 1974).

2006 river trip. The results of these measurement sessions can found in Chapter 4 (Magirl *et al.*, 2006), this chapter, and the Appendix.

5.3.1 Glen Canyon and Grand Canyon

In a project assisting researchers studying salmonid redds in Glen Canyon (Korman, *et al.*, 2005), ADV and bathymetry measurements were made at Minus 4-Mile Bar in Glen Canyon. The results of this session were published by Magirl *et al*. (2006).

The rapids measured with the ADV in Grand Canyon were all enhanced or created by debris fan aggradation from one or more new debris flows occurring after 1998. The flow measurements were made both after aggradation of the debris fan and after the 1,229 m^3/s controlled flood of November 2004. One goal of the measurements was to detect changes in the hydraulics of the rapids due to reworking. The other goal of the work was to develop a reliable measurement technique for collecting hydraulic and bathymetric data from rapids in Grand Canyon and to assemble a preliminary data set.

The first study site in Grand Canyon was a new rapid formed at Comanche Creek (Table 5.1). The tributary, entering from river left, had debris flows in 1999 and 2001 that enlarged the existing riffle into a small rapid. The rapid was measured in March 2003 and again in March 2005. Being the first measurement site for each river trip, a number of operational issues needed to be worked out; the quantity of data collected at Comanche was less than other sites. The second study site in Grand Canyon was near a campsite known to river runners as Upper Rattlesnake Camp. The tributary, entering river right, had a debris flow in 2002. The results of ADV measurements at Rattlesnake were

published by Magirl *et al.* (2006). The rapid at Escalante Creek was created by debris flows that entered the river from tributaries on both sides. The unnamed tributary on river right had debris flows in 2002 and 2003, and Escalante Creek on river left had a debris flow in 2003. Salt Creek Rapid, another study site, forms around a debris fan created by Salt Creek. A debris flow in Salt Creek in 2001 aggraded the debris fan and increased the size of the rapid. The final study site in Grand Canyon was a rapid associated with an unnamed tributary entering river left at river mile 190.1 (GCMRC, 2002). Following the naming convention of Webb *et al*. (2000), this study refers to the site as "189.7L." A debris flow occurred in this tributary in 1998. Being the final study site along the river, measured when many of the instrumentation and operational bugs were worked out of the measurement process, the data from river mile 189.7L tends to represent the highest quality of ADV data collected.

5.3.2 Cataract Canyon

Sites within Cataract Canyon were selected based on their proximity to large debris fans (Table 5.1). The debris fan at Range Canyon was the first measurement site (Figure 5.5). Range Canyon drains a large section of Canyonlands National Park and enters the river corridor from river right. Debris flows that occurred at an unknown time during the Holocene (Webb *et al.*, 2004) built a large alluvial fan pushing the river to the left and forming Rapid 13. High debris-flow activity from the steep canyon walls downstream of Range Canyon dumps copious quantities of coarse-grained alluvium into the river corridor. Coupled with reworked deposits from upstream fans, a number of

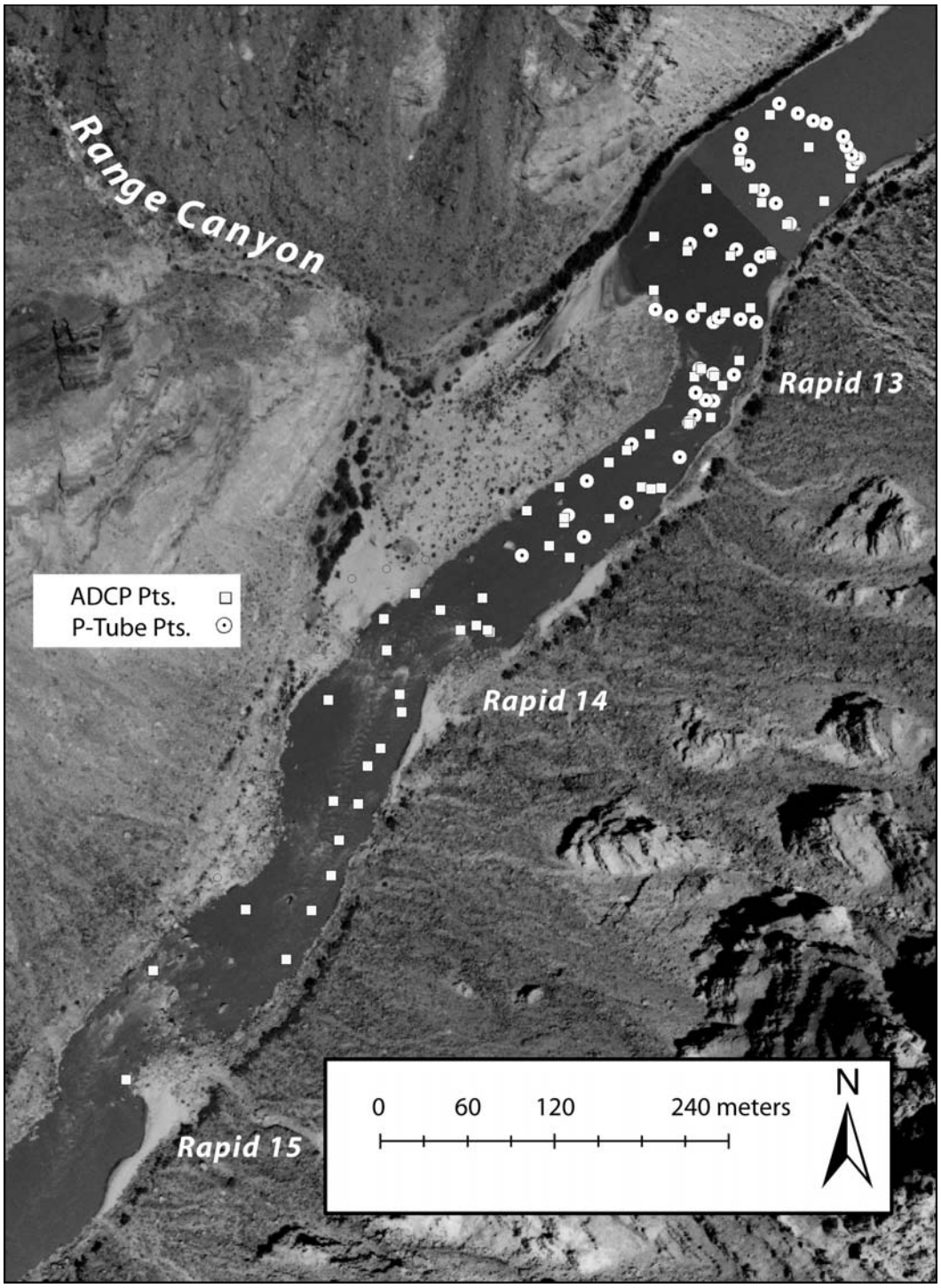

Figure 5.5: Locations of velocity measurements made in the rapid complex in Cataract Canyon at Range Canyon. This reach of closely spaced rapids is locally known as Mile Long Rapid and includes Rapids 13-20. Measurements were made in Rapid 13 and 14. Flow is from top to bottom.

rapids come in quick succession in the reach below Range Canyon, forming what is known locally as Mile Long Rapid (Webb *et al.*, 2004). Flow measurements were made with the 600 kHz ADCP and the POEM throughout Rapid 13 and Rapid 14. The water-surface profile was surveyed through Rapid 15. Rapid 13 is a relatively modest rapid with small waves and a small overall drop. Rapid 14 is larger than Rapid 13. Rapid 15, also known as Capsize Rapid or Best Rapid—both names refer to the failed James D. Best Expedition of 1891 (Webb *et al*., 2004)—is a large, steep rapid offering navigational challenges to the river runner.

The second measurement site in Cataract Canyon was the debris fan and rapid complex at Teapot Canyon which also enters from river right forming Rapid 21 (Figure 5.6). Rapid 21, also known as Big Drop 1, is the first of three large rapids that come in succession known collectively as the Big Drops (Belknap *et al.*, 1974). These three large rapids are the largest and most feared in Cataract Canyon offering the greatest navigational challenge to its river runners. The rapids become so challenging at high water that the National Park Service institutes their "catch-and-release" program for flows above 1,416 m^3/s (50,000 cfs), rescuing swimmers from boats capsized in Big Drop 2 (Rapid 22) before they are swept into Big Drop 3 (Rapid 23). Rapid 21 is the smallest of the Big Drops yet still formidable. The top of Rapid 21 begins with a small riffle accelerating flow into the middle of the main rapid (Figure 5.7), and Big Drop 1 is subjected to the dissipating turbulent structures of Rapid 20, located 500 m upstream. Time constraints prevented a full hydraulic characterization at Big Drop 1; no ADCP

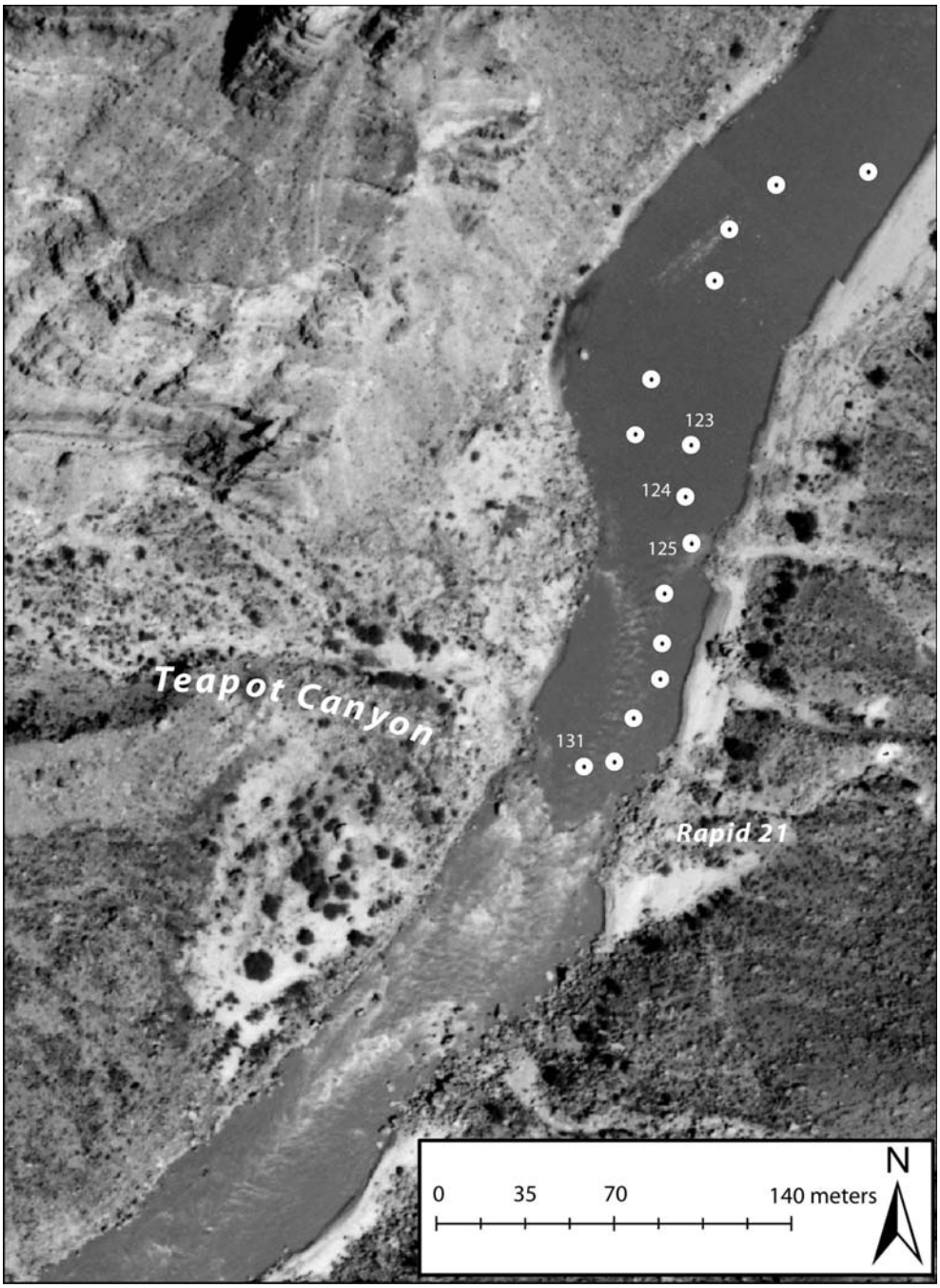

Figure 5.6: Locations of velocity measurements made in Cataract Canyon at Rapid 21. Rapid 21, also known as Big Drop 1, is one of the larger rapids in Cataract Canyon. Rapid 20 (not shown) is 500 m upstream of Rapid 21 and influences the flow in the pool above Big Drop 1. Flow is from top to bottom. Numbers refer to specific survey-point locations referenced in the text.

Figure 5.7: Looking downstream at Rapid 21 (Big Drop 1) and Teapot Canyon entering from river right. A small drop associated with a riffle precedes the main rapid. The turbulent flow structures in the pool above the rapid are readily visible. These flow structures are decaying features of Rapid 20, located 500 m upstream (photograph by T. Kenney).

measurements were taken, but a number of POEM data were collected in the smooth water leading into the tongue of the main rapid.

Imperial Canyon was the site of the final flow measurements made during the April 2006 trip (Figure 5.8). Imperial Canyon enters the canyon from river left and forms Rapid 27. The water-surface morphology of Rapid 27 is unusual. The river first funnels through a small constriction that pushes water up onto the upper end of the large debris fan debouched from Imperial Canyon. The river then turns 80° to the right and pushes through another small riffle along the middle of the debris fan before dropping into the main rapid aligned with the tributary's active channel (Figure 5.8). Measurements were made at Rapid 27 with the POEM for all sections leading into the main tongue of the rapid. Time constraints limited ADCP work to a select number of measured points covering a similar domain. The 1,200 kHz ADCP was used at Imperial. The choice was made to adjust the accuracy to allow more bins for the measurements at Imperial; the bin size was therefore 0.25 m while collecting data with the 1,200.

5.4 Results

5.4.1 ADV Measurements in Grand Canyon

Bathymetry and ADV measurements were collected at the rapid at tributary 189.7L in western Grand Canyon. In all, 253 depth points were collected over three measurement sessions. Figure 5.9 shows the bathymetric map at 189.7L; the river flows from right to left in the figure, and the debris fan enters from river left. The shoreline of the debris fan is visible in the plan view, and the subaqueous mound of course-grained

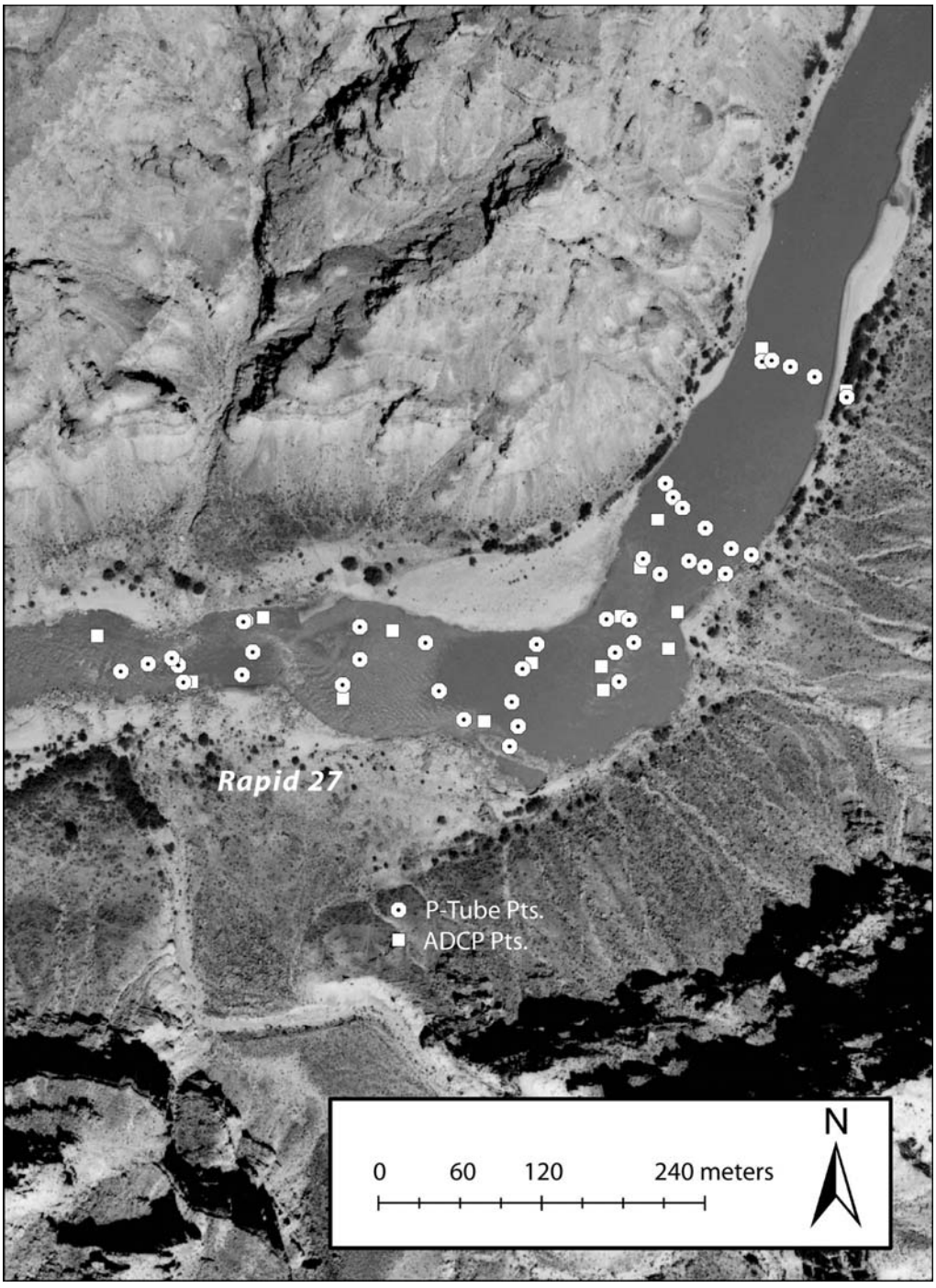

Figure 5.8: Locations of velocity measurements made in Cataract Canyon near Imperial Canyon. Imperial Canyon enters from river left and contributes to the debris fan creating Rapid 27. Flow in the river is from upper right to left.

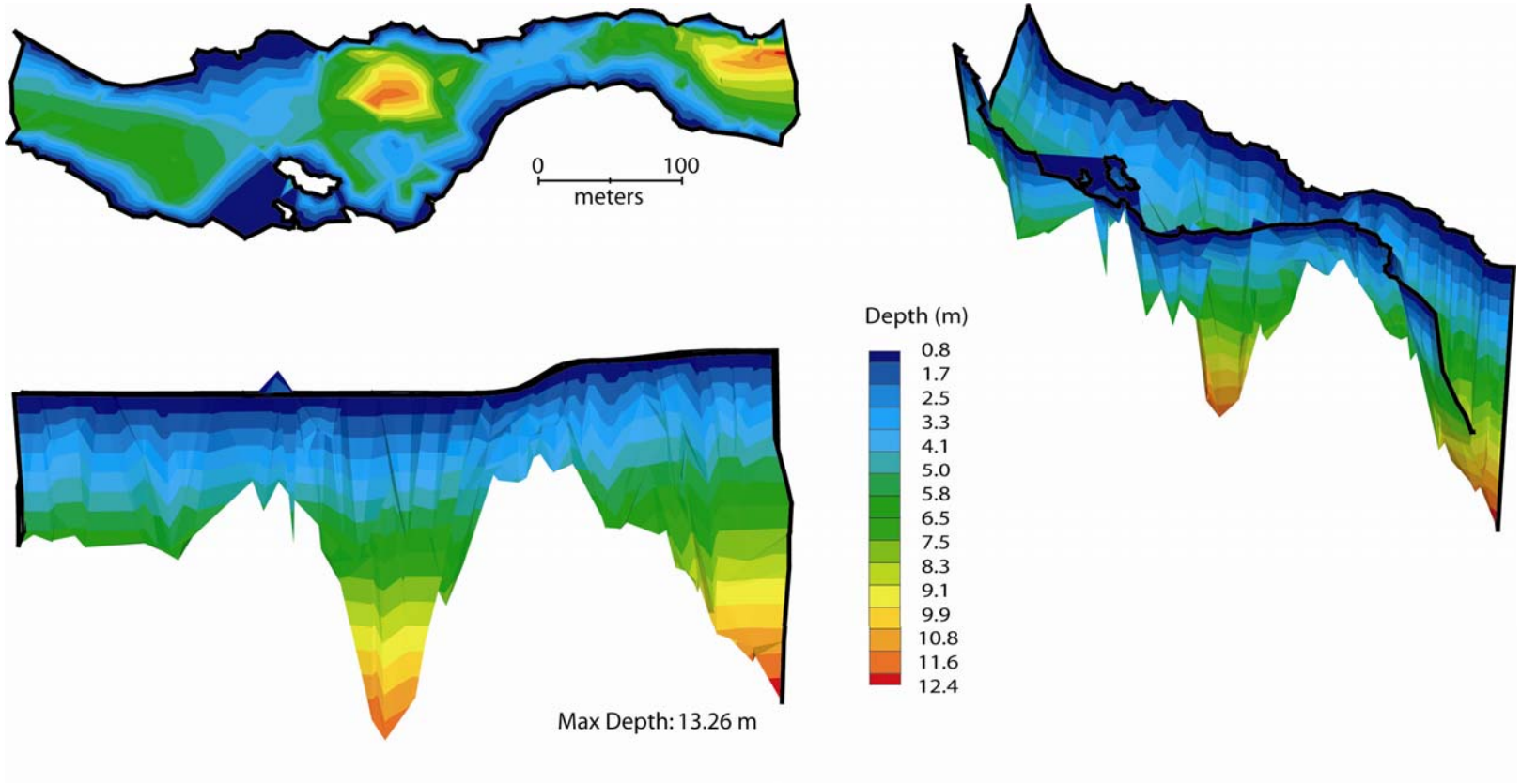

Figure 5.9: Bathymetry at rapid at river mile 189.7 (tributary left) as measured with the Lowrance X59DF fathometer. Discharge is 227 m^3/s. The river flows from right to left.

material that constricts the river into a rapid is visible in the profile view. A deep hole is visible just upstream of the rapid. Another hole formed below the rapid was probably caused by scour from water plunging over the debris fan during floods. The maximum depth through this reach was 13.26 m in the hole just above the rapid, although the bottom of the scour hole below the rapid is the lowest elevation point within the domain. Just downstream of the scour hole, a shoal of shallow water spanning the river channel adjacent the bedrock islands on river left was probably a deposition mound of cobbles and boulders reworked and transported downstream from the main debris fan. This shoal graded into the cobble bar further downstream on river right. The material comprising this cobble bar likely are boulders and cobbles reworked from the upstream debris fan.

The velocity values measured by the ADV on high water during the March 2005 trip are mapped in Figure 5.10. The length of the yellow arrows represent the scalar sum of the three velocity vectors at a given measurement point; the direction of each flow arrow was determined by evaluating the magnitude of the velocity in each principal direction. When juxtaposed against the bathymetry, the cause of the accelerated flow in the main constriction becomes apparent. The relative velocity measured in the pool above the rapid is modest. As the flow entered the constriction created by the debris fan, water accelerated into the rapid. Below the rapid, recirculation eddies were seen on both sides of the jet emanating from the rapid. Water again accelerated over the shoal before slowing while passing the downstream cobble bar. The rapid at 189.7L consisted of a smaller riffle just upstream of the main rapid producing an extended section of relatively fast water between the riffle and tongue of the main rapid. Fifteen tetherballs tossed into

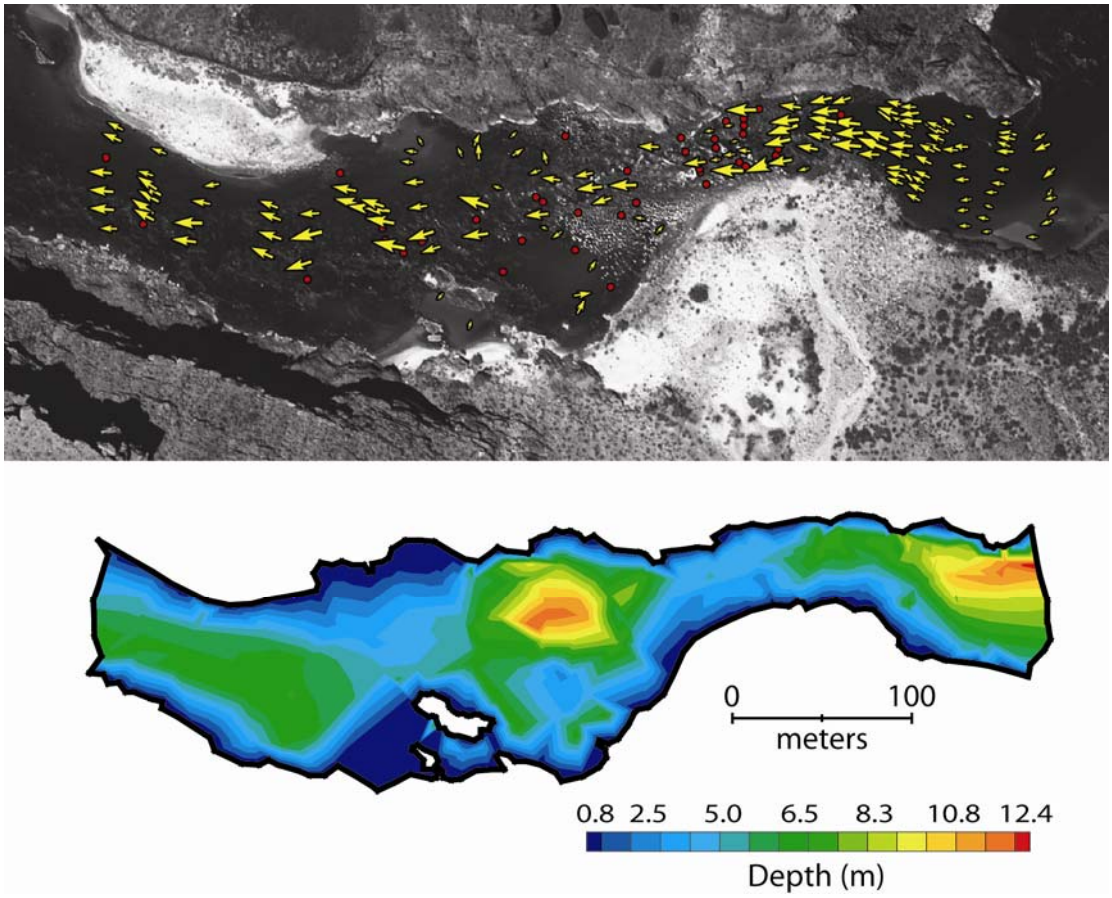

Figure 5.10: Velocity vector field measured by the ADV at river mile 189.7 on March 12, 2005 at a discharge of 518 m^3/s. For reference, the bathymetry contour map is included. Yellow arrows represent water velocity 40 cm below the surface; red dots represent data discarded due to ambiguity jumps.

the center of the river and timed over a 30 m racecourse below the preliminary riffle and above the main rapid returned an average velocity of 5.8 m/s.

In the high-velocity core of the rapid, the ADV was prone to ambiguity jumps. The criterion for eliminating velocity data affected by ambiguity jumps was two-tiered. All velocity data with measured vertical velocity magnitudes greater than 100 cm/s were eliminated. Because the instrument was placed 40 cm below the water surface, a strong vertical velocity was considered to be unrealistic. Secondly, if the measured vertical velocity was between 50-100 cm/s, the data were kept only if the magnitude of the horizontal velocity was more than twice the magnitude of the vertical velocity. Shown in Figure 5.10 as red dots, the velocity data eliminated due to ambiguity jumps were concentrated in the fastest part of the rapid within the tongue and the first set of waves below the tongue. Other data collected in the tailwaves and recirculation eddies below the rapid were also discarded.

Plotting the velocity data in profile offers insight into the ADV measurement limitations under the flow conditions at tributary 189.7L. Figure 5.11 shows ADV data at this rapid as a function of downstream position; each velocity point was projected onto the river centerline. For comparison, data affected by ambiguity jumps are also shown on Figure 5.11 as crosses; the erroneous velocity values determined from the three velocity vectors, primarily a large vertical value. The flow speed is modest in the pool above the rapid located at 0-100 m on Figure 5.11. Flow began to accelerate at 100 m and seemed to reach a maximum from 200-250 m, where ambiguity jumps begin to occur. A spread of velocity magnitude representing slow water in the eddies and the fast water in the

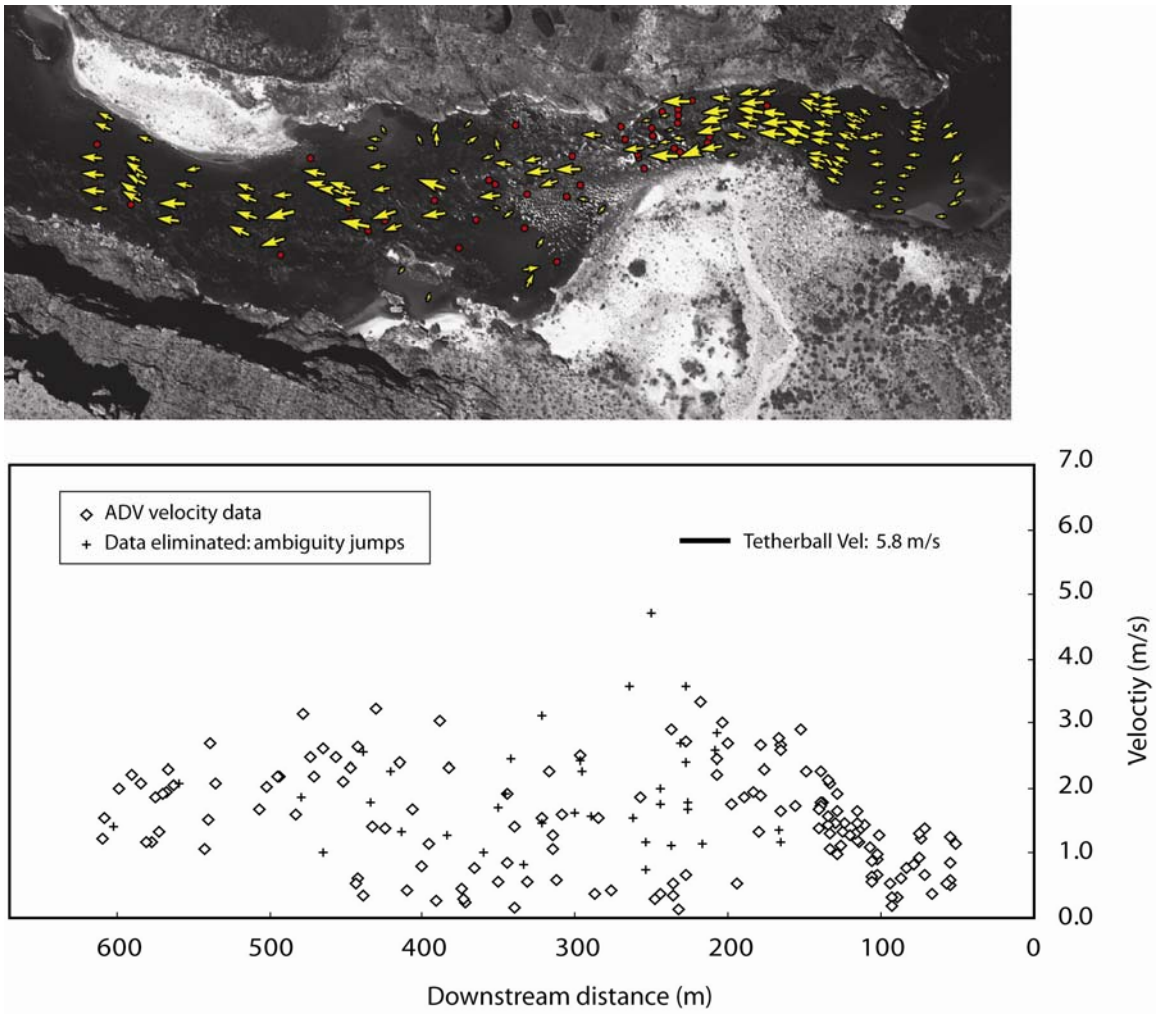

Figure 5.11: Velocity data (displayed in longitudinal profile) measured by the ADV at river mile 189.7 on March 12, 2005 at a discharge of 518 m^3/s. The vector map is included for comparison. Diamonds represent valid data; crosses represent data eliminated due to ambiguity jumps. Also shown is the average velocity of 15 tetherballs measured along a 30 m course located near 200 m.

tailwaves of the rapid prevailed from 250-450 m. Beyond 500 m, flow became nearly uniform downstream with consistent velocity ranging from 1.0-2.0 m/s. Surface-float data measured at the surface indicated the velocity in the core of the rapid is roughly 5.8 m/s. Clearly, the ADV underestimated velocity in the middle of the rapid and there seemed to be a velocity ceiling above which the instrument could not accurately measure flow. That velocity ceiling for this particular ADV device appeared to be about 3.0 m/s. Velocity and bathymetry maps from other study sites in Grand Canyon can be found in the Appendix.

A measurement bias, pronounced at some sites but only slightly apparent at 189.7L, was related to the direction (left bank to right bank or vice versa) that measurements were taken crossing the river. Groups of velocity data sometimes displayed a rotational bias (either clockwise or counterclockwise) depending on the direction transects were traversed. The final six transects at the bottom of 189.7L show this behavior. This artifact was probably an instrumentation problem; the velocity measurements with large cross-channel components do not represent real flow behavior through the rapid. Another potential source of the bias could be the influence of electrical-magnetic noise on the ADV compass. Such electrical-magnetic noise might emanate from the boat alternator or other power component.

5.4.2 ADCP Measurements in Cataract Canyon

ADCP measurements in Cataract Canyon were first made near Range Canyon at a moderate discharge, 620 m^3/s. The water-surface profile at Range Canyon is shown in

Figure 5.12 and extends through the bottom of Rapid 15. Rapid 13 is the first in a series of closely spaced rapids. Rapid 13 is positioned at the upper end of the debris fan and has a relatively small overall drop and shallow slope. Rapid 14, steeper and with a larger drop than Rapid 13, is formed by reworked debris from Range Canyon and debris flows from the steep slopes on river left (Webb *et al.*, 2004). Rapid 15, the largest rapid in this reach, is steep with a drop of about 2 m. Overall, the total drop through Rapids 13-15 is 4.9 m over a distance of 800 m.

Over 50 dwell measurements were made with the 600 kHz ADCP mounted 69 cm below the water surface. The center of the top bin was located 1.55 m below the surface with each subsequent bin located at 0.50 m increments (Figure 5.13). The highest measured velocities were in the top bin in Rapid 13 and in the middle of Rapid 14. The fastest water in each rapid, however, was not directly measured. In Rapid 13, a jet of accelerated water exited the tongue and pushed along the left shoreline. Waves and rocks in this fast-water section discouraged measurements. Where ADCP data were collected, velocity decreased with depth in the water column. The direction of flow for a given measurement site was usually uniform throughout the water column though some locations, particularly in the rapids and recirculation eddies, exhibited changing flow directions with different depths in the water column.

Two points in particular showed strongly helical flow. Points 35 and 36, labeled in Figure 5.13, had high flow velocities that pointed downstream in the uppermost bin. Moving deeper in the water column at point 36, the velocity magnitude deceased as expected. The direction of the velocity vectors, however, gradually rotated toward the left

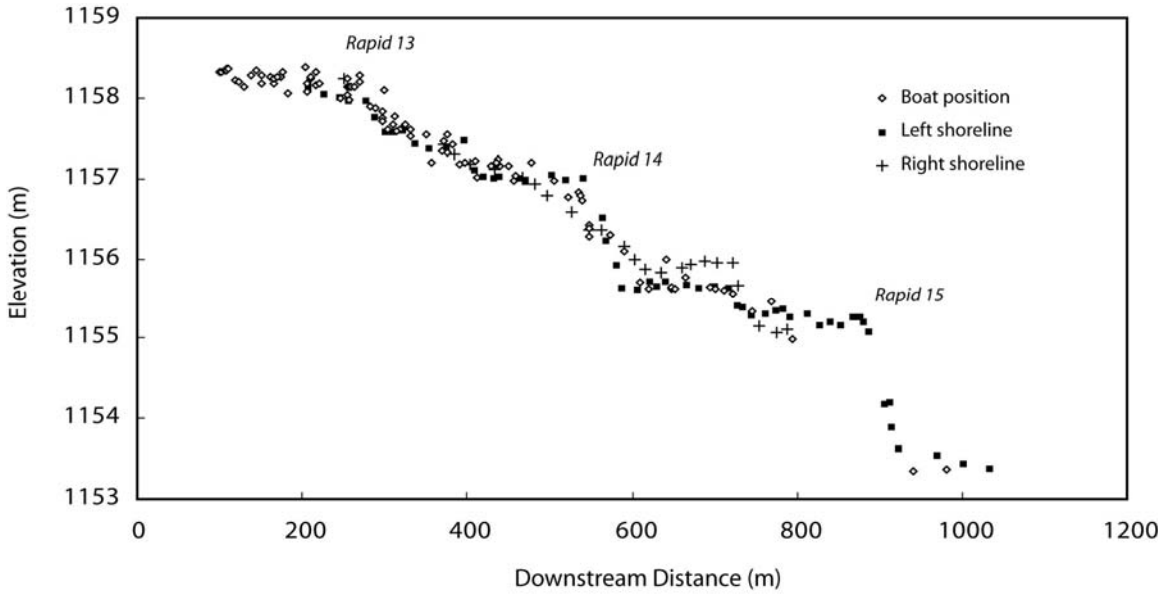

Figure 5.12: Longitudinal water-surface profile of the river near Range Canyon. Survey elevations taken along the left shoreline, right shoreline, as well as water-surface points surveyed by the boat are all included. Rapid 13 is a shallow, almost imperceptible feature with just over 1.0 m drop. Rapid 14 drops roughly 1.5 m. Rapid 15, also known as Capsize Rapid, is the largest and steepest in this reach falling roughly 2.0 meters.

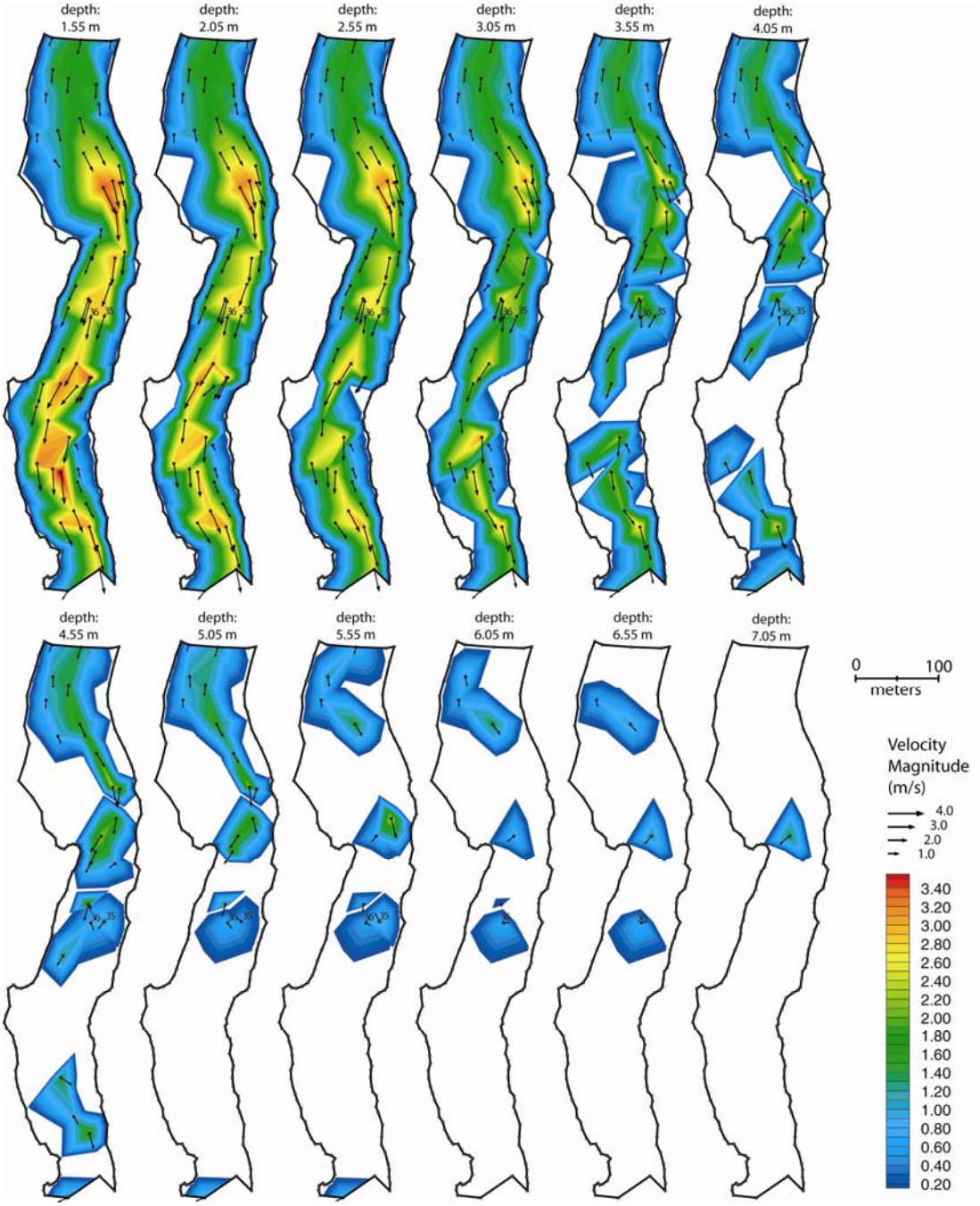

Figure 5.13: Velocity vectors measured by the ADCP at Range Canyon (Rapid 13 and Rapid 14). Data are shown in progressively deeper layers from the upper bin (depth = 1.55 m) to the deepest bin (depth = 7.05 m). Contours represent velocity magnitude; white indicates solid boundary at given point for given depth. Two points discussed in the text, 35 and 36, are labeled on the figure.

bank. The velocity vector for point 36 in the bin at 4.55 m rotated counterclockwise roughly 45° relative to the flow direction at the surface. The velocity vector in the bottom bin of point 36 (6.55 m) rotated 110° counterclockwise relative the flow direction at the surface. The flow structure at point 35 mirrored the structure at point 36. The velocity vectors in the bottom most bins at point 35 pointed toward the right bank, roughly 120° counterclockwise relative the flow direction at the surface. The flow behavior in this section of the river will be addressed in the Discussion section below.

An important aim of this work was to determine if the ADCP has the capability to make measurements directly in the fast water of rapids. One metric to gage instrument effectiveness is the percentage of missing ensembles recorded during a dwell measurement. If the instrument works flawlessly, all collected ensembles would be good, although even measurements made in slow sections of an alluvial river will occasionally contain some missing ensembles. Typically, the missing ensemble was ignored and the remaining valid ensemble data were averaged. When the ADCP (transducer) was placed 38 cm below the water surface (*e.g.*, on April 23, 2006; Table 5.1), the measurements contained a large percentage of missing ensembles, especially in the fast water of the rapid. Presumably, air entrainment under the instrument transducers created problems. Instrument placement with the transducers 69 cm below the water surface resulted in considerably better performance. Nevertheless, significant data losses occurred in some bins and within entire ensembles. Data loss could have been caused by attenuation of signal from high suspended sediment, presence of bubbles, loss of instrument bottom track, or low signal correlation.

Figure 5.14 is a contour plot showing the distribution of percentage missing ensembles as recorded by the ADCP. Instrument performance was best in the pool above Rapid 13 with most locations seeing missing ensemble percentages less than 25%. Performance in the middle of Rapid 13 was generally good. The largest percentage of missing ensembles was the section of fast water in the upper part of Rapid 14. Percentage missing ensembles rose as high as 73% in this region. This percent of missing ensembles does not necessarily indicate poor results from a given section of river—the data collected represents the average of data from good ensembles from a dwell location. The metric, instead, points out locations in the river where the ADCP may be adversely affected by high-velocity or high-turbulence flow conditions.

In addition to dwell-mode data, interdwell data were collected by the ADCP as the boat traversed the river. Variability and uncertainty arising from turbulence in the flow necessitated multiple measurements when quantifying velocity. The instrument's depth data, in contrast, was relative robust. A depth sounding from a single ensemble provided either good bathymetric information or no information at all. Therefore, while single ping velocity is not accurate enough to report for a given interdwell location, bathymetry was readily available from the interdwell transects. At Range Canyon, for example, over 1,900 depth data were collected from the dwell data, interdwell data, and POEM runs (Figure 5.15). The results of these integrated data offer a greater resolution of bathymetric data than using the rear-mounted fathometer alone.

Combining the high-density bathymetry data with water-surface survey points allows the full topological characterization of the reach of river spanning Rapids 13, 14,

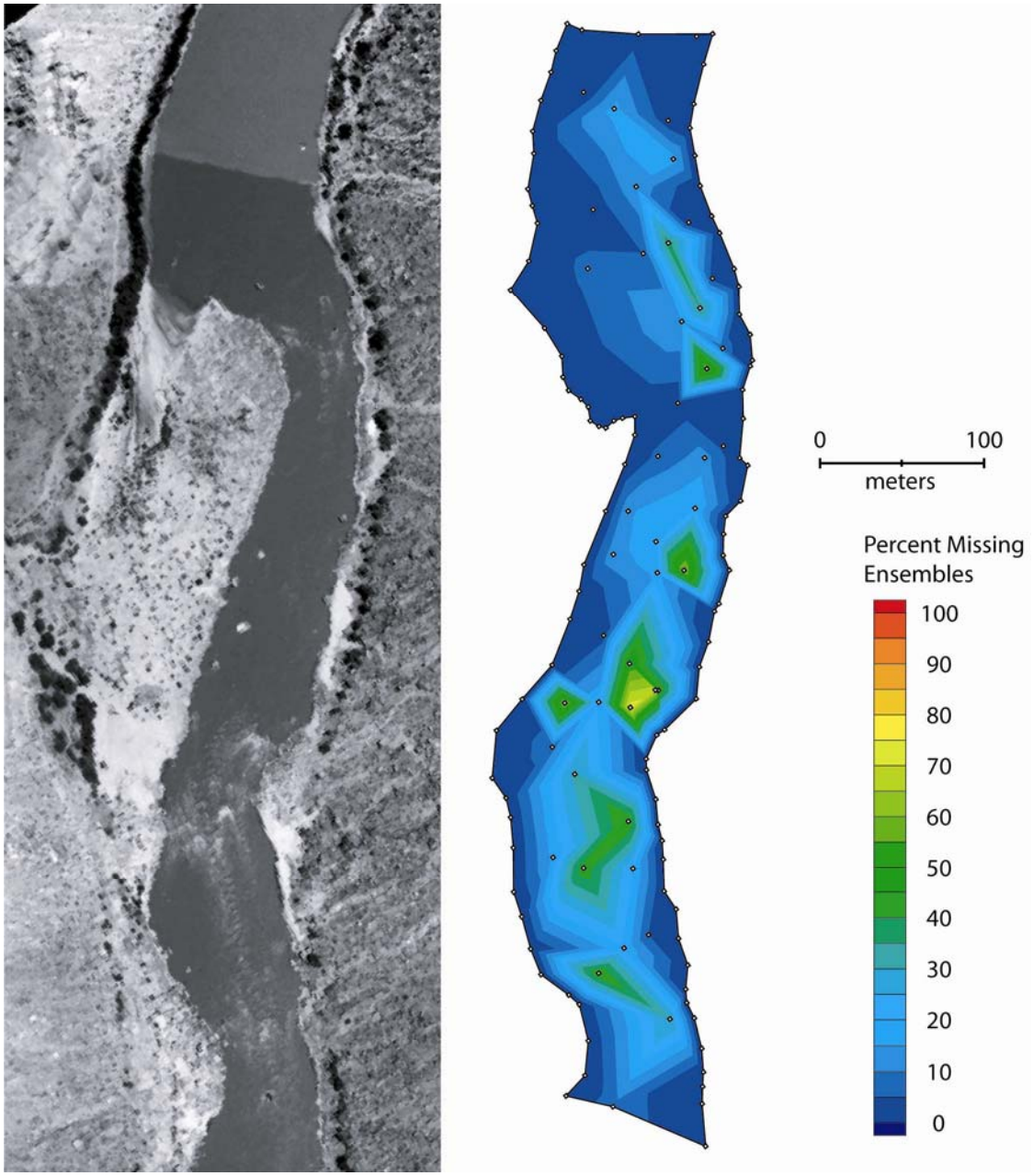

Figure 5.14: Contour plot at Rapids 13 and 14 showing the percentage of missing ensembles measured by the ADCP during each 60 second dwell. Most measured points had fewer than 30% missing ensembles. The maximum value, located just above Rapid 14 is 73%.

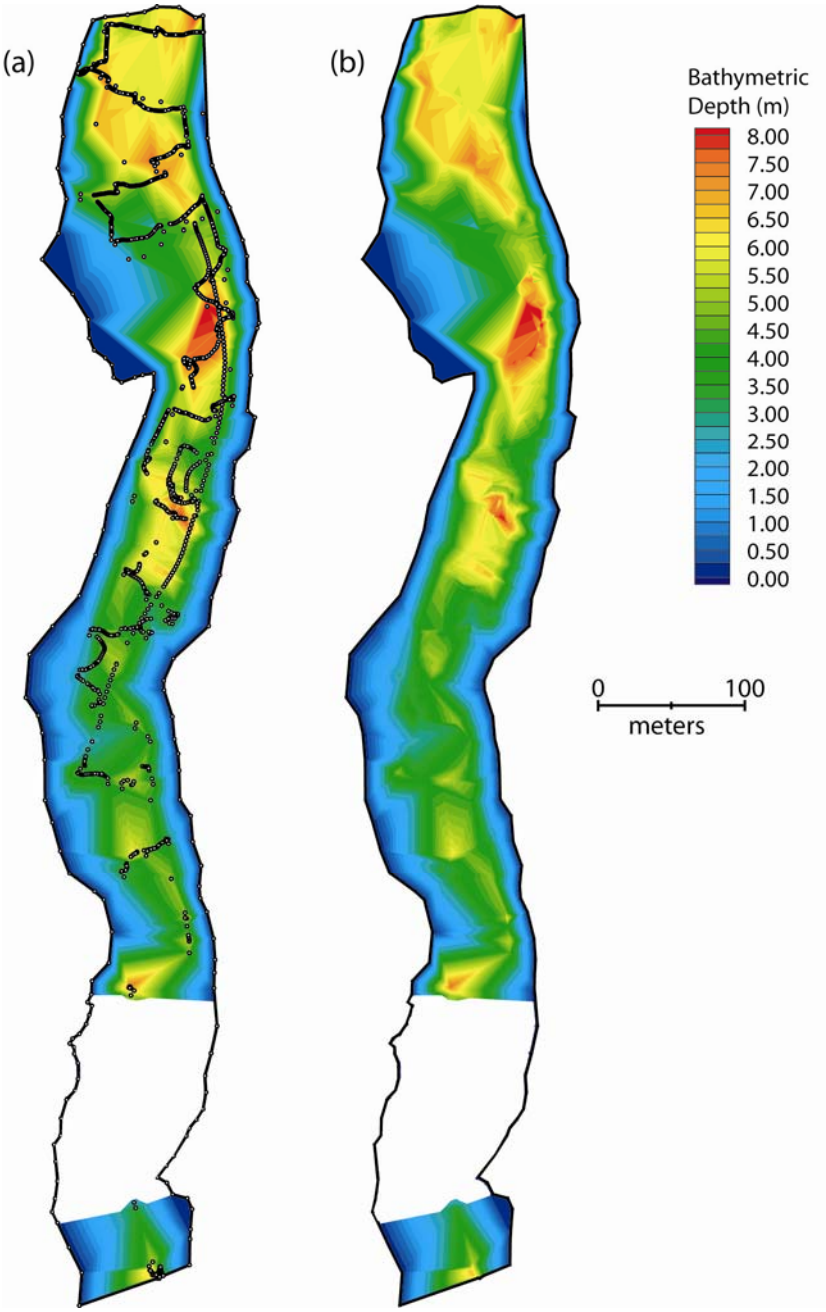

Figure 5.15: Bathymetry measured near Range Canyon (Rapids 13, 14, and 15) in Cataract Canyon. (a) Location of over 1,900 individual bathymetric data collected primarily with ADCP during the interdwell transects. (b) Contour map showing the depth through most of Rapids 13 and 14. A single point was measured below Rapid 15. The blue region just upstream of Rapid 15 (0.00 m depth) is an area of missing data. Discharge is 617 m^3/s. White sections indicate the reach where no data were collected.

and 15 (Figure 5.16). The topographic water-surface map shows the pools and rapids throughout this reach. Juxtaposed against the water-surface elevations, the contour map of slope highlights the location of alternating sections of pools and fast water. Analysis of the topology of Rapid 13 shows an unusual trait: The fast part of the rapid flows through a relatively deep section of river. It appears the mound of coarse-grained alluvium forming Rapid 13 lies roughly 40 m upstream from the upper end of the exposed debris fan constricting the flow and pushing the fastest water downstream over what may be a scour hole. This behavior is not unlike the relation between depth and surface velocity measured at Minus 4-Mile Bar in Glen Canyon (Magirl *et al.*, 2006). Rapid 13 appears to have characteristics more like a riffle and less like a rapid, at least at this moderate 620 m^3/s discharge. The superelevation of water exiting Rapid 14 and impinging on the right shoreline is visible in Figure 5.16. This superelevation can also be seen in Figure 5.12 near downstream distance 700 m.

In contrast to typical Grand Canyon bathymetry near rapids, the depth near Range Canyon is relatively consistent through the reach. The discharge in Cataract in April 2006 was on the rising limb of the snowmelt hydrograph and much sediment was mobilized into the flow. ADCP measurements confirmed significant bed movement in comparing the difference between bottom tracking and GPS tracking. It appears at least some of the holes in Cataract were filled with sand caught in bedload, smoothing the overall bathymetric appearance of this reach of river. Indeed, the bathymetry at Rapid 14 is nearly flat with no distinct mound of rapid-forming alluvium or an associated scour hole downstream.

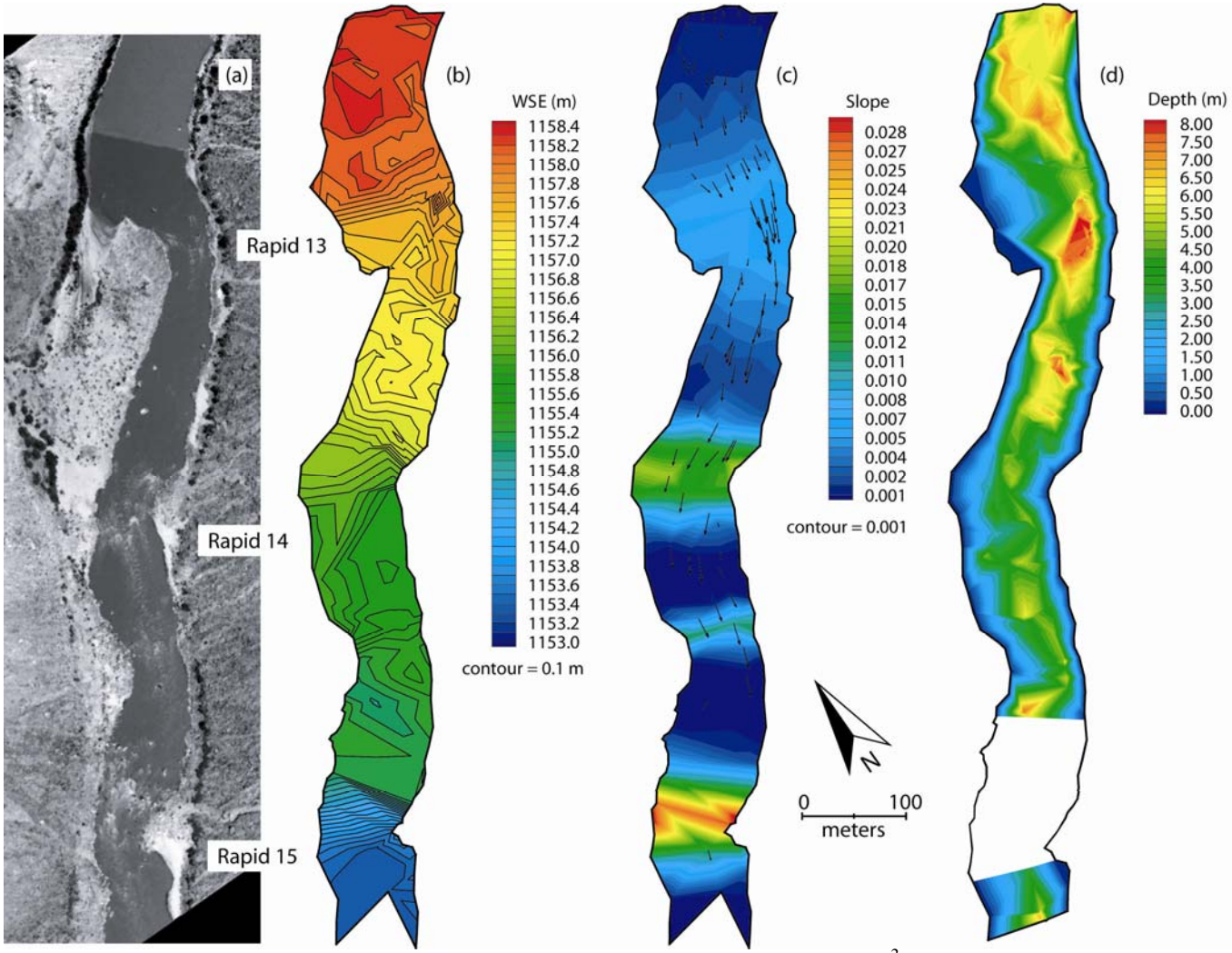

Figure 5.16: Topology near Range Canyon in Cataract Canyon at a discharge of 617 m^3/s: (a) aerial photograph of rapid complex, (b) topography of the water surface, (c) contour map of the slope of the water surface with an overlay of velocity vectors from bin 1 of the ADCP measurements, and (d) the bathymetric depth of the water.

No ADCP measurements were made at Teapot Canyon (Rapid 21), but the 1,200 kHz ADCP, with smaller bin size, was used to collect limited data at Imperial Canyon (Rapid 27; Figure 5.17). Limited time in the field precluded a full characterization of Rapid 27 with the ADCP, but the data that were collected show that flows were generally uniform with roughly logarithmic velocity profiles. The data also show that the 1,200 kHz ADCP was able to measure velocity in relatively sediment-laden conditions.

5.4.3 POEM Measurements in Cataract Canyon

Measurements were made with the POEM in Rapid 13 adjacent to Range Canyon (Figure 5.18). For each velocity measurement, the dwell position was held 60 s. Measurements of turbulent fluctuations in the flow allowed direct comparison of velocity values with relative turbulent intensity and turbulent kinetic energy, TKE (equation 5.5). As was demonstrated with the ADCP, flow accelerates into the rapids and high-velocity flow continues down the upper section of the Range Canyon debris fan. The relative turbulent intensity decreased in the upper pool in response to larger average velocity values associated with acceleration into Rapid 13. A single point near the shoreline of the debris fan on river right showed an unusually large value of $\hat{u}$. This point was located behind a strong eddy fence (*i.e.*, a vertical boundary of pronounced shear separating the free-stream flow from a recirculation eddy) on river right separating the fast water in the tongue from the slower water near the shore. In fact, this section of the river is best describes as a boil train, a section of strong, turbulent upwelling in the wake of the eddy

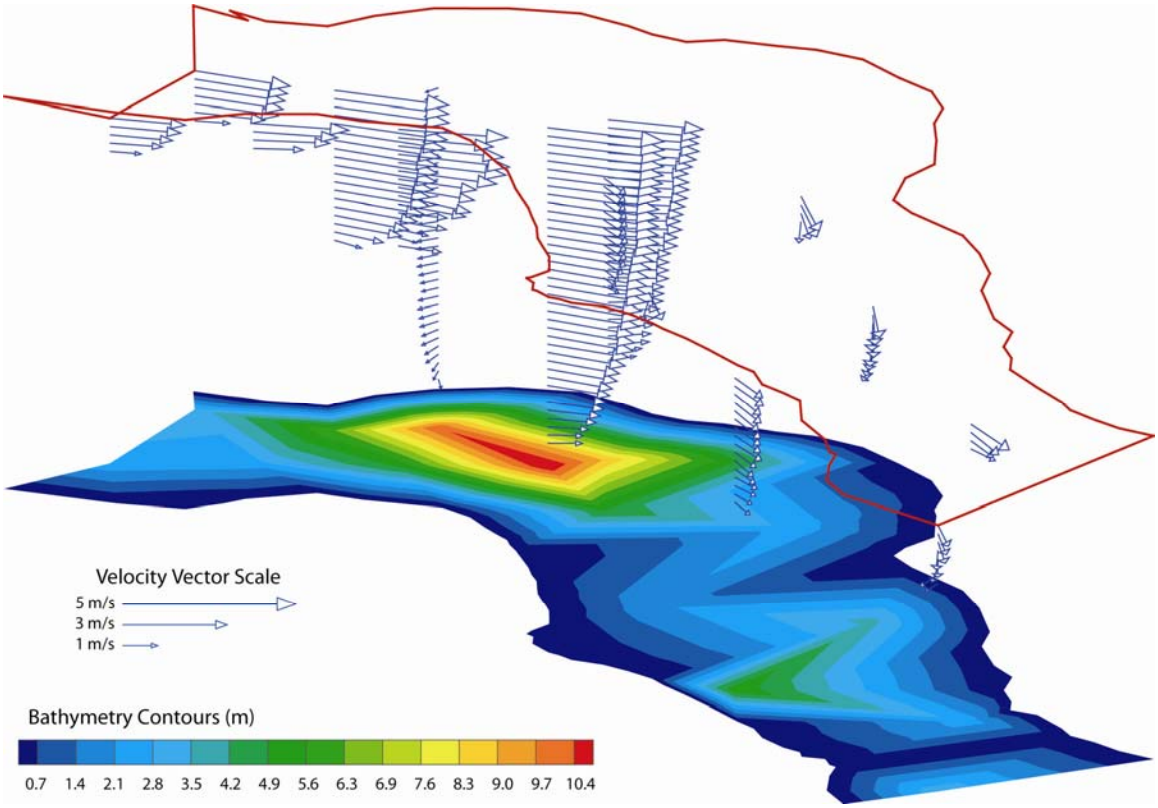

Figure 5.17: ADCP velocity vector field of the flow near Imperial Canyon (Rapid 27) viewed from the northwest. The 1,200 kHz ADCP yielded twice the number of bins as the 600 kHz unit. The bathymetry, as measured by the ADCP, is projected onto the bottom contoured layer. The maximum depth measured is 11.12 m. The floating red line represents the shoreline of the river.

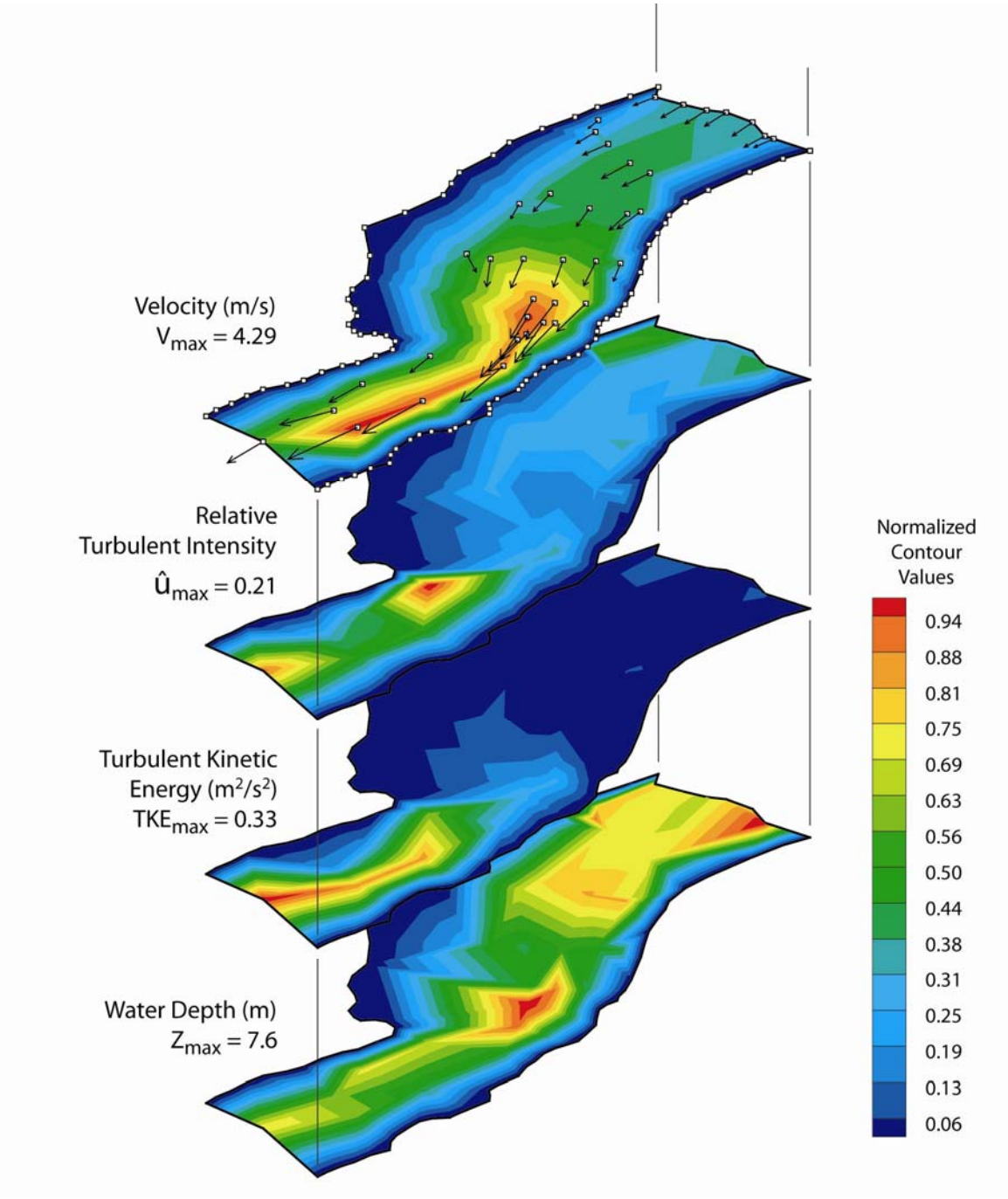

Figure 5.18: Layed contour plots of POEM measurements at Range Canyon (Rapid 13) viewed from the south showing the velocities, turbulence, and bathymetry. Contours are normalized against the maximum value for a given variable; the maximum measured values for each variable are shown next to the respective contour layer.

fence. TKE was generally small in the upper pool and within the tongue of Rapid 13. In the tailwaves below Rapid 13, TKE increased significantly.

To better compare velocity with turbulent intensity and TKE, the values of each were plotted in profile with respect to downstream distance (Figure 5.19). As was indicated in Figure 5.18, TKE is small until roughly 250 m when both average velocity and TKE began to increase. While average velocity increased until roughly 300 m then leveled off, TKE continued to rise in the downstream direction reaching its maximum measured value near 500 m downstream. Turbulent intensity, on the other hand, decreased from 100 m through the first part of the rapid, reaching a minimum value near 275 m, in the middle of the rapid. Then, from 300 m onward, $\hat{u}$ increased. The point of high turbulent intensity in the boil train is seen as the outlier with $\hat{u}$ over 0.20 near 380 m.

The POEM was used to measure flow velocities near Teapot Canyon (Rapid 21). Figure 5.20 shows the water-surface profile of Rapid 21 assembled from boat and water's-edge survey data. As was shown in Figure 5.7, a pre-rapid riffle with a drop of less than 1.0 m accelerated the flow into the tongue of Rapid 21. The water surface fell over 2.0 m through Rapid 21 and the orientation of the rapid raised the water surface onto the left shoreline near a downstream distance of 400 m.

POEM measurements were made to the end of the tongue in Rapid 21, along a series of closely spaced measurements extending down the river centerline. Figure 5.21 shows the average velocity values plotted against contours of $\hat{u}$ and TKE. Average velocity increased to a maximum value of 5.17 m/s at the farthest downstream location. This velocity is the highest value measured in Rapid 21. Relative turbulent intensity was

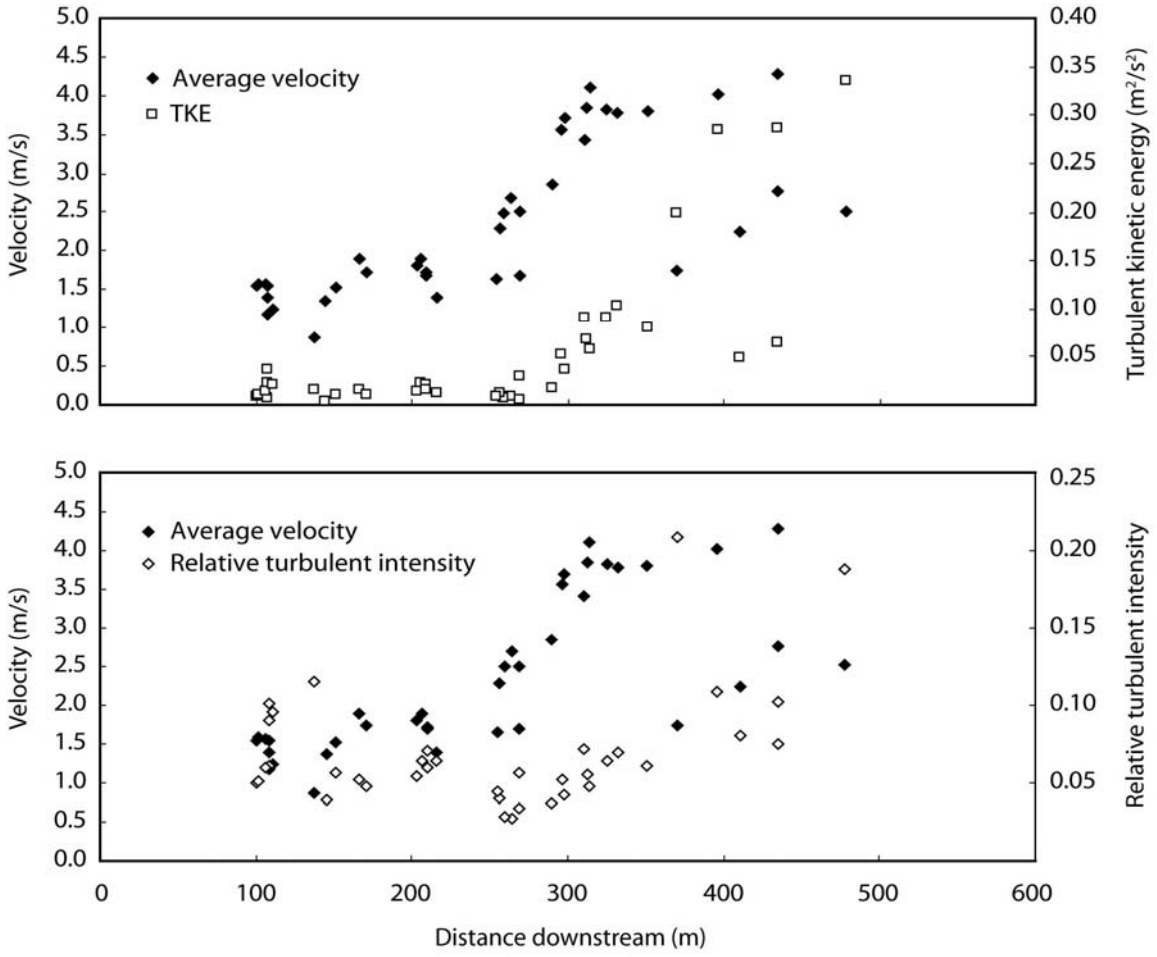

Figure 5.19: POEM-measured average velocity, turbulent kinetic energy (TKE), and relative turbulent intensity for Range 13 at Range Canyon. The tongue of the rapid is located at 300 m. Average velocity increases steeply at the beginning of the tongue of the rapid near 250 m, as does TKE. But while average velocity plateaus and begins to decrease at the first lateral waves (at 300 m), TKE continues to increase through 400 m. Relative turbulent intensity, however, stays more consistent everywhere with a general minimum in the smoothest water of the tongue; the two outlying points with values near 0.20 were measured behind an eddy fence where turbulence is high and average velocity is low.

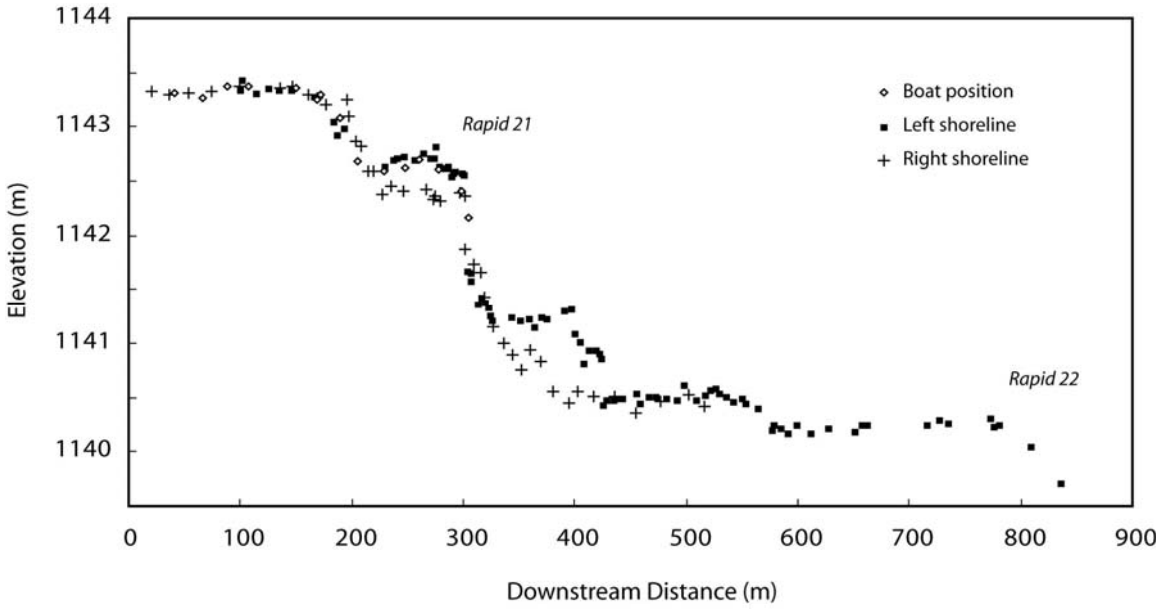

Figure 5.20: Longitudinal water-surface profile of the river near Teapot Canyon (Rapid 21). The first small drop is the lead-in riffle above Rapid 21. Rapid 21 (Big Drop 1) starts at roughly 300 m and drops more than 2.0 m. The top of Rapid 22 (Big Drop 2) is at 800 m.

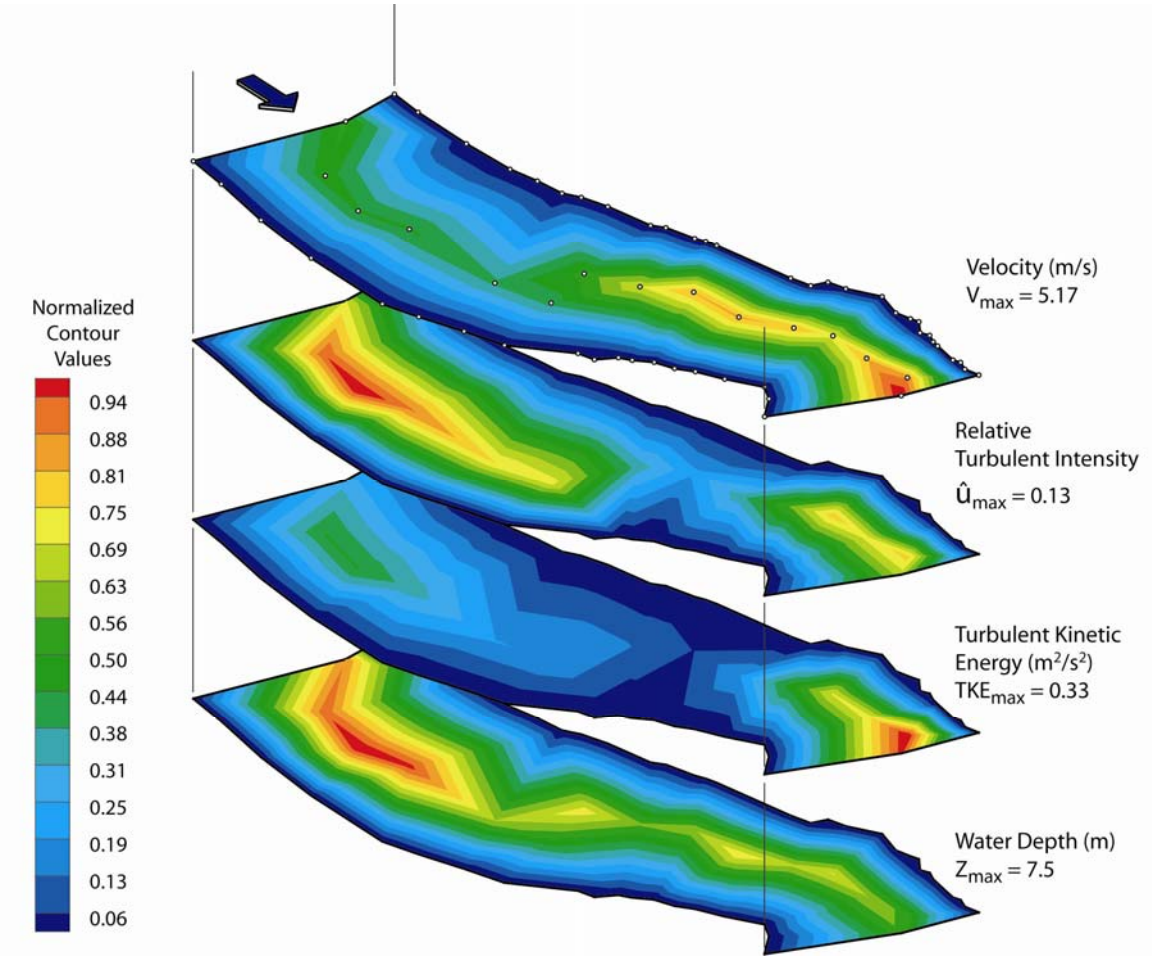

Figure 5.21: Layed contour plots of POEM measurements in Rapid 21 viewed from the west showing the velocities, turbulence, and bathymetry. Contours are normalized against the maximum value of a given variable; the maximum measured values for each variable are shown next to the respective contour layer. The blue arrow shows the direction of flow. The direction of the flow velocity in Rapid 21 was not recorded.

highest in the pool above the rapid. Rapid 21 is relatively close to Rapid 20 and the dissipating turbulent structures from Rapid 20 created high $\hat{u}$ in the upper pool. As flow accelerated into Rapid 21, velocity increased, reducing the value of $\hat{u}$. TKE, on the other hand, was small in the upper pool and increased sharply in the tongue of Rapid 21.

Plotting velocity, $\hat{u}$, and TKE in profile illustrates the trend of the three variables leading into Rapid 21 (Figure 5.22). The average velocity in the pool above the rapid was roughly 2.0-3.0 m/s, rising at the lead-in riffle near 150 m. This riffle accelerated flow within 50 m to an average velocity of roughly 4.0 m/s. Velocity then stayed constant for almost 100 m increasing again in the tongue of the main rapid. Rapid 20 created antecedent TKE that dissipates to a minimum at the top of Rapid 21, near 200 m. TKE then rose in response to turbulence generated from the riffle to a maximum in the tongue of Rapid 21. No measurements were made below the tongue and first set of breaking waves, but if Rapid 21 demonstrated behavior similar to Rapid 13, TKE would have continued to rise above 0.30 m^2/s^2 through the lower section of the rapid. Turbulence intensity, tied to the strength of TKE and average flow velocity, decreased to a minimum value near a downstream distance of 200 m.

POEM data were also collected at Imperial Canyon (Rapid 27), the final measurement site. Working across the river in transects, data were collected in the downstream direction to the center of Rapid 27. The water-surface profile reveals a complex series of lead-in riffles and superelevation shorelines before the main rapid (Figure 5.23). The first riffle was located near 200 m and the water-surface elevation dropped less than 0.5 m. The outwash of the first riffle pushed up the left shoreline near

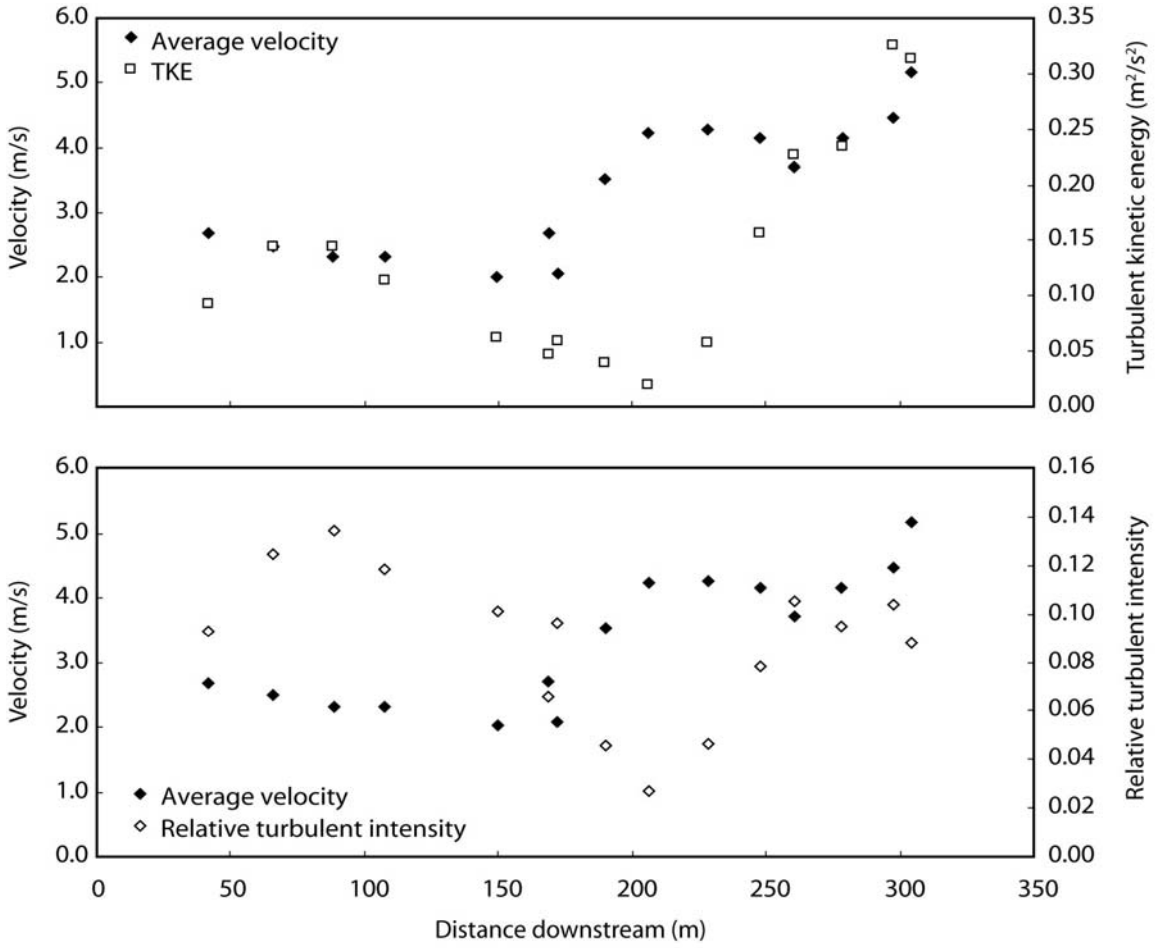

Figure 5.22: POEM-measured average velocity, turbulent kinetic energy (TKE), and relative turbulent intensity for Rapid 21 at Teapot Canyon. The rapid is two-tiered, with the first and smaller tongue located between 180-210 m; the second tongue leading into the main drop starts at 280 m. Average velocity increases at the beginning of the first tongue and then again at the second tongue. TKE climb steadily from the end of the first tongue through the second tongue. Relative turbulent intensity drops distinctly at the smoothest water of the first tongue.

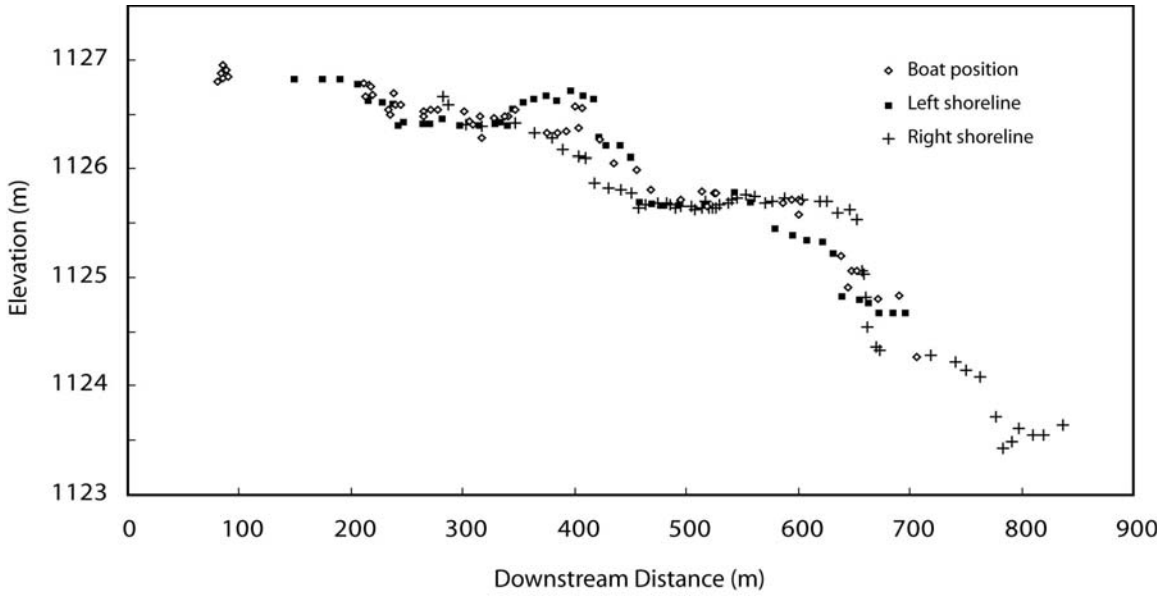

Figure 5.23: Longitudinal water-surface profile of the river near Imperial Canyon (Rapid 27). Survey elevations taken along the left shoreline, right shoreline, as well as water-surface points surveyed by the boat are all included.

350 m to an elevation nearly as high as the original water-surface elevation in the upper pool. This height of superelevation indicates that potential energy in the flow at this point is little changed; in other words, relatively little energy was consumed by wave action or friction through the first riffle. The second riffle was larger and begins at 400 m. The decrease in water-surface elevation in the second riffle was less than 1.0 m. The main part of rapid 27 began near 600 m and the total fall was roughly 1.5 m, though another small drop of 0.5 m was located just downstream near 750 m.

Velocity increased in steps moving downstream to the main rapid (Figure 5.24). A maximum average velocity of 5.28 m/s was measured in the middle of Rapid 27, the largest average velocity measured with the POEM in Cataract Canyon. Turbulent intensity also increased in the downstream direction. When viewed in profile, $\hat{u}$ appeared to increase slightly over the course of the rapid complex (Figure 5.25). The highest $\hat{u}$ was associated with a single point in the left recirculation eddy just below the first riffle. This eddy contained a strong shear zone between the high-speed water in the main flow and the slow water within the eddy. The ADCP data also showed this shear zone (Figure 5.17). As was observed with Rapid 13 and Rapid 21, TKE increased steadily downstream, reaching a peak of 0.53 m^2/s^2 at the bottom of the measurement domain in the middle of Rapid 27. Figure 5.25 shows the steady increase of TKE in the downstream direction.

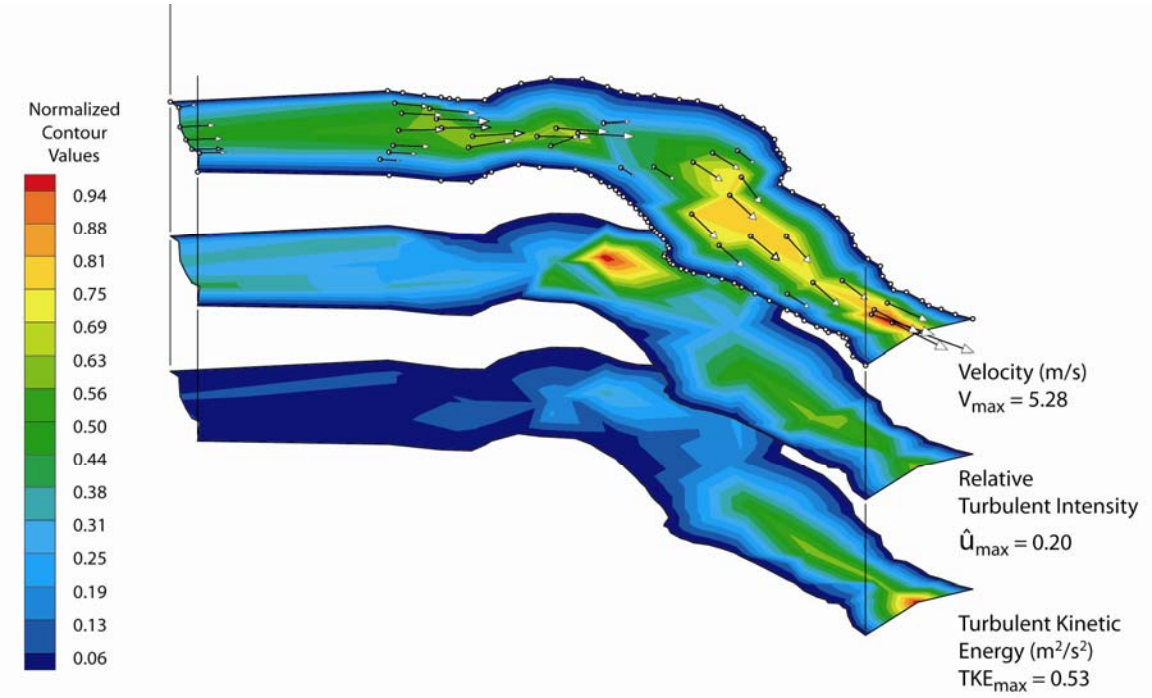

Figure 5.24: Layed contour plots of POEM measurements at Imperial Canyon (Rapid 27) viewed from the northwest showing the velocities, turbulence, and bathymetry. Contour normalized against the maximum value of a given variable; the maximum measured values for each variable are shown next to the respective contour layer.

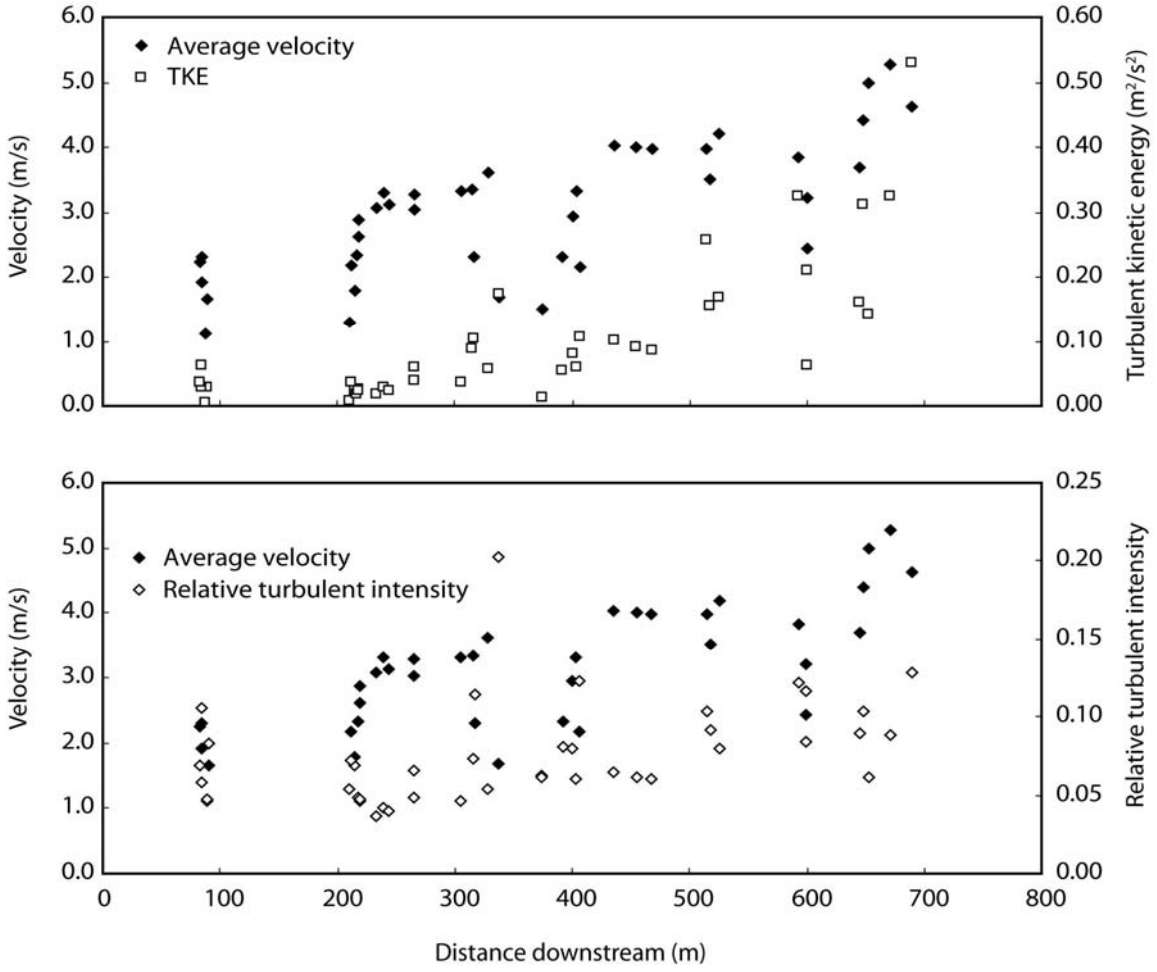

Figure 5.25: POEM-measured average velocity, turbulent kinetic energy (TKE), and relative turbulent intensity for Rapid 27. The rapid has two smaller constrictions at 220 m and 450 m; The tongue of the main rapid begins at 650 m. Average velocity rises in steps through each constriction, reaching a maximum of 5.28 m/s in the tongue of the main rapid. TKE increases steadily through the rapid complex. Relative turbulent intensity stays relatively constant throughout the rapid; the outlying point with values near 0.20 was measured behind an eddy fence where turbulence is high and average velocity is low.

5.5 Discussion

5.5.1 Flow Structures in Rapids

Insight into the helical flow structures illustrated in Figure 5.13 is gained by comparing the local flow field with the bathymetric data. Figure 5.26 shows the flow vectors associated with points 35 and 36 projected over a contour map of the bathymetry of this section of river. It appears the helical flow structure of point 36 was associated with a scour hole shown as a region of orange and red in the bathymetry contour. It is not clear what caused the scour hole or why it appeared in the middle of smooth, fast water between Rapid 13 and Rapid 14. It seems the ADCP was able to image a horseshoe vortex forming in the influence of the scour hole. The flow structure under point 35 was equally unusual and not readily explained by the bathymetry. A full characterization of this region of the river, with a large number of closely spaced velocity and bathymetry data is needed to better explain the structures of flow measured at points 35 and 36.

Comparison of the water velocity measurements collected by the POEM and the ADCP was made. Figure 5.27 shows the average velocity measured by the POEM and the average velocity in the upper bin measured by the ADCP plotted in longitudinal profile. Velocities in the upper pool matched well with respect to each instrument. As the flow was accelerated into the main section of Rapid 13, the magnitude of velocity recorded by each instrument rose in unison until a position near 300 m where velocity measured with the two instruments seems to diverge. While peak ADCP velocities were grouped around 3.0 m/s from 300 to 700 m, the POEM data indicated the fastest velocities near the surface were closer to 4.0 m/s.

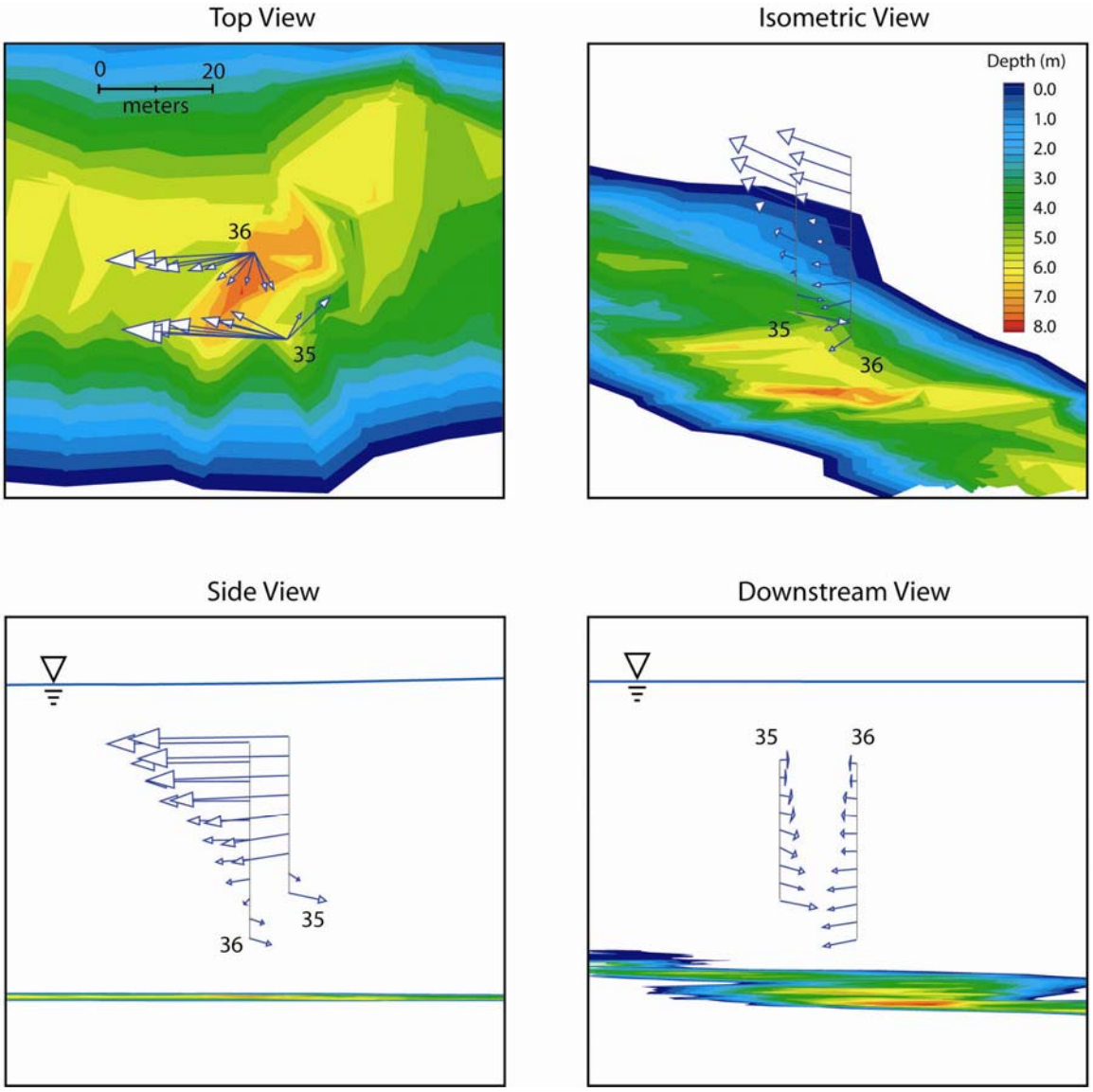

Figure 5.26: Helical flow structure shown by the ADCP measurements at the scour hole located midway between Rapid 13 and Rapid 14. Contours represent bathymetry and are projected onto the floor of the plot. Measurements at point 36 show a velocity profile progressively turning counter clockwise toward the left bank with depth in the water column. Measurements at point 35 mirror the flow structure of point 36: progressively turning clockwise toward the right bank with depth. The flow structure at point 36 is consistent with a horseshoe vortex forming in the scour hole.

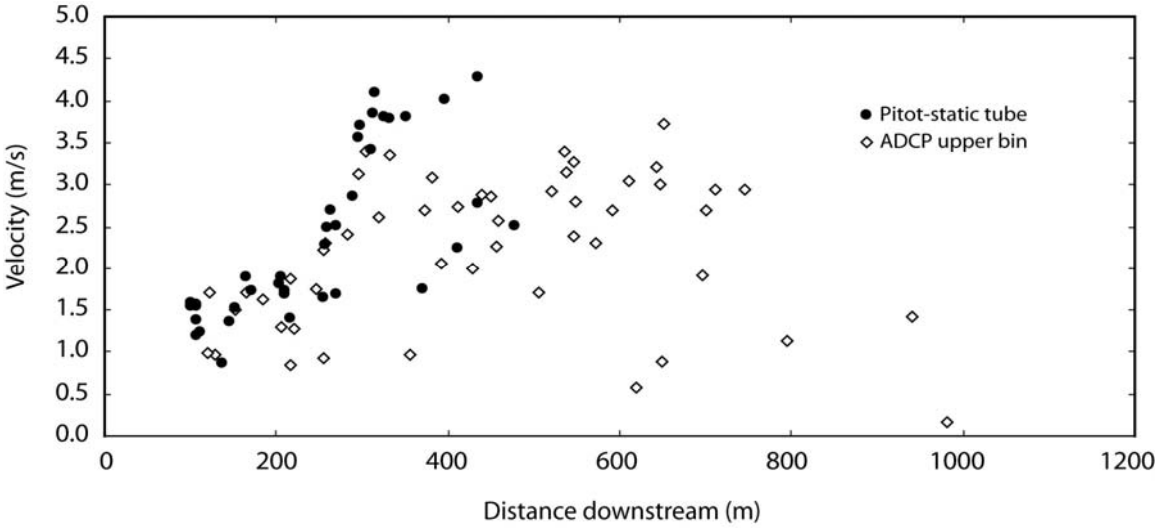

Figure 5.27: Near-surface velocity data at Range Canyon (Rapid 13). The POEM data were measured 0.40 m below the surface; the ADCP bin 1 data are located 1.55 m below the surface. The tongue of the rapid is located at a downstream distance of 300 m.

One possible explanation of the magnitude difference between instruments is that one or both instruments could be misreading the highest velocities in the flow. Given the theory of operation of both instruments, it may be more likely to suggest that the ADCP is understating velocity magnitude in the rapid. The POEM is reading a pressure difference between two ports and has been designed to operate in the condition found in a very specific place in the rapid. The ADCP, on the other hand, experienced data loss for individual bins and occasionally entire ensembles. If the dropped ADCP data were preferentially from higher velocity regions or temporary high-velocity fluctuations, the averaged velocity from the remaining good data might underestimate the actual flow magnitude. While differences in velocity illustrated by Figure 5.27 may be due to instrument error, it is also possible the results represent accurate behavior of flow in the rapids. It is important to remember the upper bin of the ADCP was 1.55 m below the water surface while the POEM was positioned 0.39 m below the water surface. Being over a meter higher in the water column, the higher velocities reported by the POEM may reflect a faster section of flow near the water surface. To test this hypothesis, the flow structures from closely aligned POEM and ADCP measurements were analyzed.

Figure 5.28 shows the velocity profile from four different locations at Rapid 13 as measured by the ADCP. These four locations were chosen due to their proximity to nearby POEM data. In each of the four cases, a POEM measurement was made within 6 m of the ADCP location. Plotted on each of the velocity profiles are the corresponding POEM data located 39 cm below the water surface. In the upper pool, the ADCP measured a velocity profile that is typical of prismatic, rough-boundary rivers:

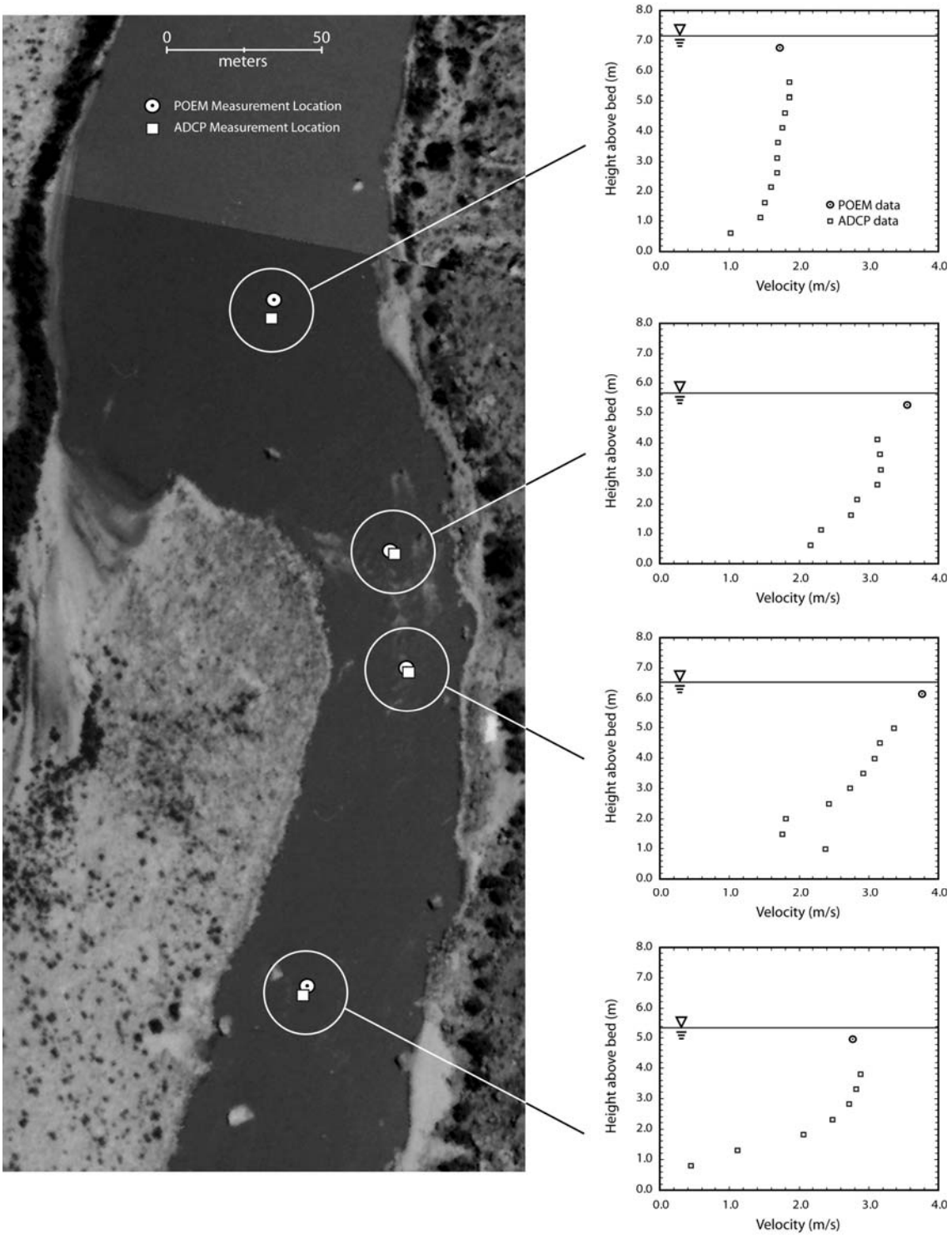

Figure 5.28: Velocity profiles for sites at Rapid 13 comparing the ADCP data (squares) and the POEM data (circles).

logarithmic in the lower part of the profile nearest the bed with a maximum value some depth below the surface and velocity at the surface slightly less than the maximum (Chow, 1959). As Figure 5.27 suggests, the velocity measurements of the POEM and ADCP agreed well in the upper pool. In the tongue of the rapid, the ADCP velocities increased away from the bed reaching a relatively uniform velocity of 3.0 m/s in the upper four bins. The POEM measurement at this location was roughly 3.6 m/s and seemed to be out of alignment with the profile measured by the ADCP. The next point downstream in Figure 5.28 was located just below the first breaking waves of the tongue. The velocity profile recorded by the ADCP is unusual with a large velocity near the bottom, minimum velocities values in the second and third bins from the bottom and flow linearly increasing with height toward the surface. When plotted on the same graph, the single POEM measurement falls in line with the trends captured by the ADCP. Finally, the comparison of ADCP data and the POEM measurement in the tailwaves below the rapid indicated good alignment between the two data sets. Analysis of Figure 5.28 alone does not offer adequate insight to suggest whether the ADCP is accurately capturing the fast flow in the rapid. The data do seem to suggest, however, that within the core of the rapid, the highest velocity flow occurs near the water surface.

Figure 5.29 is a contour map of the correlation coefficient, R^2, of the fit of the velocity profile measured with the ADCP against an idealize logarithm profile (see equation 5.6). To show extreme examples of strong and weak correlation, two profiles are plotted in Figure 5.30. One profile is from point 13 located in the pool above Rapid 13 showing a nearly logarithmic profile. The second profile is from point 28 exhibiting the

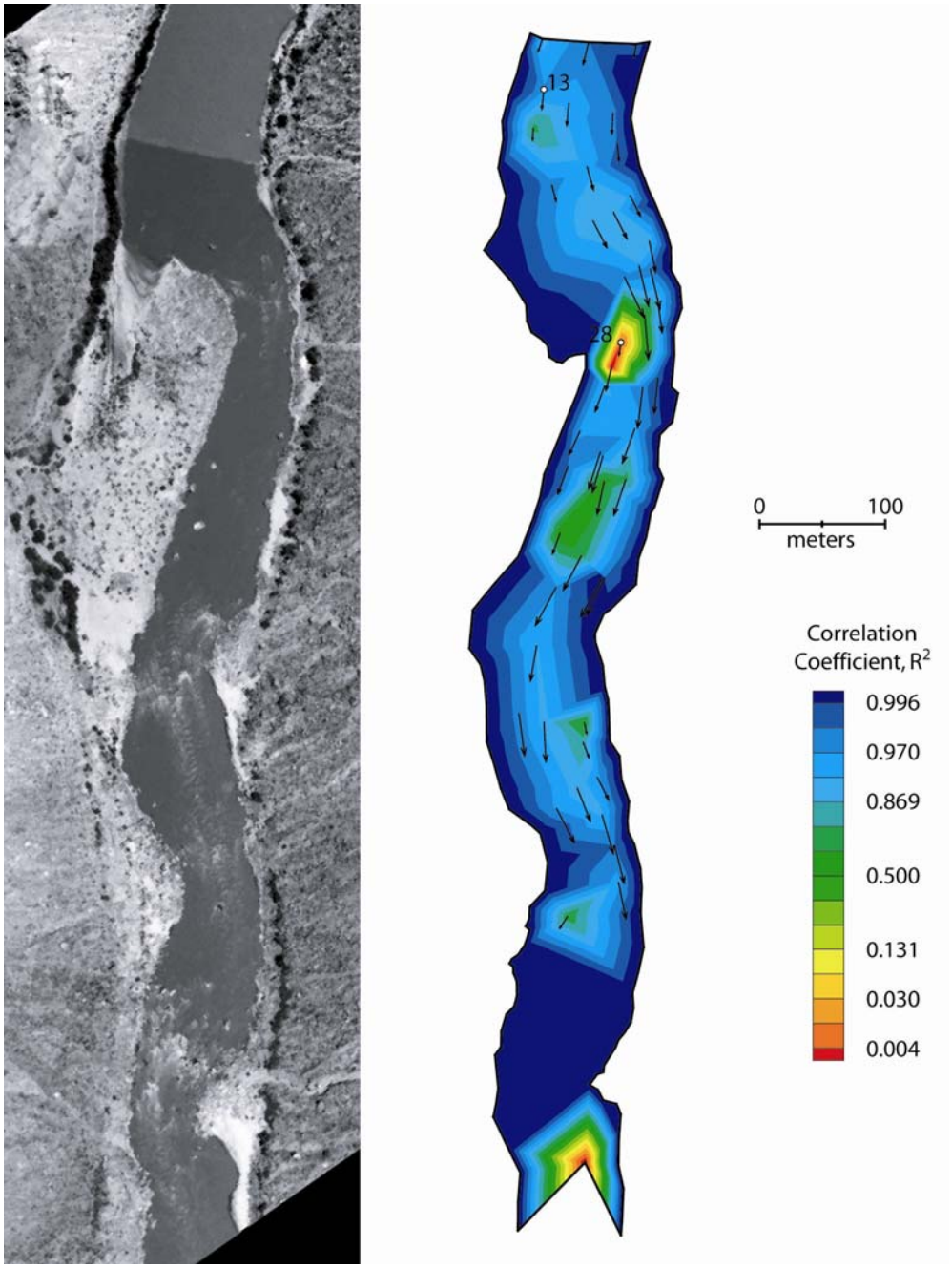

Figure 5.29: Contour plot at Range Canyon (Rapids 13, 14, and 15) of the quality of fit of the ADCP-measured velocity profile to an idealized logarithmic profile. Cool colors indicate the measured velocity closely fits a logarithmic profile. Hot colors indicate the measured velocity poorly fits a logarithmic profile. The velocity profiles of points 13 and 28, indicated on the figure, are shown in Figure 5.30.

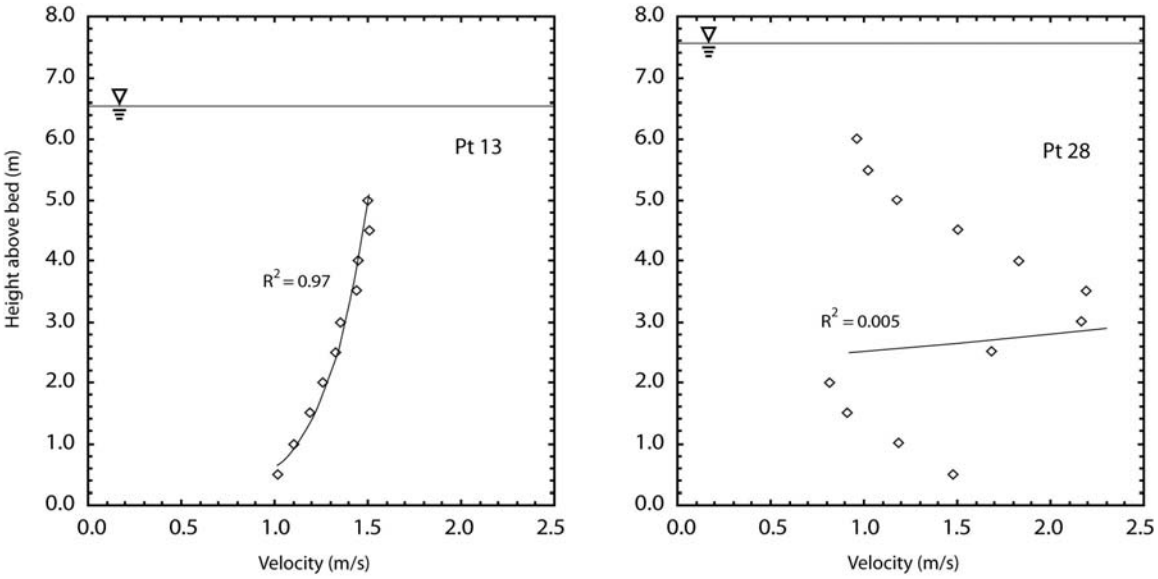

Figure 5.30: Velocity profiles from point 13 and point 28 that are mapped on Figure 5.29. The profile from point 13 (located in the pool above Range Canyon) closely fits a logarithmic profile with a correlation coefficient squared of 0.97. In contrast, the profile from point 28 (located in the turbulent boil zone behind the eddy fence next to the debris fan) correlates weakly to a logarithmic profile.

least logarithmic behavior in the domain. Point 28, labeled on Figure 5.29, is in the boil train behind the eddy fence on river right. The velocity values in the upper section of the profile are small, but a strong horizontal jet with velocity of 2.0 m/s developed 3 m above the bed. Another jet seemed to develop just above the bed. Looking again at the contour map (Figure 5.29), the areas of flow in the river that best represent a logarithmic profile were in the pool above the rapid and the tailwaves below Rapid 14. The velocity profiles in the fastest regions of the tongue of each rapid also approximated a logarithmic profile reasonably well. The velocity profiles least approximated a logarithmic profile in the high-shear zones just behind the eddy fence adjacent the debris fan.

The ADCP tracks its position in the river with multiple techniques. The primary and most accurate technique is bottom-tracking. During measurements, the ADCP pings off the bed of the river to know the water depth below the instrument. Assuming the bed is fixed with a velocity of zero, the instrument then calculates its position as it moves relative to the fixed bed. This positional location technique is called bottom-tracking. If the bed is mobile (*i.e.*, a moving bed with a finite bedload velocity), the bottom-tracking algorithm calculates a boat movement that incorrectly estimates an upstream boat drift proportional to the downstream bedload velocity. When moving-bed conditions are present in the river, GPS tracking is used. GPS tracking, while potentially less precise than bottom-tracking, is unaffected by bed movement.

Assuming that GPS tracking is accurate, one can use the difference between GPS and bottom tracking to generate an estimate of bedload transport. During a given dwell measurement, the difference in boat movement measured by GPS tracking and bottom

tracking is assumed to approximate the movement of the bed. Mueller and Wagner (2006) also used an ADCP to estimate bed movement, but without GPS tracking. Choosing a starting point, they began by first cutting directly across a river, then cutting directly back across the river to the precise location of the starting point. Calling their technique the Loop Method, they estimate bedload by evaluating the upstream distance that the bottom-tracking algorithm calculated the boat had moved; the actual upstream distance traveled was known to be zero. The method applied in Cataract Canyon is similar to the Loop Method, though the control that references the boat to a known position is GPS tracking, not the physical return to a pre-determined position in the river.

Figure 5.31 shows the estimates of bed movement, or the velocity of the bedload, as calculated through Rapid 13 and Rapid 14. The data are in the units of velocity (m/s) and represent the vector difference of the boat movement calculated by bottom-tracking and the boat movement calculated by GPS tracking. The technique seemed to work best in soft-bed regions of the upper pool where a sheet of moving sand covered section of the bed. Figure 5.31 shows that a conveyor of material entered the domain in the thalweg near the right shore. This material crossed over toward the left bank as it moved downstream and was funneled down the middle of the rapid. The bedload calculation indicated little to no bedload in the main part of the rapid, but regions of detectable bedload were identified at different locations downstream. The substrate of rapids was composed of boulders on the order of 1.0 m in size emplaced by debris flows. The bedload of sand and gravel probably flowed between boulders and could not be resolved using the ADCP technique. Where the acoustic signals could ping off large, fixed

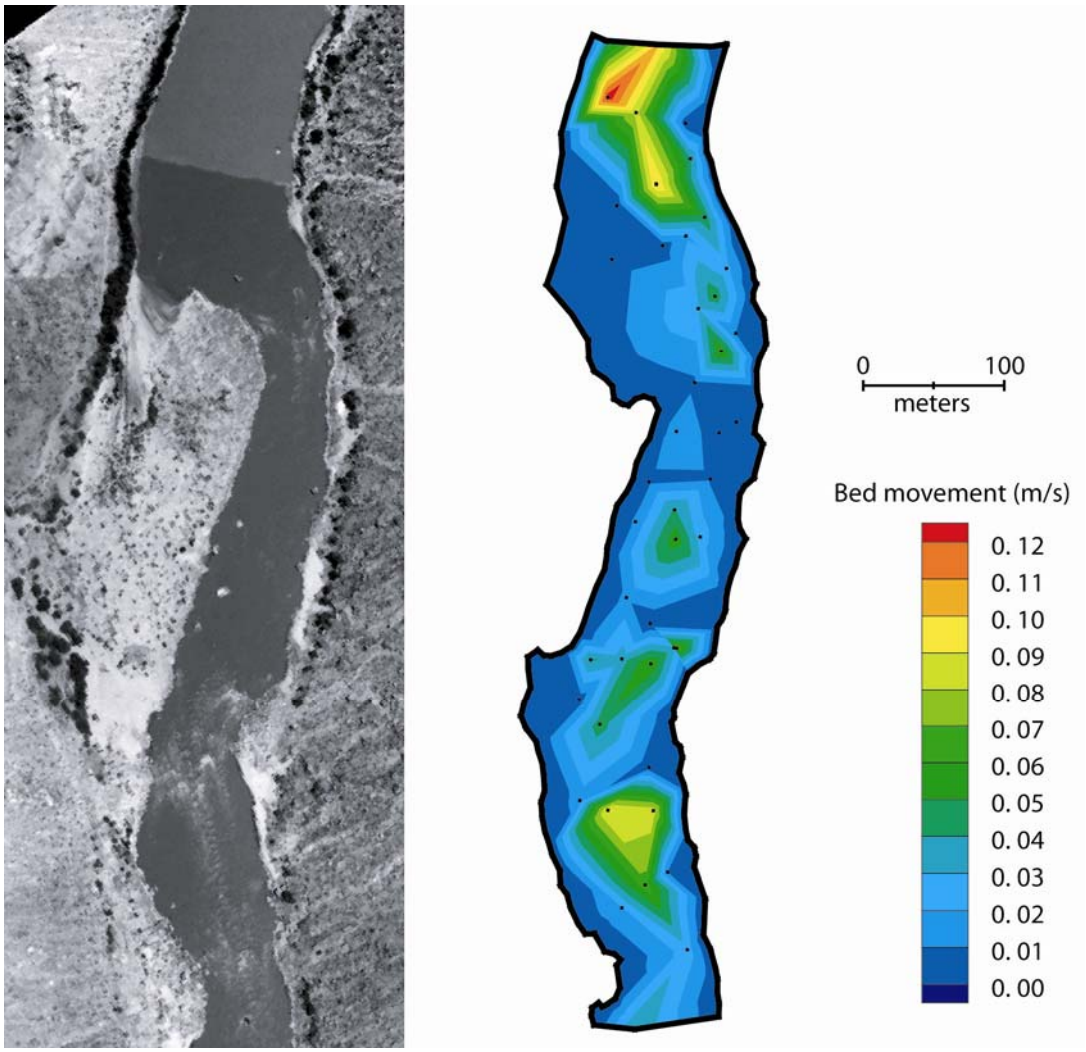

Figure 5.31: Contour plot of the bedload velocity calculated at Range Canyon (Rapid 13). The highest bedload measured was 0.12 m/s in the pool above Rapid 13.

boulders, the bottom-tracking algorithm probably worked well and bed movement would appear to be zero. Owing to the relative small bed movement detected in the middle of Rapids 13 or 14, it appears this method does not accurately estimate bedload directly within the coarse-grained substrate of rapids.

5.5.2 Turbulence in Rapids

Evident in the turbulence measurements at Range, Teapot, and Imperial is the systematic increase in the TKE progressing downstream through the rapid. Even after the velocity in the rapid peaked and began to fall, TKE increased. Figure 5.32 shows the turbulent traces measured by the POEM at four locations leading into the main section of the tongue of Rapid 21. The turbulence in point 123, positioned in the pool above the rapid was present yet relatively modest. Moving further downstream, the velocity traces of point 124 and point 125 increased but turbulent fluctuations decreased. Comparing points 123, 124, and 125, one sees that while velocity accelerated into the smooth water above the rapid, the turbulent energy continued to decrease. In other words, the POEM was detecting no new generation of turbulence from the rapid at point 125, despite the accelerated flow. The behavior of the flow, however, changed dramatically by point 131. Point 131 is the furthest downstream POEM measurements in Rapid 21 and showed accelerated velocity, averaging just over 5 m/s, with strong turbulent fluctuations. The velocity data at point 131 illustrated the turbulent energy placed into the flow by the rapid.

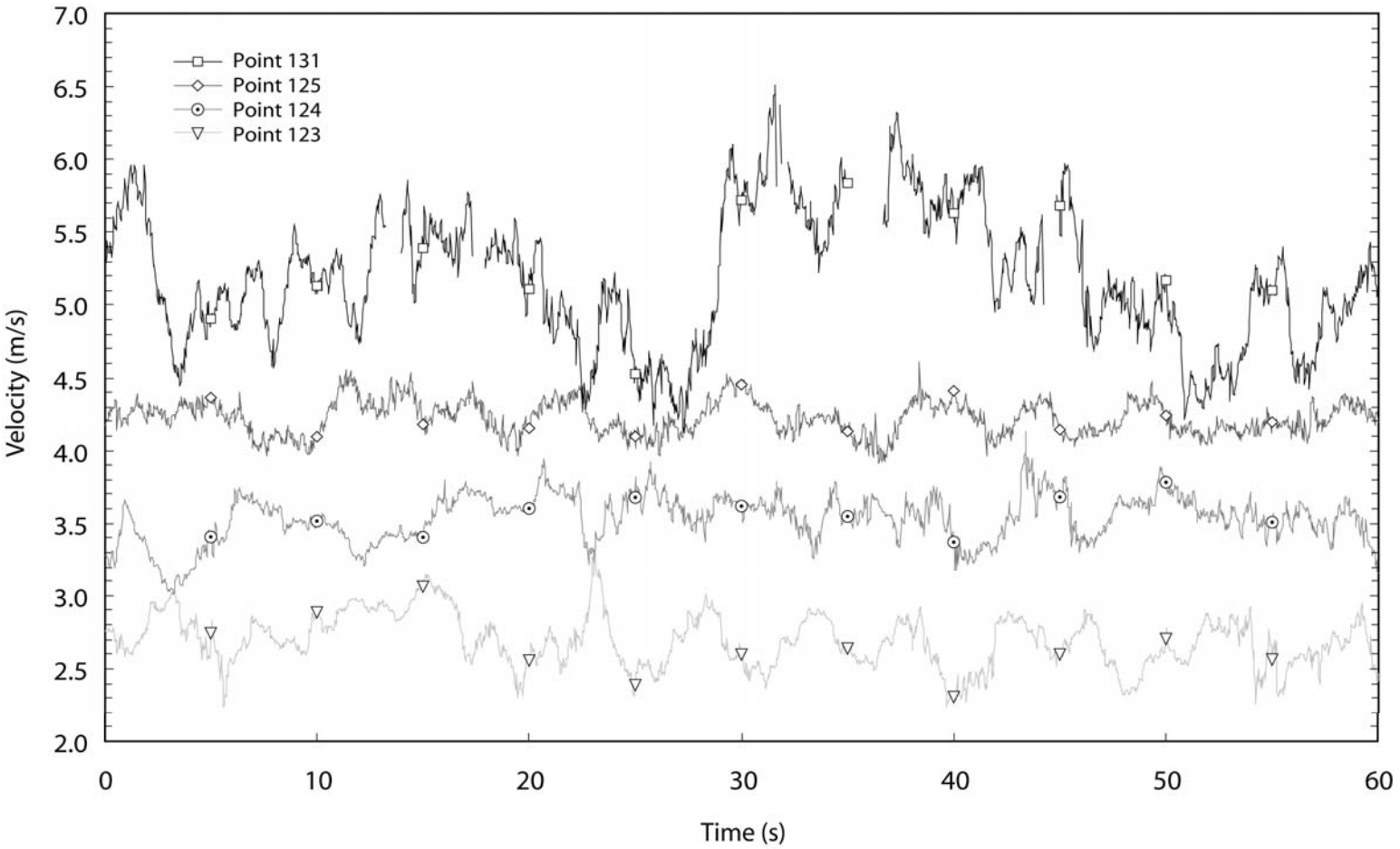

Figure 5.32: POEM velocity traces measured at Rapid 21 (Big Drop 1). The dwell time for each measurement was 60 s. Each of the four points extend close to the rapid with point 123 farthest upstream in the pool and point 131 in the middle of the tongue of Big Drop 1. Specific locations of each sample (referenced by point number) are shown on the aerial map of Big Drop 1 (Figure 5.6).

Figure 5.32 appears to implicitly show the cascade of energy as well as generation of the new turbulent energy in the rapid. The TKE of point 131 was large. More importantly, in addition to containing high-frequency turbulence, the velocity traces of point 131 show long-wavelength fluctuations associated with the largest eddies being generated by the rapid. The turbulence is presumably generated at the bed and propagates up to the water surface. An alternate hypothesis to explain these large fluctuations in velocity is relative boat movement. Because the boat is subject to movement during data collection, the variability in velocity may simply be a function of the boat moving upstream and downstream during the dwell measurement period. Based on observations during measurements, however, boat movement was small compared to the velocity of the river flowing past the boat. It is unlikely that the absolute boat velocity had an amplitude of oscillation of 1.0 m/s (*i.e.*, the amplitude of the peak turbulent fluctuations measured by the POEM and shown in Figure 5.32). Nonetheless, further analysis of the data and boat movement is required to correct velocity fluctuations for boat motion.

5.6 Conclusions

New flow measurement instruments were used to measure fluid-dynamic properties of the flow through rapids aiding the understanding of the hydraulic characteristics of rapids and enabling the development of future numerical models (*e.g.*, computational fluid dynamics). Flow and bathymetric measurements were collected at a number of rapids within the Colorado River in Grand Canyon, Glen Canyon, and Cataract Canyon. One of the instruments used, an ADV, was demonstrated to measure

velocities <3.0 m/s, and therefore was shown incapable of fully characterizing hydraulics in rapids. Two other instruments, however, proved useful for making velocity measurements in sections of fast flow in the Colorado River. The first of these instruments was an ADCP which reliably measured velocity throughout the water column within several rapids in Cataract Canyon. The second instrument, a specially designed pitot-static tube called the POEM, also proved reliable and insightful for directly measuring water velocity and turbulent structures in the fastest water on the Colorado.

The combination of the POEM and ADCP offers advantages with respect to quantifying the hydraulics of rapids. The data collected by each instrument are complimentary and elucidate different components of a rapid complex. The POEM reliably collected insightful velocity and turbulence data near the water surface. The ADCP, while less accurate than the POEM and possibly having the tendency to drop data in the fast water, reports flow structures for the entire water column. Moreover, bathymetry data collected by the ADCP is high-quality and useful. Two ADCPs used in the field, a 600 kHz unit and a 1,200 kHz unit, both adequately measured flows in the river at the sediment load and discharge of April 2006.

Using the results of the POEM and ADCP, it appears that the fastest flowing water in the middle of a rapid occurs near the water surface. In contrast to slower, rough-boundary rivers where the fastest water appears slightly below the water surface, the flow and momentum of rapids seems to be forced to the top of the water column.

Finally, employing the new measurement and survey techniques, comprehensive bathymetry, shoreline, and water-surface surfaces were collected of a number of fan-eddy complexes, advancing geomorphic understanding and enable future model development.

6. CONCLUSIONS AND FUTURE RESEARCH

A study of the fluvial geomorphology of the Colorado River in northern Arizona and eastern Utah was undertaken with a research emphasis on characterizing the fluid mechanics within rapids. Most rapids on the Colorado River are caused by the constriction of the river's flow by accumulated deposits of coarse-grained alluvium (Melis *et al.*, 1994; Webb *et al.*, 2004). Rapids, in turn, act as the dominant control on the fluvial geomorphology within Grand Canyon and Cataract Canyon, governing the water-surface profile, the bathymetry, the storage of sand, the aquatic ecology, and even the recreational value of the river (Leopold, 1969; Howard and Dolan, 1981; Schmidt and Rubin, 1995; Webb, 1996; Stevens *et al.*, 1997; Hazel *et al.*, 2006). Despite the importance of rapids on the Colorado River, relatively little research has focused on the dominant processes affecting change directly in the fastest water of the rapid.

This study began with an analysis of the long-term trends of the water-surface profile of the Colorado River in Grand Canyon between 1923 and 2000. By registering the water-surface profile as measured in 1923 with the profile of the river measured in 2000, differences in water-surface elevation at the head of individual rapids were quantified. With these data, the general rate of aggradation in the river corridor was inferred and the overall trends discussed. A detailed and comprehensive step-backwater model of most of the Colorado River in Grand Canyon was also constructed to serve as a research tool for the current study, for future studies, as well as for the broader research

community working in Grand Canyon. In an attempt to begin to decompose the fluid mechanics within rapids, flow velocity measurements were made within several Grand and Cataract Canyon rapids using several flow-measurement technologies. These measured flow-velocity, flow-structure, and topology data provided insight into the nature of the fluid mechanics in rapids.

6.1 Key Conclusions

The water-surface elevation at the head of rapids typically increases when debris flows from tributaries add coarse-grained sediment to the river corridor (Melis *et al.*, 1994). In contrast, periodic floods on the main-stem Colorado River erode sediment from debris fans effectively lowering the water-surface elevation at the head of rapids in a process termed reworking (Webb *et al.*, 1999a). By comparing water-surface profiles, the average rate of aggradation at the head of 91 rapids in Grand Canyon between 1923 and 2000 was calculated to be 0.26 ± 0.15 m. In addition, while in 1923, 50% of the cumulative drop through the river corridor occurred in just 9% of the distance (Leopold, 1969), by 2000, the cumulative drop over the same distance increased to 66%.

Howard and Dolan (1981) postulated a regulated flow regime in Grand Canyon resulting for the closure of Glen Canyon Dam in 1963 would lead to a more pronounced pool-and-rapid morphology over time. Consistent with the Howard and Dolan hypothesis, this study showed rapids in Grand Canyon became more numerous and steeper between 1923 and 2000. However, because the analysis evaluated a time period divided almost

equally between unregulated and dam-regulated flow, no definitive conclusion could be drawn of the direct influence of Glen Canyon Dam on this measured aggradation.

In the absence of large floods on the regulated Colorado River, a new one-dimensional step-backwater hydraulic model was constructed for the reach of river in Grand Canyon from Lee's Ferry to Diamond Creek, a distance of 364 km. The model was built to replace the widely used Randle and Pemberton (1987) STARS model, and includes 2,690 cross sections. The model was set to subcritical flow with a global Manning's n of 0.035 to simulate water-surface elevations for any reach along the river at variable discharge up to 5,600 m^3/s. The model was determined to be able to predict stage-discharge relations to within 0.25 m of actual values for flows below 450 m^3/s. For flows between 450-1,600 m^3/s, model accuracy is within 0.75 m. Though only limited data are available to evaluate model performance at discharge above 1,600 m^3/s, anecdotal evidence from Palisades Creek indicates model error approaches 1.4 m at 5,600 m^3/s.

To begin to assemble a data set quantifying the flow structure and flow velocities distributed within rapid on the Colorado River, an ADV was used to make flow measurements on five rapids in Grand Canyon. While the instrument was able to measure flow velocity in three dimensions up to 3.0 m/s, limitations in instrument performance rendered data unusable for flow conditions above 3.0 m/s. While useful for making measurement in small riffles (as found in Glen Canyon), the ADV, as configured, could not measure peak water velocity in rapids of substantial size.

Concurrently with ADV measurements, bathymetry was recorded below rapids in Grand Canyon with fathometer. The fathometer was able to sound the water depth in most location of the rapid, despite the turbulent and aerated flow conditions. By assembling the bathymetric data collected with the fathometer, depth maps were constructed for the five Grand Canyon rapids offering unique insight into the bottom of the Colorado River beneath rapids.

Flow-velocity and flow-structure data were successfully collected at rapids in Cataract Canyon using a combination of an ADCP and the POEM, pitot-static tube. The ADCP was able to measure flow vectors in layered increments from 1.55 m below the surface down to just above the bed of the river. The peak average velocity measured by the ADCP in Cataract Canyon was roughly 4.0 m/s while the peak average velocity measured by the POEM was roughly 5.2 m/s. In addition, the fast-response pressure transducer built into the POEM was able to measure instantaneous flow velocities up to 6.5 m/s. These values represent some of the highest velocities values measured by the USGS. The POEM was positioned 0.39 m below the water surface, and while there were some indications the ADCP underestimated the fastest velocities of flow, the presence of an ADCP measurement error could not be definitively verified. In theory, the ADCP is capable of measuring flow up to 10 m/s. Similarly, the POEM should be able to measure velocity up to 9.0 m/s.

Using the combination of ADCP and POEM, the flow structure and nature of turbulence in rapids in Cataract Canyon were analyzed. The applicability of a logarithmic velocity profile assumption in rapids was also evaluated in Cataract Canyon. Velocity

profiles are nearly logarithmic in the pool above a rapid, in the fast water in the center of the rapid, and the fast water below a rapid. In contrast, velocity profiles in eddies and behind the eddy fence closest to the debris fan are distinctively non-logarithmic. These finding are important because reworking on debris fans centers mostly on the debris fan directly behind these eddy fences. Data collected with the POEM allowed insight into the distribution of turbulent energy in rapids and appeared to measure the generation of new turbulence in the rapid tongue.

Finally, the flow-measurement procedures developed for measurements in rapids enabled detailed maps of water surface, shoreline, and bathymetric depths to be assembled for the given rapid. Such data sets for rapids and fast water are generally unavailable in the literature. This collection of detailed topologic data from rapids will enable future research efforts to detect change in rapids. These data will also enable the development of computational fluid dynamic (CFD) models to simulate the hydraulics within rapids.

6.2 Future Research Possibilities

Transport of coarse-grained sediment (*i.e.*, cobbles and boulders) is central to understanding and predicting the evolution of fluvial geomorphology in bedrock-controlled rivers. While sediment transport data are widely available, most incipient motion and bedload data have been collected for the transport of fine-grained particles. Data on coarse-grained sediment transport is uncommon within the literature, and understanding the transport of large particles from the complicated morphology of a fresh

debris-flow deposit presents further challenges. Understanding the shear stress and the flow conditions leading to movement of large particles is necessary. Research is also needed in understanding the conditions keeping large particles moving after they are set in motion. According to O'Connor (1993), the details of the nature of the flow leading to the deposition of particles is generally unknown. This last part of the problem is pertinent to paleoflood studies and post-flood forensic analysis. Coarse-particle deposition also applies to the development of secondary rapids along the Colorado River, where boulders reworked from debris fans lodge in deposition bars.

The present study began the work toward analyzing and understanding the forces and mechanics of fluid motion in rapids. Owing to the difficulties of measurement, this is a niche of hydrology and applied fluid mechanics with relatively little available data, and yet, understanding the hydraulics in these fast-water conditions is not only important to decomposing processes on the Colorado River but also to understanding the processes in many western rivers and streams, particularly during extreme flood events. Better measurement techniques and tools applied to rapids will shed insight into other extreme flows.

To better understand the processes working to control the longitudinal profiles in Grand and Cataract Canyons (Hanks and Webb, 2006), a reworking model is needed which incorporates the best available data on hydraulics in rapids and coarse-grained sediment transport. Reworking models today are mostly conceptual or empirical with little quantitative rigor (*e.g.*, Webb *et al.*, 1999; Pizzuto *et at.*, 1999). The next generation reworking model will need to include thresholds that predict the movement of coarse-

grained particles from debris fans as a function of flow characteristics through the rapid and across the debris fan. A quantitative reworking model is also need to develop a river-evolution model for Grand Canyon.

The HEC-RAS model developed for this study is intended to be the foundation of a new river-evolution model. Analogous to landscape evolution models, this river-evolution model will be stochastic in nature simulating the aggradational changes of the river corridor over time. Input to the model is coarse-grained sediment at tributary locations modeled stochastically with a debris-flow frequency model (Griffiths *et al.*, 2004) and a sediment-yield model developed for the Colorado Plateau (Webb *et al.*, 2000). Removal of material from debris fans will be accomplished by combining the HEC-RAS model (providing inundation and water velocities anywhere in the river corridor), the newly developed reworking model, and a time series or stochastic estimate of the size of floods flowing in the main-stem Colorado. By simulating multiple years of aggradation and erosion, a better understanding of the dynamic processes governing fluvial geomorphology in Grand Canyon can be analyzed.

Finally, better understanding of the fluid mechanics in rapids is possible with the development of computational fluid dynamics (CFD) models. Two-dimensional CFD models have commonly been applied to slower sections of the river in Grand Canyon (*e.g.*, Wiele *et al.*, 1999), but the nature of flow in rapids presents challenges that require fully three-dimensional models incorporating recent numerical advances including free-surface tracking, advanced turbulence modeling, deformable boundaries, and large-eddy simulations. The hydraulic and topologic data collected in the current study provides a

baseline data set from which to construct and calibrate these new models. More importantly, once built and calibrated, capable CFD models can be used to understand shear stresses on the bed of the river and the resulting effect on coarse-grained sediment transport and the evolution of fluvial geomorphology in bedrock-controlled rivers.

APPENDIX A

WATER-SURFACE PROFILE DATA FROM 1923, 2000, 2002

Appendix A contains the water-surface elevation data of the Colorado River in Grand Canyon discussed in Chapter 2 and Chapter 3. These data are two-dimensional, representing the longitudinal profile of the river as it flows from Lee's Ferry to Diamond Creek. The variable, "River Mile" is the position of the given point along the river in miles relative to Lee's Ferry. The variable, "WSE" is the water-surface elevation of the given point. The data are presented in four tables:

Table A1: Water-surface profile constructed from LIDAR data collected in May 2000 (NVGD29, Geoid99).

Table A2: Raw water-surface profile surveyed by the 1923 USGS expedition (USGS, 1924). Vertical datum is unknown but was probably North American Datum (Magirl *et al.*, 2005).

Table A3: 1923 USGS water-surface profile data that was anchored and adjusted to the 2000 LIDAR profile (NVGD29, Geoid99).

Table A4: Water-surface profile constructed from a combination of the 2000 LIDAR profile and the 2002 ISTAR DEM (NGVD88, Ellipsoid), used to calibrate the HEC-RAS model found in Chapter 3.

Table A1: Water-surface elevation data based on 2000 LIDAR.

River Mile	WSE (m)	River Mile	WSE (m)	River Mile	WSE (m)	River Mile	WSE (m)
-0.684	949.20	9.649	933.04	17.326	913.98	23.945	897.72
-0.231	949.19	9.989	932.95	17.487	913.87	24.357	897.66
0.028	949.19	10.762	932.73	17.663	913.80	24.382	896.13
0.150	949.19	11.158	932.38	17.688	913.78	24.416	896.02
0.253	948.74	11.369	932.18	17.737	912.73	24.696	895.94
0.351	948.00	11.387	931.10	17.891	912.71	24.714	895.36
0.446	947.28	11.420	929.55	18.352	912.66	24.733	894.53
0.531	946.87	11.453	929.12	18.384	911.69	24.748	893.88
0.708	946.49	11.487	928.57	18.448	911.68	24.763	893.38
0.913	946.04	11.514	928.12	18.520	911.33	24.809	893.33
0.962	945.11	11.565	927.18	18.720	911.18	24.897	893.31
1.031	944.21	11.785	926.52	19.043	911.13	24.983	893.25
1.312	944.10	12.037	926.21	19.292	911.07	25.010	892.75
1.465	944.00	12.105	925.43	19.558	910.92	25.086	892.72
1.557	943.73	12.171	925.38	19.937	910.82	25.107	891.97
2.064	943.58	12.210	924.73	20.174	910.76	25.145	891.20
2.499	943.42	12.287	924.51	20.393	910.69	25.389	891.15
2.735	943.25	12.370	923.85	20.477	910.56	25.420	889.93
2.785	942.34	12.461	923.83	20.730	910.52	25.578	889.74
2.926	942.15	12.636	923.70	20.750	909.99	25.717	889.67
2.953	941.69	12.740	923.20	20.766	908.89	25.738	887.85
3.096	941.61	12.897	922.91	20.789	908.13	25.779	887.67
3.148	941.16	12.974	922.84	20.825	907.07	25.928	887.46
3.644	941.10	13.002	922.40	20.941	906.80	25.993	887.39
3.873	941.09	13.211	922.23	21.089	906.79	26.026	886.62
4.182	941.01	13.406	922.17	21.355	906.78	26.177	886.54
4.491	940.95	13.596	921.94	21.400	905.08	26.300	886.24
5.472	940.88	13.851	921.82	21.557	905.03	26.578	886.05
5.810	940.84	13.948	921.70	21.589	904.70	26.873	885.93
5.945	940.52	14.537	921.56	21.702	904.63	26.898	884.46
6.196	940.51	14.548	920.80	21.741	903.56	27.023	884.38
6.661	940.46	14.571	919.80	21.842	903.44	27.052	883.43
7.178	940.38	14.585	919.38	21.872	902.88	27.312	883.39
7.592	940.30	14.611	919.15	22.187	902.71	27.618	883.33
7.888	940.30	14.629	919.09	22.382	902.66	27.673	883.04
7.956	940.29	14.873	918.88	22.463	902.52	27.902	882.94
7.981	939.42	15.296	918.71	22.692	902.45	27.940	882.46
8.003	938.40	15.448	918.54	22.756	901.76	28.192	882.46
8.024	937.55	15.887	918.49	22.904	901.62	28.222	882.34
8.064	936.01	16.277	918.34	23.139	901.49	28.326	882.34
8.349	935.97	16.594	918.22	23.146	901.09	28.580	882.01
8.394	935.77	16.689	918.04	23.158	900.61	28.897	881.80
8.476	934.64	17.082	917.90	23.198	899.50	29.147	881.76
8.569	934.41	17.121	916.91	23.319	899.39	29.388	881.75
8.671	933.67	17.135	915.82	23.352	899.05	29.424	879.97
9.025	933.52	17.142	915.31	23.483	898.91	29.716	879.90
9.207	933.24	17.159	914.34	23.524	897.94	29.830	879.06
9.372	933.05	17.255	914.01	23.870	897.83	30.066	879.06

Table A1: Water-surface elevation data based on 2000 LIDAR (cont'd).

River Mile	WSE (m)	River Mile	WSE (m)	River Mile	WSE (m)	River Mile	WSE (m)
30.196	879.05	40.703	863.72	52.860	848.93	59.146	831.26
30.377	878.93	41.168	863.55	52.961	848.42	59.580	831.25
30.391	878.61	41.264	862.88	53.017	846.92	59.932	831.21
30.417	878.09	41.392	862.85	53.368	846.45	60.070	831.18
30.585	878.06	41.594	862.81	53.634	846.32	60.104	831.14
30.641	877.42	41.692	862.10	53.702	845.74	60.151	829.65
30.854	877.40	41.951	862.03	53.769	845.24	60.354	829.59
30.877	877.13	42.490	861.87	53.813	844.86	60.376	828.77
31.050	877.13	42.788	861.84	53.866	844.37	60.394	828.17
31.074	877.02	43.163	861.77	53.961	844.33	60.651	828.07
31.298	876.97	43.481	861.55	54.016	844.30	61.021	827.76
31.335	876.75	43.975	861.22	54.084	843.51	61.375	827.65
31.535	876.55	44.032	859.80	54.134	843.17	61.796	827.54
31.731	876.53	44.315	859.59	54.241	843.09	61.945	826.50
31.784	876.19	44.749	859.14	54.534	843.05	62.012	825.56
31.854	875.90	44.853	858.05	54.855	843.02	62.074	824.98
32.097	875.88	45.161	857.59	55.142	842.96	62.284	824.92
32.172	875.11	45.513	857.55	55.302	842.53	62.526	824.83
32.257	874.72	45.803	857.43	55.504	842.47	62.767	824.79
32.355	873.80	46.116	857.32	55.832	842.40	62.786	824.15
32.456	873.37	46.352	857.14	56.149	842.26	62.837	823.34
32.575	872.96	46.705	856.92	56.343	842.14	63.100	823.19
32.910	872.85	46.959	856.78	56.357	841.56	63.216	823.07
33.293	872.19	47.226	856.59	56.368	841.07	63.321	822.87
33.705	871.60	47.828	855.97	56.377	840.38	63.397	822.29
34.235	870.97	48.217	855.74	56.397	839.62	63.500	821.98
34.678	870.73	48.410	855.14	56.563	839.48	63.684	821.84
34.976	870.62	48.620	854.78	56.687	839.36	63.728	821.27
35.055	870.22	48.978	854.63	56.775	838.23	63.943	821.19
35.927	869.89	49.316	854.58	56.893	838.17	64.244	821.10
36.012	869.60	49.408	853.82	56.973	837.13	64.302	820.00
36.322	869.49	49.426	853.73	57.077	836.35	64.573	819.86
36.357	868.18	49.583	853.68	57.216	836.22	64.817	819.61
37.005	868.08	49.709	853.19	57.253	835.78	65.044	819.45
37.043	867.52	49.759	853.17	57.652	835.53	65.358	819.09
37.409	867.41	49.842	853.14	57.692	835.26	65.641	818.99
37.632	867.34	49.900	852.66	57.806	835.25	65.924	818.89
37.676	866.54	50.202	852.44	57.877	834.13	65.939	818.11
38.037	866.41	50.653	852.34	58.053	833.98	65.966	817.26
38.265	866.34	51.045	852.16	58.127	833.40	66.009	816.93
38.329	865.53	51.438	852.00	58.229	833.25	66.199	816.92
38.630	865.49	52.370	851.57	58.237	833.24	66.447	816.51
38.936	865.42	52.381	850.89	58.286	832.59	66.505	816.14
39.258	865.39	52.429	850.38	58.362	832.04	66.561	815.39
39.316	864.16	52.548	850.15	58.471	831.94	66.660	814.23
39.585	864.08	52.687	849.95	58.591	831.87	66.835	813.89
39.912	863.99	52.780	849.92	58.852	831.84	67.174	813.12
40.272	863.85	52.826	849.43	58.931	831.49	67.284	812.34

Table A1: Water-surface elevation data based on 2000 LIDAR (cont'd).

River Mile	WSE (m)	River Mile	WSE (m)	River Mile	WSE (m)	River Mile	WSE (m)
67.473	812.21	74.057	788.90	79.919	762.52	88.336	737.90
67.657	812.03	74.165	788.65	79.958	761.42	88.468	737.38
67.715	811.16	74.426	788.61	80.139	760.93	88.485	737.07
67.981	810.83	74.716	788.57	80.513	760.57	88.685	736.75
68.057	809.58	75.042	788.55	80.600	759.88	88.710	735.71
68.526	809.26	75.199	788.44	80.802	759.87	88.740	734.64
68.935	809.09	75.375	788.33	82.034	759.46	88.869	734.44
68.985	809.03	75.410	788.22	82.059	759.37	88.950	733.63
69.021	808.13	75.508	787.56	82.098	758.28	89.091	733.35
69.074	807.15	75.579	787.52	82.146	756.51	89.142	732.70
69.123	806.61	75.695	787.51	82.196	754.78	89.287	732.37
69.187	806.12	75.793	787.40	82.259	754.22	89.431	732.31
69.258	805.74	75.804	786.83	82.283	753.38	89.477	731.61
69.431	805.61	75.837	785.83	82.599	753.02	89.536	731.44
69.512	805.16	75.915	785.36	82.670	752.57	89.585	730.39
69.639	804.09	75.939	784.55	82.805	752.46	89.647	729.10
69.876	803.95	76.009	784.05	82.872	751.85	89.729	728.43
69.957	803.36	76.076	783.09	83.137	751.83	89.860	728.40
70.104	803.16	76.173	782.80	83.240	751.61	89.912	727.53
70.210	802.22	76.246	782.26	83.416	751.46	90.017	727.13
70.618	802.20	76.590	782.11	83.460	750.30	90.332	726.87
70.737	801.17	77.194	782.07	83.989	749.86	90.833	726.59
70.825	801.04	77.215	781.36	84.026	749.64	90.848	725.49
70.889	800.61	77.262	779.73	84.108	749.58	90.865	724.23
71.174	800.23	77.297	778.13	84.122	748.20	90.883	723.41
71.421	800.02	77.333	776.81	84.572	748.00	91.397	723.24
71.626	799.87	77.390	776.58	84.724	747.52	92.022	722.92
71.836	799.49	77.469	776.13	84.829	747.17	92.067	722.38
71.968	798.73	77.506	775.39	84.932	746.64	92.600	722.31
72.142	798.58	77.548	774.55	84.994	745.54	92.648	721.58
72.375	798.37	77.591	773.68	85.250	745.39	92.843	721.48
72.631	798.07	77.630	772.67	85.261	744.58	92.965	721.43
72.811	798.02	77.786	772.22	85.281	743.68	93.098	721.41
72.859	797.96	78.054	772.08	85.363	742.76	93.133	720.61
72.897	796.84	78.368	771.36	85.616	742.64	93.287	720.30
72.928	795.98	78.464	770.79	85.794	742.44	93.511	720.22
72.961	795.45	79.122	770.52	85.859	741.77	93.892	720.16
72.988	795.23	79.147	769.48	85.928	741.38	93.909	719.30
73.084	795.10	79.177	768.45	86.341	741.13	93.921	718.49
73.124	794.28	79.200	767.65	86.402	740.51	93.927	717.86
73.141	793.53	79.223	767.55	86.910	740.15	93.938	717.34
73.254	792.97	79.262	766.68	87.659	740.03	93.948	716.72
73.312	792.14	79.299	765.83	87.961	739.95	93.974	715.59
73.451	791.89	79.349	765.00	88.100	739.75	94.130	715.47
73.628	791.61	79.384	764.89	88.160	739.34	94.167	714.56
73.681	790.67	79.471	764.79	88.228	739.24	94.301	714.42
73.720	789.74	79.550	763.71	88.265	739.17	94.571	714.22
73.780	789.19	79.633	762.66	88.300	738.13	94.799	714.16

Table A1: Water-surface elevation data based on 2000 LIDAR (cont'd).

River Mile	WSE (m)	River Mile	WSE (m)	River Mile	WSE (m)	River Mile	WSE (m)
94.850	713.60	101.125	688.26	113.195	648.44	123.585	629.12
95.088	713.58	101.774	688.13	113.361	647.88	123.792	628.97
95.271	713.55	101.835	685.75	113.569	647.02	124.096	628.44
95.438	713.50	102.515	685.67	113.785	646.60	124.162	627.18
95.457	712.77	102.565	683.60	114.267	646.12	124.430	626.91
95.466	711.77	103.222	683.43	114.714	645.86	124.501	625.87
95.494	710.83	103.267	682.67	114.934	645.76	124.918	625.55
95.548	709.75	104.455	682.29	115.329	645.58	125.017	625.03
95.683	709.67	104.507	680.65	115.600	645.57	125.378	624.39
96.041	709.66	104.754	680.57	115.700	644.94	125.536	624.17
96.442	709.57	104.870	680.31	115.967	644.69	125.556	623.41
96.663	709.49	105.206	680.30	116.024	643.84	125.577	622.74
96.795	709.42	105.272	677.76	116.102	643.64	125.639	622.51
97.098	709.30	106.529	675.36	116.318	643.08	125.676	621.55
97.131	708.35	106.648	672.08	116.542	642.87	125.756	621.40
97.156	707.26	106.782	671.59	116.883	642.66	125.806	620.30
97.175	706.72	106.831	671.00	117.171	642.51	125.871	620.08
97.257	705.60	108.385	670.18	117.324	641.57	126.055	619.87
97.635	705.59	108.465	668.54	117.532	640.86	126.403	619.59
97.793	705.59	109.238	668.44	117.874	640.65	126.487	618.55
97.949	705.59	109.299	666.94	118.296	640.41	126.899	618.15
98.154	705.59	109.353	665.79	118.756	640.01	126.938	617.23
98.374	705.58	109.522	665.63	118.945	639.76	127.275	616.95
98.585	705.58	109.598	664.51	119.002	638.97	127.467	616.21
98.660	705.55	109.772	664.20	119.268	638.76	127.490	615.08
98.726	705.51	109.847	663.81	119.315	637.51	127.714	614.78
98.778	705.36	109.934	662.18	119.561	637.23	128.021	614.41
98.785	705.20	110.040	661.99	119.949	637.16	128.371	613.98
98.796	704.49	110.116	660.57	120.278	637.15	128.405	612.99
98.812	703.30	110.301	659.30	120.532	636.69	129.161	612.73
98.959	702.70	110.528	658.29	120.598	636.35	129.178	611.69
99.023	701.30	110.795	657.99	120.666	636.17	129.709	611.58
99.062	699.59	110.818	657.30	120.711	634.75	129.768	609.09
99.156	698.51	110.995	657.24	120.929	634.58	131.063	608.71
99.396	698.48	111.059	657.22	120.990	634.15	131.166	606.66
99.722	698.41	111.402	656.87	121.240	634.00	131.385	606.60
99.747	697.36	111.512	656.41	121.640	633.94	131.433	605.51
99.798	695.94	111.542	654.79	121.912	633.87	131.763	605.22
99.860	694.79	111.992	654.64	122.049	633.82	132.254	605.02
100.029	694.65	112.355	654.44	122.236	633.45	132.287	603.37
100.059	693.53	112.759	654.31	122.273	632.32	132.311	602.22
100.089	692.57	112.780	653.88	122.488	632.17	132.337	600.59
100.197	692.47	112.804	653.28	122.643	631.75	132.486	600.50
100.326	690.43	112.833	652.57	122.838	631.48	132.742	600.17
100.530	690.27	112.870	651.60	123.083	631.29	133.324	599.78
100.709	690.27	112.915	650.62	123.309	631.19	133.589	599.29
100.740	689.38	112.979	650.38	123.347	630.16	133.896	599.05
100.987	689.36	113.113	649.89	123.389	629.20	134.331	598.91

Table A1: Water-surface elevation data based on 2000 LIDAR (cont'd).

River Mile	WSE (m)	River Mile	WSE (m)	River Mile	WSE (m)	River Mile	WSE (m)
134.355	597.69	144.220	569.78	154.809	545.91	167.082	529.70
134.378	596.86	144.344	568.46	155.176	545.68	167.153	529.42
134.410	596.04	144.386	568.09	155.490	545.48	167.367	529.21
134.713	595.88	144.597	567.79	155.779	545.17	167.443	528.87
134.727	594.87	144.626	567.29	155.947	544.81	167.672	528.88
134.759	594.01	144.911	566.87	156.139	544.17	168.074	528.43
134.851	593.57	144.941	565.98	156.352	543.79	168.477	528.20
135.076	593.03	145.450	565.60	156.593	543.70	168.537	527.49
135.186	592.21	145.500	564.47	156.943	543.56	168.580	526.96
135.295	592.05	145.797	564.33	157.226	543.43	168.837	526.71
135.363	591.27	145.921	563.87	157.484	542.13	169.142	526.53
135.438	590.34	146.036	563.34	157.767	542.02	169.365	526.38
135.562	589.83	146.256	562.47	158.192	541.75	169.748	526.03
136.537	589.43	146.396	562.35	158.364	541.25	170.251	525.91
136.901	589.23	146.541	562.21	158.719	540.79	170.298	525.50
136.937	588.29	146.599	561.53	158.752	539.82	170.338	525.21
137.012	588.13	146.829	561.08	159.169	539.36	170.501	525.18
137.057	586.68	147.222	560.92	159.469	539.20	170.794	525.07
137.275	586.19	147.859	560.74	159.638	539.04	171.151	524.89
137.492	586.15	148.362	560.51	159.768	538.42	171.479	524.79
137.850	585.97	148.435	558.96	159.956	537.86	171.688	524.67
138.070	585.78	148.522	558.85	160.138	537.65	171.850	524.61
138.335	585.27	148.799	558.58	160.418	537.30	171.914	524.58
138.352	584.58	149.249	558.36	160.720	536.93	171.969	523.32
138.370	583.64	149.546	558.03	161.022	536.78	171.990	522.74
138.773	583.53	149.725	557.88	161.262	536.63	172.016	522.22
138.790	582.37	150.024	557.69	161.316	535.54	172.225	522.04
139.107	582.08	150.211	557.52	161.685	535.36	172.281	521.57
139.146	581.11	150.227	556.39	161.911	535.30	172.536	521.41
139.657	581.09	150.239	555.77	162.166	535.12	172.738	521.16
139.699	579.77	150.252	555.15	162.195	534.17	172.992	520.97
139.742	578.41	150.281	554.29	162.390	534.02	173.356	520.58
139.981	578.16	150.318	553.68	162.586	533.97	173.485	520.46
140.200	577.94	150.485	553.39	162.804	533.90	173.716	520.11
140.385	577.68	150.708	553.10	163.117	533.68	173.814	519.98
140.489	577.34	151.094	552.51	163.433	533.47	173.981	519.92
140.530	576.41	151.494	551.91	163.950	533.13	174.161	519.68
140.899	576.16	151.974	551.13	164.283	533.03	174.294	519.64
141.337	575.76	152.451	551.01	164.655	532.89	174.411	519.64
141.644	575.32	152.827	550.84	164.928	532.63	174.508	519.58
141.743	574.31	152.870	549.60	165.041	531.32	174.586	519.38
142.374	573.68	153.188	549.43	165.323	531.24	174.612	519.10
144.038	573.64	153.350	548.90	165.647	531.13	174.639	518.78
144.042	573.28	153.695	548.69	166.032	530.91	174.798	518.56
144.050	572.91	153.799	547.76	166.301	530.83	174.831	518.42
144.060	572.31	154.027	547.39	166.895	530.68	174.872	517.42
144.073	571.65	154.220	546.78	166.957	530.27	174.985	517.14
144.141	570.72	154.571	546.20	167.021	530.14	175.031	516.84

Table A1: Water-surface elevation data based on 2000 LIDAR (cont'd).

River Mile	WSE (m)	River Mile	WSE (m)	River Mile	WSE (m)	River Mile	WSE (m)
175.100	516.68	181.517	499.39	191.449	477.72	201.428	458.77
175.437	516.34	181.587	499.16	191.901	477.46	201.556	457.97
175.480	515.96	181.949	498.87	192.299	476.80	201.858	457.66
175.799	515.82	182.126	498.38	192.569	476.66	201.968	457.08
176.074	515.66	182.372	498.10	193.038	476.14	202.294	456.82
176.250	515.18	182.446	497.90	193.443	475.66	202.397	456.39
176.409	515.10	182.591	497.75	193.548	474.86	202.628	456.22
176.507	514.36	182.691	496.35	193.659	474.48	203.091	456.10
176.784	514.24	183.024	496.04	193.669	474.26	203.223	455.75
177.093	514.02	183.082	495.56	193.795	474.07	203.754	455.24
177.132	513.82	183.178	495.28	193.882	473.63	203.985	455.14
177.155	513.40	183.423	495.13	194.225	473.29	204.293	454.80
177.175	512.98	183.596	494.86	194.340	472.99	204.728	454.46
177.225	512.64	183.841	494.16	194.384	472.53	204.753	453.80
177.439	512.52	184.067	493.82	194.465	471.94	205.153	453.88
177.513	512.32	184.372	493.23	194.841	471.52	205.607	453.78
177.609	511.98	184.494	492.46	195.057	471.16	205.651	453.66
177.857	511.88	184.817	491.88	195.312	470.77	205.671	453.28
177.912	511.38	184.904	491.22	195.363	470.24	205.684	452.62
178.014	511.24	185.211	490.68	195.410	469.85	205.705	451.72
178.187	511.18	185.802	489.32	195.476	469.53	205.720	450.80
178.734	511.12	185.952	489.18	195.757	469.42	205.750	450.52
179.723	511.00	186.109	489.08	195.794	469.07	205.793	450.40
179.736	510.62	186.487	488.68	195.829	468.81	205.971	450.16
179.745	510.12	187.032	488.40	195.861	468.59	206.342	449.54
179.756	509.44	187.624	488.16	196.119	468.38	206.366	448.60
179.779	508.00	187.747	487.38	196.188	467.93	206.397	447.82
179.801	506.84	188.229	487.00	196.488	467.60	206.606	447.30
179.873	506.82	188.267	486.54	196.610	467.29	207.218	447.06
179.959	506.80	188.485	486.24	196.750	467.24	207.255	446.38
180.040	506.70	188.552	485.24	196.923	466.37	207.500	445.72
180.055	506.59	188.811	485.06	197.646	466.08	207.593	445.38
180.082	505.90	188.947	484.12	197.914	465.17	207.689	444.92
180.103	505.37	189.130	483.93	198.789	464.89	207.742	444.56
180.130	505.06	189.236	483.03	198.831	464.65	207.823	443.84
180.186	504.77	189.343	482.74	198.867	464.38	208.713	443.24
180.261	504.63	189.545	482.68	198.918	463.86	208.774	442.74
180.404	504.58	189.657	482.29	198.969	463.62	209.186	442.66
180.455	503.90	189.729	482.15	199.010	463.36	209.206	441.16
180.527	503.31	189.800	481.88	199.066	462.94	209.258	440.88
180.593	502.91	190.089	481.56	199.120	462.52	209.356	440.34
180.608	502.92	190.144	480.73	199.169	461.98	209.500	439.82
180.650	502.51	191.133	480.20	199.318	461.72	209.576	439.34
180.788	502.19	191.179	479.26	199.564	461.44	209.631	439.06
180.860	501.68	191.213	478.70	199.789	460.76	209.752	438.54
180.981	500.34	191.235	478.48	200.463	459.90	209.915	438.08
181.110	499.96	191.308	478.40	200.693	459.40	210.047	437.12
181.154	499.84	191.366	478.06	201.019	459.23	210.328	436.74

Table A1: Water-surface elevation data based on 2000 LIDAR (cont'd).

River Mile	WSE (m)	River Mile	WSE (m)	River Mile	WSE (m)
210.402	436.08	221.918	413.92	228.484	393.64
210.701	435.66	221.980	413.50	228.780	393.46
210.855	435.58	222.030	412.76	229.182	393.24
210.884	435.14	222.079	412.44	229.209	392.26
211.193	434.94	222.211	412.20	229.253	391.50
211.653	434.60	222.480	412.08	229.297	391.02
211.735	434.16	222.536	411.76	229.594	390.60
211.893	433.80	222.701	411.56	229.609	390.22
211.943	433.14	222.933	411.40	229.679	389.28
212.139	432.74	222.988	410.66	229.818	388.82
212.277	431.96	223.116	410.46	230.129	388.32
212.493	431.82	223.164	409.70		
212.523	430.58	223.495	409.34		
213.053	430.12	223.548	408.70		
213.554	429.48	223.740	408.38		
214.374	429.16	223.809	407.06		
214.442	428.74	224.126	406.78		
214.590	428.58	225.029	406.58		
214.692	428.11	225.628	406.38		
215.284	427.74	225.724	406.22		
215.998	427.38	225.952	405.96		
216.070	426.44	225.972	405.38		
216.173	426.24	225.996	404.96		
216.594	425.96	226.019	404.56		
216.858	425.78	226.060	403.92		
217.198	425.59	226.100	403.26		
217.741	425.58	226.121	402.76		
217.800	423.40	226.146	402.20		
217.956	423.08	226.203	401.92		
218.011	421.82	226.243	401.50		
218.247	421.54	226.307	400.86		
218.311	420.74	226.457	400.48		
219.530	420.58	226.497	399.68		
219.621	419.80	226.732	399.36		
220.033	419.52	226.895	399.18		
220.221	419.20	226.928	398.74		
220.393	418.98	226.986	398.36		
220.627	418.88	227.162	397.26		
220.711	417.90	227.253	396.98		
220.798	416.96	227.323	396.78		
220.846	416.60	227.451	396.49		
220.927	416.34	227.637	396.18		
220.981	416.08	227.845	395.87		
221.008	415.58	228.196	395.60		
221.031	415.20	228.233	395.24		
221.232	414.94	228.257	394.90		
221.294	414.30	228.286	394.42		
221.611	414.16	228.326	393.90		

Table A2: Raw 1923 USGS (Birdseye) water-surface elevation data.

River Mile	WSE (m)	River Mile	WSE (m)	River Mile	WSE (m)	River Mile	WSE (m)
0.000	949.45	29.269	880.35	58.769	831.71	84.358	747.43
1.378	946.43	29.905	879.65	59.549	830.98	84.623	747.00
2.628	944.88	30.142	879.56	59.855	829.48	84.718	744.72
2.793	943.33	30.246	878.49	60.648	827.65	84.866	744.47
4.634	941.89	31.118	877.09	61.311	827.29	85.388	742.68
7.792	940.28	31.555	876.97	61.847	824.70	85.953	741.67
7.961	936.53	31.698	875.60	62.440	823.81	86.289	741.40
9.000	934.82	32.206	874.04	63.270	821.50	86.608	740.72
9.200	934.52	33.000	872.95	63.997	819.91	87.491	739.93
11.094	933.75	33.570	872.12	64.638	818.78	87.882	737.68
11.421	928.76	34.651	871.94	65.445	817.93	88.356	733.96
12.535	925.19	34.728	870.97	65.628	815.61	88.861	731.95
12.998	924.25	35.097	870.81	66.000	814.55	89.213	727.65
14.361	922.90	35.161	870.42	66.260	813.76	90.000	727.10
14.552	920.07	35.613	870.42	67.688	809.12	90.326	726.89
16.447	918.91	35.690	869.72	68.430	808.30	90.421	724.24
16.957	917.68	36.000	869.59	68.908	804.70	90.834	723.90
17.060	914.89	36.043	869.53	69.715	801.20	91.652	722.74
18.317	913.06	36.193	867.22	70.674	799.52	91.881	722.04
19.271	912.39	37.002	867.03	71.098	798.48	92.234	721.83
20.549	912.30	38.541	865.63	72.203	797.05	92.450	721.64
20.753	908.67	39.338	864.35	72.361	796.72	92.720	720.85
21.000	908.30	40.933	863.83	72.667	790.35	93.267	720.76
21.188	907.82	41.075	863.44	73.416	789.07	93.664	715.49
21.837	904.71	41.780	862.61	74.708	788.12	94.778	714.39
22.495	904.65	43.663	861.52	75.251	787.57	95.051	709.85
22.562	904.10	43.785	860.15	75.430	782.67	96.204	709.18
23.103	901.35	44.558	858.56	75.983	781.75	96.554	708.84
23.242	901.08	45.308	858.32	76.506	781.60	96.800	705.12
23.436	899.16	45.796	857.31	76.827	774.86	97.604	704.79
24.085	898.61	46.538	856.88	77.009	773.25	98.195	704.00
24.140	897.27	47.108	856.82	77.498	772.64	98.475	698.88
24.446	897.06	48.000	855.73	77.837	771.36	99.133	698.42
24.527	894.53	48.852	854.99	78.000	771.11	99.268	695.43
24.900	893.92	49.692	852.77	78.469	770.60	99.434	695.16
25.021	892.06	51.799	852.13	78.754	764.77	99.524	694.03
25.150	891.81	52.094	851.67	79.114	764.53	99.608	693.42
25.236	890.87	52.758	847.40	79.479	763.65	99.749	692.17
25.452	890.75	53.419	844.81	79.737	762.30	100.408	690.46
25.601	889.28	53.532	843.87	80.468	761.42	100.527	689.67
25.796	888.49	54.433	843.59	81.326	760.11	101.051	688.73
25.853	887.46	55.227	842.80	81.491	760.08	101.313	686.47
26.649	886.94	55.849	842.65	81.751	755.05	101.852	686.04
26.754	884.90	56.115	840.76	82.538	752.92	101.963	685.80
28.264	883.43	56.741	838.75	83.511	751.61	102.000	685.19
28.332	882.52	56.844	836.98	83.581	749.53	102.612	685.01
29.156	882.18	57.000	836.68	83.890	749.05	102.697	683.45

Table A2: Raw 1923 USGS (Birdseye) water-surface elevation data (cont'd).

River Mile	WSE (m)	River Mile	WSE (m)	River Mile	WSE (m)	River Mile	WSE (m)
103.782	682.39	122.695	633.04	139.465	578.88	158.193	541.05
103.888	681.29	122.835	630.94	139.580	578.14	158.571	540.87
104.092	681.17	123.429	629.26	139.871	577.99	158.730	539.95
104.200	680.80	123.532	628.47	139.985	576.68	159.149	539.65
104.601	680.65	124.314	626.85	140.298	576.47	159.443	538.15
104.737	678.24	124.416	625.97	141.130	575.40	160.706	537.24
104.886	678.18	124.766	625.75	143.471	573.97	160.830	536.23
105.041	676.90	125.324	621.21	143.981	568.51	161.681	536.08
105.881	675.83	125.786	620.91	144.194	568.15	161.815	535.41
106.127	672.60	125.866	620.27	144.299	567.48	162.445	535.26
106.396	672.02	126.239	619.78	144.501	567.29	162.841	535.02
107.046	671.38	126.380	618.87	144.615	566.71	162.955	534.47
107.418	670.59	126.680	617.22	144.944	566.62	164.091	534.07
107.977	669.34	126.866	616.09	145.000	565.71	164.449	533.80
108.549	668.88	127.563	615.51	145.019	565.46	164.553	532.64
108.758	666.29	127.950	614.63	145.569	564.15	165.079	532.49
109.000	665.99	128.458	614.48	145.698	563.09	165.184	532.18
109.249	665.07	128.565	612.34	146.056	562.84	166.418	531.91
109.514	661.60	129.012	612.31	146.385	561.84	166.564	530.41
109.730	660.81	129.102	610.51	147.003	561.44	167.211	530.11
109.821	659.62	130.384	609.97	147.859	561.14	167.970	529.47
110.276	659.25	130.479	607.59	147.987	559.80	168.106	527.88
110.378	657.94	131.430	606.55	148.392	559.46	169.000	527.30
110.666	657.73	131.588	606.52	149.054	558.73	169.819	526.48
110.895	656.81	131.744	601.98	149.627	558.39	169.930	526.05
111.012	655.23	132.202	601.86	149.860	553.85	171.356	525.57
111.455	654.31	132.314	601.28	151.026	552.57	171.553	522.58
112.000	654.16	132.953	600.70	151.596	552.05	172.521	521.97
112.097	654.10	133.000	600.46	152.342	551.08	173.232	521.79
112.302	649.93	133.140	599.60	152.440	550.16	173.354	520.69
112.682	649.10	133.638	599.27	153.197	549.55	174.261	520.39
113.295	646.82	133.853	597.35	153.291	548.64	174.673	517.89
114.975	646.72	134.041	596.80	153.492	548.64	175.168	517.34
115.094	646.02	134.160	594.79	153.568	547.42	175.719	517.09
115.697	644.07	134.362	594.15	154.012	546.75	175.811	516.45
115.999	644.04	134.952	591.25	154.802	546.41	175.964	516.30
116.494	643.77	135.104	590.70	154.899	546.11	176.100	515.36
116.743	642.46	136.182	590.46	155.401	545.84	176.694	515.33
118.617	639.87	136.407	587.75	155.504	545.23	176.867	514.05
118.713	639.38	137.631	585.16	155.687	544.68	177.361	513.50
119.228	638.98	137.749	584.85	155.790	544.13	177.502	512.28
119.952	638.19	138.039	584.70	156.674	543.46	177.832	511.76
120.062	636.27	138.168	584.12	156.845	542.42	178.189	511.76
121.000	635.81	138.563	584.03	157.000	542.39	179.000	511.15
121.090	635.72	138.703	582.93	157.647	542.27	179.256	511.03
121.558	635.26	139.061	582.26	157.775	541.78	179.399	508.04
121.650	634.11	139.179	579.21	158.117	541.63	179.618	507.19

Table A2: Raw 1923 USGS (Birdseye) water-surface elevation data (cont'd).

River Mile	WSE (m)	River Mile	WSE (m)	River Mile	WSE (m)
179.779	505.18	195.499	469.42	218.045	422.03
179.941	504.69	196.102	468.39	219.196	421.78
180.171	503.22	196.441	467.44	219.354	420.90
180.750	501.37	197.518	466.10	219.819	420.56
180.892	500.27	198.388	465.95	220.065	419.86
181.451	499.78	198.548	465.40	220.402	419.65
181.605	499.66	198.648	465.22	220.735	416.57
181.735	498.35	198.849	462.69	220.996	416.39
182.261	497.98	199.666	460.61	221.134	415.78
183.047	496.49	200.758	460.52	221.716	414.59
183.202	494.93	201.146	460.34	221.898	413.43
183.408	494.66	201.243	459.09	222.777	412.55
183.692	494.05	201.845	458.72	222.889	411.27
184.000	493.11	202.012	457.84	223.000	411.02
184.328	492.25	202.613	457.14	223.223	410.17
184.628	491.98	203.072	456.19	223.526	409.80
185.311	491.28	203.598	456.04	223.675	407.91
185.401	490.06	204.280	455.43	224.672	407.40
185.740	489.72	204.415	454.09	225.491	407.06
186.239	488.84	205.000	453.85	225.765	406.66
186.744	488.50	205.176	453.85	225.937	403.28
186.966	488.23	205.353	451.29	226.864	398.43
187.910	487.47	205.560	451.10	227.327	397.58
188.017	486.74	205.673	450.31	227.801	396.94
188.704	486.13	206.082	450.04	228.307	395.11
189.093	485.61	206.593	448.06	228.967	393.86
189.604	484.45	207.207	446.44	229.000	393.65
189.946	481.77	207.443	445.53		
190.029	481.37	207.732	444.70		
190.242	481.04	208.906	442.81		
190.528	481.00	209.332	439.13		
190.655	480.82	209.636	438.09		
190.981	479.51	210.244	436.75		
191.801	478.32	210.758	436.26		
191.954	478.32	211.526	435.13		
192.132	477.83	211.729	433.97		
193.000	476.40	212.126	433.49		
193.141	476.07	212.265	432.15		
193.241	475.98	212.961	431.23		
193.455	474.79	213.996	430.32		
194.348	472.87	214.935	429.55		
194.517	472.41	215.257	429.43		
194.592	472.23	215.888	427.94		
194.680	471.68	217.000	427.18		
194.881	471.43	217.395	426.87		
195.040	470.43	217.752	423.18		
195.370	470.09	217.932	422.82		

Table A3: Anchored 1923 USGS water-surface elevation data.

River Mile	WSE (m)	River Mile	WSE (m)	River Mile	WSE (m)	River Mile	WSE (m)
0.131	947.68	29.498	879.92	59.281	831.90	84.973	746.92
1.497	944.66	30.123	879.24	60.070	831.18	85.250	746.50
2.735	943.10	30.377	879.15	60.381	829.68	85.345	744.22
2.897	941.55	30.480	878.09	61.143	827.82	85.492	743.98
4.816	940.12	31.341	876.70	61.796	827.43	86.016	742.20
7.956	938.50	31.731	876.59	62.357	824.82	86.583	741.22
8.110	934.75	31.870	875.22	62.939	823.91	86.917	740.96
9.253	933.05	32.388	873.67	63.749	821.56	87.233	740.30
9.432	932.74	33.258	872.60	64.489	819.95	88.100	739.54
11.249	931.98	33.835	871.78	65.128	818.80	88.467	737.29
11.568	926.98	34.976	871.63	65.924	817.92	88.914	733.59
12.639	923.41	35.053	870.65	66.105	815.59	89.392	731.60
13.078	922.47	35.420	870.51	66.472	814.51	89.737	727.31
14.517	921.13	35.480	870.11	66.737	813.71	90.528	726.79
14.692	918.29	35.910	870.12	68.209	809.02	90.833	726.59
16.605	917.13	35.984	869.42	68.935	808.17	90.932	723.94
17.113	915.90	36.279	869.31	69.366	804.56	91.357	723.62
17.215	913.11	36.322	869.25	70.200	801.02	92.181	722.49
18.488	911.28	36.472	866.93	71.127	799.31	92.409	721.80
19.483	910.61	37.280	866.77	71.531	798.26	92.777	721.59
20.730	910.52	38.743	865.39	72.680	796.78	93.006	721.42
20.941	906.93	39.535	864.13	72.859	796.44	93.293	720.64
21.198	906.60	41.168	863.65	73.223	790.06	93.892	720.56
21.388	906.14	41.326	863.25	73.986	788.75	94.327	715.30
22.043	903.13	42.085	862.45	75.224	787.76	95.438	714.24
22.692	903.17	43.975	861.39	75.793	787.19	95.692	709.71
22.761	902.64	44.087	860.02	75.988	782.27	96.886	709.08
23.329	899.98	44.926	858.45	76.588	781.34	97.243	708.75
23.483	899.73	45.751	858.22	77.194	781.16	97.494	705.04
23.687	897.84	46.253	857.23	77.539	774.41	98.277	704.73
24.357	897.40	46.937	856.82	77.734	772.79	98.842	703.96
24.409	896.07	47.449	856.77	78.199	772.16	99.106	698.85
24.696	895.90	48.314	855.69	78.521	770.87	99.722	698.41
24.766	893.38	49.174	854.97	78.676	770.62	99.850	695.42
25.086	892.82	49.920	852.76	79.122	770.09	100.006	695.13
25.206	890.98	52.071	852.17	79.387	764.25	100.092	694.00
25.337	890.75	52.370	851.72	79.725	764.00	100.171	693.38
25.424	889.82	53.091	847.46	80.072	763.10	100.304	692.13
25.644	889.73	53.800	844.89	80.318	761.75	100.959	690.38
25.795	888.29	53.920	843.95	81.045	760.84	101.082	689.58
25.993	887.53	54.880	843.69	81.884	759.50	101.616	688.60
26.049	886.51	55.713	842.92	82.034	759.46	101.875	686.33
26.873	886.11	56.343	842.78	82.294	754.44	102.405	685.87
26.973	884.09	56.593	840.89	83.108	752.34	102.515	685.62
28.491	882.86	57.177	838.89	84.108	751.06	102.552	685.01
28.563	881.96	57.274	837.13	84.177	748.99	103.222	684.78
29.388	881.75	57.419	836.83	84.489	748.52	103.311	683.22

Table A3: Anchored 1923 USGS water-surface elevation data (cont'd).

River Mile	WSE (m)	River Mile	WSE (m)	River Mile	WSE (m)	River Mile	WSE (m)
104.370	682.09	123.309	631.14	140.072	577.71	158.787	539.85
104.469	680.99	123.465	629.04	140.191	576.97	159.128	539.67
104.672	680.85	124.096	627.39	140.489	576.82	159.271	538.75
104.786	680.48	124.193	626.61	140.599	575.51	159.638	538.45
105.206	680.30	124.918	625.02	140.894	575.30	159.935	536.95
105.350	677.88	125.058	624.14	141.706	574.23	161.262	536.04
105.506	677.80	125.536	623.95	144.038	572.79	161.379	535.03
105.669	676.50	126.005	619.43	144.488	567.34	162.166	534.88
106.529	675.34	126.403	619.15	144.699	566.97	162.302	534.21
106.785	672.08	126.494	618.51	144.803	566.30	162.927	534.05
107.061	671.47	126.899	618.04	145.007	566.12	163.316	533.81
107.727	670.76	127.040	617.13	145.121	565.54	163.427	533.26
108.108	669.93	127.341	615.50	145.450	565.45	164.599	532.86
108.680	668.62	127.525	614.38	145.513	564.53	164.928	532.59
109.238	668.10	128.260	613.83	145.531	564.29	165.024	531.43
109.411	665.49	128.674	612.97	146.078	562.98	165.522	531.28
109.611	665.16	129.161	612.84	146.206	561.91	165.637	530.97
109.850	664.22	129.267	610.71	146.562	561.66	166.942	530.69
110.105	660.72	129.709	610.70	146.886	560.66	167.083	529.20
110.312	659.91	129.797	608.90	147.494	560.26	167.718	528.90
110.400	658.71	131.063	608.41	148.362	559.95	168.477	528.25
110.795	658.30	131.156	606.04	148.497	558.61	168.608	526.67
110.908	656.98	132.097	605.04	148.909	558.28	169.469	526.09
111.226	656.73	132.254	605.02	149.587	557.54	170.251	525.26
111.435	655.79	132.411	600.49	150.211	557.21	170.371	524.84
111.543	654.20	132.868	600.38	150.439	552.67	171.914	524.35
112.044	653.23	132.978	599.81	151.580	551.38	172.124	521.36
112.660	653.01	133.610	599.26	152.116	550.87	173.095	520.75
112.759	652.94	133.656	599.02	152.827	549.89	173.766	520.56
112.958	648.74	133.804	598.17	152.927	548.97	173.882	519.47
113.326	647.88	134.331	597.86	153.695	548.36	174.723	519.16
113.927	645.52	134.537	595.95	153.788	547.45	175.087	516.66
115.600	645.25	134.713	595.41	153.987	547.45	175.557	516.11
115.725	644.54	134.834	593.40	154.062	546.23	176.146	515.87
116.360	642.52	135.041	592.77	154.503	545.56	176.245	515.23
116.680	642.45	135.644	589.90	155.364	545.22	176.409	515.07
117.171	642.13	135.801	589.36	155.470	544.92	176.542	514.13
117.410	640.79	136.901	589.17	155.965	544.64	177.093	514.10
119.358	637.99	137.076	586.46	156.064	544.03	177.281	512.82
119.459	637.49	138.297	583.93	156.238	543.48	177.857	512.27
119.977	637.04	138.440	583.63	156.338	542.93	178.001	511.05
120.666	636.17	138.773	583.49	157.226	542.26	178.338	510.53
120.771	634.25	138.884	582.92	157.397	541.23	178.691	510.53
121.704	633.84	139.225	582.84	157.551	541.19	179.468	509.92
121.789	633.75	139.346	581.75	158.229	541.07	179.723	509.80
122.236	633.31	139.657	581.09	158.364	540.58	179.864	506.81
122.318	632.16	139.779	578.04	158.719	540.43	180.077	505.95

Table A3: Anchored 1923 USGS water-surface elevation data (cont'd).

River Mile	WSE (m)	River Mile	WSE (m)	River Mile	WSE (m)
180.234	503.94	195.995	468.16	218.336	420.73
180.393	503.45	196.585	467.13	219.530	420.49
180.635	501.99	196.949	466.18	219.671	419.61
181.258	500.13	198.013	464.84	220.085	419.27
181.411	499.03	198.863	464.69	220.308	418.57
181.963	498.54	199.034	464.14	220.627	418.36
182.113	498.42	199.141	463.95	220.948	415.28
182.238	497.11	199.356	461.42	221.200	415.10
182.749	496.75	200.132	459.35	221.332	414.49
183.521	495.25	201.206	459.26	221.889	413.30
183.685	493.70	201.596	459.07	222.062	412.14
183.903	493.42	201.693	457.82	222.933	411.25
184.203	492.81	202.295	457.46	223.061	409.97
184.529	491.87	202.461	456.57	223.187	409.73
184.862	491.01	203.046	455.87	223.421	408.88
185.168	490.74	203.495	454.92	223.740	408.51
185.840	490.03	204.044	454.77	223.880	406.62
185.925	488.82	204.728	454.16	224.837	406.10
186.246	488.48	204.860	452.82	225.666	405.77
186.733	487.60	205.435	452.57	225.952	405.37
187.243	487.26	205.607	452.57	226.129	401.99
187.466	486.98	205.773	450.01	227.145	397.14
188.389	486.22	205.966	449.83	227.608	396.29
188.494	485.49	206.071	449.04	228.063	395.65
189.158	484.88	206.459	448.76	228.555	393.82
189.544	484.36	206.967	446.78	229.202	392.57
190.089	483.20	207.579	445.16	229.234	392.36
190.454	480.52	207.816	444.25		
190.543	480.12	208.106	443.43		
190.766	479.79	209.186	441.54		
191.067	479.75	209.638	437.85		
191.201	479.57	209.975	436.81		
191.543	478.26	210.620	435.47		
192.284	477.07	211.132	434.98		
192.423	477.07	211.897	433.85		
192.595	476.58	212.099	432.69		
193.454	475.15	212.493	432.20		
193.607	474.81	212.628	430.86		
193.715	474.72	213.307	429.95		
193.946	473.53	214.326	429.03		
194.876	471.61	215.318	428.27		
195.042	471.15	215.630	428.14		
195.115	470.97	216.225	426.65		
195.201	470.42	217.394	425.89		
195.400	470.18	217.741	425.58		
195.554	469.17	218.064	421.89		
195.871	468.84	218.227	421.53		

Table A4: Constructed water-surface profile based on 2000 and 2002 data.

River Mile	WSE (ft)	WSE (m)	River Mile	WSE (ft)	WSE (m)	River Mile	WSE (ft)	WSE (m)
-0.001	3041.24	926.97	4.650	3013.90	918.64	10.964	2986.73	910.36
0.220	3040.05	926.61	4.670	3013.89	918.63	11.181	2986.11	910.17
0.351	3036.20	925.43	4.679	3013.89	918.63	11.281	2985.81	910.07
0.549	3032.93	924.44	4.709	3013.88	918.63	11.355	2985.59	910.01
0.801	3031.22	923.92	4.899	3013.83	918.62	11.374	2984.13	909.56
0.919	3030.17	923.60	5.094	3013.78	918.60	11.384	2982.69	909.12
0.939	3029.27	923.32	5.307	3013.72	918.58	11.433	2976.04	907.10
0.948	3028.63	923.13	5.402	3013.70	918.58	11.464	2973.87	906.44
0.981	3026.77	922.56	5.452	3013.68	918.57	11.520	2971.65	905.76
1.043	3024.14	921.76	5.511	3013.66	918.56	11.591	2968.04	904.66
1.105	3023.77	921.65	5.691	3013.59	918.54	11.675	2967.61	904.53
1.167	3023.41	921.54	5.837	3013.35	918.47	11.754	2967.22	904.41
1.333	3023.18	921.47	5.847	3013.24	918.44	11.834	2966.95	904.33
1.569	3023.06	921.43	5.857	3013.13	918.40	11.914	2966.77	904.27
1.671	3022.97	921.40	5.909	3012.61	918.24	11.958	2966.67	904.24
1.892	3022.73	921.33	6.224	3012.21	918.12	12.029	2966.19	904.09
1.998	3022.61	921.29	6.606	3011.86	918.01	12.047	2965.17	903.78
2.063	3022.54	921.27	6.937	3011.75	917.98	12.058	2964.65	903.63
2.227	3022.52	921.26	7.211	3011.70	917.97	12.107	2963.84	903.38
2.351	3022.51	921.26	7.257	3011.69	917.96	12.195	2962.22	902.88
2.371	3022.51	921.26	7.283	3011.69	917.96	12.269	2960.55	902.38
2.380	3022.51	921.26	7.535	3011.65	917.95	12.299	2960.07	902.23
2.398	3022.51	921.26	7.829	3011.62	917.94	12.319	2959.74	902.13
2.466	3022.50	921.26	7.922	3011.59	917.93	12.399	2958.79	901.84
2.534	3022.09	921.13	7.957	3011.28	917.84	12.458	2958.68	901.81
2.638	3021.21	920.86	7.979	3009.25	917.22	12.613	2958.03	901.61
2.706	3021.19	920.86	7.988	3007.97	916.83	12.675	2957.60	901.48
2.727	3020.00	920.50	8.026	3003.13	915.35	12.695	2957.20	901.35
2.737	3019.28	920.28	8.068	2997.78	913.72	12.704	2957.00	901.29
2.818	3018.52	920.04	8.186	2994.62	912.76	12.734	2956.33	901.09
2.886	3018.48	920.03	8.369	2993.84	912.52	12.875	2955.77	900.92
2.916	3018.00	919.89	8.413	2993.07	912.29	12.946	2955.59	900.86
3.035	3016.69	919.49	8.488	2992.92	912.24	12.967	2955.54	900.85
3.110	3016.60	919.46	8.559	2992.79	912.20	12.976	2955.08	900.71
3.129	3016.25	919.35	8.653	2990.62	911.54	13.000	2954.00	900.38
3.138	3016.04	919.29	8.733	2989.98	911.35	13.055	2953.48	900.22
3.185	3015.04	918.98	8.754	2989.95	911.34	13.142	2953.34	900.18
3.303	3014.62	918.86	8.764	2989.94	911.33	13.260	2953.16	900.12
3.383	3014.46	918.81	8.801	2989.90	911.32	13.325	2953.12	900.11
3.483	3014.46	918.81	8.955	2989.71	911.26	13.474	2953.04	900.09
3.662	3014.45	918.80	9.162	2989.04	911.06	13.589	2952.76	900.00
3.809	3014.44	918.80	9.313	2988.63	910.93	13.757	2952.36	899.88
3.940	3014.43	918.80	9.382	2988.48	910.89	13.816	2952.27	899.85
3.996	3014.37	918.78	9.438	2988.35	910.85	13.867	2952.17	899.82
4.017	3014.31	918.76	9.718	2988.18	910.80	13.876	2952.10	899.80
4.026	3014.29	918.76	9.935	2988.08	910.77	13.885	2952.03	899.78
4.070	3014.17	918.72	10.144	2987.90	910.71	13.918	2951.83	899.72
4.206	3014.09	918.69	10.573	2987.48	910.58	14.080	2951.78	899.70
4.558	3013.92	918.64	10.769	2987.28	910.52	14.278	2951.69	899.68

Table A4: Constructed water-surface profile based on 2000 and 2002 data (cont'd).

River Mile	WSE (ft)	WSE (m)	River Mile	WSE (ft)	WSE (m)	River Mile	WSE (ft)	WSE (m)
14.370	2951.57	899.64	18.166	2921.87	890.59	21.406	2898.18	883.37
14.491	2951.40	899.59	18.222	2921.79	890.56	21.498	2898.03	883.32
14.510	2949.81	899.10	18.252	2921.75	890.55	21.536	2897.97	883.30
14.536	2947.63	898.44	18.287	2921.70	890.53	21.554	2897.36	883.12
14.556	2945.25	897.71	18.320	2921.65	890.52	21.565	2896.91	882.98
14.565	2944.19	897.39	18.340	2920.05	890.03	21.599	2896.61	882.89
14.621	2943.25	897.10	18.349	2919.25	889.79	21.652	2896.59	882.88
14.811	2942.77	896.96	18.382	2919.17	889.76	21.670	2896.02	882.71
14.950	2942.42	896.85	18.418	2919.07	889.73	21.689	2894.33	882.19
15.167	2941.87	896.68	18.445	2919.00	889.71	21.699	2893.49	881.94
15.258	2941.65	896.61	18.465	2918.06	889.42	21.738	2893.09	881.81
15.279	2941.53	896.58	18.474	2917.86	889.36	21.776	2892.98	881.78
15.299	2941.40	896.54	18.507	2917.80	889.35	21.820	2892.85	881.74
15.308	2941.34	896.52	18.663	2917.61	889.29	21.847	2891.79	881.42
15.370	2941.06	896.44	18.746	2917.55	889.27	21.888	2890.76	881.10
15.687	2940.90	896.39	18.850	2917.42	889.23	21.965	2890.16	880.92
15.910	2940.81	896.36	18.986	2917.36	889.21	22.066	2889.39	880.69
16.136	2940.79	896.35	19.110	2917.32	889.20	22.087	2889.35	880.67
16.311	2940.77	896.35	19.262	2917.29	889.19	22.096	2889.34	880.67
16.397	2940.76	896.34	19.368	2917.26	889.18	22.131	2889.30	880.66
16.417	2940.76	896.34	19.412	2917.22	889.17	22.291	2889.13	880.61
16.426	2940.76	896.34	19.433	2917.15	889.15	22.379	2889.05	880.58
16.462	2940.76	896.34	19.489	2916.98	889.10	22.525	2888.92	880.54
16.531	2940.75	896.34	19.654	2916.68	889.00	22.655	2888.79	880.50
16.594	2940.66	896.31	19.862	2916.50	888.95	22.676	2888.63	880.45
16.616	2940.06	896.13	20.069	2916.32	888.89	22.696	2887.80	880.20
16.625	2939.81	896.05	20.135	2916.26	888.88	22.705	2887.38	880.07
16.669	2938.70	895.72	20.154	2916.25	888.87	22.782	2886.95	879.94
16.876	2938.32	895.60	20.175	2916.22	888.86	22.850	2886.81	879.90
17.029	2938.04	895.51	20.184	2916.16	888.85	22.932	2886.61	879.84
17.075	2937.95	895.49	20.229	2915.89	888.76	22.994	2886.43	879.78
17.095	2935.17	894.64	20.368	2915.75	888.72	23.131	2883.77	878.97
17.104	2933.82	894.23	20.391	2915.73	888.71	23.152	2880.90	878.10
17.137	2929.10	892.79	20.400	2915.72	888.71	23.161	2879.57	877.69
17.172	2925.80	891.78	20.409	2915.71	888.71	23.180	2879.25	877.60
17.208	2925.58	891.72	20.427	2915.55	888.66	23.252	2878.84	877.47
17.277	2925.19	891.60	20.577	2914.64	888.38	23.304	2878.53	877.38
17.388	2924.85	891.49	20.695	2914.28	888.27	23.326	2878.40	877.34
17.479	2924.62	891.42	20.720	2914.20	888.25	23.335	2878.34	877.32
17.506	2924.59	891.42	20.741	2911.00	887.27	23.360	2877.27	876.99
17.526	2924.58	891.41	20.750	2909.68	886.87	23.445	2876.98	876.90
17.536	2924.58	891.41	20.785	2906.18	885.80	23.463	2876.95	876.89
17.581	2924.56	891.41	20.816	2904.38	885.26	23.484	2876.33	876.71
17.669	2924.05	891.25	20.940	2903.57	885.01	23.494	2875.73	876.52
17.690	2922.97	890.92	21.098	2903.37	884.95	23.519	2874.49	876.14
17.699	2922.50	890.78	21.335	2903.28	884.92	23.596	2873.67	875.89
17.737	2922.46	890.77	21.344	2903.02	884.84	23.634	2873.13	875.73
17.873	2922.29	890.71	21.365	2901.24	884.30	23.655	2872.78	875.62
18.042	2922.05	890.64	21.375	2900.48	884.07	23.664	2872.63	875.58

Table A4: Constructed water-surface profile based on 2000 and 2002 data (cont'd).

River Mile	WSE (ft)	WSE (m)	River Mile	WSE (ft)	WSE (m)	River Mile	WSE (ft)	WSE (m)
23.687	2872.33	875.49	26.336	2836.53	864.57	28.869	2822.12	860.18
23.841	2872.20	875.45	26.356	2836.53	864.57	29.028	2821.84	860.10
23.853	2872.19	875.44	26.377	2836.52	864.57	29.238	2821.72	860.06
23.874	2872.19	875.44	26.386	2836.52	864.57	29.375	2819.88	859.50
23.883	2872.18	875.44	26.418	2836.52	864.57	29.401	2817.81	858.87
23.916	2872.17	875.44	26.595	2836.48	864.56	29.410	2817.04	858.63
24.034	2872.11	875.42	26.614	2836.48	864.56	29.440	2815.93	858.30
24.102	2872.05	875.40	26.635	2836.48	864.56	29.602	2815.56	858.18
24.315	2871.87	875.35	26.644	2836.44	864.55	29.795	2813.05	857.42
24.342	2870.56	874.95	26.670	2836.26	864.49	29.881	2813.03	857.41
24.361	2868.47	874.31	26.756	2836.14	864.46	30.018	2813.00	857.40
24.371	2868.32	874.26	26.830	2836.12	864.45	30.040	2812.99	857.40
24.386	2868.10	874.20	26.849	2836.12	864.45	30.049	2812.99	857.40
24.445	2868.06	874.18	26.871	2834.01	863.81	30.087	2812.98	857.40
24.619	2867.94	874.15	26.880	2832.96	863.49	30.316	2812.58	857.27
24.668	2867.46	874.00	26.918	2829.41	862.40	30.348	2812.18	857.15
24.699	2865.65	873.45	26.957	2829.09	862.31	30.369	2811.69	857.00
24.720	2862.56	872.51	26.989	2828.84	862.23	30.378	2811.48	856.94
24.730	2861.28	872.12	27.010	2828.67	862.18	30.422	2809.76	856.41
24.762	2859.60	871.61	27.019	2828.59	862.15	30.546	2809.72	856.40
24.777	2859.55	871.59	27.067	2828.32	862.07	30.567	2809.71	856.40
24.880	2859.42	871.55	27.185	2827.62	861.86	30.587	2809.47	856.33
24.982	2857.98	871.11	27.374	2827.17	861.72	30.596	2808.76	856.11
25.072	2856.16	870.56	27.392	2827.15	861.72	30.656	2807.44	855.71
25.093	2855.31	870.30	27.412	2827.12	861.71	30.819	2807.09	855.60
25.113	2853.72	869.81	27.421	2827.11	861.70	30.839	2807.08	855.60
25.122	2852.77	869.52	27.451	2827.07	861.69	30.860	2806.87	855.53
25.155	2852.44	869.42	27.523	2827.05	861.68	30.869	2806.78	855.51
25.193	2852.41	869.41	27.641	2826.23	861.43	30.916	2806.62	855.46
25.365	2852.29	869.38	27.719	2825.98	861.36	31.141	2806.26	855.35
25.371	2851.99	869.29	27.756	2825.93	861.34	31.268	2806.11	855.30
25.392	2849.91	868.65	27.883	2825.27	861.14	31.274	2806.10	855.30
25.401	2849.02	868.38	27.896	2824.94	861.04	31.295	2805.57	855.14
25.436	2847.48	867.91	27.916	2824.43	860.89	31.304	2805.31	855.06
25.522	2847.22	867.83	27.925	2824.17	860.81	31.336	2805.00	854.96
25.700	2846.72	867.68	27.940	2824.17	860.81	31.472	2804.79	854.90
25.721	2845.47	867.30	28.089	2824.16	860.80	31.484	2804.75	854.89
25.731	2843.65	866.74	28.173	2824.14	860.80	31.503	2804.62	854.85
25.777	2840.49	865.78	28.191	2824.05	860.77	31.513	2804.57	854.83
25.889	2840.26	865.71	28.200	2823.98	860.75	31.552	2804.42	854.79
25.933	2840.12	865.67	28.238	2823.75	860.68	31.671	2804.38	854.78
25.980	2839.26	865.41	28.410	2823.56	860.62	31.724	2804.36	854.77
26.004	2837.89	864.99	28.472	2823.47	860.59	31.755	2803.97	854.65
26.013	2837.37	864.83	28.499	2823.31	860.54	31.777	2803.63	854.55
26.066	2837.16	864.77	28.528	2822.98	860.44	31.786	2803.50	854.51
26.197	2836.95	864.70	28.576	2822.71	860.36	31.851	2802.63	854.24
26.218	2836.84	864.67	28.812	2822.47	860.29	31.892	2802.17	854.10
26.238	2836.74	864.64	28.835	2822.33	860.25	32.000	2802.00	854.05
26.247	2836.69	864.62	28.845	2822.28	860.23	32.128	2799.95	853.42

Table A4: Constructed water-surface profile based on 2000 and 2002 data (cont'd).

River Mile	WSE (ft)	WSE (m)	River Mile	WSE (ft)	WSE (m)	River Mile	WSE (ft)	WSE (m)
32.138	2799.87	853.40	35.896	2783.27	848.34	41.181	2759.88	841.21
32.215	2799.24	853.21	35.914	2783.27	848.34	41.190	2759.79	841.18
32.283	2798.56	853.00	35.934	2783.11	848.29	41.262	2759.17	841.00
32.304	2797.44	852.66	35.943	2782.88	848.22	41.455	2758.94	840.92
32.314	2796.97	852.52	35.987	2781.80	847.89	41.589	2758.64	840.83
32.357	2796.36	852.33	36.148	2780.49	847.49	41.610	2758.31	840.73
32.588	2794.15	851.66	36.272	2780.33	847.44	41.628	2758.03	840.65
32.881	2793.92	851.59	36.291	2780.30	847.44	41.639	2757.89	840.60
33.060	2793.80	851.55	36.313	2780.15	847.39	41.719	2756.91	840.31
33.106	2793.77	851.54	36.322	2779.78	847.28	42.001	2756.38	840.14
33.126	2793.68	851.51	36.360	2778.27	846.82	42.263	2756.18	840.08
33.135	2793.43	851.44	36.589	2776.47	846.27	42.669	2755.88	839.99
33.171	2792.45	851.14	36.785	2776.43	846.26	43.129	2755.77	839.96
33.259	2790.68	850.60	36.968	2775.99	846.12	43.306	2755.75	839.95
33.417	2790.65	850.59	36.985	2775.85	846.08	43.453	2755.73	839.95
33.538	2790.35	850.50	37.006	2775.64	846.02	43.483	2755.70	839.94
33.623	2790.10	850.42	37.015	2775.55	845.99	43.503	2755.70	839.94
33.759	2790.00	850.39	37.062	2775.11	845.85	43.512	2755.69	839.93
33.768	2789.99	850.39	37.298	2774.31	845.61	43.589	2755.67	839.93
33.789	2789.97	850.38	37.488	2774.22	845.58	43.630	2755.53	839.89
33.799	2789.97	850.38	37.589	2774.18	845.57	43.766	2755.01	839.73
33.871	2789.14	850.13	37.621	2773.76	845.44	43.959	2754.29	839.51
34.023	2788.59	849.96	37.642	2772.79	845.15	43.980	2753.39	839.23
34.156	2788.21	849.85	37.651	2772.38	845.02	44.000	2750.90	838.47
34.174	2788.16	849.83	37.680	2771.13	844.64	44.009	2749.65	838.09
34.185	2788.13	849.82	37.907	2770.63	844.49	44.042	2748.72	837.81
34.209	2788.06	849.80	38.192	2769.24	844.06	44.145	2748.39	837.71
34.340	2787.90	849.75	38.233	2769.05	844.01	44.204	2748.20	837.65
34.423	2787.69	849.69	38.254	2768.92	843.97	44.304	2747.87	837.55
34.455	2787.47	849.62	38.263	2768.79	843.93	44.326	2747.68	837.49
34.476	2787.42	849.61	38.289	2768.46	843.83	44.335	2747.59	837.47
34.486	2787.41	849.60	38.512	2767.47	843.52	44.391	2747.05	837.30
34.526	2787.38	849.59	38.777	2767.34	843.49	44.459	2746.39	837.10
34.734	2787.21	849.54	39.071	2767.24	843.45	44.515	2745.98	836.97
34.804	2787.13	849.52	39.221	2767.22	843.45	44.726	2745.90	836.95
34.825	2787.11	849.51	39.233	2767.22	843.45	44.761	2745.70	836.89
34.834	2787.10	849.51	39.254	2766.03	843.09	44.782	2745.25	836.75
34.940	2786.99	849.47	39.264	2765.31	842.87	44.791	2745.05	836.69
34.955	2786.98	849.47	39.293	2763.17	842.21	44.862	2743.82	836.32
34.976	2786.95	849.46	39.544	2762.49	842.01	44.900	2743.79	836.31
34.986	2786.94	849.46	39.737	2762.32	841.96	45.024	2743.64	836.26
35.032	2785.17	848.92	40.029	2762.07	841.88	45.048	2743.40	836.19
35.097	2784.18	848.62	40.144	2761.78	841.79	45.068	2743.23	836.14
35.334	2784.06	848.58	40.234	2761.49	841.70	45.077	2743.14	836.11
35.355	2784.05	848.58	40.464	2760.85	841.51	45.155	2742.41	835.89
35.375	2783.95	848.55	40.675	2760.27	841.33	45.305	2742.29	835.85
35.384	2783.89	848.53	40.905	2760.14	841.29	45.453	2742.21	835.83
35.440	2783.52	848.42	41.086	2760.09	841.28	45.947	2741.87	835.72
35.601	2783.33	848.36	41.163	2760.04	841.26	46.044	2741.80	835.70

Table A4: Constructed water-surface profile based on 2000 and 2002 data (cont'd).

River Mile	WSE (ft)	WSE (m)	River Mile	WSE (ft)	WSE (m)	River Mile	WSE (ft)	WSE (m)
46.054	2741.79	835.70	49.909	2725.24	830.65	53.664	2702.97	823.87
46.075	2741.42	835.58	49.995	2725.10	830.61	53.673	2702.64	823.76
46.084	2741.26	835.54	50.030	2725.02	830.59	53.833	2698.27	822.43
46.128	2740.52	835.31	50.051	2724.95	830.56	53.987	2696.21	821.80
46.394	2739.23	834.92	50.060	2724.93	830.56	54.028	2696.18	821.80
46.652	2739.05	834.86	50.119	2724.74	830.50	54.049	2696.16	821.79
46.891	2738.93	834.83	50.262	2724.22	830.34	54.059	2696.16	821.79
46.926	2738.91	834.82	50.399	2724.18	830.33	54.206	2692.43	820.65
46.947	2738.90	834.82	50.439	2724.11	830.31	54.380	2692.32	820.62
46.956	2738.89	834.81	50.458	2723.96	830.26	54.484	2692.27	820.60
47.146	2738.80	834.79	50.468	2723.89	830.24	54.637	2692.15	820.57
47.367	2738.31	834.64	50.517	2723.52	830.13	54.792	2691.99	820.52
47.388	2738.10	834.57	50.623	2723.34	830.07	54.925	2691.92	820.50
47.397	2738.01	834.55	50.838	2723.33	830.07	55.191	2691.71	820.43
47.486	2737.15	834.28	50.859	2723.32	830.07	55.259	2691.40	820.34
47.545	2736.99	834.23	50.868	2723.28	830.06	55.280	2691.30	820.31
47.662	2736.97	834.23	50.889	2723.18	830.03	55.289	2691.26	820.30
47.773	2736.90	834.21	51.099	2722.91	829.94	55.354	2691.18	820.27
47.793	2736.70	834.15	51.276	2722.81	829.91	55.576	2691.09	820.24
47.802	2736.60	834.12	51.288	2722.81	829.91	55.709	2691.06	820.24
47.832	2736.27	834.02	51.309	2722.80	829.91	55.942	2690.89	820.18
48.066	2735.15	833.67	51.318	2722.79	829.91	56.271	2689.85	819.87
48.217	2734.48	833.47	51.347	2722.78	829.90	56.312	2689.76	819.84
48.237	2734.31	833.42	51.546	2722.38	829.78	56.333	2689.71	819.82
48.246	2734.23	833.39	51.673	2721.98	829.66	56.339	2689.70	819.82
48.300	2733.75	833.25	51.943	2721.14	829.40	56.380	2682.85	817.73
48.492	2733.27	833.10	52.049	2720.81	829.30	56.410	2682.39	817.59
48.525	2733.26	833.10	52.139	2720.52	829.21	56.600	2682.21	817.54
48.545	2733.26	833.10	52.161	2720.45	829.19	56.721	2680.42	816.99
48.554	2733.25	833.09	52.170	2720.42	829.18	56.759	2678.60	816.44
48.613	2733.24	833.09	52.220	2720.27	829.14	56.889	2677.59	816.13
48.702	2732.95	833.00	52.347	2719.47	828.89	56.970	2674.34	815.14
48.718	2732.79	832.95	52.368	2719.33	828.85	57.100	2671.61	814.31
48.740	2732.57	832.89	52.378	2719.27	828.83	57.221	2671.05	814.14
48.749	2732.48	832.86	52.422	2717.66	828.34	57.250	2669.97	813.81
48.781	2732.16	832.76	52.496	2716.98	828.14	57.399	2669.09	813.54
48.830	2731.72	832.63	52.581	2716.51	827.99	57.511	2668.52	813.36
48.898	2731.70	832.62	52.655	2716.19	827.89	57.620	2667.90	813.18
49.220	2731.62	832.60	52.785	2715.69	827.74	57.650	2667.53	813.06
49.424	2729.81	832.05	52.823	2714.20	827.29	57.700	2667.05	812.92
49.539	2729.64	831.99	52.984	2707.92	825.37	57.809	2666.83	812.85
49.585	2729.27	831.88	53.013	2706.28	824.87	57.830	2665.71	812.51
49.607	2729.03	831.81	53.034	2705.98	824.78	57.839	2665.23	812.36
49.616	2728.92	831.77	53.043	2705.92	824.76	57.890	2663.29	811.77
49.688	2728.12	831.53	53.093	2705.61	824.67	58.029	2662.97	811.67
49.797	2727.75	831.42	53.261	2704.54	824.34	58.061	2662.68	811.58
49.830	2727.59	831.37	53.383	2703.84	824.13	58.179	2660.73	810.99
49.850	2727.39	831.31	53.507	2703.64	824.07	58.259	2659.71	810.68
49.859	2726.99	831.19	53.643	2703.42	824.00	58.301	2657.65	810.05

Table A4: Constructed water-surface profile based on 2000 and 2002 data (cont'd).

River Mile	WSE (ft)	WSE (m)	River Mile	WSE (ft)	WSE (m)	River Mile	WSE (ft)	WSE (m)
58.340	2656.53	809.71	62.991	2628.56	801.19	66.843	2596.14	791.30
58.419	2656.35	809.66	63.000	2628.52	801.17	66.928	2595.37	791.07
58.520	2655.95	809.53	63.050	2628.28	801.10	67.012	2594.60	790.83
58.602	2655.60	809.43	63.100	2628.05	801.03	67.104	2593.75	790.58
58.801	2655.47	809.39	63.159	2627.83	800.96	67.275	2592.47	790.18
58.909	2655.09	809.27	63.200	2627.68	800.92	67.364	2592.28	790.13
58.990	2654.60	809.12	63.269	2627.32	800.81	67.509	2591.93	790.02
59.102	2653.83	808.89	63.349	2626.29	800.49	67.639	2591.51	789.89
59.310	2653.42	808.76	63.380	2625.47	800.24	67.654	2591.46	789.88
59.461	2653.39	808.75	63.399	2625.02	800.11	67.673	2590.19	789.49
59.751	2653.34	808.74	63.411	2624.84	800.05	67.683	2589.55	789.29
59.999	2653.24	808.71	63.448	2624.31	799.89	67.725	2587.57	788.69
60.061	2653.16	808.68	63.569	2623.71	799.71	67.814	2587.23	788.59
60.100	2652.37	808.44	63.680	2623.62	799.68	67.935	2586.76	788.44
60.121	2650.73	807.94	63.701	2623.03	799.50	68.068	2583.41	787.42
60.130	2650.02	807.73	63.710	2622.73	799.41	68.207	2582.47	787.14
60.171	2648.60	807.29	63.749	2621.45	799.02	68.285	2582.44	787.13
60.201	2648.57	807.28	63.849	2620.80	798.82	68.459	2582.37	787.11
60.251	2648.52	807.27	63.911	2620.68	798.78	68.720	2582.19	787.05
60.331	2648.44	807.24	63.961	2620.60	798.76	68.929	2581.75	786.92
60.351	2648.42	807.24	64.121	2620.51	798.73	68.975	2581.65	786.89
60.360	2647.96	807.10	64.159	2620.49	798.73	68.994	2579.80	786.32
60.419	2644.83	806.14	64.250	2620.44	798.71	69.003	2578.99	786.08
60.499	2644.71	806.11	64.269	2619.07	798.29	69.068	2574.59	784.74
60.600	2644.56	806.06	64.281	2617.97	797.96	69.299	2568.86	782.99
60.701	2644.03	805.90	64.319	2616.32	797.45	69.453	2568.42	782.85
60.900	2643.50	805.74	64.501	2616.21	797.42	69.731	2564.22	781.57
61.041	2643.34	805.69	64.591	2615.97	797.35	69.808	2564.07	781.53
61.081	2643.23	805.66	64.719	2615.29	797.14	69.841	2564.00	781.51
61.301	2642.84	805.54	64.849	2615.17	797.10	69.861	2563.97	781.50
61.500	2642.16	805.33	64.899	2615.15	797.10	69.870	2563.95	781.49
61.600	2641.60	805.16	65.001	2615.13	797.09	69.953	2561.97	780.89
61.751	2639.26	804.45	65.051	2615.03	797.06	70.021	2561.68	780.80
61.801	2638.45	804.20	65.299	2613.96	796.74	70.087	2561.41	780.72
62.000	2635.28	803.23	65.499	2613.95	796.73	70.240	2557.63	779.57
62.050	2633.97	802.83	65.651	2613.91	796.72	70.388	2557.46	779.51
62.081	2633.26	802.62	65.719	2613.85	796.70	70.545	2557.36	779.48
62.121	2633.22	802.61	65.760	2613.82	796.69	70.653	2557.30	779.47
62.159	2633.18	802.59	65.911	2613.78	796.68	70.687	2556.72	779.29
62.239	2633.11	802.57	65.930	2613.77	796.68	70.820	2554.40	778.58
62.351	2632.71	802.45	65.940	2611.41	795.96	71.054	2552.28	777.93
62.500	2631.94	802.22	66.000	2607.24	794.69	71.281	2551.47	777.69
62.568	2631.62	802.12	66.083	2607.19	794.67	71.468	2550.96	777.53
62.699	2631.48	802.08	66.248	2606.80	794.55	71.569	2550.70	777.45
62.783	2630.26	801.70	66.447	2605.05	794.02	71.755	2549.80	777.18
62.801	2629.04	801.33	66.568	2600.18	792.53	71.861	2548.86	776.89
62.810	2628.83	801.27	66.610	2599.50	792.33	71.974	2546.79	776.26
62.899	2628.79	801.26	66.639	2599.06	792.19	72.101	2546.31	776.12
62.970	2628.67	801.22	66.680	2598.45	792.01	72.199	2545.97	776.01

Table A4: Constructed water-surface profile based on 2000 and 2002 data (cont'd).

River Mile	WSE (ft)	WSE (m)	River Mile	WSE (ft)	WSE (m)	River Mile	WSE (ft)	WSE (m)
72.403	2545.36	775.83	76.457	2493.01	759.87	79.418	2435.99	742.49
72.536	2544.97	775.71	76.478	2492.79	759.80	79.469	2435.80	742.43
72.832	2544.45	775.55	76.487	2492.70	759.77	79.483	2434.88	742.15
72.853	2544.35	775.52	76.549	2492.07	759.58	79.538	2431.13	741.01
72.862	2543.96	775.40	76.643	2491.65	759.45	79.560	2429.95	740.65
72.924	2537.45	773.41	76.880	2491.62	759.45	79.569	2429.44	740.49
72.986	2534.71	772.58	76.960	2491.60	759.44	79.626	2428.71	740.27
73.080	2534.36	772.47	76.981	2491.60	759.44	79.774	2428.50	740.21
73.096	2533.27	772.14	76.991	2491.60	759.44	79.895	2428.32	740.15
73.157	2528.90	770.81	77.108	2491.58	759.43	79.901	2428.31	740.15
73.288	2525.73	769.84	77.173	2491.57	759.43	79.921	2427.20	739.81
73.501	2523.54	769.17	77.193	2491.56	759.43	79.930	2426.54	739.61
73.625	2522.71	768.92	77.202	2490.99	759.25	79.963	2424.71	739.05
73.645	2521.64	768.60	77.279	2481.65	756.41	80.052	2424.17	738.89
73.654	2521.10	768.43	77.354	2475.75	754.61	80.070	2423.89	738.80
73.687	2518.96	767.78	77.448	2472.94	753.75	80.079	2423.74	738.76
73.753	2515.72	766.79	77.540	2469.61	752.74	80.138	2422.83	738.48
73.806	2514.86	766.53	77.566	2468.21	752.31	80.271	2422.61	738.41
73.924	2514.46	766.41	77.587	2466.77	751.87	80.277	2422.56	738.40
74.024	2514.13	766.31	77.596	2465.97	751.63	80.297	2422.33	738.33
74.092	2513.72	766.18	77.658	2462.71	750.63	80.306	2422.22	738.29
74.244	2513.11	766.00	77.733	2462.03	750.43	80.336	2421.83	738.17
74.440	2513.01	765.97	77.753	2461.86	750.37	80.418	2421.66	738.12
74.462	2513.00	765.96	77.762	2461.77	750.35	80.471	2421.62	738.11
74.471	2513.00	765.96	77.821	2461.31	750.21	80.493	2421.51	738.08
74.542	2512.97	765.95	77.995	2460.10	749.84	80.502	2421.43	738.05
74.705	2512.89	765.93	78.087	2459.25	749.58	80.564	2420.91	737.89
74.838	2512.79	765.90	78.106	2459.02	749.51	80.650	2420.17	737.67
74.995	2512.66	765.86	78.116	2458.91	749.48	80.768	2419.71	737.53
75.176	2512.51	765.81	78.187	2458.04	749.21	80.797	2419.67	737.52
75.347	2512.38	765.77	78.289	2457.56	749.06	80.818	2419.66	737.51
75.365	2512.37	765.77	78.358	2457.40	749.02	80.827	2419.66	737.51
75.385	2512.28	765.74	78.368	2457.38	749.01	80.898	2419.64	737.51
75.394	2512.20	765.72	78.389	2457.21	748.96	81.058	2419.58	737.49
75.480	2509.81	764.99	78.433	2456.87	748.85	81.229	2419.52	737.47
75.534	2509.76	764.97	78.566	2455.82	748.53	81.458	2419.44	737.45
75.726	2509.58	764.92	78.575	2455.75	748.51	81.468	2419.44	737.45
75.779	2509.42	764.87	78.596	2455.58	748.46	81.490	2419.43	737.44
75.800	2507.77	764.37	78.606	2455.51	748.44	81.499	2419.43	737.44
75.810	2506.88	764.10	78.662	2455.07	748.31	81.543	2419.41	737.44
75.872	2503.55	763.08	78.718	2454.87	748.24	81.700	2419.36	737.42
75.960	2499.59	761.88	78.951	2454.66	748.18	81.890	2418.03	737.02
76.066	2496.60	760.96	79.100	2454.62	748.17	81.993	2417.79	736.94
76.167	2496.19	760.84	79.126	2454.19	748.04	82.046	2417.78	736.94
76.252	2494.09	760.20	79.147	2451.21	747.13	82.067	2416.79	736.64
76.273	2493.98	760.17	79.156	2450.09	746.79	82.076	2415.79	736.33
76.282	2493.93	760.15	79.256	2442.43	744.45	82.182	2403.43	732.57
76.347	2493.59	760.05	79.342	2436.87	742.76	82.244	2400.73	731.74
76.442	2493.11	759.90	79.389	2436.09	742.52	82.292	2397.70	730.82

Table A4: Constructed water-surface profile based on 2000 and 2002 data (cont'd).

River Mile	WSE (ft)	WSE (m)	River Mile	WSE (ft)	WSE (m)	River Mile	WSE (ft)	WSE (m)
82.400	2397.29	730.69	84.963	2374.41	723.72	89.061	2331.88	710.76
82.534	2396.79	730.54	85.035	2373.29	723.38	89.183	2329.38	710.00
82.617	2396.13	730.34	85.112	2372.83	723.24	89.310	2329.21	709.94
82.638	2395.64	730.19	85.224	2372.53	723.15	89.418	2329.02	709.89
82.648	2395.43	730.13	85.245	2372.47	723.13	89.446	2328.19	709.63
82.694	2394.95	729.98	85.255	2370.89	722.65	89.467	2327.06	709.29
82.804	2394.71	729.91	85.333	2364.85	720.81	89.476	2326.70	709.18
82.825	2394.11	729.72	85.363	2363.80	720.49	89.550	2324.94	708.64
82.835	2393.85	729.65	85.458	2363.55	720.41	89.618	2320.36	707.25
82.884	2392.48	729.23	85.603	2363.29	720.33	89.695	2317.98	706.52
82.972	2392.45	729.22	85.739	2363.00	720.24	89.739	2317.64	706.42
82.993	2392.44	729.22	85.804	2361.23	719.70	89.866	2317.18	706.28
83.002	2392.44	729.22	85.824	2360.72	719.55	89.887	2316.00	705.92
83.043	2392.42	729.21	85.833	2360.46	719.47	89.937	2314.34	705.41
83.132	2392.39	729.20	85.889	2359.23	719.09	90.062	2312.88	704.97
83.152	2392.35	729.19	86.017	2358.41	718.84	90.363	2310.96	704.38
83.161	2392.30	729.17	86.259	2357.96	718.71	90.618	2310.55	704.26
83.233	2391.92	729.06	86.336	2357.81	718.66	90.792	2310.26	704.17
83.342	2391.62	728.97	86.357	2357.17	718.47	90.816	2310.22	704.16
83.381	2391.51	728.93	86.367	2356.86	718.37	90.837	2308.25	703.55
83.401	2391.46	728.92	86.420	2355.69	718.01	90.847	2306.29	702.96
83.410	2391.25	728.85	86.505	2355.61	717.99	90.923	2298.79	700.67
83.443	2390.46	728.61	86.538	2355.58	717.98	91.096	2298.31	700.52
83.626	2387.37	727.67	86.557	2355.42	717.93	91.316	2297.92	700.41
83.633	2387.36	727.67	86.567	2355.31	717.90	91.506	2297.65	700.32
83.653	2387.33	727.66	86.622	2354.63	717.69	91.618	2297.49	700.27
83.662	2387.32	727.66	86.846	2354.33	717.60	91.627	2297.48	700.27
83.736	2386.50	727.41	87.097	2354.08	717.52	91.655	2297.43	700.26
83.804	2386.16	727.30	87.319	2353.85	717.45	91.842	2297.17	700.18
83.963	2385.95	727.24	87.414	2353.75	717.42	92.012	2296.92	700.10
83.984	2385.92	727.23	87.588	2353.57	717.37	92.047	2296.62	700.01
83.993	2385.81	727.19	87.668	2353.50	717.35	92.056	2296.52	699.98
84.028	2385.41	727.07	87.688	2353.48	717.34	92.245	2295.48	699.66
84.087	2385.30	727.04	87.697	2353.48	717.34	92.438	2295.11	699.55
84.102	2385.27	727.03	87.741	2353.44	717.33	92.550	2294.82	699.46
84.111	2383.20	726.40	87.946	2353.29	717.28	92.618	2294.64	699.41
84.177	2381.12	725.77	88.097	2353.05	717.21	92.639	2294.41	699.34
84.274	2381.10	725.76	88.116	2352.72	717.11	92.649	2294.25	699.29
84.428	2381.06	725.75	88.126	2352.57	717.06	92.784	2293.16	698.96
84.522	2381.04	725.74	88.186	2351.95	716.87	92.805	2293.13	698.95
84.612	2380.53	725.59	88.319	2349.04	715.99	92.814	2293.12	698.94
84.693	2379.52	725.28	88.421	2346.82	715.31	92.846	2293.08	698.93
84.715	2379.25	725.20	88.502	2343.98	714.45	93.018	2292.93	698.89
84.724	2379.13	725.16	88.570	2343.81	714.39	93.074	2292.89	698.87
84.817	2378.14	724.86	88.686	2343.53	714.31	93.100	2292.88	698.87
84.851	2377.50	724.66	88.701	2342.35	713.95	93.121	2291.60	698.48
84.860	2377.28	724.59	88.710	2340.15	713.28	93.130	2291.05	698.31
84.901	2376.23	724.27	88.754	2336.56	712.18	93.187	2288.29	697.47
84.954	2374.55	723.76	88.911	2334.54	711.57	93.454	2287.93	697.36

Table A4: Constructed water-surface profile based on 2000 and 2002 data (cont'd).

River Mile	WSE (ft)	WSE (m)	River Mile	WSE (ft)	WSE (m)	River Mile	WSE (ft)	WSE (m)
93.678	2287.88	697.35	98.752	2239.56	682.62	102.525	2174.18	662.69
93.870	2287.86	697.34	98.785	2238.71	682.36	102.536	2173.86	662.59
93.889	2286.99	697.07	98.805	2236.29	681.62	102.607	2171.42	661.85
93.899	2286.13	696.81	98.814	2235.30	681.32	102.741	2168.66	661.01
93.961	2276.01	693.73	98.873	2232.22	680.38	102.865	2168.43	660.94
94.006	2275.28	693.51	98.935	2230.76	679.94	103.128	2168.29	660.89
94.075	2275.14	693.46	99.009	2226.68	678.69	103.213	2168.25	660.88
94.095	2275.10	693.45	99.018	2226.06	678.50	103.232	2168.24	660.88
94.104	2275.08	693.44	99.102	2219.21	676.42	103.253	2167.44	660.64
94.137	2274.29	693.20	99.220	2217.04	675.75	103.262	2166.97	660.49
94.190	2270.11	691.93	99.418	2216.97	675.73	103.330	2165.21	659.96
94.340	2269.79	691.83	99.690	2216.72	675.66	103.590	2164.49	659.74
94.536	2269.42	691.72	99.720	2216.69	675.65	103.874	2164.00	659.59
94.557	2269.38	691.71	99.740	2214.01	674.83	104.211	2163.42	659.41
94.566	2269.37	691.70	99.749	2212.67	674.42	104.412	2163.07	659.30
94.613	2269.29	691.68	99.799	2206.93	672.67	104.442	2163.02	659.29
94.775	2269.17	691.64	99.879	2203.29	671.56	104.462	2161.51	658.83
94.805	2268.87	691.55	100.054	2201.89	671.14	104.471	2160.76	658.60
94.824	2268.00	691.29	100.078	2199.92	670.54	104.518	2157.99	657.76
94.834	2267.57	691.16	100.087	2199.17	670.31	104.697	2157.81	657.70
94.870	2266.26	690.76	100.134	2196.40	669.46	104.770	2157.74	657.68
95.116	2266.19	690.73	100.193	2196.20	669.40	104.791	2157.52	657.61
95.302	2266.13	690.72	100.202	2195.88	669.30	104.800	2157.36	657.56
95.396	2266.06	690.70	100.211	2195.43	669.17	104.835	2156.76	657.38
95.435	2265.19	690.43	100.233	2194.36	668.84	105.099	2156.12	657.19
95.456	2264.17	690.12	100.279	2193.64	668.62	105.182	2156.10	657.18
95.465	2260.89	689.12	100.288	2193.55	668.59	105.198	2155.49	656.99
95.524	2255.89	687.60	100.308	2193.36	668.54	105.208	2154.57	656.71
95.563	2254.31	687.11	100.338	2192.67	668.33	105.263	2149.06	655.03
95.799	2254.08	687.04	100.379	2190.48	667.66	105.318	2148.12	654.75
96.057	2253.96	687.01	100.584	2190.00	667.51	105.463	2147.31	654.50
96.237	2253.85	686.97	100.687	2189.96	667.50	105.546	2147.22	654.47
96.418	2253.70	686.93	100.737	2188.92	667.18	105.567	2146.89	654.37
96.437	2253.62	686.90	100.746	2188.57	667.08	105.577	2146.67	654.31
96.447	2253.57	686.89	101.022	2187.50	666.75	105.623	2145.50	653.95
96.483	2253.40	686.84	101.054	2186.98	666.59	105.847	2141.95	652.87
96.750	2253.28	686.80	101.075	2186.09	666.32	106.149	2141.48	652.72
96.841	2253.24	686.79	101.084	2185.71	666.20	106.220	2141.37	652.69
96.986	2252.96	686.70	101.119	2184.31	665.78	106.238	2141.34	652.68
97.123	2250.43	685.93	101.349	2183.75	665.61	106.247	2141.28	652.66
97.142	2248.14	685.23	101.655	2183.66	665.58	106.285	2140.61	652.46
97.151	2246.83	684.83	101.767	2183.63	665.57	106.339	2139.66	652.17
97.238	2241.49	683.21	101.788	2182.94	665.36	106.444	2138.79	651.90
97.465	2240.61	682.94	101.797	2181.93	665.05	106.525	2136.20	651.11
97.761	2240.58	682.93	101.877	2175.80	663.18	106.546	2134.72	650.66
98.110	2240.52	682.91	102.066	2175.63	663.13	106.555	2134.09	650.47
98.255	2240.50	682.90	102.288	2175.13	662.98	106.652	2129.94	649.21
98.403	2240.48	682.90	102.464	2174.72	662.85	106.774	2129.04	648.93
98.618	2240.43	682.88	102.507	2174.61	662.82	106.795	2128.44	648.75

Table A4: Constructed water-surface profile based on 2000 and 2002 data (cont'd).

River Mile	WSE (ft)	WSE (m)	River Mile	WSE (ft)	WSE (m)	River Mile	WSE (ft)	WSE (m)
106.804	2128.08	648.64	110.797	2085.22	635.58	114.665	2045.66	623.52
106.848	2127.11	648.34	110.806	2085.08	635.53	114.851	2045.28	623.40
107.007	2127.02	648.32	110.878	2084.01	635.21	114.888	2045.27	623.40
107.196	2126.87	648.27	111.002	2083.63	635.09	114.911	2045.17	623.37
107.214	2126.63	648.20	111.039	2083.54	635.06	114.920	2045.11	623.35
107.223	2126.39	648.12	111.097	2083.19	634.96	114.957	2045.00	623.32
107.259	2125.75	647.93	111.271	2082.44	634.73	115.088	2044.81	623.26
107.442	2125.67	647.90	111.357	2082.35	634.70	115.301	2044.48	623.16
107.555	2125.62	647.89	111.443	2081.35	634.40	115.535	2044.43	623.14
107.575	2125.26	647.78	111.490	2080.80	634.23	115.647	2044.42	623.14
107.584	2124.99	647.70	111.499	2080.69	634.19	115.659	2044.42	623.14
107.608	2124.27	647.48	111.529	2077.35	633.18	115.680	2043.69	622.92
107.895	2123.66	647.29	111.582	2075.21	632.52	115.689	2043.32	622.80
108.129	2123.53	647.25	111.792	2075.12	632.50	115.721	2042.33	622.50
108.380	2123.39	647.21	111.857	2075.08	632.48	115.908	2041.75	622.33
108.401	2122.42	646.91	112.095	2074.61	632.34	116.006	2040.99	622.09
108.410	2121.93	646.76	112.292	2074.25	632.23	116.026	2040.48	621.94
108.448	2120.00	646.18	112.455	2074.02	632.16	116.035	2040.23	621.86
108.612	2119.11	645.90	112.620	2073.84	632.11	116.091	2038.71	621.40
108.789	2119.01	645.87	112.736	2073.71	632.07	116.331	2036.27	620.66
108.910	2118.94	645.85	112.775	2072.50	631.70	116.352	2036.10	620.60
108.929	2118.93	645.85	112.798	2070.83	631.19	116.361	2036.05	620.59
108.939	2118.93	645.85	112.807	2070.07	630.96	116.389	2035.90	620.54
108.984	2118.90	645.84	112.902	2062.27	628.58	116.553	2035.49	620.42
109.206	2118.78	645.80	113.040	2060.14	627.93	116.718	2035.40	620.39
109.233	2118.76	645.80	113.109	2059.38	627.70	116.739	2035.28	620.35
109.243	2118.21	645.63	113.136	2058.69	627.49	116.748	2035.20	620.33
109.274	2116.35	645.06	113.155	2057.71	627.19	116.790	2034.83	620.22
109.413	2111.11	643.47	113.165	2057.23	627.04	116.982	2034.52	620.12
109.538	2109.90	643.10	113.233	2054.15	626.10	117.147	2034.29	620.05
109.551	2109.31	642.92	113.381	2052.29	625.54	117.159	2034.00	619.96
109.561	2108.86	642.78	113.440	2052.10	625.48	117.168	2033.57	619.83
109.603	2107.04	642.23	113.475	2051.90	625.42	117.222	2031.18	619.10
109.818	2105.18	641.66	113.496	2051.25	625.22	117.461	2029.60	618.62
109.880	2102.52	640.85	113.505	2050.96	625.13	117.482	2029.46	618.58
109.901	2101.23	640.45	113.543	2049.83	624.79	117.491	2029.37	618.55
109.910	2100.67	640.28	113.590	2048.91	624.51	117.556	2028.72	618.35
110.026	2098.82	639.72	113.648	2048.29	624.32	117.576	2028.54	618.30
110.073	2096.51	639.02	113.795	2047.79	624.17	117.585	2028.44	618.27
110.094	2095.09	638.58	113.816	2047.71	624.14	117.654	2027.94	618.12
110.103	2094.48	638.40	113.825	2047.69	624.14	117.790	2027.86	618.09
110.156	2092.94	637.93	113.916	2047.38	624.04	117.843	2027.45	617.97
110.351	2089.31	636.82	114.053	2046.93	623.90	118.011	2026.98	617.82
110.371	2088.22	636.49	114.121	2046.70	623.83	118.240	2026.64	617.72
110.380	2087.67	636.32	114.319	2046.21	623.68	118.390	2026.31	617.62
110.421	2086.18	635.87	114.453	2046.17	623.67	118.501	2026.04	617.54
110.549	2085.86	635.77	114.588	2046.13	623.66	118.523	2025.97	617.52
110.718	2085.45	635.65	114.609	2046.06	623.64	118.532	2025.94	617.51
110.777	2085.30	635.60	114.618	2045.99	623.62	118.589	2025.75	617.45

Table A4: Constructed water-surface profile based on 2000 and 2002 data (cont'd).

River Mile	WSE (ft)	WSE (m)	River Mile	WSE (ft)	WSE (m)	River Mile	WSE (ft)	WSE (m)
118.675	2025.69	617.43	122.577	2000.32	609.70	126.622	1957.10	596.52
118.695	2025.56	617.39	122.662	1999.72	609.51	126.714	1956.72	596.41
118.704	2025.49	617.37	122.684	1999.71	609.51	126.735	1956.47	596.33
118.737	2025.24	617.29	122.693	1999.70	609.51	126.744	1956.36	596.30
118.813	2024.85	617.17	122.882	1998.02	609.00	126.815	1955.54	596.05
118.834	2024.76	617.15	123.047	1997.87	608.95	126.949	1953.97	595.57
118.843	2024.71	617.13	123.296	1997.51	608.84	126.998	1953.29	595.36
118.952	2024.08	616.94	123.311	1997.14	608.73	127.018	1953.03	595.28
119.104	2021.76	616.23	123.317	1996.43	608.51	127.027	1952.90	595.24
119.234	2021.72	616.22	123.388	1991.30	606.95	127.077	1952.24	595.04
119.254	2021.55	616.17	123.509	1991.14	606.90	127.235	1951.42	594.79
119.263	2021.04	616.01	123.610	1991.02	606.86	127.424	1949.98	594.35
119.319	2018.19	615.14	123.681	1990.98	606.85	127.489	1948.07	593.77
119.361	2018.06	615.10	123.752	1990.93	606.84	127.508	1946.92	593.42
119.480	2017.77	615.02	123.832	1990.88	606.82	127.518	1946.35	593.25
119.562	2017.63	614.97	123.941	1990.63	606.74	127.554	1945.19	592.89
119.592	2017.57	614.96	124.104	1989.23	606.32	127.699	1945.09	592.86
119.660	2017.46	614.92	124.116	1988.48	606.09	127.720	1945.03	592.85
119.796	2017.36	614.89	124.137	1987.16	605.69	127.729	1944.98	592.83
119.825	2017.25	614.86	124.146	1986.60	605.52	127.753	1944.82	592.78
119.846	2017.11	614.82	124.215	1985.09	605.06	127.956	1944.37	592.64
119.855	2017.05	614.80	124.361	1983.54	604.58	128.054	1943.98	592.53
119.887	2016.85	614.74	124.554	1980.83	603.76	128.075	1943.84	592.48
120.080	2016.35	614.58	124.604	1980.05	603.52	128.084	1943.76	592.46
120.245	2016.21	614.54	124.625	1979.83	603.45	128.133	1943.31	592.32
120.432	2015.86	614.43	124.634	1979.82	603.45	128.344	1942.69	592.13
120.545	2015.60	614.35	124.675	1979.76	603.43	128.378	1942.68	592.13
120.673	2012.84	613.51	124.899	1979.39	603.32	128.397	1941.74	591.84
120.692	2011.28	613.04	125.001	1978.42	603.02	128.403	1941.27	591.70
120.701	2010.51	612.80	125.060	1978.03	602.90	128.450	1939.34	591.11
120.766	2009.08	612.37	125.290	1976.92	602.57	128.658	1938.78	590.94
120.870	2008.79	612.28	125.418	1976.14	602.33	128.847	1938.60	590.89
120.962	2007.85	611.99	125.516	1975.26	602.06	129.049	1938.58	590.88
121.121	2006.99	611.73	125.536	1975.09	602.01	129.134	1938.58	590.88
121.160	2006.92	611.71	125.545	1973.88	601.64	129.155	1938.58	590.88
121.180	2006.89	611.70	125.598	1970.14	600.50	129.164	1938.13	590.74
121.189	2006.87	611.69	125.699	1967.00	599.54	129.208	1934.28	589.57
121.228	2006.80	611.67	125.912	1962.25	598.09	129.341	1934.28	589.57
121.354	2006.62	611.62	126.066	1961.82	597.96	129.581	1934.00	589.48
121.406	2006.54	611.59	126.128	1961.58	597.89	129.670	1933.85	589.44
121.444	2006.48	611.58	126.148	1961.38	597.83	129.711	1933.83	589.43
121.730	2006.12	611.47	126.157	1961.28	597.80	129.732	1932.79	589.11
121.956	2005.94	611.41	126.187	1961.04	597.72	129.742	1931.75	588.80
122.187	2005.82	611.37	126.341	1960.82	597.66	129.823	1926.79	587.29
122.220	2005.27	611.21	126.393	1960.74	597.63	130.043	1926.29	587.13
122.240	2004.21	610.88	126.400	1960.73	597.63	130.267	1926.24	587.12
122.249	2003.68	610.72	126.421	1959.96	597.40	130.513	1926.19	587.10
122.299	2001.67	610.11	126.430	1959.58	597.28	130.742	1926.14	587.09
122.397	2000.68	609.81	126.471	1957.92	596.77	131.022	1926.09	587.07

Table A4: Constructed water-surface profile based on 2000 and 2002 data (cont'd).

River Mile	WSE (ft)	WSE (m)	River Mile	WSE (ft)	WSE (m)	River Mile	WSE (ft)	WSE (m)
131.063	1926.08	587.07	135.061	1874.82	571.45	138.298	1849.14	563.62
131.084	1924.43	586.57	135.076	1874.60	571.38	138.333	1848.75	563.50
131.093	1923.72	586.35	135.096	1874.37	571.31	138.354	1846.74	562.89
131.187	1918.49	584.76	135.105	1874.26	571.27	138.363	1845.68	562.56
131.386	1918.19	584.66	135.144	1873.75	571.12	138.404	1843.34	561.85
131.433	1917.75	584.53	135.244	1873.13	570.93	138.475	1843.25	561.82
131.454	1917.07	584.32	135.268	1873.08	570.91	138.529	1843.18	561.80
131.463	1916.78	584.23	135.338	1871.82	570.53	138.585	1843.12	561.78
131.575	1915.35	583.80	135.360	1871.21	570.34	138.697	1843.03	561.76
131.691	1915.22	583.76	135.369	1870.79	570.22	138.712	1843.02	561.75
131.700	1915.22	583.76	135.422	1867.95	569.35	138.733	1842.70	561.65
131.721	1914.99	583.69	135.469	1866.54	568.92	138.742	1842.39	561.56
131.731	1914.89	583.66	135.537	1865.26	568.53	138.827	1839.61	560.71
131.783	1914.47	583.53	135.570	1864.73	568.37	139.035	1838.36	560.33
131.969	1913.64	583.28	135.620	1864.42	568.28	139.091	1838.33	560.32
132.224	1912.52	582.94	135.720	1864.09	568.17	139.132	1837.69	560.13
132.253	1912.40	582.90	135.832	1863.98	568.14	139.153	1836.58	559.79
132.262	1911.32	582.57	136.005	1863.82	568.09	139.162	1836.11	559.65
132.324	1902.03	579.74	136.052	1863.77	568.08	139.203	1835.15	559.35
132.377	1899.28	578.90	136.073	1863.75	568.07	139.408	1834.95	559.29
132.504	1899.01	578.82	136.083	1863.74	568.07	139.429	1834.93	559.29
132.777	1898.49	578.66	136.111	1863.72	568.06	139.439	1834.92	559.28
132.904	1898.24	578.58	136.242	1863.59	568.02	139.473	1834.89	559.27
132.924	1898.08	578.53	136.394	1863.45	567.98	139.618	1834.76	559.23
132.933	1897.94	578.49	136.558	1863.29	567.93	139.653	1834.74	559.23
132.983	1897.18	578.26	136.576	1863.27	567.92	139.674	1832.72	558.61
133.235	1896.38	578.02	136.596	1863.25	567.92	139.683	1831.72	558.31
133.463	1895.74	577.82	136.605	1863.24	567.92	139.777	1827.13	556.91
133.579	1895.43	577.73	136.652	1863.20	567.90	139.958	1826.58	556.74
133.608	1895.23	577.67	136.854	1862.99	567.84	140.073	1826.09	556.59
133.629	1895.04	577.61	136.891	1862.57	567.71	140.094	1825.97	556.56
133.638	1894.96	577.58	136.913	1861.22	567.30	140.103	1825.92	556.54
133.718	1894.24	577.36	136.922	1860.63	567.12	140.135	1825.75	556.49
133.975	1893.76	577.22	136.960	1858.32	566.42	140.221	1825.43	556.39
134.138	1893.59	577.17	137.005	1857.26	566.09	140.393	1824.64	556.15
134.291	1893.44	577.12	137.099	1856.05	565.72	140.420	1823.98	555.95
134.330	1892.97	576.98	137.174	1854.89	565.37	140.470	1822.80	555.59
134.350	1890.36	576.18	137.195	1854.28	565.18	140.520	1820.72	554.96
134.359	1889.24	575.84	137.205	1854.02	565.11	140.570	1818.69	554.34
134.440	1884.18	574.30	137.236	1853.28	564.88	140.744	1818.58	554.30
134.605	1882.59	573.81	137.404	1852.76	564.72	140.881	1818.35	554.23
134.709	1881.57	573.50	137.591	1852.72	564.71	141.103	1817.77	554.06
134.729	1881.39	573.45	137.739	1852.36	564.60	141.257	1817.62	554.01
134.738	1881.30	573.42	137.830	1852.14	564.53	141.278	1817.58	554.00
134.785	1880.85	573.28	137.940	1851.80	564.43	141.287	1817.53	553.98
134.866	1880.08	573.05	137.975	1851.69	564.40	141.331	1817.32	553.92
134.887	1879.23	572.79	138.094	1851.31	564.28	141.420	1817.02	553.83
134.896	1878.82	572.66	138.131	1851.06	564.20	141.467	1816.89	553.79
134.946	1876.65	572.00	138.215	1850.10	563.91	141.505	1816.81	553.76

Table A4: Constructed water-surface profile based on 2000 and 2002 data (cont'd).

River Mile	WSE (ft)	WSE (m)	River Mile	WSE (ft)	WSE (m)	River Mile	WSE (ft)	WSE (m)
141.650	1816.28	553.60	146.450	1772.33	540.21	152.317	1736.05	529.15
141.676	1815.42	553.34	146.544	1771.96	540.09	152.494	1735.89	529.10
141.698	1814.66	553.11	146.584	1771.32	539.90	152.702	1735.39	528.95
141.707	1814.34	553.01	146.603	1771.08	539.83	152.823	1735.37	528.94
141.763	1813.00	552.60	146.612	1771.02	539.81	152.829	1735.37	528.94
141.949	1812.02	552.30	146.663	1770.69	539.71	152.850	1734.78	528.76
142.035	1811.83	552.25	146.793	1769.82	539.44	152.860	1733.91	528.50
142.055	1811.79	552.23	147.019	1769.33	539.29	152.906	1731.27	527.69
142.064	1811.77	552.23	147.278	1768.88	539.15	153.022	1731.15	527.65
142.136	1811.61	552.18	147.451	1768.70	539.10	153.196	1730.96	527.60
142.242	1811.38	552.11	147.690	1768.38	539.00	153.344	1730.79	527.54
142.520	1810.99	551.99	147.973	1768.12	538.92	153.353	1730.78	527.54
142.778	1810.81	551.93	148.042	1768.05	538.90	153.373	1730.69	527.51
142.996	1810.66	551.89	148.063	1768.01	538.89	153.382	1730.57	527.48
143.046	1810.63	551.88	148.072	1767.97	538.88	153.469	1729.48	527.15
143.331	1810.43	551.82	148.107	1767.85	538.84	153.693	1728.04	526.71
143.612	1810.24	551.76	148.370	1767.42	538.71	153.758	1727.10	526.42
143.923	1810.03	551.70	148.373	1767.42	538.71	153.773	1726.88	526.35
143.985	1809.99	551.68	148.393	1767.02	538.59	153.792	1726.61	526.27
144.015	1809.97	551.68	148.402	1765.84	538.23	153.802	1726.48	526.23
144.034	1809.13	551.42	148.449	1762.23	537.13	153.851	1725.76	526.01
144.044	1808.37	551.19	148.566	1761.74	536.98	154.019	1724.36	525.58
144.118	1802.65	549.45	148.704	1761.06	536.77	154.038	1724.16	525.52
144.236	1797.60	547.91	148.909	1760.25	536.52	154.048	1724.05	525.49
144.310	1794.82	547.06	149.021	1759.95	536.43	154.090	1723.53	525.33
144.450	1792.65	546.40	149.154	1759.19	536.20	154.264	1721.45	524.70
144.577	1791.53	546.06	149.346	1758.67	536.04	154.486	1719.78	524.19
144.742	1789.16	545.34	149.619	1758.39	535.96	154.659	1718.96	523.94
144.751	1789.01	545.29	149.903	1757.51	535.69	154.777	1718.80	523.89
144.798	1788.35	545.09	150.074	1757.00	535.53	154.794	1718.79	523.89
144.988	1786.85	544.63	150.181	1756.67	535.43	154.815	1718.60	523.83
145.145	1785.59	544.25	150.204	1756.61	535.41	154.821	1718.54	523.81
145.361	1784.49	543.91	150.213	1756.05	535.24	154.880	1718.01	523.65
145.404	1784.29	543.85	150.332	1744.89	531.84	155.072	1716.92	523.32
145.426	1784.18	543.82	150.554	1743.73	531.49	155.224	1716.70	523.25
145.435	1783.72	543.68	150.806	1742.60	531.14	155.368	1716.48	523.18
145.497	1780.63	542.74	151.068	1741.26	530.74	155.374	1716.47	523.18
145.630	1780.27	542.63	151.332	1739.77	530.28	155.395	1716.25	523.11
145.814	1779.79	542.48	151.477	1738.93	530.03	155.404	1716.13	523.08
145.882	1778.96	542.23	151.652	1738.05	529.76	155.457	1715.44	522.87
145.901	1778.73	542.16	151.906	1737.33	529.54	155.693	1715.10	522.76
145.911	1778.62	542.12	151.925	1737.03	529.45	155.921	1714.94	522.71
145.967	1777.94	541.92	151.944	1736.73	529.36	155.942	1714.93	522.71
146.044	1776.99	541.63	151.953	1736.58	529.31	155.951	1714.85	522.69
146.065	1776.68	541.53	151.983	1736.28	529.22	156.004	1714.26	522.51
146.074	1776.41	541.45	152.187	1736.21	529.20	156.140	1712.75	522.05
146.152	1774.18	540.77	152.208	1736.20	529.19	156.238	1712.13	521.86
146.293	1773.01	540.41	152.258	1736.18	529.19	156.259	1711.85	521.77
146.395	1772.53	540.27	152.288	1736.11	529.17	156.268	1711.68	521.72

Table A4: Constructed water-surface profile based on 2000 and 2002 data (cont'd).

River Mile	WSE (ft)	WSE (m)	River Mile	WSE (ft)	WSE (m)	River Mile	WSE (ft)	WSE (m)
156.306	1711.03	521.52	161.783	1682.90	512.95	167.603	1659.64	505.86
156.523	1710.51	521.36	162.115	1682.33	512.77	167.707	1659.58	505.84
156.782	1709.79	521.14	162.221	1681.15	512.41	167.727	1659.56	505.83
156.989	1709.61	521.09	162.250	1680.62	512.25	167.736	1659.55	505.83
157.238	1709.20	520.96	162.271	1680.21	512.13	167.798	1659.50	505.82
157.250	1709.00	520.90	162.280	1680.04	512.08	167.928	1659.36	505.77
157.269	1708.69	520.81	162.330	1679.10	511.79	168.015	1659.26	505.74
157.279	1708.53	520.76	162.517	1678.99	511.76	168.109	1659.17	505.72
157.347	1707.39	520.41	162.600	1678.95	511.74	168.257	1658.51	505.51
157.540	1704.97	519.67	162.765	1677.87	511.41	168.414	1658.24	505.43
157.717	1704.52	519.54	162.979	1677.70	511.36	168.461	1658.18	505.41
157.886	1704.09	519.41	163.168	1677.50	511.30	168.482	1657.98	505.35
158.220	1703.93	519.36	163.374	1677.18	511.20	168.491	1657.71	505.27
158.241	1703.50	519.23	163.386	1677.16	511.20	168.594	1654.70	504.35
158.250	1703.31	519.17	163.407	1676.90	511.12	168.745	1654.24	504.21
158.325	1702.13	518.81	163.417	1676.77	511.08	169.003	1653.26	503.91
158.505	1701.04	518.48	163.473	1675.99	510.84	169.221	1652.67	503.73
158.694	1700.80	518.40	163.786	1675.30	510.63	169.451	1652.44	503.66
158.714	1700.79	518.40	164.064	1675.21	510.60	169.739	1651.74	503.45
158.723	1700.13	518.20	164.244	1675.15	510.59	169.932	1651.59	503.40
158.732	1699.16	517.90	164.387	1675.10	510.57	170.234	1651.35	503.33
158.904	1697.34	517.35	164.461	1674.69	510.45	170.275	1651.32	503.32
159.090	1697.12	517.28	164.470	1674.62	510.42	170.296	1650.90	503.19
159.105	1697.02	517.25	164.546	1674.08	510.26	170.305	1650.50	503.07
159.126	1696.69	517.15	164.771	1673.76	510.16	170.417	1648.68	502.52
159.136	1696.55	517.11	164.928	1673.72	510.15	170.694	1648.56	502.48
159.235	1695.98	516.93	164.973	1672.76	509.86	170.743	1648.55	502.48
159.422	1695.67	516.84	164.993	1671.81	509.57	170.763	1648.50	502.46
159.643	1695.20	516.70	165.002	1671.33	509.42	170.772	1648.47	502.45
159.688	1695.09	516.66	165.117	1669.35	508.82	170.846	1648.17	502.36
159.708	1694.65	516.53	165.260	1669.21	508.78	171.198	1647.98	502.30
159.717	1694.34	516.43	165.412	1669.14	508.75	171.411	1647.96	502.30
159.820	1691.98	515.72	165.594	1669.09	508.74	171.443	1647.96	502.30
159.913	1690.80	515.36	165.617	1668.85	508.67	171.514	1647.49	502.15
160.176	1690.08	515.14	165.626	1668.49	508.56	171.535	1647.21	502.07
160.241	1689.77	515.04	165.671	1667.15	508.15	171.544	1647.09	502.03
160.262	1689.58	514.98	165.844	1667.06	508.12	171.654	1646.23	501.77
160.271	1689.48	514.95	166.126	1666.78	508.03	171.793	1646.15	501.75
160.369	1688.76	514.73	166.334	1666.12	507.83	171.893	1645.83	501.65
160.706	1688.19	514.56	166.564	1665.76	507.72	171.914	1645.47	501.54
160.724	1688.12	514.54	166.838	1665.69	507.70	171.923	1644.78	501.33
160.733	1688.02	514.51	166.872	1665.68	507.70	172.054	1637.88	499.23
160.810	1687.23	514.27	166.893	1665.61	507.68	172.166	1637.75	499.19
161.013	1687.19	514.26	166.903	1665.42	507.62	172.411	1636.40	498.77
161.262	1687.13	514.24	167.014	1663.92	507.16	172.633	1636.02	498.66
161.283	1685.55	513.76	167.077	1662.54	506.74	172.796	1635.60	498.53
161.292	1684.88	513.55	167.121	1661.92	506.55	172.974	1634.89	498.31
161.360	1683.25	513.05	167.165	1661.47	506.42	172.993	1634.86	498.31
161.546	1683.09	513.01	167.393	1660.82	506.22	173.003	1634.82	498.29

Table A4: Constructed water-surface profile based on 2000 and 2002 data (cont'd).

River Mile	WSE (ft)	WSE (m)	River Mile	WSE (ft)	WSE (m)	River Mile	WSE (ft)	WSE (m)
173.225	1634.02	498.05	176.796	1611.38	491.15	181.093	1564.38	476.82
173.340	1633.60	497.92	176.805	1611.35	491.14	181.102	1564.30	476.80
173.636	1633.20	497.80	176.852	1611.23	491.10	181.146	1563.92	476.68
173.683	1632.38	497.55	176.903	1611.12	491.07	181.273	1563.64	476.60
173.704	1631.46	497.27	177.078	1610.84	490.98	181.477	1563.45	476.54
173.713	1631.06	497.15	177.215	1607.47	489.96	181.498	1563.37	476.52
173.784	1630.95	497.11	177.323	1606.92	489.79	181.508	1563.30	476.49
174.036	1630.78	497.06	177.426	1606.58	489.69	181.561	1562.89	476.37
174.192	1630.52	496.98	177.539	1606.18	489.56	181.757	1561.74	476.02
174.235	1630.45	496.96	177.560	1606.02	489.51	181.894	1561.12	475.83
174.257	1630.04	496.84	177.569	1605.95	489.49	182.028	1559.80	475.43
174.266	1629.80	496.76	177.637	1605.45	489.34	182.146	1559.45	475.32
174.317	1628.90	496.49	177.696	1605.06	489.22	182.338	1558.98	475.18
174.574	1628.43	496.35	177.817	1604.85	489.16	182.484	1558.02	474.88
174.743	1627.53	496.07	177.864	1604.37	489.01	182.699	1552.96	473.34
174.764	1627.32	496.01	177.885	1603.42	488.72	182.817	1552.67	473.25
174.773	1627.24	495.98	177.895	1603.01	488.60	182.916	1552.43	473.18
174.950	1622.60	494.57	177.974	1602.27	488.37	182.997	1552.23	473.12
174.997	1622.05	494.40	178.026	1602.22	488.36	183.152	1549.54	472.30
175.018	1621.54	494.25	178.036	1602.21	488.35	183.347	1549.18	472.19
175.027	1621.32	494.18	178.125	1602.16	488.34	183.373	1549.13	472.17
175.092	1620.79	494.02	178.341	1601.90	488.26	183.395	1549.04	472.15
175.175	1620.38	493.89	178.604	1601.50	488.14	183.404	1549.01	472.14
175.299	1619.78	493.71	178.672	1601.40	488.11	183.457	1548.80	472.07
175.438	1619.72	493.69	178.743	1601.30	488.08	183.687	1548.11	471.86
175.459	1619.60	493.65	178.930	1601.26	488.06	183.824	1546.28	471.31
175.468	1619.43	493.60	179.216	1601.19	488.04	183.871	1545.89	471.19
175.509	1618.69	493.38	179.421	1601.11	488.02	183.972	1545.65	471.11
175.589	1618.35	493.27	179.663	1600.60	487.86	183.984	1545.58	471.09
175.609	1618.32	493.26	179.708	1600.32	487.78	184.004	1545.27	471.00
175.618	1618.31	493.26	179.729	1598.19	487.13	184.013	1545.11	470.95
175.658	1618.24	493.24	179.738	1596.15	486.51	184.075	1544.00	470.61
175.693	1618.18	493.22	179.838	1586.82	483.66	184.226	1541.46	469.84
175.805	1617.98	493.16	180.007	1586.48	483.56	184.280	1541.27	469.78
175.855	1617.74	493.09	180.030	1586.20	483.47	184.371	1540.96	469.68
175.876	1617.64	493.06	180.051	1584.76	483.03	184.383	1540.92	469.67
175.885	1617.59	493.04	180.060	1583.79	482.74	184.404	1540.49	469.54
175.962	1617.22	492.93	180.101	1581.14	481.93	184.413	1540.28	469.48
176.040	1617.02	492.87	180.263	1579.55	481.45	184.478	1539.28	469.17
176.172	1616.76	492.79	180.374	1579.33	481.38	184.599	1538.86	469.04
176.193	1616.53	492.72	180.406	1578.96	481.27	184.777	1538.25	468.86
176.202	1616.43	492.69	180.427	1577.94	480.96	184.854	1537.13	468.52
176.261	1615.86	492.51	180.436	1577.50	480.82	184.877	1536.60	468.36
176.429	1614.81	492.19	180.542	1574.51	479.91	184.886	1536.37	468.29
176.482	1613.67	491.85	180.695	1572.30	479.24	184.930	1535.93	468.15
176.563	1612.15	491.38	180.835	1570.49	478.69	185.028	1535.72	468.09
176.643	1611.87	491.30	180.980	1565.48	477.16	185.047	1535.46	468.01
176.721	1611.60	491.22	181.054	1564.75	476.94	185.057	1535.33	467.97
176.776	1611.43	491.16	181.071	1564.60	476.89	185.109	1534.58	467.74

Table A4: Constructed water-surface profile based on 2000 and 2002 data (cont'd).

River Mile	WSE (ft)	WSE (m)	River Mile	WSE (ft)	WSE (m)	River Mile	WSE (ft)	WSE (m)
185.247	1533.90	467.53	189.511	1506.74	459.25	193.538	1480.77	451.34
185.293	1533.58	467.44	189.579	1505.62	458.91	193.600	1480.28	451.19
185.368	1533.07	467.28	189.701	1504.48	458.57	193.828	1477.14	450.23
185.420	1532.83	467.21	189.822	1503.20	458.18	193.982	1476.29	449.97
185.566	1532.75	467.18	189.922	1503.14	458.16	194.191	1475.71	449.80
185.617	1532.38	467.07	190.046	1503.07	458.14	194.275	1474.86	449.54
185.676	1531.53	466.81	190.067	1503.06	458.13	194.434	1470.70	448.27
185.721	1530.85	466.60	190.087	1503.05	458.13	194.644	1469.94	448.04
185.741	1530.59	466.52	190.096	1502.50	457.96	194.781	1469.83	448.00
185.750	1530.45	466.48	190.192	1499.72	457.11	194.799	1469.81	448.00
185.786	1529.91	466.32	190.342	1499.58	457.07	194.810	1469.76	447.98
185.917	1529.33	466.14	190.398	1499.53	457.06	194.862	1469.45	447.89
185.995	1529.15	466.08	190.540	1499.40	457.02	194.961	1468.88	447.71
186.070	1529.00	466.04	190.680	1499.27	456.98	194.993	1468.70	447.66
186.091	1528.96	466.03	190.709	1499.24	456.97	195.014	1468.53	447.61
186.101	1528.95	466.02	190.739	1498.86	456.85	195.023	1468.45	447.58
186.163	1528.73	465.96	190.777	1498.35	456.70	195.073	1468.03	447.46
186.312	1528.19	465.79	190.925	1498.17	456.64	195.160	1467.52	447.30
186.333	1528.11	465.77	191.075	1498.11	456.62	195.257	1467.46	447.28
186.342	1528.07	465.76	191.098	1497.24	456.36	195.285	1466.63	447.03
186.421	1527.79	465.67	191.121	1496.37	456.09	195.396	1463.28	446.01
186.653	1527.16	465.48	191.143	1495.55	455.84	195.544	1461.33	445.41
186.765	1526.89	465.40	191.166	1494.68	455.58	195.648	1460.68	445.22
186.915	1526.54	465.29	191.189	1493.81	455.31	195.769	1460.59	445.19
187.046	1526.26	465.20	191.209	1493.29	455.15	195.869	1459.74	444.93
187.188	1526.12	465.16	191.218	1493.12	455.10	195.961	1459.66	444.90
187.306	1526.01	465.13	191.280	1492.17	454.81	196.121	1459.46	444.84
187.392	1525.82	465.07	191.428	1490.61	454.34	196.228	1457.98	444.39
187.523	1525.32	464.92	191.544	1489.83	454.10	196.287	1457.48	444.24
187.703	1522.71	464.12	191.680	1489.51	454.00	196.319	1457.22	444.16
187.836	1521.36	463.71	191.765	1489.31	453.94	196.437	1456.99	444.09
188.046	1521.03	463.61	191.842	1489.13	453.89	196.464	1456.95	444.08
188.173	1520.98	463.59	191.934	1488.91	453.82	196.484	1456.78	444.03
188.229	1520.96	463.59	192.047	1488.67	453.75	196.494	1456.67	443.99
188.250	1519.79	463.23	192.127	1488.51	453.70	196.550	1456.04	443.80
188.259	1519.29	463.08	192.221	1488.23	453.61	196.716	1454.99	443.48
188.300	1518.96	462.98	192.321	1487.78	453.48	196.866	1453.99	443.18
188.490	1517.87	462.65	192.494	1486.41	453.06	196.913	1453.65	443.07
188.623	1514.88	461.74	192.736	1485.01	452.63	196.935	1453.49	443.02
188.762	1514.29	461.56	192.884	1484.74	452.55	197.012	1452.94	442.86
188.851	1511.07	460.57	193.067	1484.63	452.52	197.154	1452.63	442.76
189.005	1510.74	460.47	193.206	1484.17	452.38	197.210	1452.51	442.73
189.129	1510.59	460.43	193.227	1483.96	452.31	197.403	1452.10	442.60
189.148	1509.85	460.20	193.236	1483.88	452.29	197.665	1450.57	442.13
189.158	1509.47	460.09	193.289	1483.38	452.13	197.907	1448.47	441.49
189.256	1507.58	459.51	193.343	1483.24	452.09	198.112	1448.20	441.41
189.348	1507.30	459.43	193.467	1482.57	451.89	198.165	1448.12	441.39
189.443	1507.29	459.42	193.508	1481.56	451.58	198.338	1447.99	441.35
189.502	1506.90	459.30	193.529	1481.01	451.41	198.515	1447.89	441.32

Table A4: Constructed water-surface profile based on 2000 and 2002 data (cont'd).

River Mile	WSE (ft)	WSE (m)	River Mile	WSE (ft)	WSE (m)	River Mile	WSE (ft)	WSE (m)
198.680	1447.79	441.29	202.193	1422.16	433.47	206.575	1389.30	423.46
198.773	1447.74	441.27	202.269	1422.00	433.43	206.584	1389.22	423.43
198.793	1447.68	441.25	202.290	1421.95	433.41	206.714	1389.03	423.38
198.802	1447.51	441.20	202.299	1421.70	433.33	206.910	1388.95	423.35
198.944	1444.97	440.43	202.340	1420.47	432.96	206.966	1388.67	423.27
198.991	1444.16	440.18	202.453	1420.16	432.86	207.037	1387.93	423.04
199.112	1441.14	439.26	202.645	1419.66	432.71	207.208	1386.43	422.58
199.133	1440.43	439.04	202.790	1419.54	432.68	207.463	1384.24	421.92
199.142	1440.10	438.94	202.808	1419.53	432.67	207.569	1382.32	421.33
199.264	1438.66	438.50	202.819	1419.52	432.67	207.590	1381.82	421.18
199.373	1438.10	438.33	202.888	1419.46	432.65	207.600	1381.77	421.16
199.473	1437.67	438.20	203.113	1419.08	432.54	207.681	1381.30	421.02
199.550	1437.52	438.16	203.263	1417.95	432.19	207.752	1379.77	420.55
199.752	1435.83	437.64	203.447	1417.38	432.02	207.802	1378.25	420.09
199.846	1434.69	437.29	203.616	1416.86	431.86	208.038	1377.35	419.82
199.917	1434.04	437.10	203.872	1416.25	431.67	208.287	1377.01	419.71
200.106	1433.34	436.88	204.107	1414.84	431.24	208.309	1376.70	419.62
200.261	1432.55	436.64	204.276	1413.17	430.73	208.318	1376.57	419.58
200.420	1432.43	436.60	204.297	1413.02	430.69	208.359	1376.00	419.40
200.453	1432.41	436.60	204.307	1413.02	430.69	208.581	1375.89	419.37
200.473	1432.28	436.56	204.326	1413.01	430.69	208.690	1375.88	419.37
200.482	1432.20	436.53	204.489	1412.98	430.68	208.741	1375.69	419.31
200.550	1431.61	436.35	204.539	1412.97	430.67	208.762	1375.42	419.23
200.663	1430.76	436.10	204.558	1412.96	430.67	208.771	1375.31	419.19
200.699	1430.66	436.07	204.568	1412.96	430.67	208.853	1374.33	418.90
200.719	1430.62	436.05	204.617	1412.94	430.66	208.995	1374.07	418.82
200.728	1430.60	436.05	204.686	1412.88	430.65	209.101	1373.98	418.79
200.808	1430.40	435.99	204.708	1412.86	430.64	209.164	1372.48	418.33
200.932	1430.10	435.89	204.717	1412.56	430.55	209.185	1370.77	417.81
201.036	1429.82	435.81	204.785	1410.93	430.05	209.194	1370.03	417.59
201.089	1429.63	435.75	204.977	1410.81	430.01	209.229	1368.61	417.15
201.110	1429.55	435.73	205.083	1410.74	429.99	209.288	1367.50	416.81
201.119	1429.51	435.71	205.359	1410.67	429.97	209.327	1366.79	416.60
201.160	1429.36	435.67	205.521	1410.66	429.97	209.368	1366.15	416.40
201.234	1429.08	435.58	205.622	1410.29	429.86	209.445	1365.22	416.12
201.361	1428.61	435.44	205.643	1407.29	428.94	209.501	1364.53	415.91
201.445	1427.69	435.16	205.652	1405.68	428.45	209.542	1363.66	415.64
201.465	1427.09	434.98	205.720	1400.15	426.77	209.584	1362.80	415.38
201.474	1426.80	434.89	205.867	1399.22	426.48	209.622	1362.23	415.21
201.511	1425.70	434.55	205.909	1399.04	426.43	209.637	1362.00	415.14
201.569	1425.33	434.44	205.988	1398.60	426.29	209.657	1361.74	415.06
201.622	1425.00	434.34	206.171	1396.81	425.75	209.667	1361.61	415.02
201.707	1424.78	434.27	206.270	1395.84	425.45	209.738	1360.60	414.71
201.817	1424.74	434.26	206.294	1395.60	425.38	209.778	1360.17	414.58
201.870	1423.72	433.95	206.317	1395.38	425.31	209.847	1359.55	414.39
201.889	1423.22	433.80	206.326	1395.29	425.28	209.892	1359.12	414.26
201.899	1422.96	433.72	206.388	1391.34	424.08	209.960	1358.16	413.97
201.953	1422.70	433.64	206.516	1389.78	423.60	210.048	1356.73	413.53
202.145	1422.27	433.51	206.554	1389.48	423.51	210.173	1355.27	413.09

Table A4: Constructed water-surface profile based on 2000 and 2002 data (cont'd).

River Mile	WSE (ft)	WSE (m)	River Mile	WSE (ft)	WSE (m)	River Mile	WSE (ft)	WSE (m)
210.194	1355.10	413.03	214.314	1329.38	405.20	218.239	1304.03	397.47
210.203	1355.03	413.01	214.369	1329.36	405.19	218.260	1303.30	397.25
210.265	1354.56	412.87	214.392	1328.97	405.07	218.269	1302.87	397.11
210.396	1352.50	412.24	214.401	1328.78	405.01	218.301	1301.47	396.69
210.498	1351.88	412.05	214.435	1328.08	404.80	218.363	1301.02	396.55
210.608	1351.38	411.90	214.522	1327.66	404.67	218.428	1300.99	396.54
210.775	1350.77	411.71	214.596	1327.25	404.55	218.576	1300.93	396.52
210.847	1350.32	411.58	214.605	1327.07	404.49	218.822	1300.83	396.49
210.868	1349.99	411.48	214.759	1325.39	403.98	219.002	1300.75	396.47
210.877	1349.84	411.43	214.780	1325.36	403.97	219.210	1300.66	396.44
210.942	1349.11	411.21	214.789	1325.34	403.96	219.269	1300.63	396.43
211.037	1348.80	411.11	214.836	1325.28	403.95	219.443	1300.56	396.41
211.093	1348.66	411.07	214.963	1325.09	403.89	219.471	1300.54	396.40
211.211	1348.44	411.00	215.141	1324.84	403.81	219.543	1300.09	396.27
211.321	1347.74	410.79	215.265	1324.66	403.76	219.561	1299.58	396.11
211.469	1346.84	410.52	215.392	1324.46	403.70	219.570	1299.33	396.04
211.537	1346.41	410.39	215.454	1324.36	403.66	219.645	1297.91	395.60
211.720	1346.01	410.26	215.594	1324.14	403.60	219.863	1297.42	395.45
211.741	1345.93	410.24	215.688	1323.98	403.55	219.993	1297.12	395.36
211.750	1345.85	410.22	215.883	1323.67	403.45	220.044	1296.97	395.32
211.880	1344.63	409.84	215.978	1323.52	403.41	220.136	1296.46	395.16
211.913	1343.63	409.54	215.999	1323.49	403.40	220.155	1296.35	395.13
211.934	1342.71	409.26	216.008	1323.09	403.28	220.165	1296.30	395.11
211.943	1342.32	409.14	216.067	1320.57	402.51	220.210	1296.04	395.03
211.993	1341.98	409.04	216.165	1320.27	402.42	220.282	1295.73	394.94
212.102	1341.25	408.81	216.342	1319.98	402.33	220.381	1295.31	394.81
212.229	1339.30	408.22	216.476	1319.75	402.26	220.532	1295.06	394.73
212.463	1338.07	407.84	216.502	1319.58	402.21	220.580	1294.98	394.71
212.484	1338.03	407.83	216.523	1319.40	402.15	220.680	1292.81	394.05
212.493	1337.61	407.70	216.532	1319.33	402.13	220.760	1289.67	393.09
212.543	1333.85	406.56	216.576	1318.98	402.03	220.931	1286.12	392.01
212.646	1333.54	406.46	216.715	1318.61	401.91	221.015	1283.28	391.14
212.800	1333.08	406.32	216.827	1318.39	401.85	221.056	1282.44	390.89
212.947	1332.64	406.19	217.032	1317.99	401.72	221.145	1282.05	390.77
212.969	1332.57	406.17	217.110	1317.79	401.66	221.230	1281.69	390.66
212.978	1332.54	406.16	217.132	1317.69	401.63	221.251	1280.94	390.43
213.013	1332.44	406.13	217.141	1317.64	401.62	221.260	1280.62	390.33
213.064	1332.39	406.11	217.185	1317.44	401.56	221.313	1279.55	390.01
213.087	1332.22	406.06	217.362	1317.34	401.53	221.408	1279.51	389.99
213.096	1332.15	406.04	217.393	1317.34	401.53	221.562	1279.44	389.97
213.143	1331.80	405.93	217.490	1317.31	401.52	221.580	1279.44	389.97
213.229	1331.41	405.81	217.662	1317.27	401.50	221.591	1279.43	389.97
213.307	1331.34	405.79	217.747	1316.50	401.27	221.662	1279.29	389.93
213.425	1330.88	405.65	217.768	1313.86	400.46	221.902	1278.68	389.74
213.537	1330.44	405.52	217.777	1312.73	400.12	221.917	1278.64	389.73
213.640	1330.24	405.46	217.828	1309.77	399.22	221.938	1278.15	389.58
213.739	1330.08	405.41	217.946	1308.39	398.80	221.947	1277.95	389.52
213.925	1330.04	405.40	218.073	1304.84	397.72	222.156	1272.98	388.00
214.218	1329.41	405.20	218.176	1304.34	397.56	222.177	1272.85	387.96

Table A4: Constructed water-surface profile based on 2000 and 2002 data (cont'd).

River Mile	WSE (ft)	WSE (m)
222.186	1272.79	387.95
222.251	1272.50	387.86
222.376	1272.28	387.79
222.405	1272.16	387.75
222.426	1271.96	387.69
222.435	1271.87	387.67
222.633	1270.77	387.33
222.769	1270.33	387.20
222.802	1270.23	387.17
222.967	1269.41	386.92
222.988	1268.71	386.70
223.016	1267.81	386.43
223.137	1265.79	385.81
223.222	1264.15	385.31
223.311	1263.68	385.17
223.438	1263.27	385.04
223.550	1261.64	384.55
223.627	1260.67	384.25
223.657	1260.53	384.21
223.686	1260.39	384.17
223.716	1260.25	384.12
223.737	1260.13	384.09
223.755	1259.16	383.79
223.766	1258.47	383.58
223.828	1255.63	382.72
223.935	1255.24	382.60
224.085	1254.70	382.43
224.191	1254.50	382.37
224.399	1254.32	382.32
224.610	1254.14	382.26
224.799	1253.98	382.21
224.870	1253.92	382.19
225.064	1253.88	382.18
225.228	1253.86	382.18
225.246	1253.86	382.18
225.488	1253.84	382.17
225.633	1253.67	382.12
225.654	1253.23	381.98
225.663	1253.04	381.93
225.722	1251.83	381.56
225.822	1251.69	381.52
225.927	1251.54	381.47
225.950	1251.51	381.46
225.959	1250.87	381.27

APPENDIX B

ADDITIONAL VELOCITY AND BATHYMETRY MEASUREMENTS FROM GRAND CANYON

ADV and fathometer data were collected in 2003 and 2005 at five rapids within Grand Canyon (see Table 5.1). Appendix B presents the flow velocity and bathymetry maps constructed for each site. As discussed in Chapter 3, a directional bias affected the ENU velocity vectors collected by the ADV from the particular measurement session. All data from that session were rotated using a correction angle so that the maps realistically show the water flowing downstream. The angular correction factors for each session are given below in Table B1.

Table B1: Angular correction factor used to post-process ADV data from each measurement session.

Site	Date	Angular correction
Comanche	3/18/03	-45°
Comanche	3/3/05	-45°
Rattlesnake	3/20/03	-22°
Rattlesnake	3/21/03	-22°
Rattlesnake	3/5/05	-11°
Escalante	3/21/03	-13°
Escalante	3/5/05	-13°
Salt	3/25/03	-20°
Salt	3/26/03	-20°
Salt	3/8/05	-20°
RM 189.7L	3/30/03	-10°
RM 189.7L	3/11/05	0°
RM 189.7L	3/12/05	0°

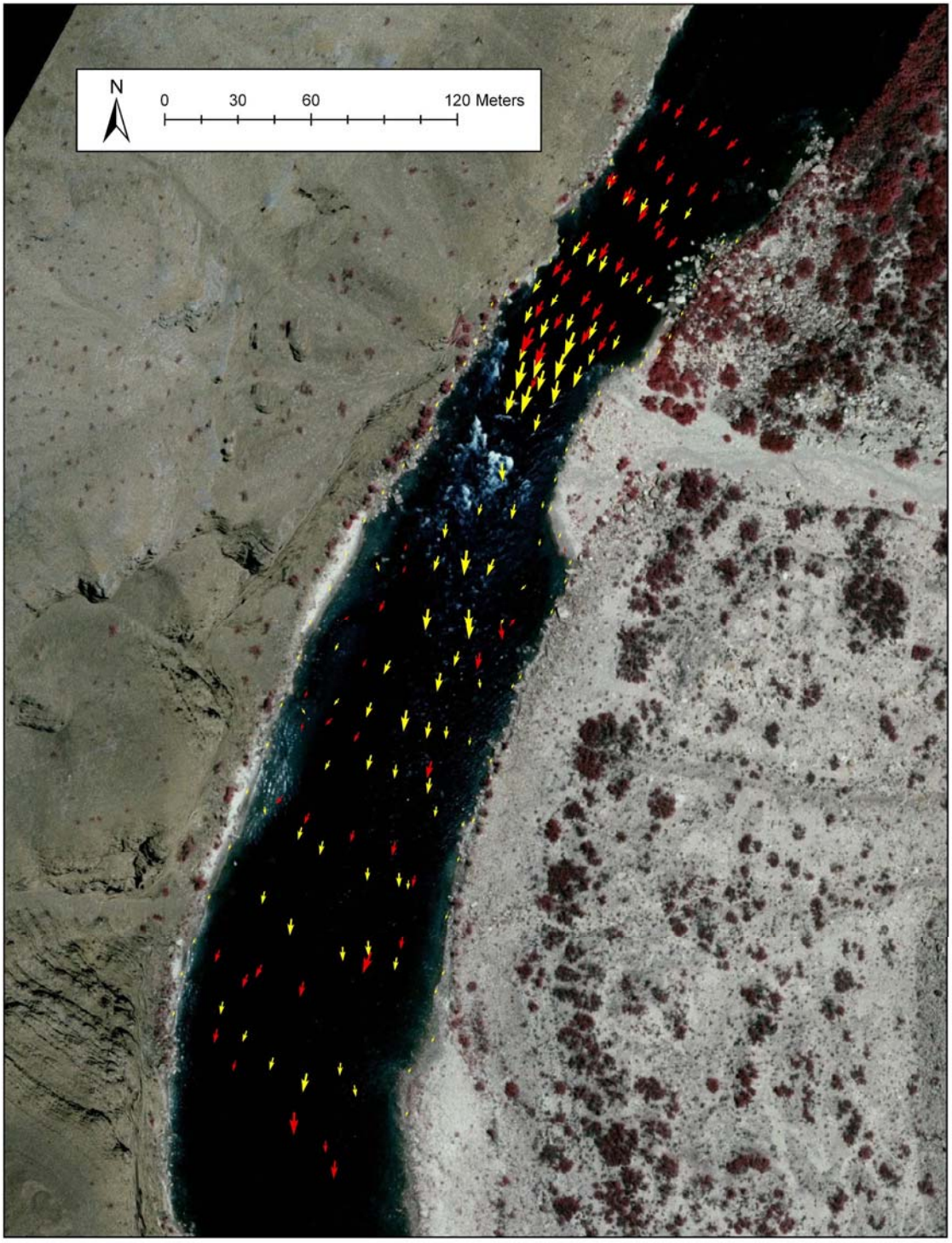

Figure B.1: Flow velocity vector field at the rapid at Comanche Creek as measured with the ADV. Red arrows represent data collected in 2003; Yellow arrows represent data collected in 2005. See Table 5.1 and Chapter 5 for details.

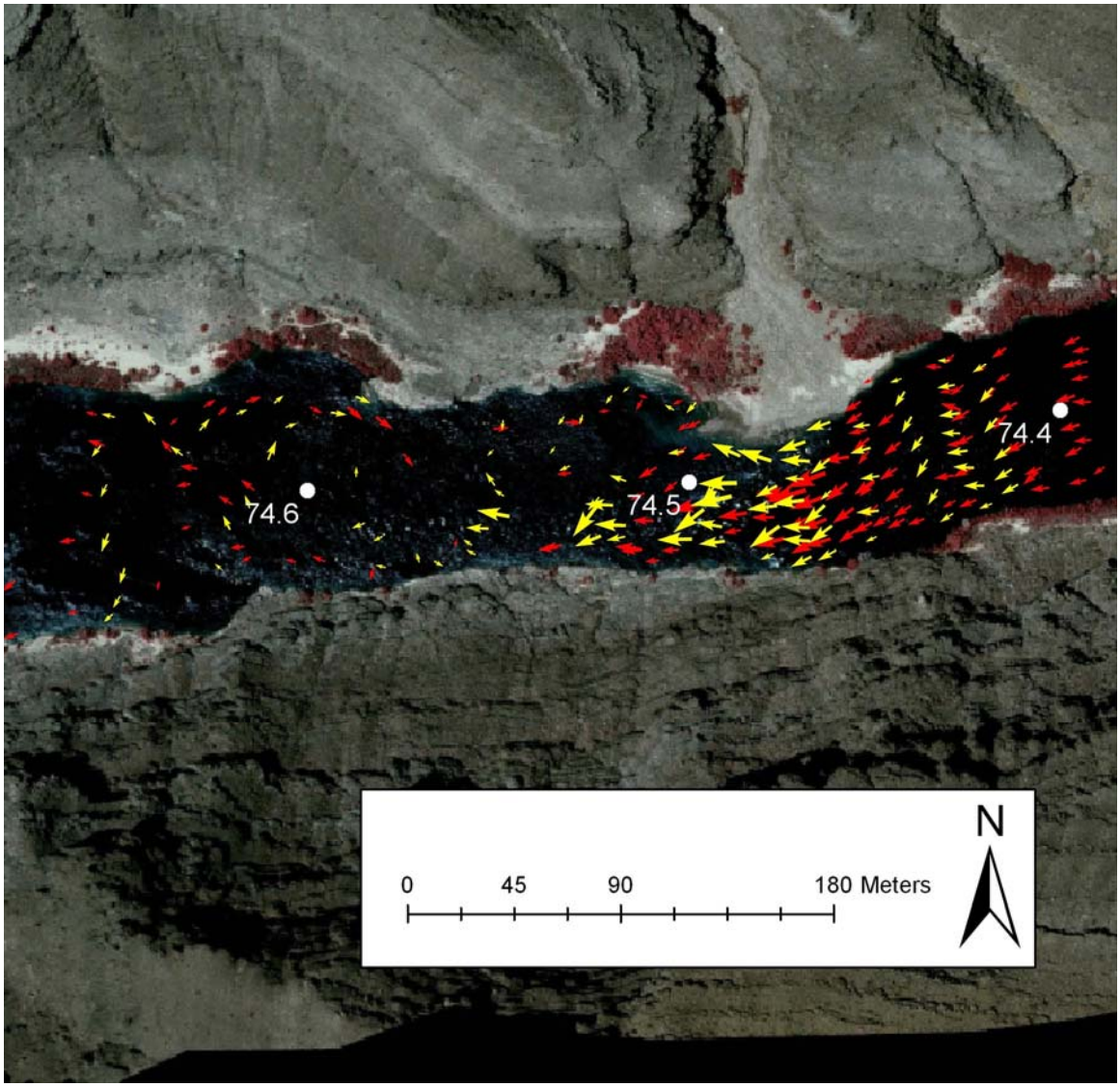

Figure B.2: Flow velocity vector field at the rapid at Upper Rattlesnake Camp as measured with the ADV. Red arrows represent data collected in 2003; Yellow arrows represent data collected in 2005. See Table 5.1 and Chapter 5 for details.

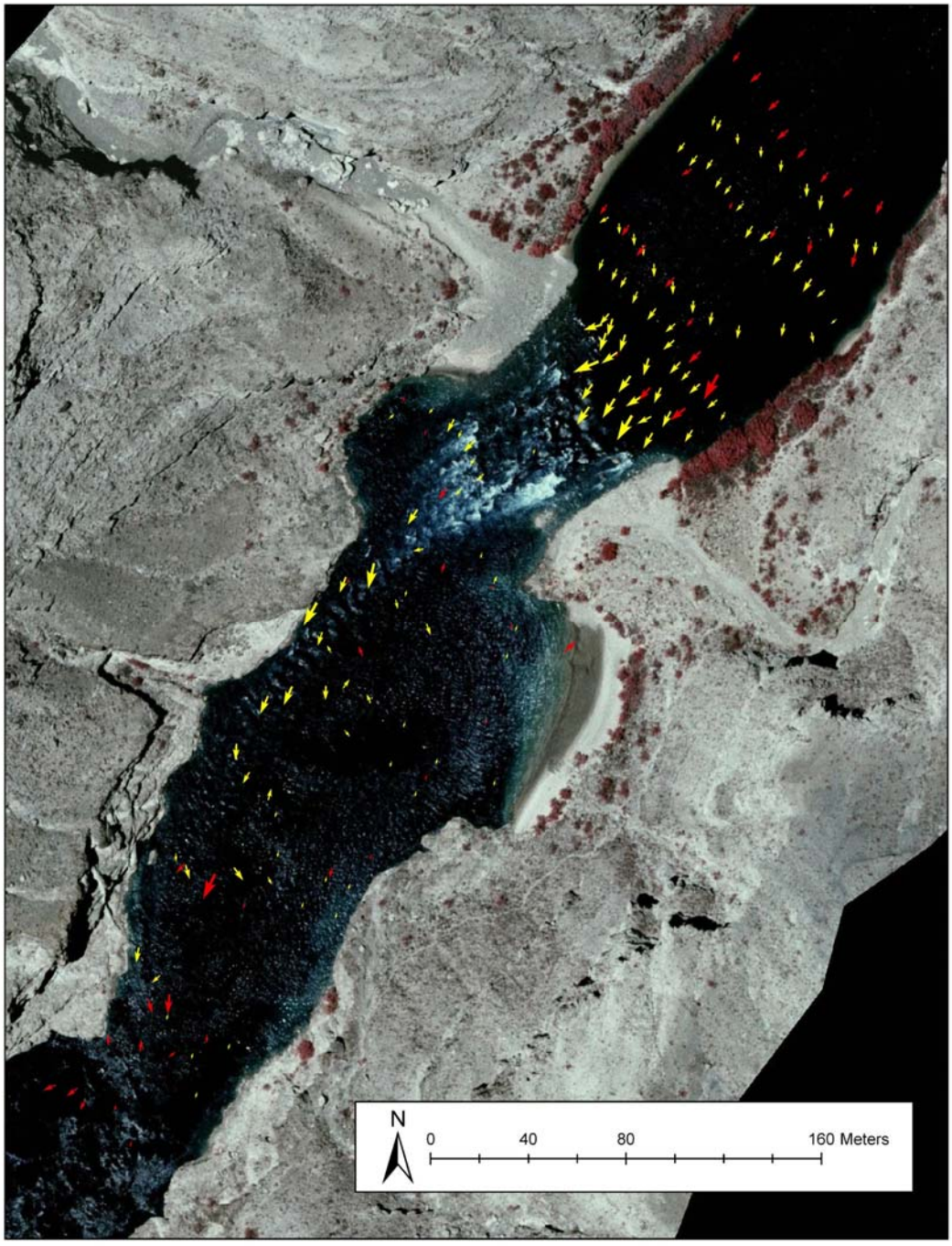

Figure B.3: Flow velocity vector field at the rapid at Escalante Creek as measured with the ADV. Red arrows represent data collected in 2003; Yellow arrows represent data collected in 2005. See Table 5.1 and Chapter 5 for details.

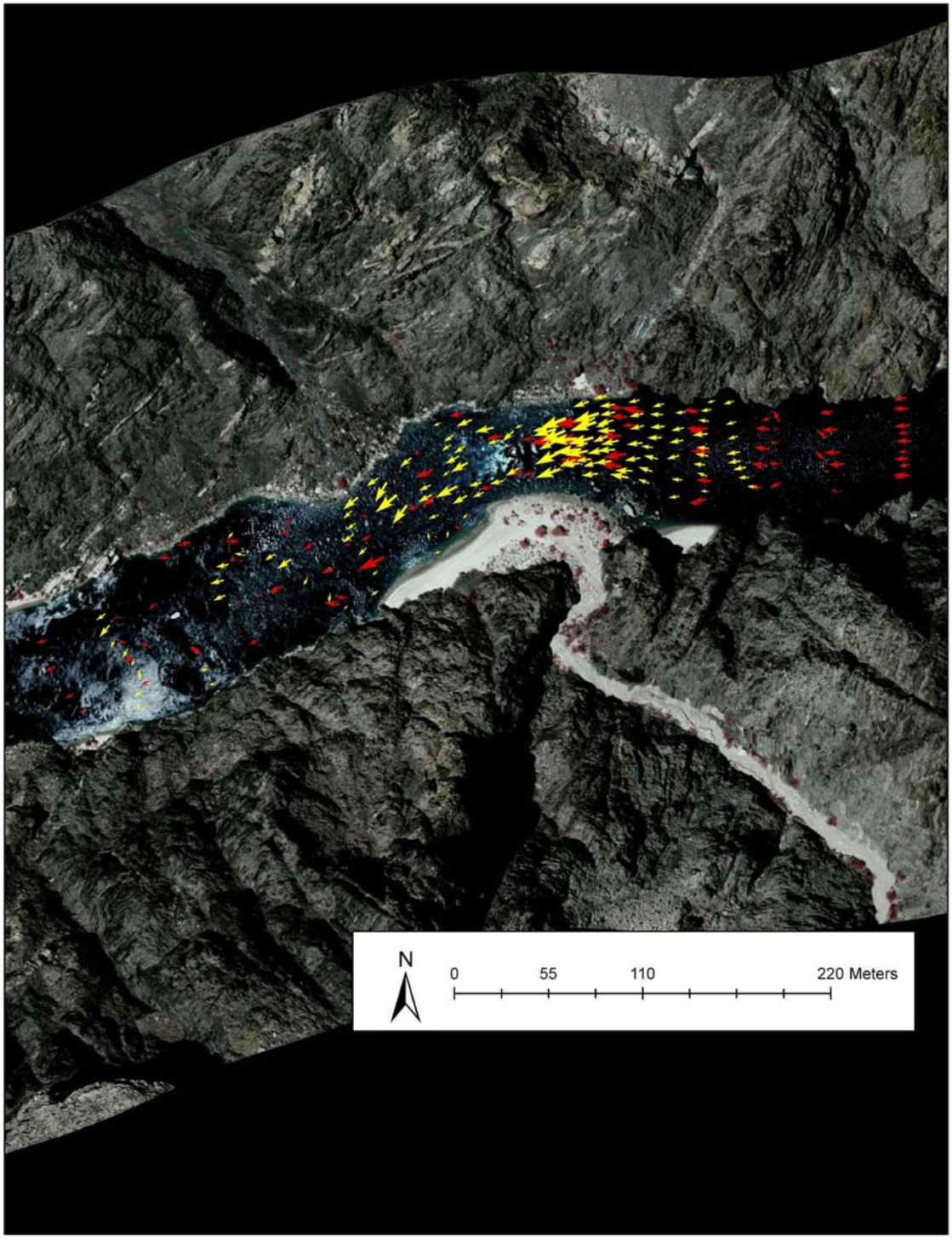

Figure B.4: Flow velocity vector field at Salt Creek Rapid as measured with the ADV. Red arrows represent data collected in 2003; Yellow arrows represent data collected in 2005. See Table 5.1 and Chapter 5 for details.

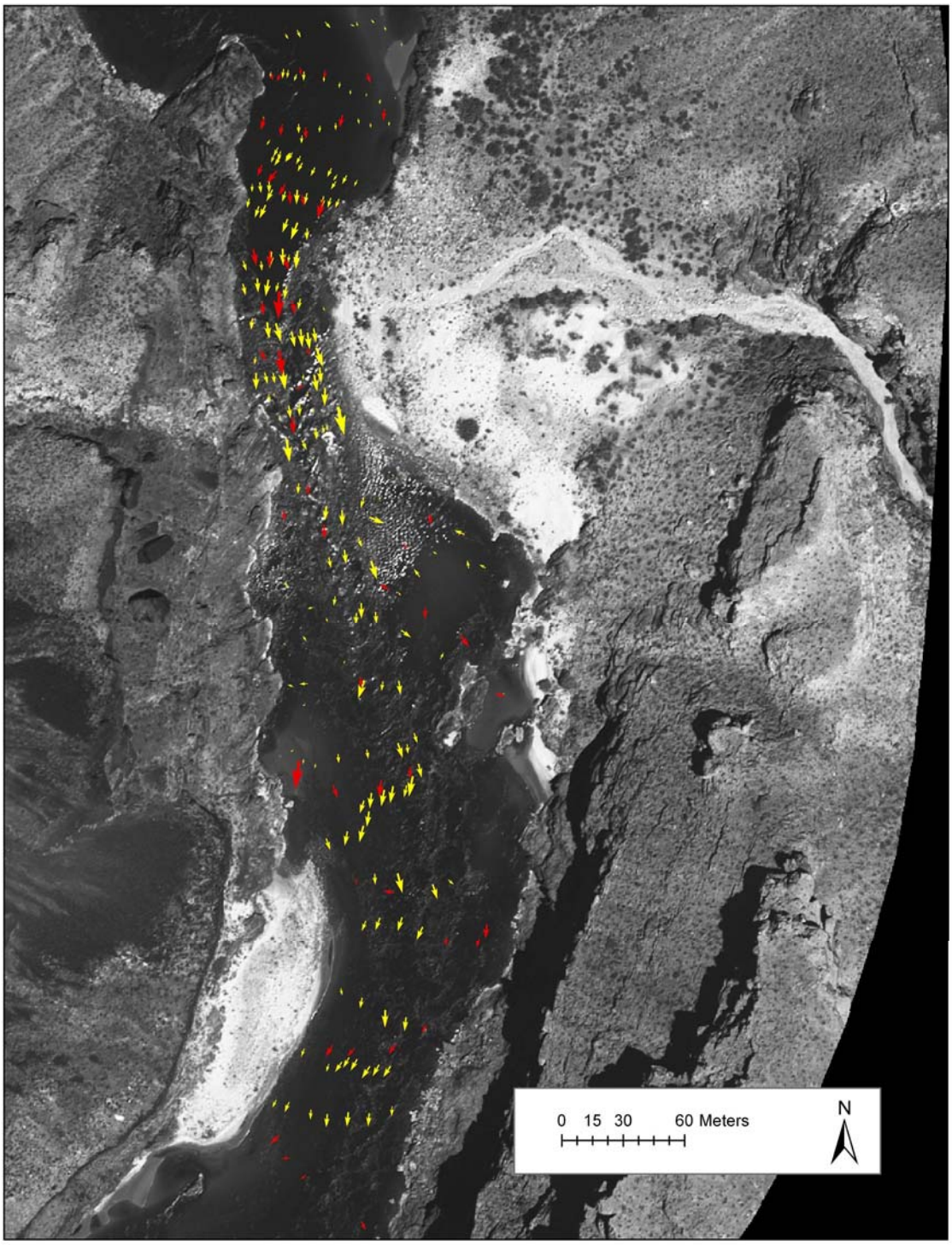

Figure B.5: Flow velocity vector field at 189.7L as measured with the ADV. Red arrows represent data collected in 2003; Yellow arrows represent data collected in 2005. See Table 5.1 and Chapter 5 for details.

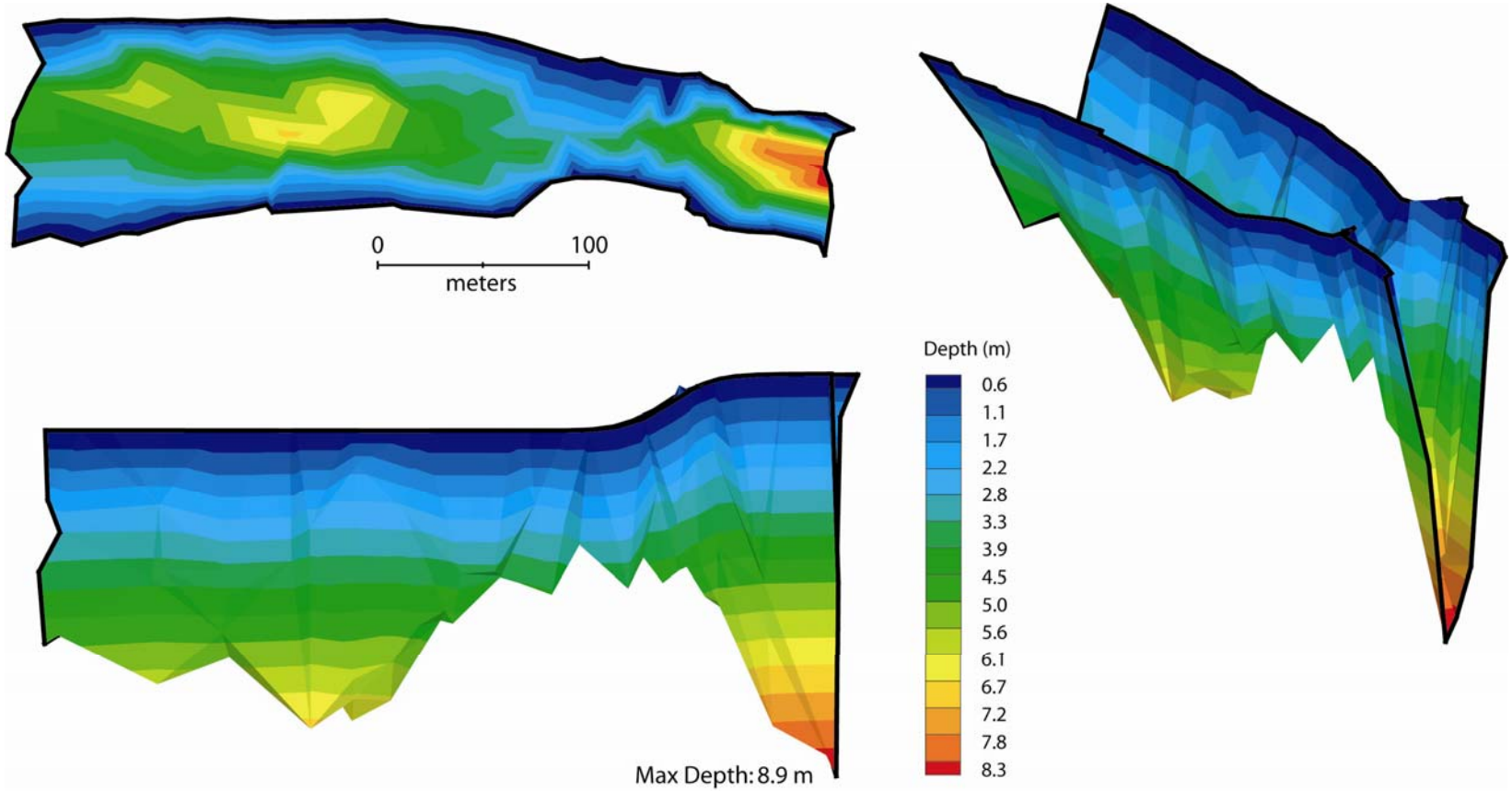

Figure B.6: Bathymetry at Comanche Rapid (river mile 67.7) as measured with the Lowrance X59DF fathometer. Discharge is 227 m^3/s.

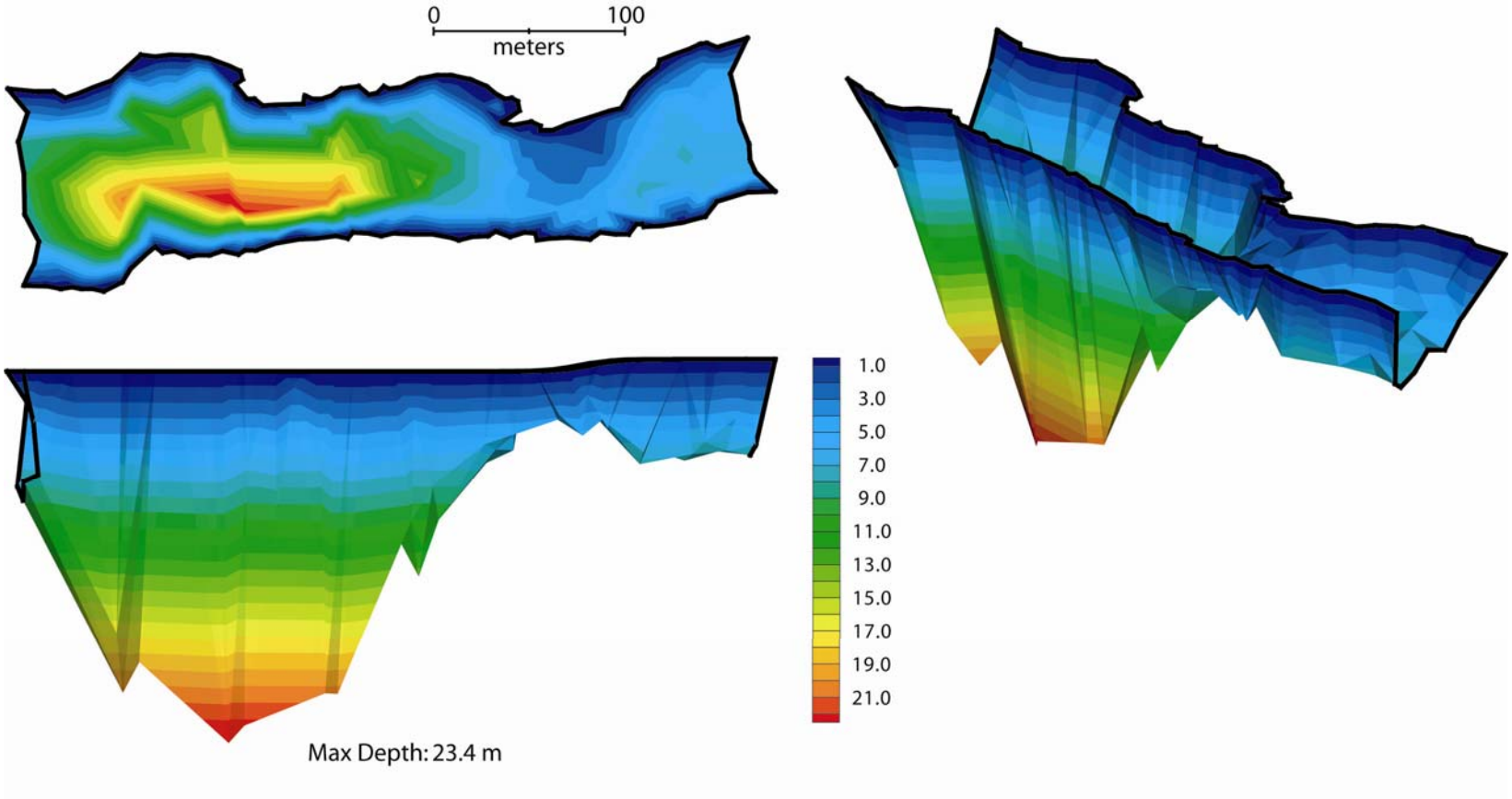

Figure B.7: Bathymetry at Rattlesnake (river mile 73.9) as measured with the Lowrance X59DF fathometer. Discharge is 227 m^3/s.

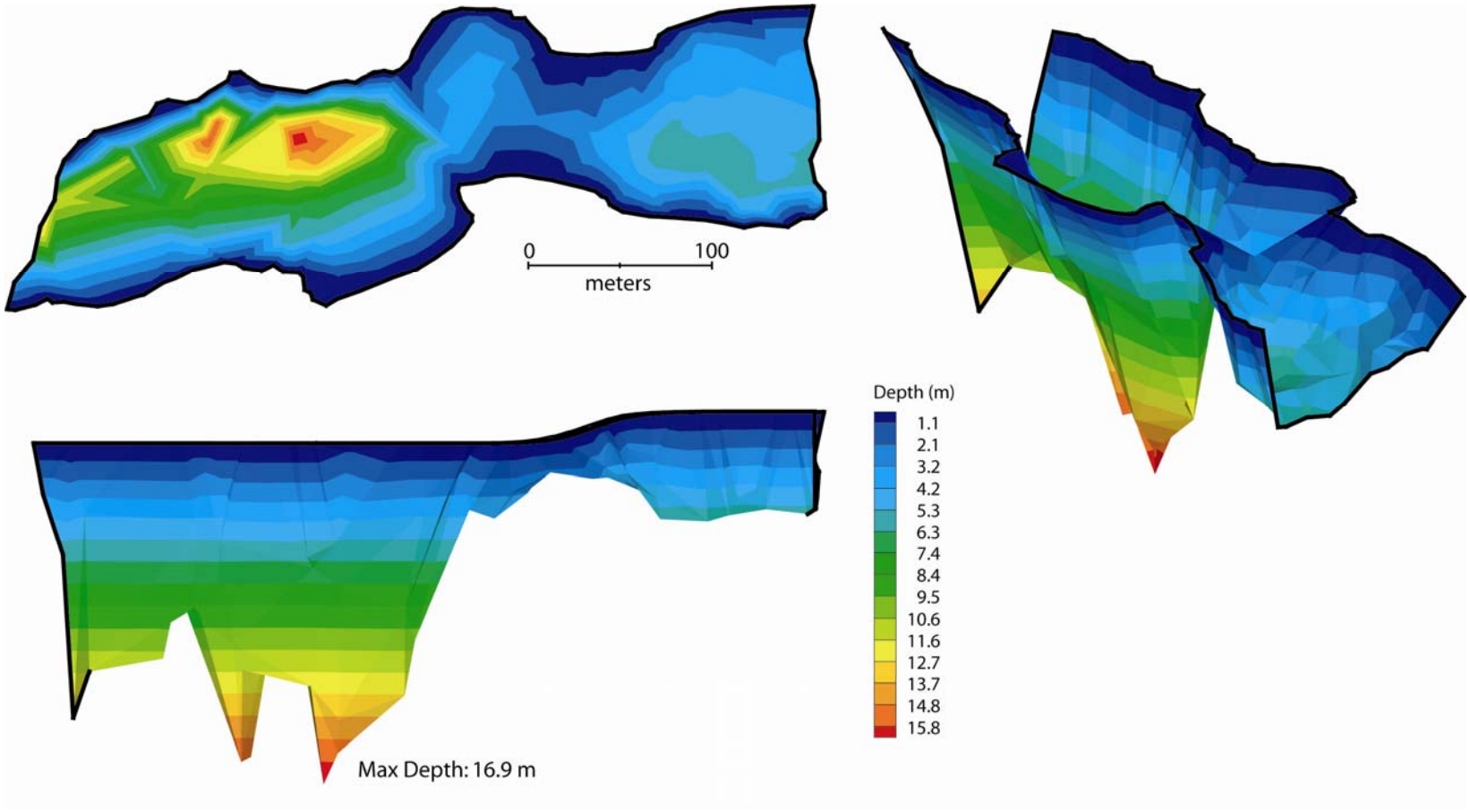

Figure B.8: Bathymetry at Escalante Rapid (river mile 75.4) as measured with the Lowrance X59DF fathometer. Discharge is 227 m^3/s.

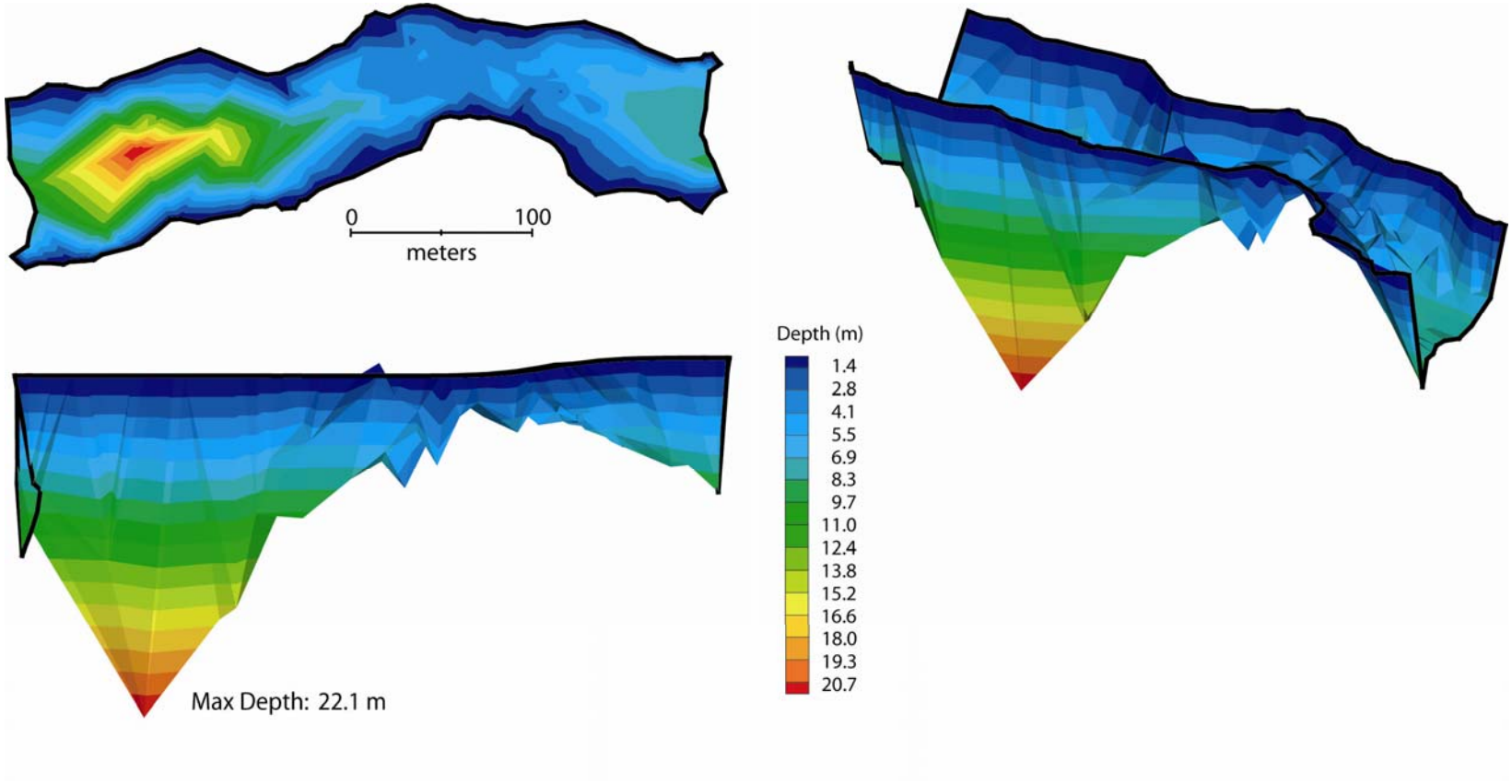

Figure B.9: Bathymetry at Salt Creek Rapid (river mile 93.1) as measured with the Lowrance X59DF fathometer. Discharge is 227 m^3/s.

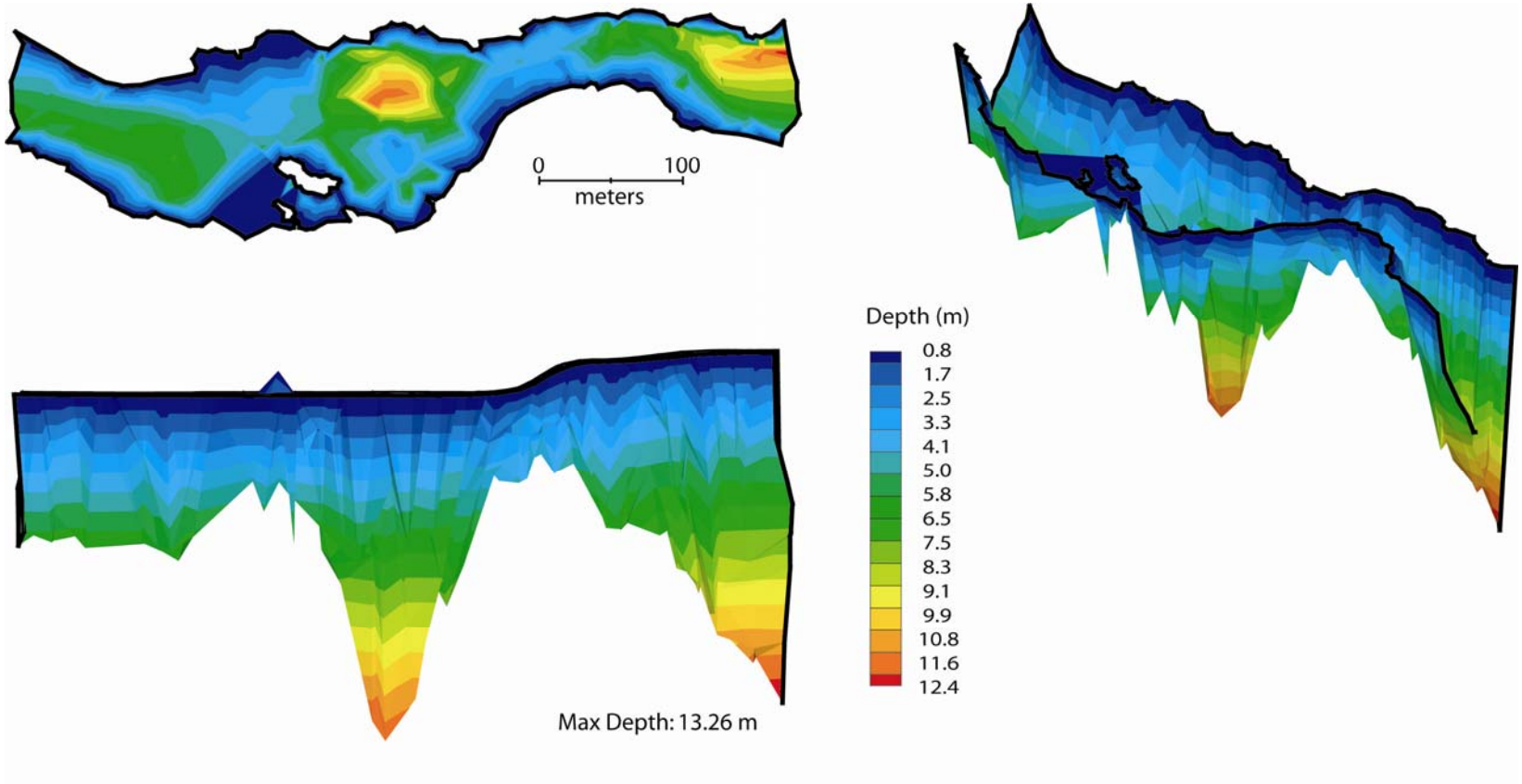

Figure B.10: Bathymetry at tributary 189.7L as measured with the Lowrance X59DF fathometer. Discharge is 227 m^3/s.

REFERENCES

Allen, J.R.L. (1985), *Principles of Physical Sedimentology*, George Allen & Unwin, London, 272 pp.

Anderson, R.E. (1978), Geologic Hap of the Black Canyon 15-minute Quadrangle, Mohave County, Arizona, and Clark County, Nevada. *U.S. Geological Survey Geologic Quadrangle Map* GQ 1394.

Belknap, B. and L. Belknap Evans (1969), *Grand Canyon River Guide*, Westwater Books, Evergreen, Colorado, 96 pp.

Belknap, B., B. Belknap, and L. Belknap Evans (1974), *Canyonlands River Guide*, Westwater Books, Evergreen, Colorado, 79 pp.

Belknap, L., C. Walbridge, M. Thornton, and R. Browers (1998). *Safety Code of American Whitewater*, American Whitewater, Margaretville, NY.

Bennett, J.P. (1993) Sediment transport simulations for two reaches of the Colorado River, Grand Canyon, Arizona, *U.S. Geol. Surv. Water-Resour. Invest. Rep., 93-4034,* 42 p.

Birdseye, C.H. (1928), Topographic Instruction of the United States Geological Survey, *U.S. Geological Survey Bulletin*, *788*, 432 pp.

Blackwelder, E. (1934), Origin of the Colorado River, *GSA Bulletin*, *45*, 551-565.

Boyer D.E. and R.H. Webb (in press), *In Search of Dam Sites: The U.S. Geological Survey Expedition of 1923 in Grand Canyon*. Utah State University Press, Logan, Utah.

Brunner, G.W. (2001), HEC-RAS river analysis system: hydraulic reference manual, *US Army Corps of Engineers, Institute for water resources, Hydrologic Engineering Center.*

Bureau of Reclamation (1996), Environmental assessment on the experimental flood: Glen Canyon Dam. *Bureau of Reclamation*, Salt Lake City, Utah.

Cheng, R.T. and J.W. Gartner (2003), Complete velocity distribution in river cross-sections measured by acoustic instruments, in *Proc. of the IEEE/OES Seventh Working Conference on Current Measurement Technology*, IEEE.

Chow, V.T. (1959), *Open-Channel Hydraulics*, McGraw-Hill Book Company, New York, 680 pp.

Cluer, B.L. (1997), Eddy bar responses to the sediment dynamics of pool-riffle environments, Ph.D. diss. Colorado State University, 128 pp.

Cooley, M.E., B.N. Aldridge, and R.C. Euler (1977), Effects of the catastrophic flood of December, 1966, North Rim area, eastern Grand Canyon, Arizona, *U.S. Geol. Surv. Prof. Pap., 980*.

Crumbo, K. (1981), *A river runners' guide to the history of the Grand Canyon*, Johnson Books, Boulder, Colo.

Damon, P.E., M. Shafiqullay, and R.B. Scarborough (1978), Revised Chronology for Critical Stages in the Evolution of the Lower Colorado River [abs.] *Geological Society of America Abstracts with Programs, 10 (3)*, p. 101.

Davis, P.A., M.R. Rosiek, and D.M. Galuszka (2002a), Evaluation of airborne image data and LIDAR main-stem data for monitoring physical resources within the Colorado River ecosystem, *U.S. Geol. Surv. Open File Rept.*, *02-469*. 35 pp.

Davis, P., M. Manone, S. Mietz, K. Kohl, M. Rosiek, J. Hazel, M. Kaplinski, and M. Gonzales (2002b), Evaluation of LIDAR and photogrammetry for monitoring volume changes in riparian resources within the Grand Canyon, Arizona, Pecora 15/Land Satellite Information IV Conference, Nov. 10-14, Denver, CO.

Dey, S. and A.K. Barbhuiya (2006), Velocity and turbulence in a scour hole at a vertical-wall abutment, *Flow Meas. and Instr*. 17, 13-21, doi:10.1016/j.flowmeasinst.2005.08.005.

Douglas, M.E. and P.C. Marsh (1996), Population estimates/population movements of Gila cypha, an endangered cyprinid fish in Grand Canyon region of Arizona, *Copeia, 1996 (1)*, 15-28.

Elgar, S., B. Raubenheimer, and R.T. Guza (2005), Quality control of acoustic Doppler velocimeter data in the surfzone, *Meas. Sci. Technol*.,16, 1889-1893, doi:10.1088/0957-0233/16/10/002.

Fenton, C.R., R.H. Webb, P.A. Pearthree, T.E. Cerling, and R.J. Poreda (2001), Displacement rates on the Toroweap and Hurricane faults: Implications for Quaternary downcutting in the Grand Canyon, Arizona, *Geology, 29 (11)*, 1035-1038.

Ferro, V. (2003) ADV measurements of velocity distributions in a gravel-bed flume, *Earth Surf. Process. Landforms*, *28*, 707-722, doi:10.1002/esp.467.

Flynn, M.E. and N.J. Hornewer (2003), Variations in sand storage measured at monumented cross sections in the Colorado River between Glen Canyon Dam and Lava Falls Rapid, Northern Arizona, 1992-99, *U.S. Geol. Surv. Water-Resour. Invest. Rep., 03-4104*, 39 p.

Fox, R.W. and A.T. McDonald (1985), *Introduction to Fluid Mechanics*, John Wiley & Sons, New York, 741 pp.

Gartner, J.W. and N.K. Ganju (2002), A preliminary evaluation of near-transducer velocities collected with low-blank acoustic Doppler current profiler, in Proceedings: ASCE Conference, Hydraulic Measurements and Experimental Methods 2002, Estes Park, CO, July 28-August 1, 2002.

Ghiglieri, M.P. and T.M. Myers (2001), *Over the Edge: Death in Grand Canyon,* Puma Press, Flagtaff, Ariz., 408 pp.

Graf, W.L. (1979), Rapids in canyon rivers, *J. of Geology, 87*, 533-551.

Grams, P.E. and J.C. Schmidt (2002), Streamflow regulation and multi-level flood plain formation: channel narrowing on the aggrading Green River in the eastern Uinta Mountains, Colorado and Utah, *Geomorphology, 44*, 337-360.

Grand Canyon Monitoring and Research Center (2002), A Guide to the Colorado River in the Grand Canyon: From Glen Canyon Dam to Pierce Ferry, U.S. Geological Survey, Grand Canyon Monitoring and Research Center, Flagstaff, AZ.

Grant, G.E. (1997), Critical flow constraints flow hydraulics in mobile-bed streams: A new hypothesis, *Water Resour. Res., 33 (2)*, 349-358.

Griffiths, P.G., R.H. Webb, and T.S. Melis (1996), Initiation and frequency of debris flows in Grand Canyon, Arizona: *U.S. Geological Survey Open-File Report 96-491*, 35 pp.

Griffiths, P.G., R.H. Webb, and T.S. Melis (1997), Initiation of debris flows in bedrock canyons of the Colorado River, USA, *in* Debris-flow hazards mitigation: Mechanics, prediction, and assessment, edited by Chen, C.L., American Society of Civil Engineers, 12-20. New York.

Griffiths, P.G., R.H. Webb, and T.S. Melis (2004), Initiation and frequency of debris flows in Grand Canyon, Arizona, *J. Geophys. Res., Surf. Processes*, *109*, F04002, doi: 10.1029/2003JF000077.

Hamblin, W.K. (1994), Late Cenozoic lava dams in the western Grand Canyon: *Geological Society of America Memoir 183*, 139 p.

Hanks, T.C. and R.H. Webb (2006), Effects of tributary debris on the longitudinal profile of the Colorado River in Grand Canyon, *J. Geophys. Res., Surf. Processes*, *111*, F02020, doi:10.1029/2004JF000257.

Hazel, J.E. Jr., D.J. Topping, J.C. Schmidt, and M. Kaplinski (2006), Influence of a dam on fine-sediment storage in a canyon river, *J. Geophys. Res., Surf. Processes, 111*, F01025, doi:10.1029/2004JF000193.

Henderson, F.M. (1966) *Open Channel Flow*, Macmillan, New York, 522 pp.

Helsel, D.R., and R.M. Hirsch (1992), *Statistical Methods In Water Resources*, Elsevier, New York.

Hotchkiss, R.H., D. Faber, M.C. Stone, H.M. Tritico, and P.J. Flanagan (2003), Velocity measurements in vicinity of a removable spillway weir, in World Water and Environmental Resources Congress 2003 and Related Symposia, Philadelphia, PA, ASCE.

Howard, A., and R. Dolan (1981), Geomorphology of the Colorado River in Grand Canyon, *J. Geology*, *89*, 269-298.

Hunt, C.B. (1969), Geological History of the Colorado River, in: The Colorado River Region and John Wesley Powell, *U.S. Geological Survey Professional Paper 669*, 145 pp.

Huntoon, P.W. (1977), Holocene faulting in the western Grand Canyon, Arizona, *GSA Bulletin*, *88*, 1619-1622.

Irish, J.L., and J.W. Lillycrop (1999), Scanning laser mapping of the coastal zone: the SHOALS system, *ISPRS J. Photogr. & Remote Sens.*, *54*, 123-129.

Kearsley, M.J.C. and T.J. Ayers (1999), Riparian vegetation responses: snatching defeat from the jaws of victory and vice versa, in *The Controlled Flood in Grand Canyon, Geophys. Monogr. Ser.,* vol. 110, edited by R.H.Webb et al., pp. 309-327, AGU, Washington, D.C.

Kieffer, S.W. (1985), The 1983 hydraulic jump in Crystal Rapid: Implications for river-running and geomorphic evolution in the Grand Canyon, *J. Geology*, *93*, 385-406.

Kieffer, S.W. (1987), The waves and rapids of the Colorado River, Grand Canyon, Arizona, *U.S. Geological Survey Open File Report 87-096*, 69 pp.

Kieffer, S.W. (1988), Hydraulic map of Lava Falls Rapid, Grand Canyon, Arizona, *U.S. Geol. Surv. Misc. Invest. Series Map I-1897-J*, scale 1:1,000, 1 sheet.

Kieffer, S.W. (2003), Hydraulics and geomorphology of the Colorado River in the Grand Canyon, *in Grand Canyon Geology,* edited by Bues, S.S. and M. Morales, 275-312, Oxford University Press, New York.

Korman, J., M. Kaplinski, J.E. Hazel III, T.S. Melis (2005), Effects of the experimental fluctuating flows from Glen Canyon Dam in 2003 and 2004 on the early life history stages of Rainbow Trout in the Colorado River, Final Report prepared from the Grand Canyon Research and Monitoring Center, 171 pp.

Lai, Yong G. (2005), River and watershed modeling: Current effort and future direction, in US-China Workshop on Advanced Computational Modelling in Hydroscience & Engineering, September 19-21, 2005, Oxford, Mississippi, USA.

Lane, S.N., P.M. Biron, K.F. Bradbrook, J.B. Butler, J.H. Chandler, M.D. Crowell, S.J. McLelland, K.S. Richards, and A.D. Roy. (1998) Three-dimensional measurement of river channel flow processes using acoustic Doppler velocimetry, *Earth Surf. Process. Landforms*, *23*, 1247-1267.

Leopold, L.B. (1969), The rapids and the pools—Grand Canyon, pp. 131-145 in The Colorado River Region and John Wesley Powell, *U.S. Geol. Surv. Prof. Pap., 669*.

Leopold, L.B., M.G. Wolman, and J.P. Miller (1964), *Fluvial Processes in Geomorphology*, W.H. Freeman, San Francisco, 522 pp.

Loomis, J. Douglas, A.J., Harpman, D.A. (2005), Recreation use values and nonuse values of Glen and Grand Canyons, in The State of the Colorado River Ecosystem in Grand Canyon, edited by Gloss, S.P. et al., p. 153-164, *U.S. Geological Survey Circular 1282*.

Lucchitta, I. (1966), Cenozoic geology of the upper Lake Mead area adjacent to the Grand Wash Cliffs, Arizona, Ph.D. thesis, State College, Pennsylvania State University, 218 pp.

Lucchitta, I., (1972), Early history of the Colorado River in the basin and range prvince: *GSA Bulletin, 83*, 1933-1947.

Lucchitta, I. (1975), The Shivwitz Plateau, In: Application of ERTS Images and Image Processing to Regional Geologic Problems and Geologic Mapping in Northern Arizona, *Jet Propulsion Laboratory Technical Report 32-1597*, 41-72.

Lucchitta, I. (1990), History of the Grand Canyon and of the Colorado River in Arizona, in Grand Canyon Geology, edited by S.S. Beus and M. Morales, 311-332, Oxford University Press, New York.

Magirl, C.S., R.H. Webb, and P.G. Griffiths (2005), Changes in the water surface profile of the Colorado River in Grand Canyon, Arizona, between 1923 and 2000, *Water Resour. Res.*, *41*, W05021, doi:10.1029/2003WR002519.

Magirl, C.S., P.G. Griffiths, and R.H. Webb (2006), ADV point measurements within rapids of the Colorado River in Grand Canyon, in Graham, R. (editor), Examining the Confluence of Environmental and Water Concerns, Proceedings of the 2006 World Environmental and Water Resources Congress, Omaha, Nebraska, May 21-25, 2006: Reston, Virginia, American Society of Civil Engineers Publication.

Martin, R.A. (1989), *A Story that Stands Like a Dam*, New York, Henry Holt Company 368 pp.

McKee, E.D., R.F. Wilson, W.J. Breed, and C.S. Breed (1967), Evolution of the Colorado River in Arizona, *Museum of Northern Arizona Bulletin*, *44*, 67 pp.

McKee, E.D., and E.H. McKee (1972), Pliocene Uplift of the Grand Canyon Region: Time of Drainage Adjustment, *GSA Bulletin*, *83 (7)*, 1923-1932.

Meek, N. and J. Douglass (2001), Lake overflow: an alternative hypothesis for Grand Canyon incision and development of the Colorado River, in *Colorado River: Origin and Evolution*, Proceedings of a symposium held at Grand Canyon National Park in June, 2000, edited by Young, R.A. and E.E. Spamer, p. 199-204, Grand Canyon Association, Grand Canyon, Arizona.

Melis, T.S. (1997), Geomorphology Of Debris Flows And Alluvial Fans In Grand Canyon National Park And Their Influences On The Colorado River Below Glen Canyon Dam, Arizona, Ph.D. diss., University of Arizona, Tucson.

Melis, T.S., R.H. Webb, P.G. Griffiths, and T.J. Wise (1994), Magnitude and frequency data for historic debris flows in Grand Canyon National Park and vicinity, Arizona, *U.S. Geol. Surv. Water Resour. Invest. Rep., 94-4214*. 285 pp.

Melis, T.S., W.M. Phillips, R.H. Webb, and D.J. Bills (1996), When the blue-green waters turn red; historical flooding in Havasu Creek, Arizona, *U.S. Geol. Surv. Water Resour. Invest. Rep., 96-4059*, 136 pp.

Milligan, M. (2004), *Westwater Lost and Found*, Utah State University Press, Logan, Utah, 300 pp.

Morlock, S.E. and G.T. Fisher (2002), Hydroacoustic Current Meters for the Measurement of Discharge in Shallow Rivers and Streams, in *Hydraulic Measurements and Experimental Methods 2002, proceedings, July 28-Aug 1, 2002, Estes Park, Co*. ASCE.

Mueller, D.S. and C.R. Wagner (2006), Application of the Loop Method for correcting acoustic Doppler current profiler discharge measurements biased by sediment transport, *U.S. Geol. Surv. Scient. Invest. Rep., 2006-5079*, 18 pp.

Nikora, V.I. and G.M. Smart (1997), Turbulence characteristics of New Zealand gravel-bed rivers, *Journal of Hydraulic Engineering, 123 (9)*, 764-773.

O'Connor, J.E. and R.H. Webb (1988), Hydraulic modeling for paleoflood analysis, in *Flood Geomorphology*, edited by V.R. Baker et al., Wiley, New York, 393-402.

O'Connor, J.E. (1993), Hydrology, Hydraulics, and Geomorphology of the Bonneville Flood, *Geol. Soc. of Amer. Special Paper 274*, 83 pp.

O'Connor, J.E., L.L. Ely, E.E. Wohl, L.E. Stevens, T.S. Melis, V.S. Kale, and V.R. Baker (1994), A 4500-year record of large floods on the Colorado River in the Grand Canyon, Arizona, *J. Geology, 102*, 1-9.

Parnell, R.A. Jr., J.B. Bennett, and L.E. Stevens (1999), Mineralization of riparian vegetation buried by the 1996 controlled flood, in *The Controlled Flood in Grand Canyon, Geophys. Monogr. Ser.,* vol. 110, edited by R.H.Webb et al., pp. 224-239, AGU, Washington, D.C.

Pederson, J., K. Karlstrom, W. Sharp, and W. McIntosh (2002), Differential incision of the Grand Canyon related to Quaternary faulting—Constraints from U-series and Ar/Ar dating, *Geology, 30 (8)*, 739-742.

Peirce, H.W. (1984), The Mogollon Escarpment, *Arizona Bureau of Geology and Mineral Technology Fieldnotes, 14 (2)*, 8-11.

Pizzuto, J.E., R.H. Webb, P.G. Griffiths, J.G. Elliot, and T.S. Melis (1999), Entrainment and transport of cobbles and boulders from debris fans, in *The Controlled Flood in Grand Canyon, Geophys. Monogr. Ser.,* vol. 110, edited by R.H.Webb et al., pp. 53-70, AGU, Washington, D.C.

Pope, S.B. (2000) *Turbulent Flows*, Cambridge University Press, New York, 771 pp.

Potochnik, A.R. and J.E. Faulds (1998), A tale of two rivers: Tertiary structural inversion and drainage reversal across the southern boundary of the Colorado Plateau, in Geologic excursions in northern and central Arizona (GSA Rocky Mountain Section field trip guidebook), edited by Duebendorfer, E.M, p. 149-174, Flagstaff, Northern Arizona University.

Powell, J.W. (1895), Canyons of the Colorado: Flood and Vincent. Reprinted as, *The Exploration of the Colorado River and its Canyons*. New York: Dover, 400 pp.

Randle, T.J., and E.L. Pemberton (1987), Results and analysis of STARS modeling efforts of the Colorado River in Grand Canyon, *NTIS report no. PB88-183421, Glen Canyon Environmental Studies*, Flagstaff, Arizona.

RDInstruments, Inc. (1996), *Acoustic Doppler current profilers—Principles of operation: A practical primer*, RDInstruments, Inc., San Diego, Calif., 54 pp.

Reisner M. (1986), *Cadillac Desert, The American West and its Disappearing Water*, Penguin Books, New York, 582 pp.

Reynolds, O. (1895), On the dynamical theory of incompressible viscous fluids and the determination of the criterion, *Philosophical Transactions of the Royal Society of London, Series A, 186*, 123 pp..

Roy, A.G., P.M. Biron, T. Buffin-Bélanger, and M. Levasseur. (1999) Combined visual and quantitative techniques in the study of turbulent flows, *Water Resour. Res., 35(3)*, 871-877.

Schmidt, J.C. (1990), Recirculating flow and sedimentation in the Colorado River in Grand Canyon, Arizona, *J. of Geology, 98*, 709-724.

Schmidt, J.C., and J.B. Graf (1990), Aggradation and degradation of alluvial sand deposits, 1965-1986, Colorado River, Grand Canyon National Park, Arizona, *U.S. Geol. Surv. Prof. Pap., 1493*.

Schmidt, J.C. and D.M. Rubin (1995), Regulated streamflow, fine-grained deposits, and effective discharge in canyons with abundant debris fans, in *Natural and anthropogenic influences in fluvial geomorphology,* edited by J.E. Costa, et al., p. 177-195, AGU, Geophys. Mono. 89, Washington, DC.

Schmit, L.M. S.P. Gloss, and C.N. Updike (2005), Overview, in The State of the Colorado River Ecosystem in Grand Canyon, edited by Gloss, S.P. et al., p. 1-16, *U.S. Geological Survey Circular 1282*.

Sklar, L.S. and W.E. Dietrich (2004), A mechanistic model for river incision into bedrock by saltating bed load, *Water Resour. Res., 40*, W06301, doi:10.1029/2003WR002496.

Smart, G.M. (1994), Turbulent Velocities in a Mountain River, in Hydraulic Engineering '94: proceedings of the 1994 Conference: Buffalo, New York, August 1-5, 1994, ASCE, 844-848.

Smart, G.M. (1999), Turbulent velocity profiles and boundary shear in gravel bed rivers, *Journal of Hydraulic Engineering, 125 (2)*, 106-116.

Spencer, J.E. and P.A. Pearthree (2001), Headward erosion versus closed-basin spillover as alternative causes of Neogene capture of the Ancestral Colorado River by the Gulf of California, in *Colorado River: Origin and Evolution*, Proceedings of a symposium held at Grand Canyon National Park in June, 2000, edited by Young, R.A. and E.E. Spamer, p. 215-219, Grand Canyon Association, Grand Canyon, Arizona.

Stevens, J.E. (1988), *Hoover Dam: An American Adventure*, University of Oklahoma Press, Norman, Okla.

Stevens, L.E. (1983), *The Colorado River in Grand Canyon, A Guide*, Red Lake Books, Flagstaff, Ariz.

Stevens, L.E., J.P. Shannon, and D.W. Blinn (1997), Colorado River benthic ecology in Grand Canyon, Arizona, USA: Dam, tributary and geomorphological influences, *Regulated Rivers: Research and Management, 13*, 129-149.

Taylor, J.R. (1997), *An Introduction to Error Analysis*, University Science Books, Sausalito, Calif.

Tinkler, K.J. (1997), Indirect Velocity Measurement from Standing Waves in Rockbed Rivers, *Journal of Hydraulic Engineering*, *123 (10)*, 918-921.

Topping, D.J., D.M. Rubin, and L.E. Vierra Jr. (2000), Colorado River sediment transport 1. Natural sediment supply limitation and the influence of Glen Canyon Dam, *Water Resour. Res., 36 (2)*, 515-542.

Topping, D.J., J.C. Schmidt, and L.E. Vierra Jr. (2003), Computation and Analysis of the Instantaneous-Discharge Record for the Colorado River at Lees Ferry, Arizona—May 8, 1921, through September 30, 2000, *U.S. Geol. Surv. Prof. Pap., 1677*.

Turner, R.M. and M.M. Karpiscak (1980), Recent vegetation changes along the Colorado River between Glen Canyon Dam and Lake Mead, Arizona, *U.S. Geological Survey Professional Paper 1132*, 125 pp.

United States Geological Survey (1924), Plan And Profile of Colorado River From Lees Ferry, Ariz., to Black Canyon, Ariz.- Nev. and Virgin River, Nev., *U.S. Geol. Surv.*

Walters, C., J. Korman, L. E. Stevens, and B. Gold (2000), Ecosystem modeling for evaluation of adaptive management policies in the Grand Canyon. *Conservation Ecology*, *4 (2)*.

Webb, R.H. (1996), *Grand Canyon, a Century of Change*, University of Arizona Press, Tucson, Ariz.

Webb, R.H., P.T. Pringle, and G.R. Rink (1989), Debris flows from tributaries of the Colorado River, Grand Canyon National Park, Arizona, *U.S. Geol. Surv. Prof. Pap., 1492*.

Webb, R.H., T.S. Melis, P.G. Griffiths, and J.G. Elliot (1997), Reworking of aggraded debris fans by the 1996 controlled flood on the Colorado River in Grand Canyon National Park, Arizona, *U.S. Geol. Surv. Open File Report 97-16.*

Webb, R.H., T.S. Melis, P.G. Griffiths, and J.G. Elliot (1999a), Reworking of aggraded debris fans, in *The Controlled Flood in Grand Canyon, Geophys. Monogr. Ser.,* vol. 110, edited by R.H.Webb et al., pp. 37-51, AGU, Washington, D.C.

Webb, R.H., D.L. Wegner, E.D. Andrews, R.A. Valdez, and D.T. Patten (1999b), Downstream effects of Glen Canyon Dam on the Colorado River in Grand Canyon: A review, in *The Controlled Flood in Grand Canyon, Geophys. Monogr. Ser.,* vol. 110, edited by R.H.Webb et al., pp. 1-21, AGU, Washington, D.C.

Webb, R.H., T.S. Melis, P.G. Griffiths, J.G. Elliott, T.E. Cerling, R.J. Poreda, T.W. Wise, and J.E. Pizzuto (1999c), Lava Falls Rapid in Grand Canyon, effects of late Holocene debris flows on the Colorado River, *U.S. Geol. Surv. Prof. Pap., 1591*.

Webb, R.H., P.G. Griffiths, T.S. Melis, and D.R. Hartley (2000), Sediment delivery by ungaged tributaries of the Colorado River in Grand Canyon, *U.S. Geol. Surv. Water-Resour. Invest. Rep., 00-4055*.

Webb, R.H., T.S. Melis, and R.A. Valdez (2002), Observations of Environmental Change in Grand Canyon, Arizona, *U.S. Geol. Surv. Water-Resour. Invest. Rep., 02-4080*.

Webb, R.H., J. Belnap, and J. Weisheit (2004), *Cataract Canyon: A Human and Environmental History of the Rivers in Canyonlands*, University of Utah Press, Salt Lake City, Utah, 268 pp.

Webb, R.H, P.G. Griffiths, and L.P. Rudd (in press), Occurrence of Holocene debris flows on the Colorado Plateau, *GSA Bulletin*.

Wehr, A., and U. Lohr (1999), Airborne laser scanning—an introduction and overview, ISPRS *J. Photogr. & Remote Sens., 54*, 68-82.

Wiele, S.M. and Smith, J.D. (1996) A reach-averaged model of diurnal discharge wave propagation down the Colorado River through the Grand Canyon, *Water Resour. Res. 32 (5)*, 1375-1386.

Wiele, S. M. and Griffin, E.R. (1997) Modifications to a one-dimensional model of unsteady flow in the Colorado River through the Grand Canyon: *U.S. Geol. Surv. Water-Resour. Invest. Rep.* 97-4046.

Wiele, S.M., E.D. Andrews, E.R. Griffin (1999), The effect of sand concentration on depositional rate, magnitude, and location in the Colorado River below the Little Colorado River, in *The Controlled Flood in Grand Canyon, Geophys. Monogr. Ser.,* vol. 110, edited by R.H.Webb et al., pp. 131-145, AGU, Washington, D.C.

Wilcox, D.C. (1993), *Turbulence Modeling for CFD*, DCW Industries, La Cañada, California, 537 pp.

Wilson, R.M. (1941), Claude Hale Birdseye obituary, *Trans. Am. Soc. Civ. Engrs., 106*, 1549-1553.

Wilson, R.T. (1986), Sonar patterns of Colorado River bed, Grand Canyon: Las Vegas, Nevada, Proceedings of the Fourth Federal Interagency Sedimentation Conference,v. 2, p. 5-133 to 5-142.

Wohl, E.E. (1998), Bedrock channel morphology in relation to erosional processes, in *Rivers Over Rock: Fluvial Processes in Bedrock Rivers*, edited by Tinkler, K.J. and E.E. Wohl, p. 133-151, Geophys. Mono. 107, American Geophysical Union, Washington, D.C.

Wright, S.A. and J.W. Gartner (2006), Measurements of velocity profiles and suspended-sediment concentrations in a Colorado River eddy during high flow, in Proceedings, 8th Federal Interagency Sedimentation Conference, April 2-6, 2006, Revo, NV.

Yanites, B.J., R.H. Webb, P.G. Griffiths, and C.S. Magirl (2006), Debris flow deposition and reworking by the Colorado River in Grand Canyon, Arizona, *Water Resour. Res., 42,* W11411, doi:10.1029/2005WR004847.

Yorke, T.H. and K.A. Oberg. (2002) Measuring river velocity and discharge with acoustic Doppler profilers, *Flow Meas. and Instr*. *13*, 191-195.

Young, R.A. (2001), The Laramide-paleogene history of the western Grand Canyon region: Setting and Stage, in *Colorado River: Origin and Evolution*, Proceedings of a symposium held at Grand Canyon National Park in June, 2000, edited by Young, R.A. and E.E. Spamer, p. 7-15, Grand Canyon Association, Grand Canyon, Arizona.

Young, R.A. and W.J. Brennan (1974), Peach Springs Tuff, Its Bearing on Structural Evolution of the Colorado Plateau and Development of Cenozoic Drainage in Mohave County, Arizona, *GSA Bulletin, 85*, 1745-1750.

Young, R.A. and E.E. Spamer, editors (2001), *Colorado River: Origin and Evolution*, Proceedings of a symposium held at Grand Canyon National Park in June, 2000, Grand Canyon Association, Grand Canyon, Arizona.